A FUNDAMENTAL STUDY ON SIMPLIFIED ANALYSIS OF BUCKLING, LOAD-CARRYING CAPACITY AND DEFORMABILITY OF GIRDERS

by

Hachirho Takeda

2004

A Fundamental Study on Simplified Analysis of Buckling, Load-Carrying Capacity and Deformability of Girders

Index

Acknowledgement

Chapter 1

Introduction

1.1 Background and purpose of study

Girder bridges such as plate and box girder bridges can be considered to be the most common steel bridges. Since those girders have traditionally fundamental and rational form, they will continue to be used in future as well. The typical construction of those girders mainly consists of flanges, webs and stiffeners and the behavior of these components and the general behavior have been intensively studied by many researchers in the past in the wide areas including buildings and other engineering fields.

The fall-off of box girders during construction stage due to insufficient compressive strength of stiffened plates and lateral buckling of plate girders and due to poor detailing of connections are typical examples of accidents of girder structures. Furthermore, in the Great Hanshin-Awaji Earthquake, that occurred more than nine years ago, cyclic web buckling due to shear in the cross beam of rigid frame piers either combined or not with damages of piers or bearings or buckling of main girders caused by the collapse of piers have been reported. With such damages in mind, the studies on the design to improve the safety and rationality should be directly incorporated into the improved structural design. Recently, with remarkable improvements in the computer simulation as the background, the non-linear material and large displacement analysis is frequently applied by means of finite element methods and other powerful methods. Such verification is finally desirable; nevertheless, simplified but practical analyses using proper modeling is yet deemed necessary on the more natural and instinctive ground of structural mechanics. As a matter of fact, experimental and inductive methods, or so-called semi-inverse method, are also useful and essential as well as the analytical method.

The main purpose of this dissertation is to investigate the fundamental property and characteristics on various points of girder structures toward their rational design by means of experimental methods in combination with several approximate analyses. Although the clarification on the buckling and load-carrying capacity of girder structure is emphasized, the viewpoint of the deformability will also be stressed for mitigation of seismic force on the girders. The latter viewpoint may be thought very important from the standpoint of absorption of earthquake energy, as it is evident from the damaged states on the Great Hanshin-Awaji Earthquake.

1.2 Literature survey and specifications

The study on girder bridges that are most common steel bridges has been carried out numerously.[1] Since main components of these girders consist of flanges, webs and stiffeners and the loading pattern are compression, bending, shear and those combinations, it is necessary to carry out the research from various viewpoints. Concerning the type of loading, the examination on the behavior of girders subjected to static and cyclic loadings is required. Furthermore, tapered members, namely the

girders with varying depth are often used.

In this article, literature survey and the application to specifications are described. Especially, The Japanese Specifications for Highway Bridges[2] is mainly mentioned.

An allowable compressive stress of girders due to bending moment has been determined based on the lateral buckling strength of girders. Timoshenko and Gere lead to a closed-form solution by elastic buckling analysis.[3] Nethercot[4] summarized the results based on buckling analysis as the simple and direct design methods in which various loading and support cases have been considered for the elastic lateral buckling of beams. Buckling in the elastic range is in particular useful when the strength of girders during the construction phase is considered. If the end moments are unequal, the solution for the case under uniform moment must be modified. Salvadori[5] proposed a modifier for the case that moment gradient affected on the critical moment. This modifier is adopted in Reference 2) and the equivalent uniform moment on a girder under unequal end moments has been defined. Woolcock and Trahair[9],[10] investigated the problem on post-buckling strength.

In Japan the load-carrying capacity curves had been obtained by inelastic buckling tests[6] have been used in Reference 2). Further, when a local buckling strength falls below a lateral buckling strength, in order to consider the effect of the local buckling on the load-carrying capacity the allowable stress for the local buckling has been adopted as the allowable compressive stress due to bending moment. The simultaneous buckling of flanges and web plate has not been considered. Elastic buckling of plate girders under pure bending has been analyzed by Konishi et al.[32] as the simultaneous buckling between a web plate and vertical stiffeners. The researches on the overall lateral buckling of girders are also presented. The study on the lateral-torsional buckling strength of steel twin girder bridges under erection[7] is reflected in Reference 8).

When long-span steel girder bridges are constructed, those web plates need generally multiple longitudinal and transverse stiffeners. Richmond[11] solved the elastic buckling of rectangular plates orthogonally stiffened under bending and combined bending and compression by using the orthotropic plate theory. Such design procedure was proposed in several specifications, for example BS5400[12]. The Japanese Specifications for Highway Bridges does not explicitly contain any design provision applicable to the multi-stiffened webs.[2] Therefore, the necessity for any simple theory which can cover the prediction of the bending strength of plate girders whose web has the multiple stiffeners is high. A plate girder with many longitudinal stiffeners has been tested[13], and the experiments on the ultimate strength of the plate girders and box girders with multi-stiffened webs have been carried out.[14]-[16]

The web plate of plate girders subjected to shear force has been noticed for its characteristic behavior. Wagner[17] proposed a complete tension field to the panel strength under shear. Basler is a pioneer in the study on the shear strength of plate girders[18],[19]. There have been many experimental studies on the ultimate shear of plate girders subjected to shear force.[1] And then, various models to predict the shear strength of plate girders have been also formulated.[1] Another analytical method is the elasto-plastic finite displacement analysis using means such as the finite element

method. Marsh[20], Nakazawa et al.[21,22] and Lee et al.[23] carried out the elasto-plastic finite displacement analysis on the ultimate shear behavior of the plate girder panel using the finite element method considering both material and geometric non-linearity. Lee et al.[33] also carried out the experiment in order to verify the theory. The post-buckling strength of girder panels had been clarified from these analyses and experimental results is not utilized sufficiently in The Japanese Specifications for Highway Bridges.[2] In this Specification, considering the post-buckling strength of web plate the safety factor for calculated buckling stress of web panel is reduced.

In the meantime, tapered girders are also usually used. In such type of girders, the girder with varying web depth has been often constructed. The studies on the load-carrying capacity of girders with variable web and tapered panels are comparatively few. Falby[24] has proposed a calculation method to predict shear strength by means of plastic analysis in Basler's style[19]. Also, Mandal et al.[25,26] have given a predicting method extending the theory of Porter et al.[27]. In Reference 2), plate girders with the web tapered in depth have not been described yet.

Most of the panels in plate girders are subjected to the combined loading of varying bending moments in longitudinal direction and shear forces. Many studies on a plate panel subjected simultaneously to bending moments and shear forces in its plane have been carried out and the interaction curves have been proposed[28-29]. Since a girder panel has four edges, the effects of these frame members must be considered. These analytical results are often expressed using interaction curves[1]. The investigations on the interaction of girder panels in inelastic range under combined loading have been proposed[30-31]. In The Japanese Specifications for Highway Bridges[2], as an interaction curve, the formula of the circular type has been adopted. In the meantime, although the works of general design procedures for the ultimate strength of panels with variable depth under the combined action of bending moments and shear forces are required such investigation is few.

The behavior of structures or structural members subjected to the cyclic load under strict condition such as seismic load and traffic load has been much studied at various fields in recent years. To begin with, there is the problem as a fatigue under high cycle and low stress. As an example of such problem, the studies that regard such problems as fatigue ones owing to web breathing under repetitive loading have been made. For examples, these problems are discussed at Ref.5) which is a publication by ECCS[34] and have been adapted as a design standard in Eurocode No.3[35]. Okura has introduced the research results on such problems and discussed in detail[36]. In addition, there is the problem of structures with low cycle and high stress. In such type of cyclic loadings, the research on the behavior of inelastic repetitive buckling for plate girders and girder panels is also necessary. Up to now, for this kind of subject Popov et al. have proceeded with a series of studies on the case in which shear links are subjected to cyclic shear loads[37-39]. In these studies, the width-to-thickness ratio of a web panel and the spacing of stiffeners are chosen as parameters and many load-displacement hysteresis diagrams have been described.

As obtained results, a fact that shear links exhibit excellent energy absorption has been shown and its availability has been discussed. Test girders are wide flange beams of which the web has comparatively small width-to-thickness ratio. Although limited to shear link beams under cyclic loading, many loading tests have been conducted, and the behavior up to the ultimate state has been clarified considerably in detail by Hjelmstad[37] Also in Japan, for an example, Suzuki et al. has researched inelastic behavior of beams under non-uniform moment[40].

As recent applied research, there is the study by Takahashi et al.[41] Recently, Lubell showed that steel plate shear walls exhibit many desirable structural characteristics in the area of high seismic risk[42] and similarly, the use of shear links is proposed for the main tower of the new San Francisco-Oakland Bay self-anchored suspension bridge for its ability of dissipating the hysteretic plastic strain energy by making the links finally removable without causing difficulties from the rest of the main members after its significant inelastic deformation[43].

1.3 Summary of study

The substance of this study is to mainly clarify the fundamental behavior of girder structures by means of several approximate analyses and experimental methods. The outline of each chapter except chapters 1 and 7 are summarized as follows.

In Chapter 2, the flexural buckling, particularly the elastic lateral buckling of the girder subjected to moment gradient is treated as the simultaneous buckling between flanges and a web by using an orthotropic plate theory. The elastically supported and elastically built-in edges are adopted as the boundary condition at flanges. Numerical computations are carried out by using the finite difference method and it is investigated how the rigidity of flanges and stiffeners affect the buckling load. To verify the validity of this theory, loading tests are also carried out using model girders. By applying this theory to the web panel of the girder with unequal end moments, the magnitude of reduced bending moments and the position where the moment is reduced can be obtained. That is useful for checking on the buckling of the web panel with combined bending moment and shear forces.

In Chapter 3, girder bridges with large depth are analyzed by the approximate method for the bending strength of the girder with multi-stiffened web plate by means of the orthotropic theory. In the proposed method, the stress distribution at the ultimate state is assumed and the simultaneous buckling of flanges and a web plate is evaluated. For the case of inelastic buckling the reduced coefficients are assumed. Besides, the formula on an equivalent rigidity is given in the case of the web plate with unequally spaced stiffeners. The effect of the flexural rigidity of flanges, the flexural and torsional rigidities of web plates, the aspect ratio of web panels and the width-to-thickness ratio of web panels on the buckling loads are investigated, respectively. The proposed method is verified by using the existing result of the loading test under bending of the girder with horizontal and vertical

stiffeners.

In Chapter 4, the static strength on girder panels subjected to shearing forces is examined. In the first half of this chapter, the girder with equal depth is chosen as the subject of the study. Firstly, by testing small girder models the strength and deformation behavior are investigated. In this description, the comparison between proposed several methods of plastic analysis on the shearing strength of such girders are provided. Subsequently, the strength and the deformation behavior on the shear panel of girders are investigated in detail by means of elasto-plastic finite deformation analyses using finite element method. In particular, it is taken into account how the flange rigidity and the ductility influence the result. In this analytical process and on the basis the experimental results the adequacy of a few main methods by plastic analysis is examined. In the latter half of this chapter, the load-carrying capacity of the girder with linearly varying depth under shear is investigated. In the first place the plastic analysis for the girder with equal depth is extended to that for the girder with trapezoidal panels. The shear buckling load of a trapezoidal panel is obtained on basis of the calculated results by finite element method. And the stress on tension strips is also obtained on basis of the stress distribution suggested by Ostapenko. Then, by testing the model girder with the varying depth, the characteristics of such girders is found and the validity of the plastic analysis is verified. Finally, about the intermediate vertical stiffeners on this trapezoidal girder, efforts are chiefly concentrated at the effects of the rigidity on failure modes on the basis of the experimental examination and the theoretical consideration by the modeling analysis.

In Chapter 5, the load-carrying capacity of the girder panel subjected to the combined forces of bending and shear is investigated. For the girder with equal depth the results of plastic analysis, elastic finite deformation analysis, elasto-plastic finite deformation analysis, experiments and so on which have been proposed formerly by many researchers are summarized and compared first. Then, the method to predict by the plastic analysis the load-carrying capacity of the girder with the trapezoidal panels of linearly varying depth is given. The method of plastic analysis on the shear strength of the girder with linearly varying depth is expanded to the case of the combined loads. Finally, by using the model girders with the varying cross section the loading test is done and the validity is investigated by comparing these experimental results with the results by the plastic analysis.

In Chapter 6, the strength and the deformation capacity of the girder panels subjected to cyclic shear load are investigated. Namely, the alternating inelastic shear buckling behavior of girder panels is clarified. This belongs to the subject of high stress and remarkably low cycle fatigue. Firstly, the strength and deformability for single panel of plate girders is investigated in detail. The analytical method is based on the elasto-plastic finite displacement analysis using finite element method. Subsequently, inelastic repetitive shear and flexural buckling of plate girders with multi-panel is treated. The loading test by means of small-sized model girders, the width-to-thickness ratio of the web, flange rigidity and loading pattern being introduced as the main parameters is carried out and the influences on the collapse modes, strength and deformation behaviors of these panels are examined. Then, the

elasto-plastic finite displacement analysis is carried out for such girders with multi-panel. The validity of this analysis is verified by comparison with loading tests. Finally, the energy absorbing capacity of such panels is discussed in view point of plastic damper effect.

In Chapter 7, a steel beam that simulated the intermediate cross beam in the bridge piers of two-story portal steel frame is analyzed. The strength and deformability of this steel beam subjected to the monotonously increasing shear force or alternatively repetitive shear force are clarified by the elasto-plastic finite displacement analysis using the finite element method. Effect of energy dissipation due to the shear buckling deformation in the relatively thin web plate near the center of the crossbeam is investigated. Namely, the energy dissipation effect by the deformation of the web panel is noticed in order to reduce the damage in the earthquake of the bridge pier as much as possible.

1.4 References

1) Galambos, T. V.: Stability Design Criteria for Metal Structures, 5th ed., John Wiley & Sons, 1998.
2) Specification for Highway Bridges, Japan Road Association, 1990.
3) Timoshenko, S. P., and Gere, J. M.: Theory of Elastic Stability, McGraw-Hill, New York, 1961.
4) Nethercot, D. A. and Rockey, K. C.: A Unified Approach to the Elastic Lateral Buckling of Beams, The Structural Engineer, Vol.49, No.7, pp.321-330, 1971.
5) Salvadori, M. G.: Lateral Buckling of I-beams, Trans. Am. Soc. Civ. Eng., Vol.120, 1955.
6) Fukumoto, Y., et al.: Inelastic Lateral Buckling Tests on Welded Beams and Girders, Proc. of Japan Society of Civil Engineers, No.189, pp.39-51, 1971 (in Japanese).
7) Hotta,T., Naito,J. and Nsshimura, N.: Lateral-Torsional Buckling Strength of Steel Twin Girder Bridges under Erection, Journal of JSCE,No.612/ I-46,pp.287-296,1999 (in Japanese).
8) Recommendation's for Erection Design and Construction of Steel Structures-2001, JSCE, 2001.
9) Woolcock, S. T., and Trahair, N. S.: Post-buckling of Determinate I-beams, ASCE J. Eng. Mech. Div., Vol.100, No.EM.2, pp.157-172, 1974.
10) Woolcock, S. T., and Trahair, N. S.: Post-buckling of Redundant I-beams, ASCE J. Eng. Mech. Div., Vol.102, No.EM2, pp.293-312, 1976.
11) Richmond, B.: Approximate buckling criteria for multi-stiffened rectangular plates under bending and compression, Proc. ICE, Vol.20, pp.141-150, 1961.
12) Draft BS5400: Steel, Concrete and Composite Bridges, Part 3: Code of Practice for Design of Steel Bridges, British Standard Institution, London, 1979.
13) Mikami, I. et al.: A test on ultimate strength of multi-stiffened plate girders in bending, Technology Reports of Kansai Univ., No.22, pp.149-161, 1981.

14) Mikami, I. et al.: Inelastic coupled buckling of steel box girders under bending, Proc. of JSCE, No.301, pp.23-36, 1980(in Japanese).

15) Mikami, I., Dogaki, M. and Yonezawa, H.: Ultimate load tests on multi-stiffened steel box girders, Technology Report of Kansai Univ., No.21, pp.157-169, 1980.

16) Niwa, Y., Watanabe, E. and Nishigome, A.: A study on shear ultimate capacity of box girder webs with multi-stiffeners, Preliminary Report of Annual Meeting, Kansai Branch of JSCE, June, 1979.

17) Wagner, H.: Flat Sheet Metal Girder with Very Thin Metal Webs, NACA Tech. Memo. Nos.604, 605, 606, 1931.

18) Basler,K., Yen,B.T., Muller,J.A. and Thürlimann,B.: Web Buckling Tests on Welded Plate Girders, Weld. Res. Counc. Bull., No.64, 1960.

19) Basler,K. : Strength of Plate Girders in Shear, Journal of the Structural Division, ASCE, Vol.87,No.ST7, pp.151-180., 1961.

20) Marsh C., Ajam W. and Ha H.: Finite Element Analysis of Postbuckled Shear Webs, Journal of Structural Engineering, ASCE, Vol.114, No. 7, pp.1571-1586, 1988.

21) Kuranishi,S., Nakazawa,M. and Iwakuma,T.: On the tension field action and collapse mechanism of a panel under shear, structural Eng./earthquake Eng., JSCE, Vol.5,No.1,pp.161s-171s, 1988.

22) Kuranishi,S., Nakazawa,M. and Iwakuma,T.: A new formula to predict the ultimate shear strength of a plate girder, Structural Eng./Earthquake Eng., JSCE, Vol.6,No.2, pp.239s-250s, 1989.

23) Lee, S. C., and Yoo, C. H.: Strength of Plate Girder Web Panels under Pure Shear, Journal of Structural Engineering, ASCE, Vol.125, No.8, 1999.

24) Falby,W.E. and Lee,G.C. : Tension-Field Design of Tapered Webs, AISC, Engineering Journal, Vol.13, No.1, pp.11-17, 1976.

25) Davis,G. and Mandal,S.N. : The collapse Behaviour of Tapered Plate Girders Loaded within the Tip, Proc. Instn. Civ. Engrs., Part2, Vol.67,pp.65-80,1979.

26) Davis,G. and Mandal,S.N. : Tapered Steel Beams Loaded within Tip, Journal of the Structural Division, ASCE, Vol.105,No.ST3,pp.589-599,1979.

27) Porter,D.M., Rockey,K.C. and Evans,H.R. : The collapse behaviour of plate girders loaded in shear, Structural Engineer, Vol.53,No.8,pp.313-325,1975.

28) Timoshenko, S. P.: The stability of the webs of plate girders, Engineering, Vol.138, pp.207-209, 1934.

29) Way, S.: Stability of rectangular plates under shear and bending forces, Journal of Applied Mechanics, Vol.3, No.4, pp. A 131-A 135, 1936.

30) Basler, K.: Strength of Plate Girders under Combined Bending and Shear, Trans. Am. Soc. Civ. Eng., Vol.128, Part Ⅱ, p.720. 1963.

31) Chern, C. and Ostapenko, A.: Unsymmetrical Plate Girders under Shear and Moment, Fritz Eng. Lab. Rep., No.328.9, Lehigh Univ., Bethlehem, Pa., 1970.

32) Konishi, I., Yonezawa, H., and Mikami, I.: Elastic Buckling of Plate Girders under Pure Bending, Proc. JSCE, No.143, 1967 (in Japanese).

33) Lee, S. C. and Yoo, C. H.: Experimental Study on Ultimate Shear Strength of Web Panels, Journal of Structural Engineering, ASCE, Vol.125, No.8, 1999.

34) Dubas, P. and Gehri, E. (edited): Behaviour and Design of Steel Plated Structures, ECCS, 1986.

35) Eurocode No.3, Chapter 9: Design of Steel Structures, Edited draft issue 3, Comission of the European Communities, April, 1990.

36) Okura, I.: Fatigue of Steel Bridges, Toyo-Shoten, 1994 (in Japanese).

37) Hjelmstad, K. D. and Popov, E. P.: Cyclic Behavior and Design of Link Beams, Journal of Structural Engineering, ASCE, Vol.109, No.10, Oct., 1983.

38) Malley, J. O. and Popov, E. P.: Shear Links in Eccentrically Braced Frames, Journal of Structural Division, ASCE, Vol.110, No.9, Sep., 1984.

39) Kasai, K. and Popov, E. P.: Cyclic Web Buckling Control for Shear Link Beams, Journal of Structural Division, ASCE, Vol.112, N0.ST3, Mar. 1986.

40) Suzuki, T. and Ono, T.: An Experimental Study on Inelastic Behavior of Steel Members Subjected Repeated Loading, World Conf EE, No.6, pp.3163-3167, Jan., 1977.

41) Takahashi, Y. and Tanaka, K.: Development of Hysteretic Damper using Eccentrical Brace System, Steel Construction Engineering, Vol.4, No.14, pp. 39-52, 1997 (in Japanese).

42) Lubell, A. S., Prion H. G. L. and Ventura, C. E.: Unstiffened Steel Plate Shear Wall Performance under Cyclic Loading, Journal of Structural Engineering, ASCE, Vol.126, No.4, pp.453-460, 2000.

43) McDaniel, C. C., Uang, Chia-Ming and Seible, F.: Cyclic Testing of Built-up SteelShear Links for the New Bay Bridge, Journal of Structural Engineering, ASCE, Vol. 129, No. 6, pp. 801-809, 2003.

Chapter 2

Lateral-torsional buckling of girders

2.1 General description

As long as girders are properly braced, they can have satisfactory strength. But if the bracing against lateral deflection and twisting is not set up enough, they may fail due to lateral-torsional buckling in an early stage. Therefore, the lateral-torsional buckling is a limit state in which structural members lose their usefulness in bending. The tendency to this type of buckling is particularly remarkable during construction because of insufficient braces.

The case in which a girder section is subjected to bending moment alone is real. On the other hand since the case under combined bending moments and shear forces is usual, the bending moment distribution in the longitudinal direction is necessarily non-uniform.

In such buckling curves, there are three ranges composed of elastic buckling, inelastic buckling and plastic behavior. Among these, elastic buckling is especially of importance during construction phase. On the other hand, the remaining ranges are important for completed girder structures.

Extensive researches have been conducted in this field. Nethercot[1] summarized these results as the simple and direct design methods in which various loading and support cases have been considered for the elastic lateral buckling of beams. Vinnakota[2] has considered the effects of initial geometric imperfections. Woolcock and Trahair[3,4] investigated the problem on postbuckling strength.

The lateral stability must be influenced by the existence of a web. Therefore, in the analysis on such problem the deformation of a web plate should be considered in order to obtain the buckling strength exactly. In most research, the deformation of a web plate is not considered usually.

Recently, the bridge with twin girders has been constructed in order to realize rationalization and reduction of labor. In such structural type of bridge, it may especially worry about the generation of lateral-torsional buckling. In addition, such type of girder bridge with very thin web plate is especially noticed in Europe. Therefore, the lateral-torsional buckling on such girders with large width-to-thickness ratio of web plate will become an important interest. In the girder under construction, it is still more important.

Overall lateral buckling of the bridge composed of twin girders has been also studied[44,45]. Recently, research on overall lateral buckling of rational 2-girder bridges under erection is presented[46]. Researches on such overall behavior are very much also required.

In this chapter the elastic lateral buckling of girders with relatively thin web will be investigated. Accordingly, this problem is closely related with the girder under construction. For twin girder bridges above mentioned, such investigation is especially effective.

The simultaneous buckling of the flange and web is analyzed by means of the theory of orthotropic plate. The numerical computations are carried out by the finite difference method. Loading tests are also carried out and theoretical and experimental results are

compared.

Furthermore, when a girder panel is subjected to unequal end moments a problem how equivalent uniform moment is estimated arises. It becomes a matter of important concern for checking on the buckling of a girder panel. Therefore this problem is brought up for the last study of this chapter. The method that has been applied in the lateral-torsional buckling analysis is also adopted to investigate this problem.

2.2 Elastic lateral-torsional buckling of girders under uniform moment

The research in this case has been dealt with intensively formerly. In this article, at first a typical critical buckling moment of beams is given. Subsequently, an analytical method in which the deformation of a web is included as a variable is introduced.

2.2.1 Simply supported beam

It is assumed that the ends of a beam are prevented from lateral deflection and twisting. On the other hand, it is assumed that they are free to rotate laterally and the end cross section is free to warp. The critical moment of a doubly symmetric beam for which the simply supported condition can be satisfied has been obtained as follows[5].

$$M_{0cr} = \frac{\pi}{l} \sqrt{E I_y G J} \sqrt{1 + W^2} \qquad (2.1)$$

$$W = \frac{\pi}{l} \sqrt{\frac{E C_w}{G J}}$$

where l is span length, E and G are the elastic and shear moduli, respectively. I_y, J and C_w are the minor axis moment of inertia, the St-Venant torsion constant and warping constant, respectively.

2.2.2 Various end support conditions

End-restrained conditions have a considerable influence on the elastic lateral-torsional buckling strength. Some of these end support conditions are shown in Fig.2. 1. Nethercot[1] has given the following equation that can be applied in these cases.
.

$$M_{cr} = \alpha \sqrt{E I_y G J} \frac{\pi}{l} \sqrt{1 + \frac{\pi^2}{R^2}} \qquad (2.2)$$

where α varies with loading and support conditions and the value of α has been presented for symmetrical I-beams loaded with equal end moments.
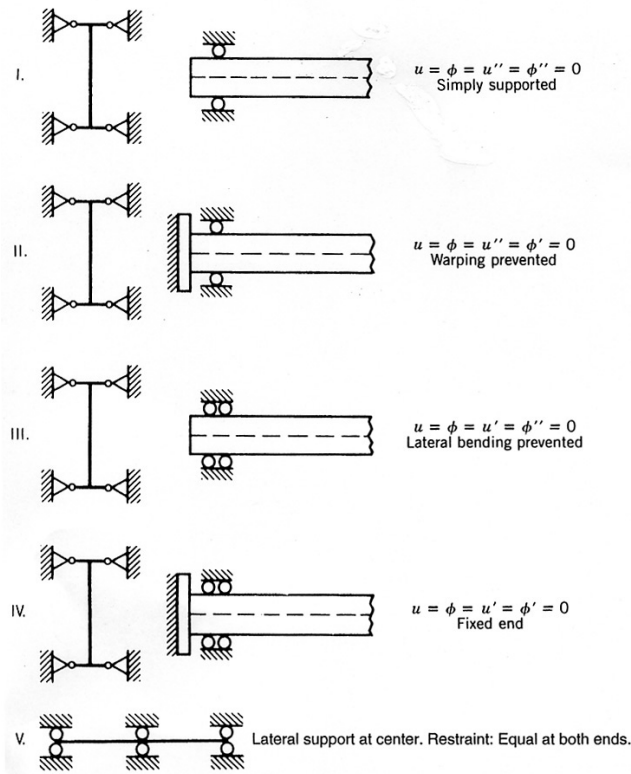
Fig.2.1 Idealized end restraints[16].

In this figure, u and φ denote the lateral displacement and the twisting of the beam, respectively.

2.2.3 Elastic buckling of plate girders under pure bending

Elastic buckling of plate girders under pure bending has been analyzed by Konishi et al.[6] as the simultaneous buckling between a web plate and vertical stiffeners. The stiffened plate (Fig.2.2) is regarded as an orthotropic plate. The differential equation of the deflection surface for the buckled orthotropic plate is

$$D_x \frac{\partial^4 w}{\partial x^4} + 2H \frac{\partial^4 w}{\partial x^2 \cdot \partial y^2} + D_y \frac{\partial^4 w}{\partial y^4} = N_0 \left(1 - \alpha \frac{y}{b}\right) \frac{\partial^2 w}{\partial x^2}$$
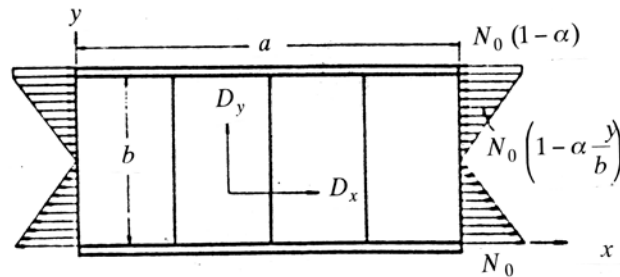

Fig.2.2   Stiffened plate.

11

where D_x and D_y are the flexural rigidities of the stiffened web plate in the direction of x and y, respectively, $H = \kappa\sqrt{D_x D_y}$, N_0 is the maximum axial force per unit length at $y=0$ and α is the constant which can be settled by the position of the neutral axis. The boundary condition at upper flange is assumed as laterally supported and built-in edge. The effects of vertical stiffeners and the flexural and torsional rigidities of the upper flange on the buckling loads have been investigated in detail.

2.3 Elastic lateral-torsional buckling of girders under unequal end moments

Most of the plate girder panels are usually subjected to combined loading of bending moments and shear forces. In these cases due to the existence of shear forces the distribution of bending moments in the longitudinal direction becomes necessarily non-uniform. Consequently it is supposed to be actual and general that the subject on the lateral-torsional buckling of plate girders should be also treated in consideration of this effect.

2.3.1 Beams under unequal end moments

If the applied end moments are unequal, the moment gradient arises in the longitudinal direction of beams. Salvadori[7] has presented that the influence of moment gradient may be taken into account by a simple modifier to Eq.2.1.

$$M_{cr} = C_b M_{0cr}$$

where C_b is the equivalent uniform moment factor.

This value can be estimated with good accuracy by use of the following formulas.

$$C_b = 1.75 + 1.05\kappa + 0.3\kappa^2 \leq 2.56$$

$$\frac{1}{C_b} = 0.6 + 0.4\kappa \leq 0.4$$

where κ is the end moment ratio.

In Eq.(2.2), as α for buckling moments of the beam under unequal end moments the following simple expression has been summarized by Nethercot[1].

$$\alpha = 1.16 + [0.6 - \kappa] - [\kappa - 0.6]^2 \qquad (-0.8 \leq \kappa \leq 1)$$

$$\alpha = 2.56 \qquad (\kappa \leq -0.8)$$

In the above expression, terms in square brackets are used only when positive. These results agree well with the original values obtained by Horne[8].

2.3.2 Plate girders under unequal end moments

It is supposed that for the case when the web has relatively large width-to-thickness

ratio, such as plate girders, the deformation of the web should be taken into consideration. This fact has been left out of consideration in most studies on the lateral buckling. And the restraint caused by the flanges must be also given thought. In this article the elastic lateral buckling of plate girders loaded with unequal end moments is analyzed as the simultaneous buckling between the flanges and the web.

(1) Stiffened web subjected to unequal end moments

The plate girder under the action of unequal end moments that has a symmetrical section about both the major and minor axes is shown in Fig.3.1. The web plate has a length a and a width b (aspect ratio $\alpha = a/b$). It is assumed that the shearing stresses which are distributed parabolically along both ends of the web ($x = 0$, a) and uniformly along the joints between the web and the flange are in equilibrium with both end moments. Considering that the uniformly distributed shearing force is in equilibrium with the axial force at the top and bottom flanges, respectively, the value of τ is determined:

$$\tau = (1 - \beta)\sigma_0 \, F / (ah)$$

By using the value of τ and taking the moments of all forces acting on the web, the shearing stress τ_{xy} at any point in the web is obtained as follows:

$$\tau_{xy} = (1 - \beta)\sigma_0 \left[-\left(\frac{y}{b}\right)^2 + \left(\frac{y}{b}\right) + F / (bh) \right] / \alpha$$
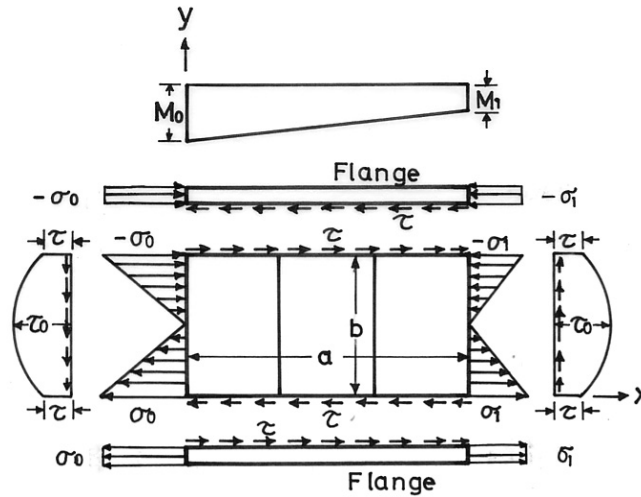

Fig.3.1 Plate girder under unequal end moments.

By assuming that the normal stress σ_x at any point in the web varies linearly in the x-direction, σ_x becomes:

$$\sigma_x = \sigma_0 [1 - (1 - \beta)(x / a)](1 - 2y / b)$$

where $\beta = \sigma_1 / \sigma_0$, $F =$ the cross-sectional area of the flange, $h =$ the thickness of the web plate.

It is assumed that the web under these stresses is simply supported along the edges $x = 0$ and $x = a$ and elastically supported and elastically built-in along the edges $y = 0$ and $y = b$. The web plate stiffened by the transverse stiffeners may be regarded as the orthotropic plate and the simultaneous buckling between the web and the flange is analyzed. The differential equation of the deflection surface for the buckled orthotropic plate is

$$D_x \frac{\partial^4 w}{\partial x^4} + 2H \frac{\partial^4 w}{\partial x^2 \partial y^2} + D_y \frac{\partial^4 w}{\partial y^4} = h \left[\sigma_x \frac{\partial^2 w}{\partial x^2} + 2\tau_{xy} \frac{\partial^2 w}{\partial x \partial y} \right] \tag{3.1}$$

where D_x and D_y are the flexural rigidities of the stiffened web plate in the direction of x and y, respectively, $H = \nu_y D_x + 2 D_{xy}$ (D_{xy} = the torsional rigidity of the stiffened plate), and it is assumed that the value of Poisson's ratio associated with the force in the y-direction, ν_y, takes 0.3. When the numerical factor κ is used, in which $H = \kappa \sqrt{D_x D_y}$, κ can be determined theoretically. For simplification in the following analysis the computation is carried out for the case in which $\kappa = 0$. The differential equations of the deflection curve for the buckled flanges, if the warping rigidity of the flanges may be neglected, become

$$B_b \frac{\partial^4 w}{\partial x^4} \pm (\sigma_0 F - \tau h x) \frac{\partial^2 w}{\partial x^2} \mp \tau h \frac{\partial w}{\partial x} = \pm \left[D_y \frac{\partial^3 w}{\partial y^3} + (4 D_{xy} + D_1) \frac{\partial^3 w}{\partial x^2 \partial y} \right] \tag{3.2}$$

$$C_b \frac{\partial^3 w}{\partial x^2 \partial y} \mp \frac{1}{F} \left[(\sigma_0 F - \tau h x) \frac{\partial^3 w}{\partial x^2 \partial y} - \tau h \frac{\partial^2 w}{\partial x \partial y} \right] I_0 = \pm \left[D_y \frac{\partial^2 w}{\partial y^2} + D_1 \frac{\partial^2 w}{\partial x^2} \right] \tag{3.3}$$

where in these equations the upper sign is applied to the top flange and the lower sign to the bottom flange, and B_b, C_b and I_0 are the flexural and torsional rigidities of the flange and the polar moment of inertia respect to the center of gravity of the flange, respectively. Eqs. (3.2) and (3.3) represent the conditions of elastically supported and elastically built-in edges, respectively.

The problem will be solved by converting the differential equations (3.1), (3.2) and (3.3) into a set of the finite difference equations considering the simply supported boundary condition along the edges $x=0$ and $x=a$. The result is represented in the following matrix form:

$$[A]\{w\} = k_\sigma [B]\{w\} \tag{3.4}$$

where k_σ is the buckling coefficient and represented as $\sigma_0 b^2 h / (\pi^2 D_x)$. For the positive minimum given value obtained by solving Eq.(3.4), the buckling stress can be determined.

(2) Critical loads

The computed results are as follows.

The relationship between the number of subdivisions in the finite difference equations and the convergence of the solutions must be investigated in advance. An example of this result is shown in Fig.3.2 where Nx and Ny are the number of subdivisions in the direction of x and y, respectively. It seems to be quite all right in an engineering problem to consider the solution for $Nx=Ny=20$ as the sufficiently accurate value. Practically the value of k_σ in the case of $Nx=Ny=20$ almost agrees with the estimated value obtained by means of Salvadori's[14] method.

Figures 3.3 and 3.4 show how k_σ varies with α for five values of β in the case of $Dy/Dx=50$. In these figures each solid line shows the simultaneous buckling curve. On the other hand the values calculated by using the lateral buckling theory of beams in Ref. 1 are shown by the broken lines. It is obvious that the difference between the two curves for each value of β does not always show the same tendency and becomes larger as α becomes smaller. In the following analysis the computed results for $\beta=0$ will be examined, since the influence of the shearing force seems to be most remarkable.
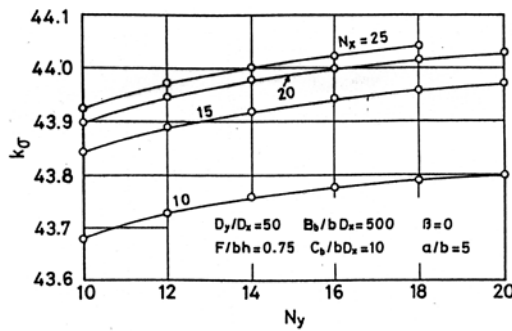

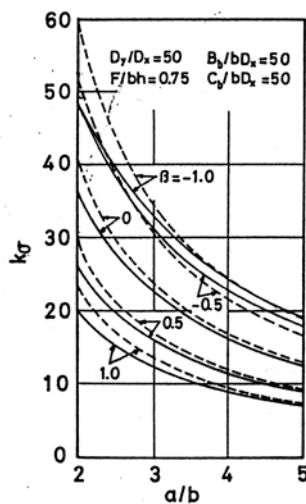Fig.3.2 Buckling coefficient vs. number of subdivisions in finite difference method.

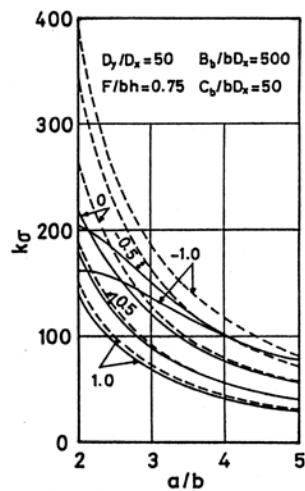Fig.3.3 Comparison of simultaneous buckling load with value obtained by means of beam theory.

Fig.3.4 Comparison of simultaneous buckling load with value obtained by means of beam theory.

15

Figure 3.5 shows the effect of the flexural rigidity of the flange on the critical load. It is obvious that k_σ increases considerably according to the increase of B_b. But for the comparatively small values of α the horizontal deflection of the flange is small and k_σ is significantly influenced by the torsional rigidity of the flange as shown later. Figure 3.6 shows the effect of the torsional rigidity of the flange on the critical load and it is noted that k_σ does not so much increase as C_b increases. From Figs. 3.5 and 3.6, it may be considered that the effect of the flexural rigidity of the flange on the critical load is almost dominant for the values of $\alpha \geqq 2$ and as α increases k_σ decreases considerably on account of the influence of horizontal deflection of the flange.
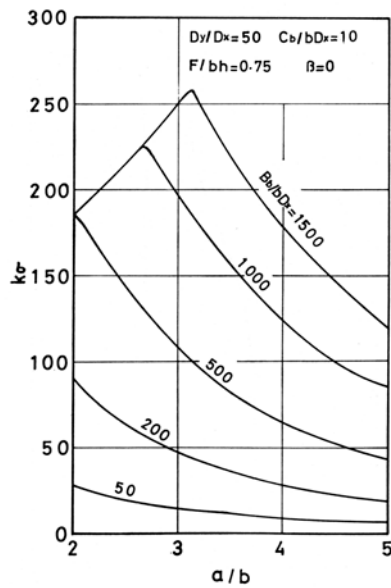

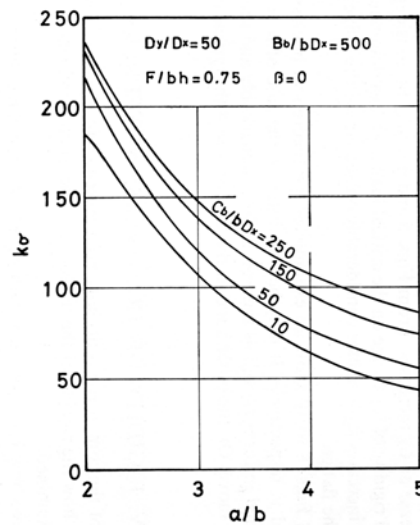Fig.3.5 Relationship between buckling coefficient and flexural rigidity of flange.

Fig.3.6 Relationship between buckling coefficient and torsional rigidity of flange.

Figure 3.7 and Figs 3.8 to 3.10 show an example of the theoretical buckling mode in the direction of x and y, respectively. It may be noted that in the case of $\alpha = 2$ the buckling mode is complicated in form as well as the web deflects remarkably and the bottom flange has a tendency to move. On the other hand in the case of $\alpha = 4$ the typical lateral buckling mode is given.

(3) Rigidity of transverse stiffeners

In Art.(2) all of the computed results have been presented for the case in which $D_y/D_x = 50$. In Art(3), how the rigidity of the transverse stiffeners has influence on the buckling strength will be examined.

Figure 3.11 shows how k_σ-values vary with B_b/bD_x for the three different values of D_y/D_x. As it has been shown in Art.(2) k_σ increases rapidly as B_b/bD_x increases. It may be also seen from Fig.3.11 that k_σ-values are elevated comparatively well up to a
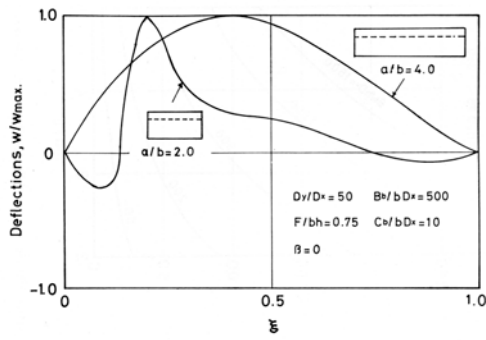
16

Fig.3.7 Theoretical buckling mode (longitudinal direction).
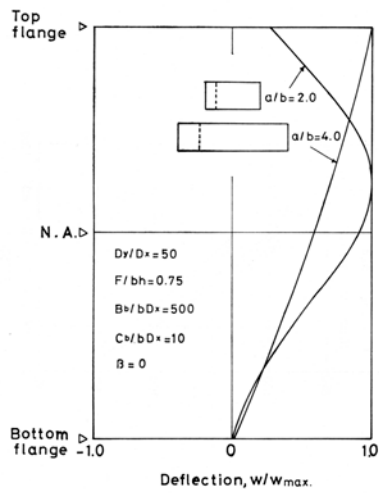

Fig.3.8 Theoretical buckling mode
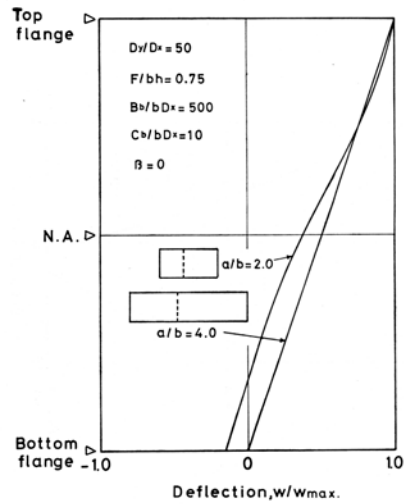(transverse direction).

Fig.3.9 Theoretical buckling mode
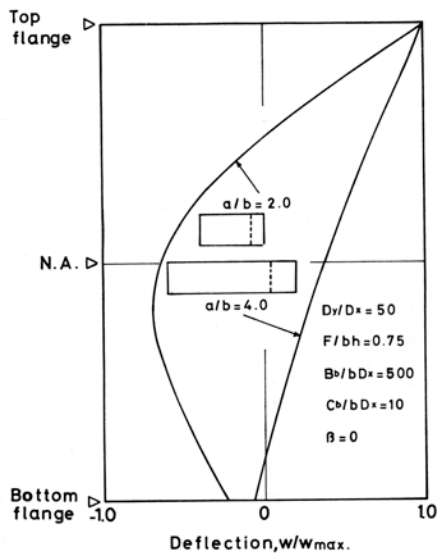(transverse   direction).

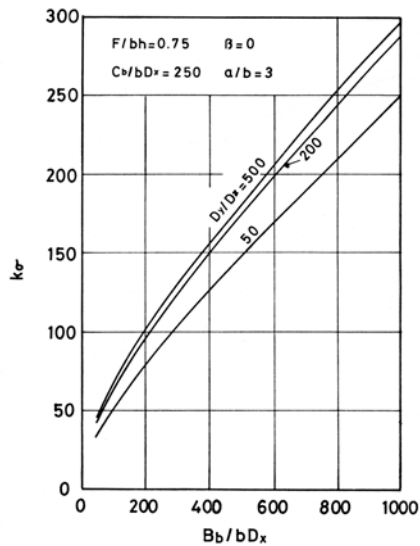Fig.3.10 Theoretical buckling mode
(transverse direction).

Fig.3.11 Influence of flexural rigidities
of flange and transverse stiffener on
critical load.

17

value of D_y/D_x=200, but gradually for values of D_y/D_x=200 and over. Figure 3.12 shows how k_σ-values vary with C_b/bD_x for the three different values of D_y/D_x. As it has been shown in (2) k_σ increases gradually according to the increase of C_b/bD_x. It may be also seen from Fig. 3.12 that when the values of D_y/D_x vary from 50 to 200 an increase in D_y/D_x leads to a considerable increase in k_σ-value, but a further increase in D_y/D_x does not so much influence the critical load.
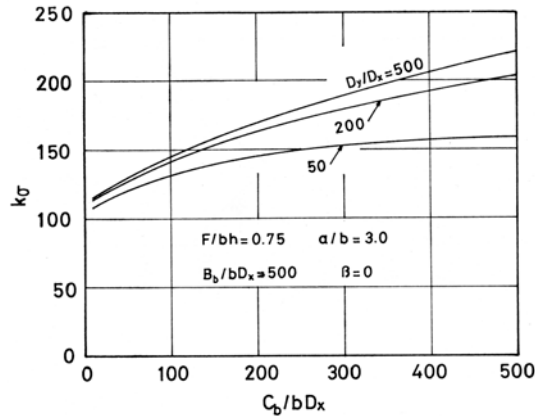

Fig.3.12 Influence of torsional rigidity of flange and flexural rigidity of
transverse stiffener on critical load.

Figures 3.13 to 3.19 show how k_σ-values vary with α for various values of D_y/D_x in seven combinations of the width-to-thickness ratio of the web, b/h, the width-to-thickness ratio of the flange, c/t, and the ratio of the cross-sectional area of flange to web, F/bh. In these Figs. each broken line shows the value calculated by means of the theory of lateral buckling of beams (Ref. 1). On referring to Figs. 3.13 to 3.15 the influence of alternating the value of b/h for the case in which t c/t=10 and F/bh=0.75 may be seen. It is obvious from these Figs. that when the values of α are between 2 and 3 the difference between the buckling loads obtained by means of the two theories is considerable even for the case in which D_y/D_x=200. Figures 3.14, 3.16 and 3.17 show the effect of alternating the value of c/t for the case in which b/h=250 and F/bh=0.75. It may be seen that the difference between the two theories increases by degrees according to the increase of c/t. By referring to Figs.3.14, 3.18 and 3.19 the influence of alternating the value of F/bh may be examined. It may be seen that as F/bh increases the difference between the two theories increases considerably. It may be obvious from Fig. 3.18 that when the values of α are between 2 and 4 the simultaneous buckling curve for the value of D_y/D_x=200 agrees well with the broken line and in the region of 4 even the simultaneous buckling curve for the value of D_y/D_x=30 almost agrees with the broken line.
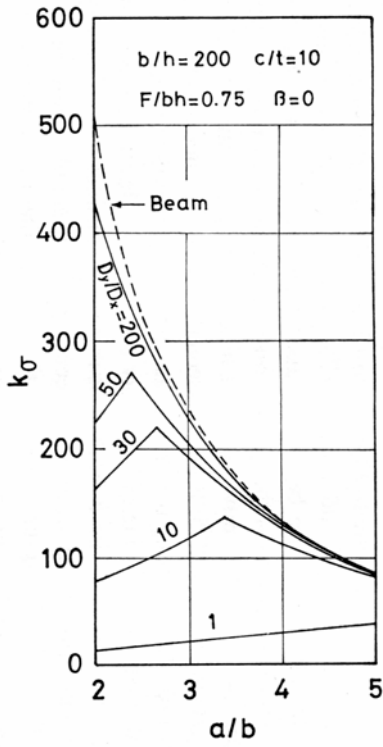
Fig.3.13 Effect of transverse stiffener.
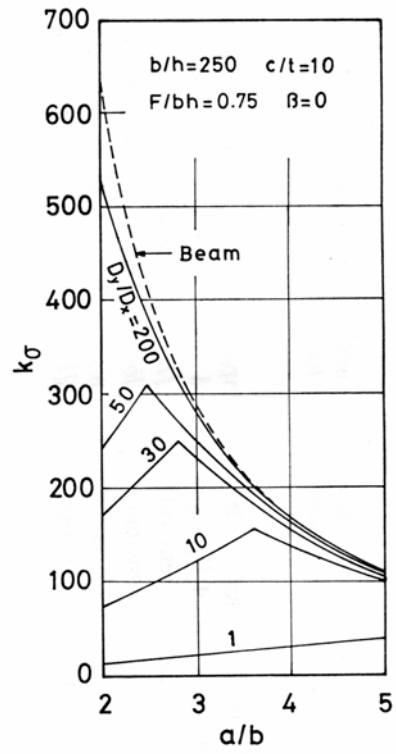
Fig.3.14 Effect of transverse stiffener.
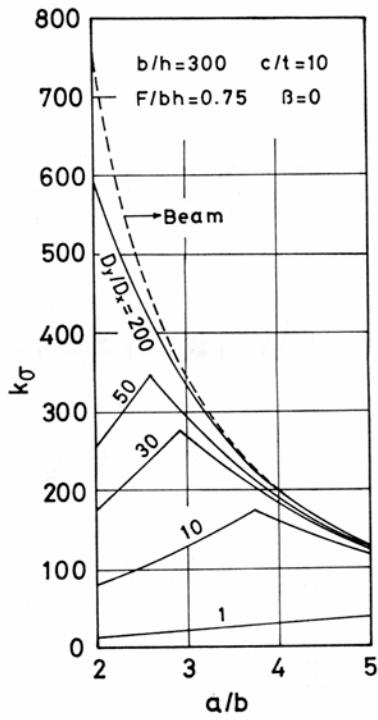
Fig.3.15 Effect of transverse stiffener.
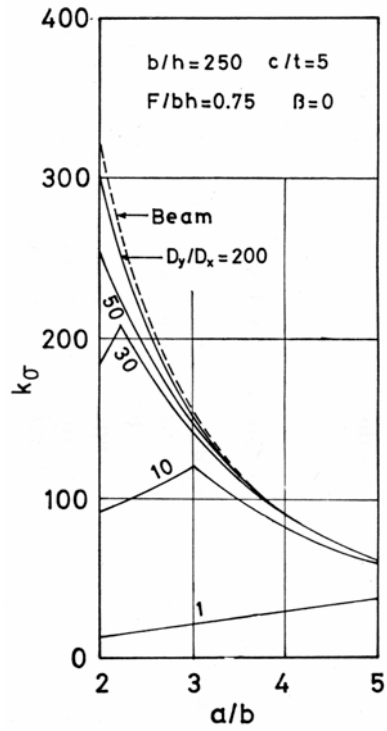
Fig.3.16 Effect of transverse stiffener.

19
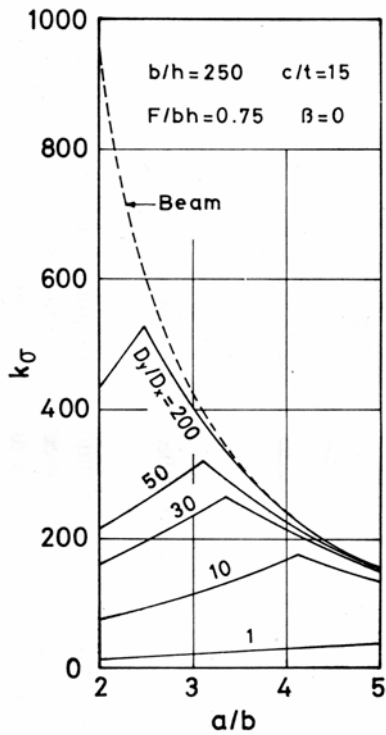
Fig.3.17 Effect of transverse stiffener.
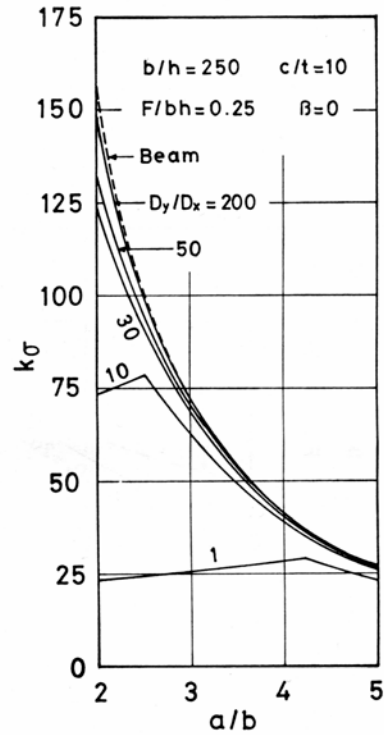
Fig.3.18 Effect of transverse stiffener.
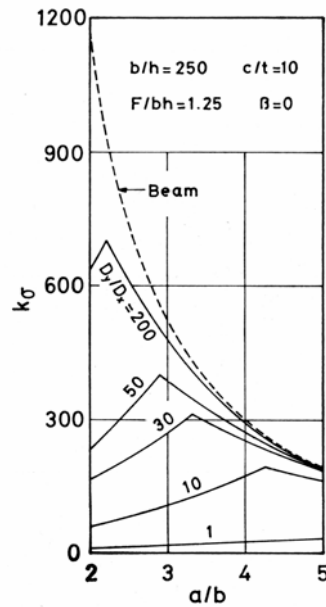
Fig.3.19 Effect of transverse stiffener.

It may be seen from Figs. 3.13 to 3.19 that the simultaneous buckling loads for D_y/D_x above a certain value almost or fairly well agree with the buckling loads obtained by using the beam theory. So on referring to Figs. 3.11 and 3.12 we may regard the minimum value of D_y/D_x in the limit when the simultaneous buckling loads approach the buckling loads obtained by means of the beam theory as the necessary rigidity of the transverse

stiffeners. Then as seem from Figs. 3.13 to 3.19 when the values of α are between 2 and 5 it may be quite all right to consider the value of D_y/D_x=200 for comparatively small values of α and the value of D_y/D_x=30 to 50 for comparatively large values of α as the necessary rigidity of the transverse stiffeners, respectively.

(4) Conclusions

The elastic lateral buckling of plate girders under the action of unequal end moments has been analyzed by using the theory of orthotropic plates. As a result of the computations the simultaneous buckling loads between the flange and the web are obtained for various cases. The obtained critical loads are compared with those calculated by means of the beam theory for various end moment ratios. And the effect of the flexural and torsional rigidities of the flange and the flexural rigidity of the transverse stiffeners on the critical loads has been examined.

As a result of these investigations, it follows:

1) It is obvious that for comparatively large values of α the critical loads are influenced considerably by the values of the flexural rigidity of the flange, while they are not so much affected by the values of the torsional rigidity of the flange.

2) It has been shown that the increase in the critical load almost reaches the limit when the rigidity of the transverse stiffeners approaches a certain value in the case of β =0, and the necessary rigidity of the transverse stiffeners is presented.

3) It is evident that the lateral buckling loads should be determined by considering the rigidities of the flange and the transverse stiffeners.

2.3.3 Elastic lateral buckling of plate girders of mono-symmetrical cross section

Although the elastic lateral buckling of I-beams and plate girders loaded with equal or unequal end moments has been studied by many investigators[5),9),10),16),17)] , as was stated previously, the deformation of the web has been left out of consideration in many researches. When the web has relatively large width-to-thickness ratio, it is supposed that the web deformation should be taken into consideration. The restraint caused by the flanges must be also given thought. As the compression flange of the steel girder of composite girders has the small cross section, the girder under construction is considered to be in a dangerous state concerning the lateral buckling. The elastic buckling of rectangular plates loaded with linearly distributed normal and parabolically distributed shearing stresses has been investigated by Radulovic[18)-20)] , but it has been assumed that all boundary edges are simply supported. In this article the elastic lateral buckling of plate girders of mono-symmetrical cross section subjected to equal or unequal end moments is analyzed as the simultaneous buckling between the flange and the web.

Computed buckling loads are compared with those calculated by means of the beam theory[1)], and the effect of the flexural rigidity of the transverse stiffeners on the buckling strength is studied. The effect of the flexural rigidity of the flange on the buckling strength is examined. Further a few examples of theoretical buckling modes are shown. Consequently the property of the elastic lateral buckling of plate girders is clarified.

(1) Stiffened web

The plate girder under the action of unequal end moments that has a mono-symmetrical cross section is shown in Fig. 3.20. The web plate has a length a width b (aspect ratio α =a/b). It is assumed that the shearing stresses which are distributed parabolically along both ends of the web (x=0, a) and uniformly along the joints between the web and the flange are in equilibrium with both end moments.
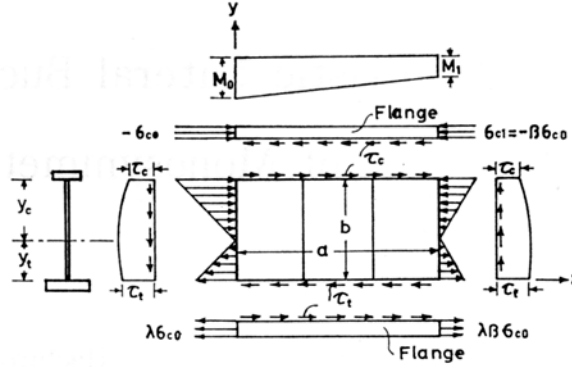

Fig.3.20 Stiffened web plate.

Considering that the uniformly distributed shearing force is in equilibrium with the axial force at the top and bottom flanges, respectively, the value of τ_c and τ_t are determined:

$$\tau_c = (1-\beta)\,\sigma_{c0}\,F_c/(ah)$$

$$\tau_t = \lambda(1-\beta)\,\sigma_{c0}\,F_t/(ah)$$

where $\beta = \sigma_{c1}/\sigma_{c0}$, $\lambda = y_t/y_c$ h = the thickness of the web plate, F_c and F_t are the cross-sectional areas of the compression and the tension flanges, respectively. λ is equal to $(0.5+F_c/bh)/(0.5+F_t/bh)$, provided that t_c/b and t_t/b are considered to be zero from the industrial point of view (t_c and t_t are the thickness of the compression and tension flanges, respectively.). By using the values of τ_c and τ_t and taking the moments of all forces acting on the web, the shearing stress τ_{yw} at any point in the web is obtained as follows:

$$\tau_{xy} = (1-\beta)\left\{-\frac{1+\lambda}{2}\left(\frac{y}{b}\right)^2 + \lambda\left(\frac{y}{b}\right) + \frac{1-\lambda}{2} + \frac{F_c}{bh}\right\}\sigma_{c0}/\alpha$$

The above expression corresponds to the value of the shearing stress in the web calculated by means of the elementary beam theory, when it can be regarded that t_c/b and t_t/b vanish. By assuming that the normal stress σ_x at any point in the web varies linearly in the x-direction, σ_x becomes:

$$\sigma_x = \left\{\lambda - (1+\lambda)\left(\frac{y}{b}\right)\right\}\left\{1 - (1-\beta)\left(\frac{x}{a}\right)\right\}\sigma_{c0}$$

The normal stress σ_y at any point in the web is assumed to be zero.

It is assumed that the web under these stresses is simply supported along the edges x=0 and x=a and elastically supported and elastically built-in along the edges y=0 and y=b.

The web plate stiffened by the transverse stiffeners may be regarded as the orthotropic plate and the simultaneous buckling between the web and the flange is analyzed. The differential equation of the deflection surface for the buckled orthotropic plate is

$$D_x \frac{\partial^4 w}{\partial x^4} + 2H \frac{\partial^4 w}{\partial x^2 \partial y^2} + D_y \frac{\partial^4 w}{\partial y^4} = h \left[\sigma_x \frac{\partial^2 w}{\partial x^2} + 2\tau_{xy} \frac{\partial^2 w}{\partial x \partial y} \right] \tag{3.5}$$

where D_x and D_y are the flexural rigidities of the stiffened web plate in the direction of x and y, respectively, $H = v_y D_x + 2 D_{xy}$ (D_{xy} = the torsional rigidity of the stiffened plate), and it is assumed that the value of Poisson's ratio in the y-direction, v_y, takes 0.3. When the numerical factor κ is used, in which $H = \kappa \sqrt{D_x D_y}$, κ can be determined theoretically[15]. For simplification in the following analysis the computation is carried out for the case in which $\kappa = 0$. The differential equations of the deflection curve for the buckled flanges, if the warping rigidity of the flanges may be neglected, are obtained as follows. For the compression flange the expression becomes:

$$B_{bc} \frac{\partial^4 w}{\partial x^4} + \left(\sigma_{c0} F_c - \tau_c hx \right) \frac{\partial^2 w}{\partial x^2} - \tau_c h \frac{\partial w}{\partial x} = D_y \frac{\partial^3 w}{\partial y^3} + \left(4 D_{xy} + D_1 \right) \frac{\partial^3 w}{\partial x^2 \partial y}$$

$$C_{bc} \frac{\partial^3 w}{\partial x^2 \partial y} - \frac{1}{F_c} \left[\left(\sigma_{c0} F_c - \tau_c hx \right) \frac{\partial^3 w}{\partial x^2 \partial y} - \tau_c h \frac{\partial^2 w}{\partial x \partial y} \right] I_{0c}$$

$$= \left(D_y \frac{\partial^2 w}{\partial y^2} + v_y D_x \frac{\partial^2 w}{\partial x^2} \right)$$

$$\tag{3.6}$$

where B_{bc}, C_{bc} and I_{oc} are the flexural and torsional rigidities of the compression flange and the polar moment of inertia respect to the center of gravity of the compression flange, respectively. For the tension flange the expression becomes:

$$B_{bt} \frac{\partial^4 w}{\partial x^4} - \left(\sigma_{t0} F_t - \tau_t hx \right) \frac{\partial^2 w}{\partial x^2} + \tau_t h \frac{\partial w}{\partial x} = - \left[D_y \frac{\partial^3 w}{\partial y^3} + \left(4 D_{xy} + D_1 \right) \frac{\partial^3 w}{\partial x^2 \partial y} \right]$$

$$C_{bt} \frac{\partial^3 w}{\partial x^2 \partial y} + \frac{1}{F_t} \left[\left(\sigma_{t0} F_t - \tau_t hx \right) \frac{\partial^3 w}{\partial x^2 \partial y} - \tau_t h \frac{\partial^2 w}{\partial x \partial y} \right] I_{0t}$$

$$= - \left(D_y \frac{\partial^2 w}{\partial y^2} + v_y D_x \frac{\partial^2 w}{\partial x^2} \right)$$

$$\tag{3.7}$$

where B_{bt}, C_{bt} and I_{ot} are the flexural and torsional rigidities of the tension flange and the

polar moment of inertia respect to the center of gravity of the tension flange, respectively. Eqs.3.6 and 3.7 represent the conditions of elastically supported and elastically built-in edges.

The problem will be solved by converting the differential equations 3.5, 3.6 and 3.7 into a set of the finite difference equations considering the simply supported boundary conditions along the edges $x=0$ and $x=a$. Thus the obtained positive minimum eigen value represents the buckling coefficient which $k_\sigma = \sigma_{c0} b^2 h / \left(\pi^2 D_x \right)$ and the buckling stress can be determined.

(2) Computed results

When the number of subdivisions in the finite difference equations is represented by N, the following computed results are the solutions for $N=10$ in the direction of both x and y, respectively.

Fig. 3.21 shows the effect of the flexural rigidity of the compression flange on the critical load. It is obvious that k_σ increases considerably according to the increase of B_{bc}. For the comparatively small values of α the deflection of the compression flange is small and k_σ is influenced by the torsional rigidity of the flange as shown later in Figs. 3.22 to 3.24. Fig. 3.22 and Figs. 3.23 and 3.24 show examples of the theoretical buckling mode in the direction of x and y in the case of $\beta =0$. It may be noted that in the case of $\alpha =2$ the buckling mode is complicated in form as well as the web deflects remarkably. On the other hand in the case of $\alpha =4$ the typical lateral buckling mode is given.
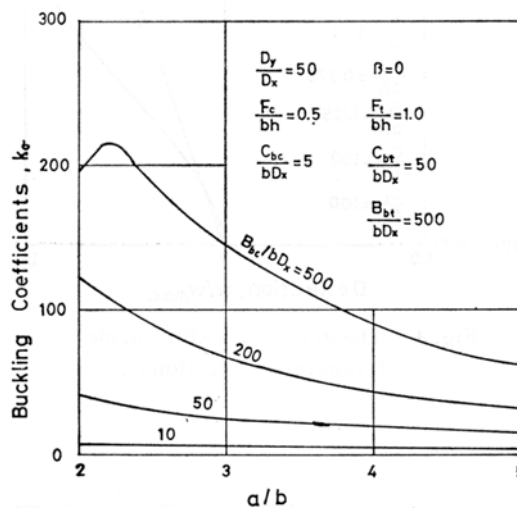
Fig.3.21 Relationship between buckling coefficient and flexural rigidity
of compression flange.
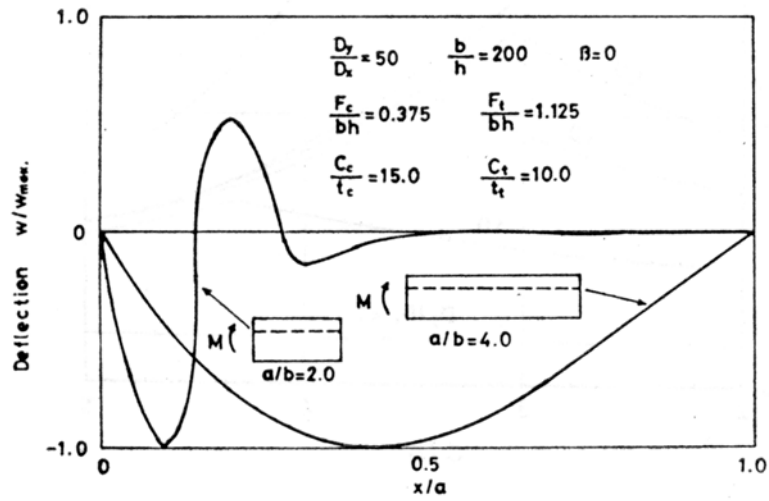
Fig.3.22 Theoretical buckling mode
(longitudinal direction).
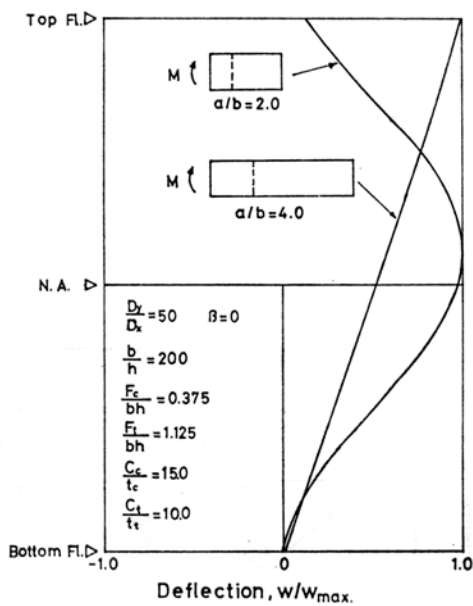
Fig.3.23 Theoretical buckling mode
(transverse direction).
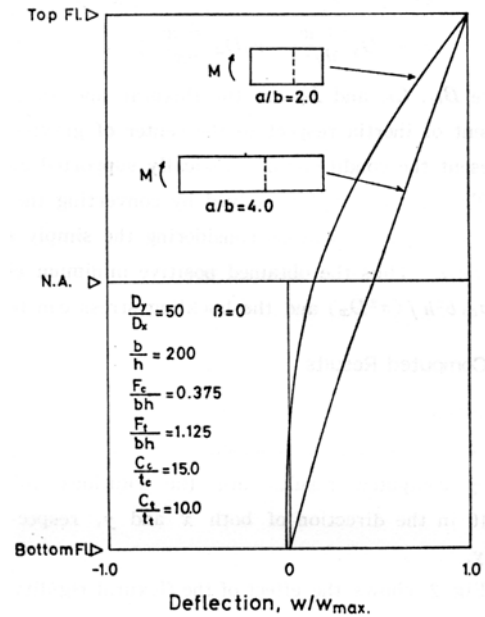
Fig.3.24 Theoretical buckling mode
(transverse direction).

Figs. 3.25 to 3.30 show how the rigidity of the transverse stiffeners has influence on the buckling strength. Figs. 3.25 to 3.27 show how k_σ-values vary with α for various values of D_y/D_x in three combinations of the ratio of the cross-sectional area of compression and tension flange to web in the case of $\beta = 0$ and Figs. 3.28 to 3.30 show the same relation in the case of $\beta = 1$. In these Figures, each broken line shows the value calculated by means of the theory of lateral buckling of beams (Ref. 1). It may be seen that the simultaneous buckling loads show lower values and the difference between the two theories increases considerably   according to the decrease of α . For comparatively large

25

values of α k_σ values approach more rapidly a certain value in the case of β =1 than β =0 as the value of D_y/D_x increases. From these Figures, the necessary rigidity of transverse stiffeners can be roughly estimated.

Fig.3.25 Effect of transverse stiffener.　　Fig.3.26 Effect of transverse stiffener.

Fig.3.27 Effect of transverse stiffener.　　Fig.3.28 Effect of transverse stiffener.
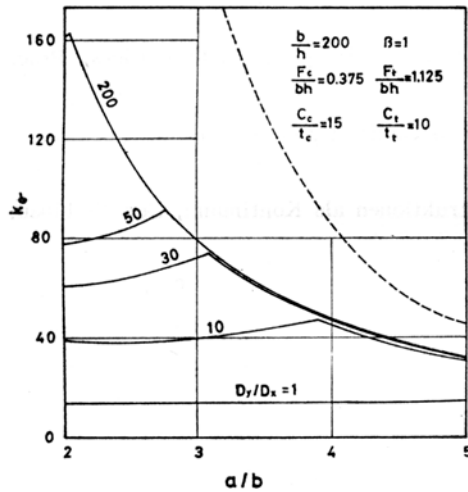
Fig.3.29 Effect of transverse stiffener.　　Fig.3.30 Effect of transverse stiffener.
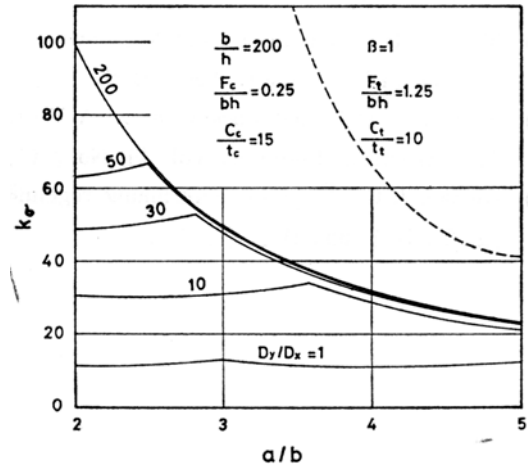
(3) Conclusions

　　The elastic lateral buckling of plate girders of mono-symmetrical cross section under the action of unequal end moments has been analyzed by using the theory of orthotropic plates. As a result of the computations the simultaneous buckl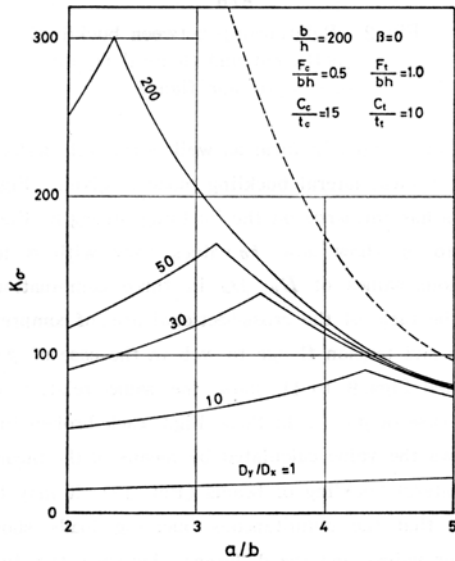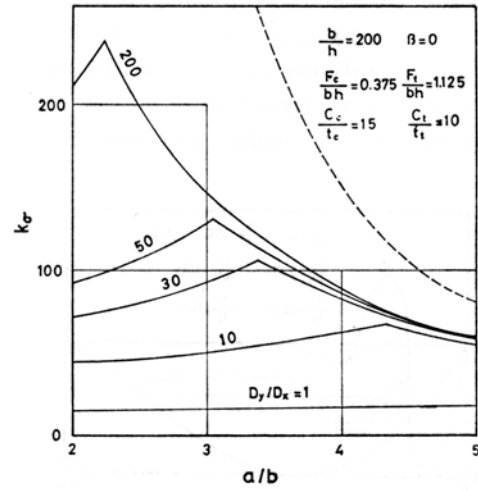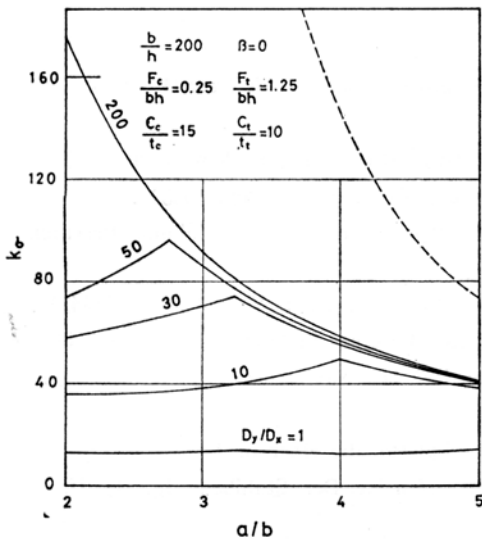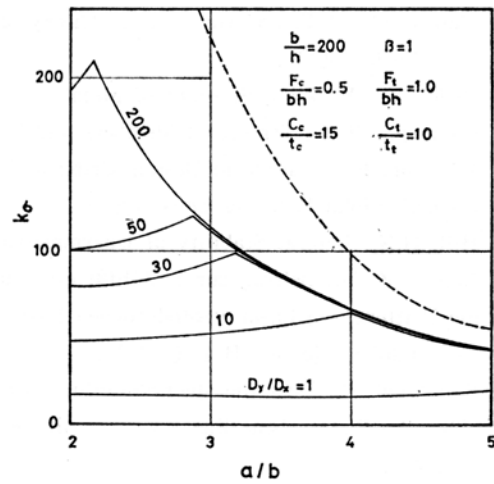ing loads between the flange and the web are obtained. The obtained critical loads are compared with those calculated by means of the beam theory. And the effect of the flexural rigidity of the compression flange and the flexural rigidity of the transverse stiffeners on the critical loads has been examined.

　　As a result of these investigation it is obvious that for comparatively large values of α the critical loads are influenced considerably by the values of the flexural rigidity of the compression flange. Further it has been shown that the increase in the critical load almost reaches the limit when the rigidity of the transverse stiffeners approaches a certain value and the necessary rigidity of the transverse stiffeners is estimated. It is evident that the lateral buckling loads should be determined by considering the rigidities of the flange and the transverse stiffeners.

2.4 Lateral-torsional buckling tests of girders under unequal end moments

　　The ultimate strength of a plate girder subjected to bending moment primarily depends on the strength of the compression flange. Basler[21] has proposed three buckling modes of compression flanges. Of these, lateral buckling has been studied both theoretically and experimentally by many researchers[16].

　　In the case of girders under varying moment, the ultimate strength can be predicted by using the equivalent constant bending moment[22]. There has, however, been little experimental verification for this case. Fukumoto[23] has tested the lateral-torsional buckling of welded I-girders with a web plate of comparatively small depth-to-thickness ratio.

　　In the preceding articles, the elastic lateral buckling of plate girders under varying

27

moment in consideration of web plate deformation was examined theoretically. This analysis is especially suitable for girders with web plates of large depth-to-thickness ratio.

In this article, two welded plate girders with web plate of relatively large depth-to-thickness ratio are tested. They are designed so as to collapse within the elastic range. Each girder is simply supported at both the ends subjected to a concentrated load at the center. Namely the applied bending moment varies from a maximum value at the center to zero at the bearing stiffeners.

The test results of the load carrying capacity are compared with the values predicted by the previously given theory in which the effect of moment gradient is taken into account. This theory gives the elastic buckling strength for coupled buckling of stiffened web-plate and flanges.

(1) Description of tests
 1) Test models
Two welded girder models, LP-1 and LP-2, made of SS400 steel were tested. As shown in Fig. 4.1, the side of each of these lying on the right-hand side of the load is chosen as the testing panel. The testing panel is composed of several single panels bounded by the top and bottom flanges and the transverse stiffeners: Model LP-1 has five single panels and Model LP-2 four. The dimensions of the testing panel on each girder are summarized in Table 4.1.

Intermediate transverse stiffeners are attached on both sides of web plate in addition to bearing stiffeners at the loading point and at the supports. The web plate and the top and bottom flanges have each a cross-section constant throughout the whole length. Both models were designed so as to collapse within the elastic range.

The loading point is indicated by the thick arrow in Fig.4.1. As the load is single and concentrated, the testing panel is subjected to bending moment varying from maximum value to zero.
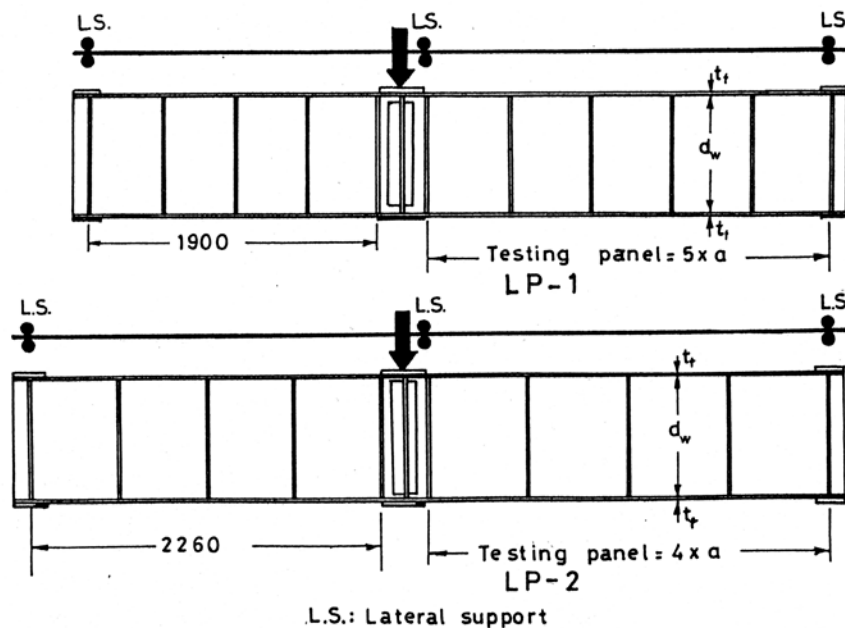

Fig.4.1 Testing plate girder models.

28

Table 4.1 Dimensions of testing plate girders

Model	LP-1	LP-2
Flange b (mm) $\times$ t_f (mm)	80$\times$9	80$\times$7.2
Web plate d_w (mm) $\times$ t (mm)	782$\times$3.2	800$\times$3.2
Stiffener b_s (mm) $\times$ t_s (mm)	19$\times$4.5	15$\times$3.2
Single panel length a (mm)	520	640
Aspect ratio of single panel	0.665	0.80
Depth-to-thickness ratio of web plate	244	250

2) Material testing

   Prior to testing the models, standard material testing according to JIS Z2241-1968 was conducted to obtain the yield stress of each component. The results are shown in Table 4.2.

Table 4.2 Results of standard material testing

Model		LP-1	LP-2
Yield stress (MPa)	Flange σ_{Yf}	323.6	353.0
	Web plate σ_{Yw}	274.6	313.8

3) Test setup

   Each model was simply supported with roller supports at both ends and tested under a concentrated load on the top flange using an oil jack. It was ensured that the applied load remains vertical, even when the models twisted and deflected laterally. To prevent any horizontal movement of the model, rigid support frames bolted to the floor of laboratory were provided at the locations shown in Fig. 4.1. Each frame was attached to the model using a roller. The frames prevented rotation about longitudinal axis and lateral displacement of the model, but permitted lateral bending. Fig.4.2 shows the lateral supports at the loading point and at the bearing stiffeners. The frames also allowed the flanges of the model to rotate independently in their own planes, so that the models are free to warp.

4) Instrumentation

   Dial gauges and electrical displacement transducers were used to measure the deflection on each model. In order to measure the out-of-plane deflections of the web plates relative to the boundaries of single panel, a frame clamped to the bearing stiffeners was used. Dial gauges were mounted underneath the bottom flange to measure the vertical girder deflections. The horizontal and vertical deflections and the angle of torsion on the top flange were detected using cathetometers. Fig.4.3 shows the poles for these measurents.

   Electrical resistance strain gauges, of uniaxial and rosette types, were used to measure the strains on web plate, and top and bottom flanges on each model. The strain gauges were bonded on to both the surfaces of the model components, and thus it is possible to separate the membrane and the plate-bending strains.
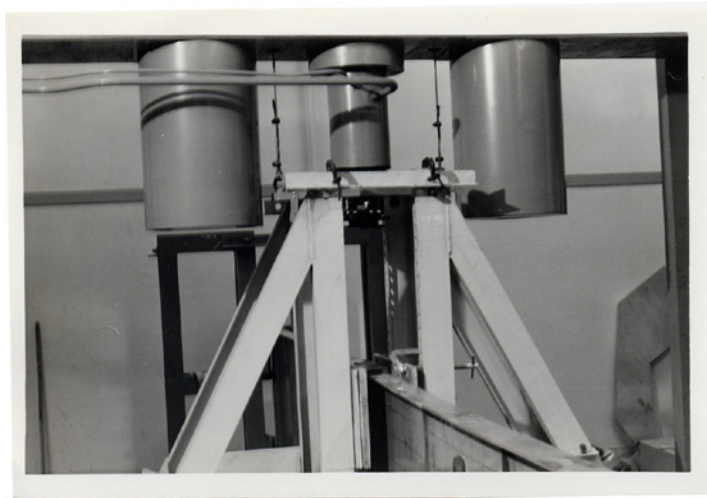
Fig.4.2 (a) Lateral support
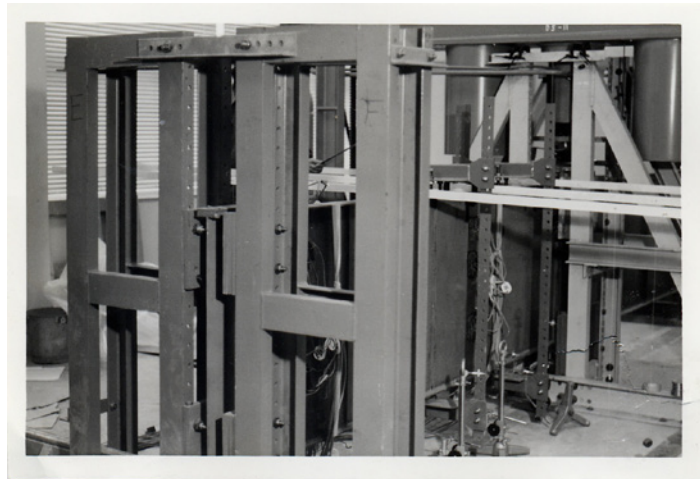
Fig.4.2 (b) Lateral support
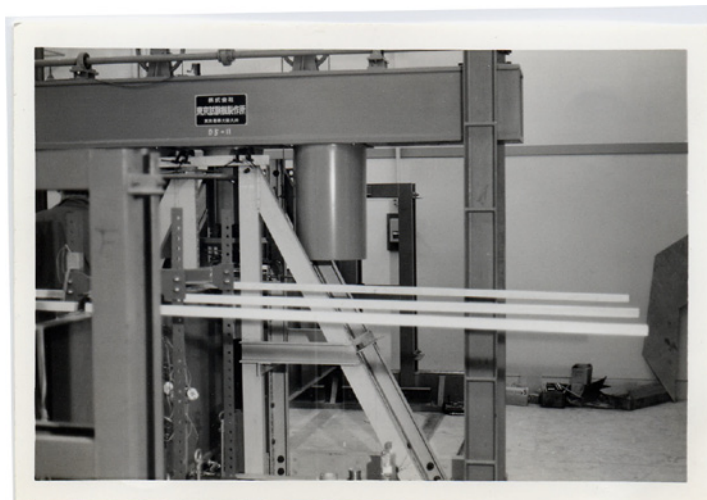
Fig.4.3 Pole for measurement of deflection and torsion

5) Testing procedure

After each model was set up, the eccentricity of the loading was checked and the initial out-of-plane deflection of web plate was also measured. The distribution of the obtained initial deflection is shown in Fig. 4.4. The maximum initial deflection of the web plate for Model LP-1 is 5 mm and for Model LP-2 3 mm. Each maximum imperfection is relatively large owing to the use of so thin a plate.
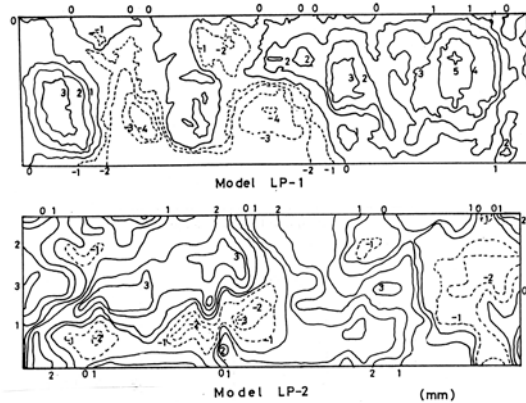
Fig.4.4 Initial deflection of web plates.

The step-by-step loading procedure was used in each girder test. After attaining maximum load, unloading was conducted.

(2) Results of loading tests and interpretation
1) Collapse mode

The collapse of the two models was due to lateral coupled buckling of their compression flanges and stiffened webs. As an illustration, Model LP-2 after collapse is shown in Figs. 4.5 and 4.6.
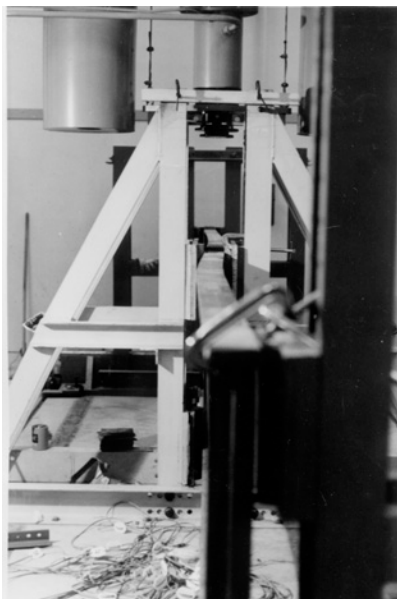
Fig.4.5 Collapsed girder.

Fig.4.6 Buckled web plate.

2) Load-deflection curves

Figures 4.7 and 4.8 show the horizontal deflection and angle of torsion on the top flange and the vertical deflection of the girder for the loading sequences in the cases of Models LP-1 and LP-2, respectively. In these figures the chain line shows the relationship between load and girder deflection predicted by elastic beam theory. The observed relationship remains linear up to the neighborhood of the collapse except in the early stage of the loading. As seen from these figures, the horizontal deflection of the compression flange increases rapidly as the girder approaches collapse point.
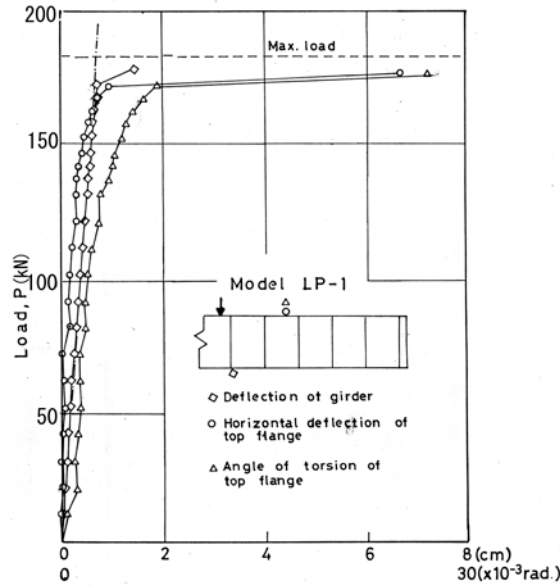
Fig.4.7 Load-deflection curves for Model LP-1.
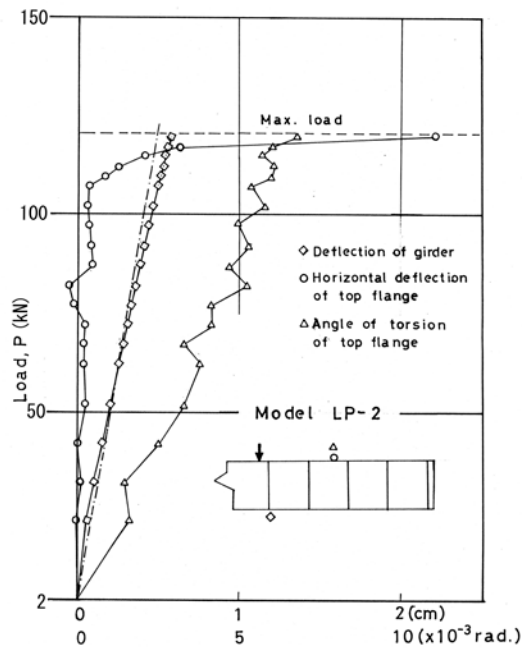
Fig.4.8 Load-deflection curves for Model LP-2.

3) Out-of-plane deflection of web panels

In Fig. 4.9, the deflection of various points on the web panel is shown for the three different loading steps. It can be seen from Fig. 4.9 that the web plate of Model LP-1 buckled in a deformed shape of a half-wave, while the web plate of model LP-2 buckled showing two half-waves. It is clear from comparison of Fig. 4.9 with Fig. 4.4 that the initial deflection influenced the buckling shape of the web plate.
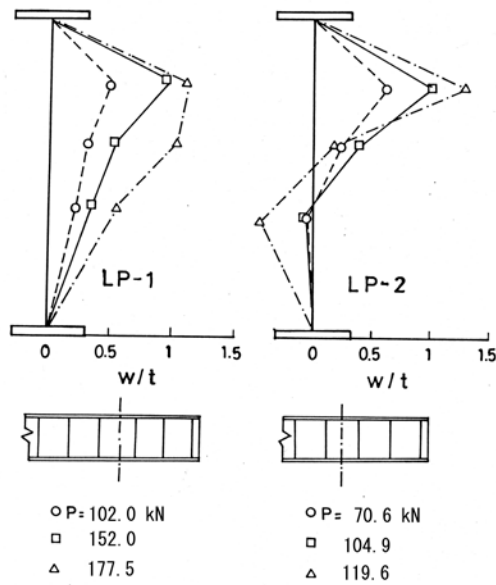
Fig.4.9 Deflection distribution of web plates.

4) Bending strain of girder

The observed distribution of girder-bending strain is shown in Fig. 4.10. The strain distribution departs from linear distribution as the loading approaches the ultimate state. It is obvious from the figure that a portion of the web plate loses its load carrying capacity as the applied load increases.
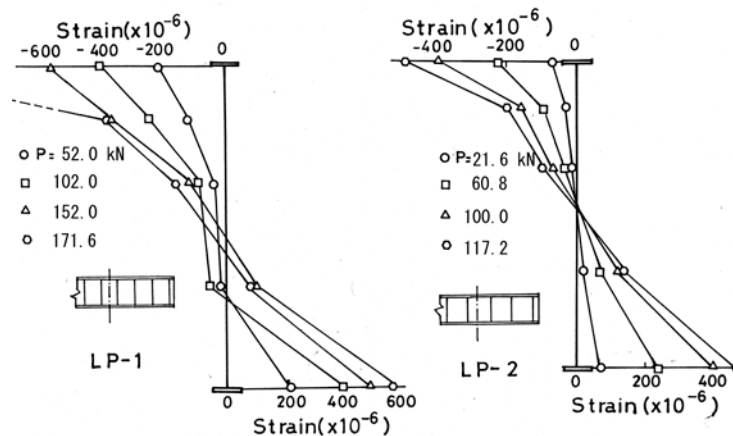
Fig.4.10 Distribution of strains due to girder bending.

5) Ultimate strength

Table 4.3 shows the observed maximum load P_{max}, the observed ultimate moment M_{max}, and the full plastic moment M_p for each girder. In addition, the elastic coupled buckling load predicted theoretically P_{ult} is also indicated. As seen from a comparison of the experimental result with calculated result, theoretical buckling loads are 13～15% lower than experimental values for both models.

The strains on top flange due to lateral bending at the load step approaching ultimate state are shown in Fig. 4.11. In each model the effective buckling length reduces which is why the experimental buckling loads were made higher than the predicted values.

The ultimate strength obtained by test are plotted with several theoretical curves for the buckling strength of I-beams in Fig. 4.12, where σ_Y the yield stress, σ_{cr} the critical stress, E=Young's modulus, d=the girder depth, L_e=the effective length, r_x=the radius of gyration about strong axis, r_y=the radius of gyration about weak axis, β =the end moment ratio. The ultimate strength of the tested girder models is higher than the theoretical curves for the case of β =0.
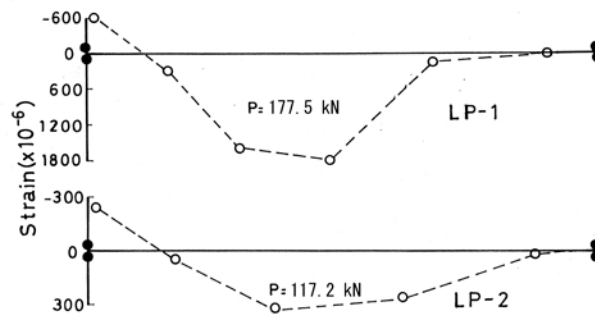
Fig.4.11 Strains of top flanges due to lateral bending.

Table 4.3 Comparison between experimental and predicted results

Model	Experimental					Theory[13]
	P_{max} (kN)	V_{max} (kN)	M_{max} (kN・m)	M_p (kN・m)	M_{max}/M_p	P_{ult} (kN)
LP-1	177.5	75.7	197.1	316.7	0.62	151.0
LP-2	118.7	55.9	143.2	323.6	0.44	103.7
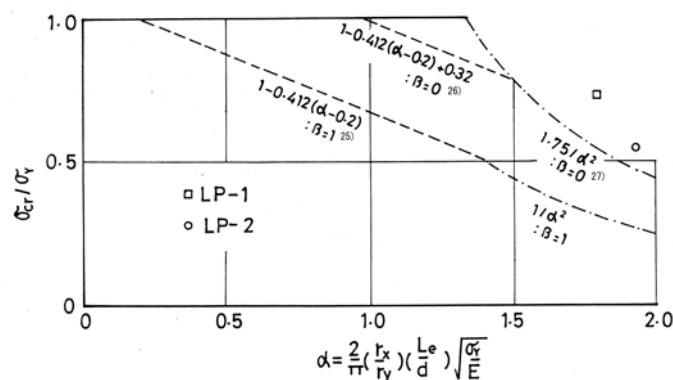
Fig.4.12 Experimental strength and theoretical curves.

(3) Conclusions

Two model girders were tested to investigate the lateral buckling strength and behavior of plate girders with transverse stiffeners under varying moment. They have the web plate of large depth-to-thickness ratio.

Such matters as the effect of initial deflection on the web plate, the distribution of strains due to girder bending, and the load-deflection relationship, were discussed. Experimental buckling loads were compared with the elastic coupled buckling loads predicted theoretically, with particular attention to out-of-plane deformation of web panels. Further, the experimentally obtained ultimate strength was also compared with the theoretically proposed lateral buckling curves for I-beams under varying moment.

The theoretical buckling loads agreed comparatively well with experimental values. It is effective sufficiently to use the elastic coupled buckling strength of stiffened web-plate and flanges for the prediction of the lateral-torsional buckling loads.

2.5 Equivalent uniform moment on a girder for unequal end moments

When a girder panel is subjected to the combined bending moments and shearing forces, interaction curves are often used in order to estimate the ultimate strength[16]. In this case as the applied moment varies in the longitudinal direction of a girder, it becomes a serious problem that as the value of the bending moment that is used for the interaction curve what section is adequate. In regard to this problem, the position of the equivalent uniform moment is formularized also according to the expression to convert into the uniform compression[28]. By the method of the elastic or elasto-plastic large displacement analysis on the plate under varying moments, the studies to examine its ultimate behavior are also carried out[29],[30]. But it is considered that the position of the equivalent uniform moment has not been yet suggested as a general formula.

In this article the method in order to obtain the position of the equivalent uniform moment is presented for single vertically stiffened girder panel and in the elastic range. By applying a parametric analysis, the influences of degree of the moment gradient, the panel aspect ratio, the torsional rigidity of the panel edge and so on are examined. In numerical calculation the finite difference method is used[13].

The position of the equivalent uniform moment is expressed as the function of the panel aspect ratio and the end moment ratio on the basis of the data analysis. Making use of these results, the value of the equivalent uniform moment can be obtained easily.

(1) Analysis

A girder panel under unequal end moments is shown in Fig.5.1. When the panel length and the panel depth are assumed to a and b, respectively, the panel aspect ratio can be expressed $\alpha = a/b$. In order to be in equilibrium with unequal end moments, it is assumed that applied shearing stresses are parabolically distributed along $x = 0$ and
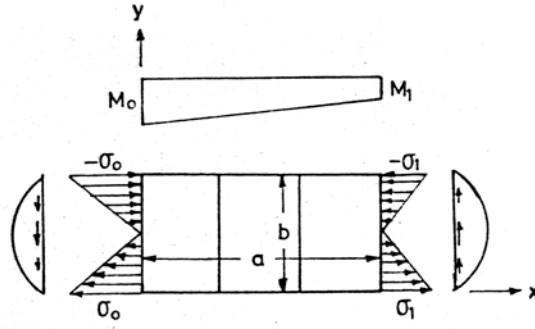
Fig.5.1 Panel under unequal end moments.

$x = a$. From equilibrium of force, the shearing stress at any point in a panel, τ_{xy}, is as follows.

$$\tau_{xy} = (1-\beta)\sigma_0 \left[-\left(\frac{y}{b}\right)^2 + \left(\frac{y}{b}\right) \right] / \alpha \tag{5.1}$$

If the normal stresses at any point in a panel, σ_x, varies linearly in the direction of x, it is as follows.

$$\sigma_x = \sigma_0 \left[1 - (1-\beta)\frac{x}{a} \right] \left(1 - \frac{2y}{b} \right) \tag{5.2}$$

where $\beta = \sigma_1/\sigma_0$ and h is the thickness of the panel.

It is assumed that as the boundary conditions of the girder panel the edges $x = 0$ and $x = a$ are simply supported and along the edges $y = 0$ and $y = b$ the deflections are zero and also these edges are built-in. So as to extend this method for a vertically stiffened girder panel, the panel may be regarded as an orthotropic plate, and then the differential equation of the deflection surface for a buckled plate is as follows.

$$D_x \frac{\partial^4 w}{\partial x^4} + 2H \frac{\partial^4 w}{\partial x^2 \partial y^2} + D_y \frac{\partial^4 w}{\partial y^4} = h \left[\sigma_x \frac{\partial^2 w}{\partial x^2} + 2\tau_{xy} \frac{\partial^2 w}{\partial x \partial y} \right] \tag{5.3}$$

When D_x, D_y and D_{xy} denote the flexural rigidity in the direction of x, that in the direction of y and the torsional rigidity, respectively in the above equation, H equals to $v_y D_x + 2 D_{xy}$ (v_y = Poisson's ratio in connection with the applied force in the y direction) and H can be expressed as $\kappa \sqrt{D_x D_y}$ by means of a parameter κ.

The built-in conditions at upper and lower edges are expressed as follows.
when $y=b$

$$C_b \frac{\partial^3 w}{\partial x^2 \partial y} = -\left[D_y \frac{\partial^2 w}{\partial y^2} + D_1 \frac{\partial^2 w}{\partial x^2} \right] \tag{5.4}$$

36

when $y=0$

$$C_b \frac{\partial^3 w}{\partial x^2 \partial y} = \left[D_y \frac{\partial^2 w}{\partial y^2} + D_1 \frac{\partial^2 w}{\partial x^2} \right] \tag{5.5}$$

where, C_b is the torsional rigidity.

By converting equations (5.3),(5.4) and (5.5) into a set of the finite difference equations and so as to satisfy the simply supported conditions at $x=0$ and $x=a$ and the conditions, $w=0$, at $y=0$ and $y=b$, the buckling coefficient $k_\sigma (= \sigma_0 b^2 h / \pi^2 D_x)$ can be obtained.

(2) Computed results and considerations

Single panel of vertically stiffened web is taken up in actual computations. Accordingly, the value of $\kappa = 1$ is adopted.

In order to examine how solutions converge under the application of the finite difference method, the case of the square plate subjected to pure bending and simply supported at all edges is chosen. In Fig.5.2 the broken line shows the result obtained by the energy method[5]. As it is supposed that the convergence is practically good when the number of subdivisions is 20 in the direction of x and y, the computations are carried out using these subdivisions.

In Fig.5.3, the position in which the non-uniform moment is converted into the equivalent bending moment is shown in broken line at the single panel under unequal end moment. If the value of ξ which indicates this position is once obtained, the equivalent bending moment , M_{eq}, can be estimated in the following expression.

$$M_{eq} = M_0 \left(1 - \xi + \xi\beta \right) \tag{5.6}$$
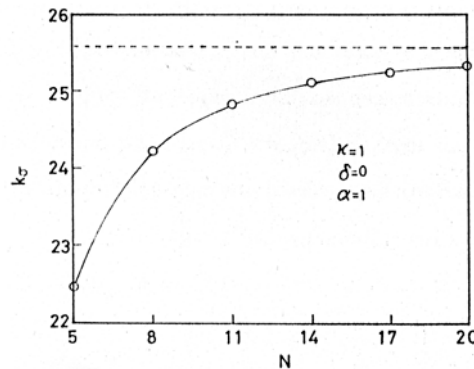
Fig.5.2 Buckling coefficient vs. number of subdivisions.
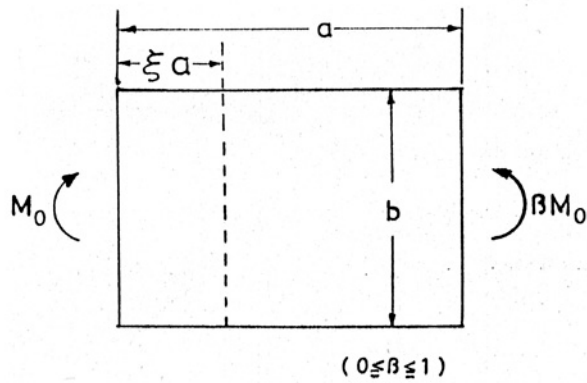
Fig.5.3 Conversion into equivalent bending moment.

When the upper and lower edges are simply supported($\delta = C_b / b D_x = 0$), how ξ varies with the value of β ($0 \leqq \beta \leqq 1$) is shown in Fig.5.4(a) and Fig.5.4(b). As α increases the curved lines change to the convex pattern downward and the value of ξ decreases by degrees. In regard to the parameter β, since the shearing stress increases with the decrease of β, the position of ξ transfers to the edge in which the larger moment acts. The similar relation for the case in which the upper and lower edges are fixed is shown in Fig.5.5(a) and Fig.5.5(b). It is seen in these figures that ξ shows smaller value than that obtained for the simply supported edges on condition that α and β are the same value, respectively.
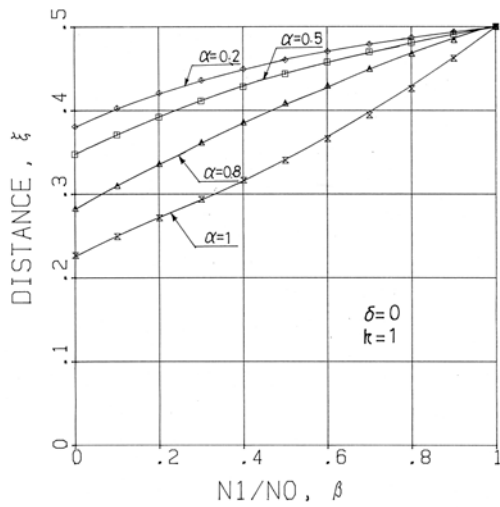
Fig. 5.4(a) Position of equivalent bending moment.
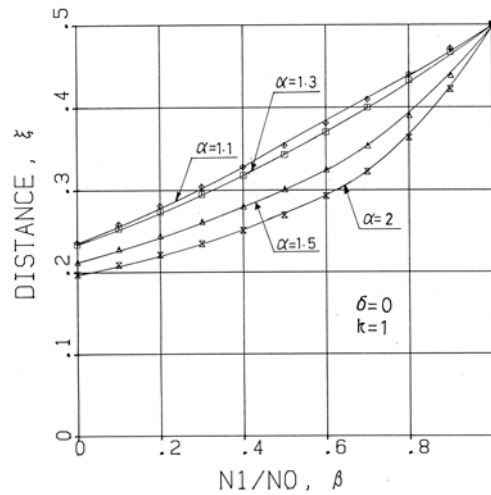
Fig. 5.4(b) Position of equivalent bending moment.
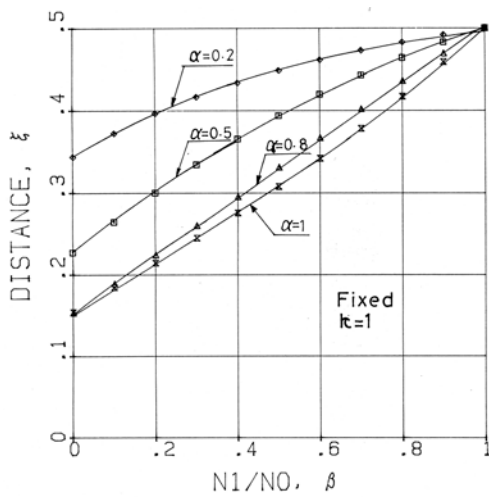
Fig. 5.5(a) Position of equivalent
bending moment.
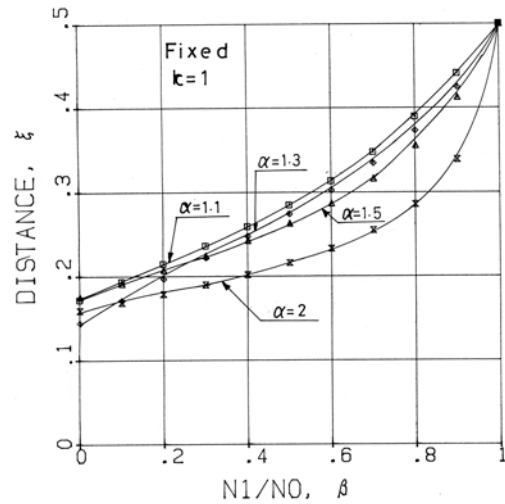
Fig. 5.5(b) Position of equivalent
bending moment.

In Fig.5.6, how ξ varies with the value of δ is shown on the case that $\alpha =1$. If δ is smaller than 1, the value of ξ changes with slight increases of δ. But if δ approaches 1, the value of ξ almost agrees with that obtained for the fixed edges. It is supposed that this is caused by the fact that the increase of the torsional rigidity C_b considerably influences on the buckling load for each value of β because of the restraint effect. However, it is considered that this influence becomes constant for δ of the order of 1.
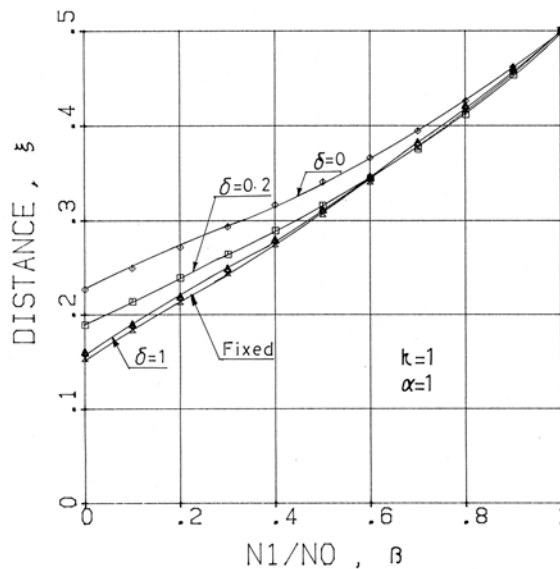
Fig.5.6 Influence of torsional rigidity.

Figs.5.7(a) and 5.7(b) show the relation between α and ξ for several values of β. The state that ξ decreases with the reduction of β is shown well in these figures.
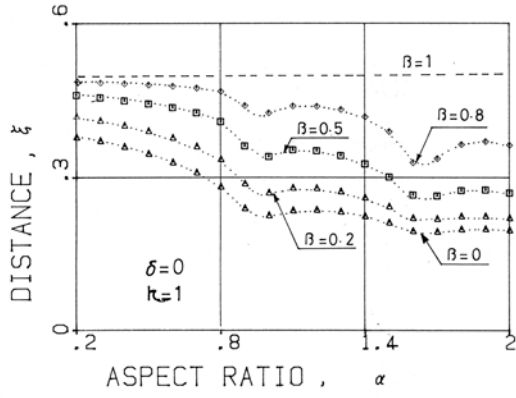
Fig. 5.7 (a) Position of equivalent
bending moment.
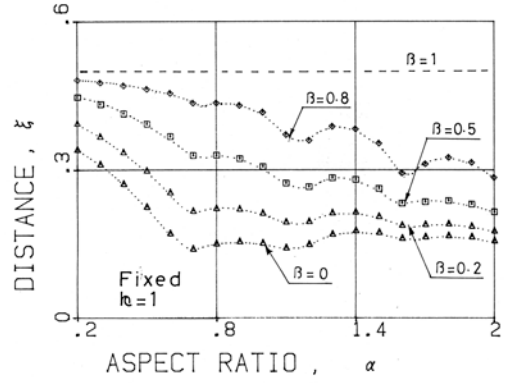
Fig. 5.7(b) Position of equivalent
bending moment.

From the above results, the position of the equivalent bending moment ξ can be expressed as the following form.

I. For simply supported upper and lower edges.

$0.2 \leq \alpha \leq 0.94$

$$\xi = 0.378 + 0.0609\alpha + 0.114\beta - 0.23\alpha^2 + 0.393\alpha\beta + 0.00512\beta^2$$
$$- 0.271\alpha^2\beta - 0.445\alpha\beta^2 + 0.495\alpha^2\beta^2$$

$0.94 < \alpha \leq 1.63$

$$\xi = 0.0238 + 0.359\alpha - 1.257\beta - 0.151\alpha^2 + 2.566\alpha\beta + 1.297\beta^2$$
$$- 1.13\alpha^2\beta - 2.189\alpha\beta^2 + 0.957\alpha^2\beta^2$$

$1.63 < \alpha \leq 2.0$

$$\xi = 0.0251 + 0.207\alpha - 5.08\beta - 0.0575\alpha^2 + 5.371\alpha\beta + 3.684\beta^2$$
$$- 1.427\alpha^2\beta - 3.631\alpha\beta^2 + 0.974\alpha^2\beta^2$$

$$(5.7)$$

II. For fixed upper and lower edges.

$0.2 \leq \alpha \leq 0.66$

$$\xi = 0.387 - 0.124\alpha + 0.222\beta - 0.394\alpha^2 + 0.069\alpha\beta - 0.114\beta^2$$
$$+ 0.542\alpha^2\beta + 0.0617\alpha\beta^2 - 0.148\alpha^2\beta^2$$

$0.66 < \alpha \leq 1.15$

$$\xi = -0.041 + 0.407\alpha - 0.392\beta - 0.209\alpha^2 + 2.225\alpha\beta + 0.76\beta^2$$
$$- 1.582\alpha^2\beta - 2.203\varepsilon\beta^2 + 1.529\alpha^2\beta^2$$

$$1.15 < \alpha \le 1.62$$

$$\xi = -0.501 + 0.932\alpha - 3.391\beta - 0.314\alpha^2 + 5.442\alpha\beta + 2.876\beta^2$$
$$- 2.122\alpha^2\beta - 4.128\alpha\beta^2 + 1.601\alpha^2\beta^2$$

$$1.62 < \alpha \le 2.0$$

$$\xi = -0.0548 + 0.274\alpha - 4.463\beta - 0.0778\alpha^2 + 4.924\alpha\beta + 2.52\beta^2$$
$$- 1.39\alpha^2\beta - 2.485\alpha\beta^2 + 0.721\alpha^2\beta^2$$

$$(5.8)$$

Approximate curves obtained by applying Eqs.(5.7) and (5.8) are indicated by solid lines in Figs.5.8(a) and 5.8(b). As seen from these figures, it is supposed that these approximate expressions are sufficiently useful so as to estimate the position of the equivalent bending moment. By substituting the value of ξ into Eq.(5.6) the equivalent bending moment M_{eq} can be easily obtained.
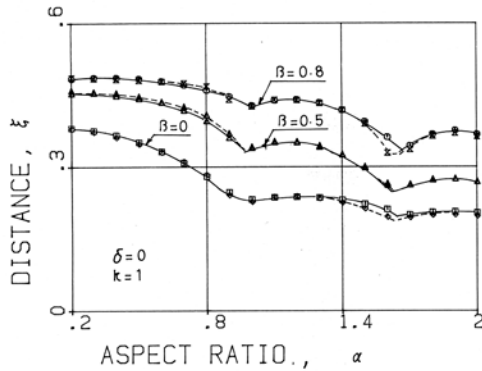
Fig. 5.8 (a) Position of equivalent
bending moment.
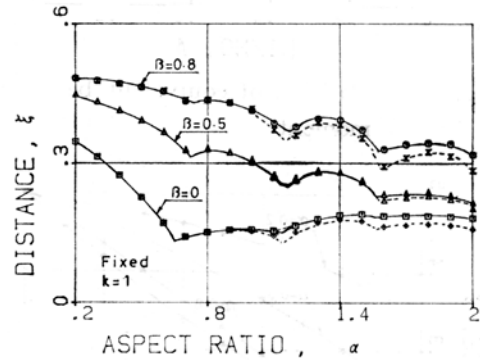
Fig. 5.8(b) Position of equivalent
bending moment.

(3) Conclusions

As the result of the buckling analysis for the single girder panel under unequal end moments, the position of the equivalent bending moment was obtained. In computation the finite differences method was adopted. The conclusions are summarized as follows.

1) As panel aspect ratio α grows large, the position of the equivalent bending moment shifts to the edge in which larger moment acts.

2) With the increase of the torsional rigidity at the upper and lower edges the position of the equivalent bending moment moves to the edge in which larger moment acts.

3) As end moment ratio decreases, the position of the equivalent bending moment

approaches the edge in which larger moment acts. In this case the degree of fall differs according to the panel aspect ratio.

4) The position of the equivalent bending moment was expressed as a function of the panel aspect ratio and the end moment ratio. The good accuracy of this expression was given.

2.6 Discussions

Elastic buckling is important for the beams with relatively slender web and the analysis on this problem is actually useful for the beams under construction. Hancock has considered the effect of web distorsion.[31] He has indicated that a beam with web width-to-thickness ratio of 68 has a flexural-torsional buckling load that is approximate 10% lower than the Timoshenko and Gere estimate, which assumes no distortion. Recently, Hughes et al. have presented an energy method allowing for the effect of web distortion on the lateral buckling of mono-symmetric beams subjected to a concentrated vertical load.[37] They have pointed out that the disparity between the distortional and classical critical load increases as web height to beam length ratio increases and the classical method seriously overestimates the critical load for short beams. The accuracy of this method is verified by results obtained from ABAQUS. Plum and Svensson have presented a simple method to improve the lateral free and restrained buckling capacity of double-symmetric I-beams.[38] They presented a solution to the problem consisting of warping-preventing devices in form U-sections connected to the web and flanges of the I-section. Cheung has examined the elastic distortional buckling behavior of beams with very slender webs through the findings of a parametric study on section geometries.[42]

In addition to linear buckling analysis, Woolcock and Trahair have considered the post buckling of determinate and redundant I-beams.[3,4] They have pointed out that the effect of nonlinear torsion does not change the critical load and the elastic post-buckling behavior of redundant I-beams will rarely be important. Recently, Nakazawa et al. have investigated analytically the post-buckling behavior of a simply supported panel subjected to combined loading of bending and shear.[29] They have given the suggestive results on the panel stress distribution after buckling. Kounadis and Ioannidis have examined that the elastic lateral postbuckling response of geometrically perfect beams, under simultaneously uniform bending and axial compression in the vicinity of the critical bifurcation state.[39]

The studies on inelastic lateral-torsional buckling have been mostly based upon the tangent-modulus theory and it is supposed that the satisfactory results are obtained. The effect of the residual stress on inelastic lateral-torsional buckling of beams was started by Galambos's research.[32] The combined effects of residual stresses and geometrical imperfections on inelastic lateral-torsional buckling of beams were initiated by Linder.[33] Tuda et al.[30] and Nakazawa et al.[36] have investigated the ultimate strength of a plate girder panel under unequal end moments by using finite difference method and finite element method, respectively. They proposed several interaction curves on the ultimate strength of a girder panel.

The literature on the experimental researches are collected and reported.[34,35] In Ref. 34) an empirical formula is proposed. In Ref. 35) a statistical consideration is given for the tests of laterally unsupported welded beams. Kemp has analyzed the rotation capacities in

many tests and given them as a function of the interactive local flanges and web buckling and lateral-torsional buckling that can be represented by a simple set of equations.[40] Recently, Trahair et al. have examined the inelastic combined bending and torsion of I-section beams using the finite-element method.[41] In that paper, the elastic-plastic load-deformation relationships of beams under combined bending and torsion were determined by taking into account the effects of large deformations, material inelasticity, and initial conditions of residual stresses and geometric imperfections. They have pointed out that a commonly quoted circular interaction equation for combined bending and torsion does not always provide a true lower bound for I-section beams. Subsequently, Trahair has given a consistent set of multiple curves for the design of steel beams against lateral buckling.[43]

Hereafter, the method of limit state design will be introduced. Accordingly, it is supposed that the subject of stress redistribution is one of the research needs for the purpose of rational design. And the rotation capacity of girders must be also important problem to be examined with much enthusiasm. In addition, the research on overall lateral-torsional buckling of twin girders with very thin web plate will be needed.

2.7 References

1) Nethercot, D. A. and Rockey, K. C.: A Unified Approach to the Elastic Lateral Buckling of Beams, The Structural Engineer, Vol.49, No.7, pp.321-330, 1971.
2) Vinnakota, S.: Inelastic Stability of Laterally Unsupported Beams, Comput. Struct.,Vol.7, No.3, 1977.
3) Woolcock, S. T., and Trahair, N. S.: Post-buckling of Determinate I-beams, ASCE J. Eng. Mech. Div., Vol.100,No.EM.2, pp.157-172, 1974.
4) Woolcock, S. T., and Trahair, N. S.: Post-buckling of Redundant I-beams, ASCE J. Eng. Mech. Div., Vol.102,No.EM2, pp.293-312,1976.
5) Timoshenko, S. P., and Gere, J. M.: Theory of Elastic Stability, McGraw-Hill, New York,1961.
6) Konishi, I., Yonezawa, H., and Mikami, I.: Elastic Buckling of Plate Girders under Pure Bending, Proc. JSCE, No.143, 1967(in Japanese).
7) Salvadori, M. G.: Lateral Buckling of I-beams, Trans. Am. Soc. Civ. Eng., Vol.120,1955.
8) Horne, M.R.: The Flexural-torsional Buckling of Members of Symmetrical I-section under Combined Thrust and Unequal Terminal Moments, Q. J. of Mech. And App. Maths., Vol.Ⅶ, Pt.4,1954.
9) Bleich, F.: Buckling Strength of Metal Structures, McGraw-Hill Book Co., New York, 1952.
10) Galambos, T. V.: Structural Members and Frames, Prentice-Hall, New Jersey, 1968.
11) Schmidt, L. C.: Restrains against Elastic Lateral Buckling, Proc. ASCE, Vol.91, No.EM6, pp.1-10, 1965.
12) Hartmann, A. J.: Elastic Lateral Buckling of Continuous Beams, Proc. ASCE, Vol.93, No.ST4, pp.11-26, 1967.
13) Takeda, H., Mikami, I. And Yonezawa, H.: Elastic Lateral Buckling of Plate Girders, Theoretical and Applied Mechanics, Univ. of Tokyo Press, Vol.24, 1974.

14) Salvadori, M. G.: Numerical Computation of Buckling Loads by Finite Differences, Trans. ASCE, Vol.116, pp.590-636, 1951.

15) Gienke, E. G.: Uber die Berechnung regelmassiger Konstruktionen als Kontinuum, Der Stahlbau, Jg.33, H.1 und H.2, 1964.

16) Galambos, T. V.: Guide to Stability Design Criteria for Metal Structures, 4th ed., John Wiley & Sons, 1988.

17) Hill, H. N.: Lateral Stability of Unsymmetrical I-beams, Jour. Aero. Sci. Vol.9, No.5, 1942.

18) Radulovic, B.: Beitrag zur Stabilität einer Rechteckplatte, die einer in beiden Richtungen über die Plattenebene linear veränderlichen Last unterworfen ist, bei Navierschen Randbedingungen, Der Stahlbau, Jg.42, H.7, 1973.

19) Radulovic, B.: Über die Querversteifungen einer Rechteckplatte, die einer in beiden Richtungen über die Plattenebene linear veränderlichen Last unterworfen ist, Der Stahlbau, Jg.43, H.4, 1974.

20) Radulovic, B.: Zur Stegblechbeulung unter in zwei Richtungen linear veränderlichen Normalspannungen und in einer Richtung parabolisch veränderlichen Schubspannungen, Der Stahlbau, Jg.44, H.7, 1975.

21) Basler, K. and Thurlimann, B.: Strength of Plate Girders in Bending, Journal of Structural Division, ASCE, Vol.87, No.ST6, pp.153-181, 1961.

22) Specification for Highway Bridges, Japan Road Association, 1990.

23) Fukumoto, Y., et al.: Lateral-torsional Buckling Tests of Welded I-girders under Moment Gradient, Proc. Of Japan Society of Civil Engineers, No.362/I-4, pp.323-332, 1985 (in Japanese).

24) Takeda, H., Mikami, I. and Yonezawa, H.: Lateral Buckling Test of Steel Plate Girders under Varying Bending, Technology Reports of Kansai University, No.33, 1991.

25) Fukumoto, Y., et al.: Inelastic Lateral Buckling Tests on Welded Beams and Girders, Proc. of Japan Society of Civil Engineers, No.189, pp.39-51, 1971(in Japanese).

26) Usami, T.: Inelastic Lateral Buckling Strength of Monosymmetric I-girders, Research Bulletin of the Faculty of Engineering, Gifu University, No.23, pp.81-94, 1973.

27) Nethercot, D. A. and Trahair, N. S.: Lateral Buckling Approximations for Elastic Beams, The Structural Engineer, Vol.54, No.6, pp.197-204, 1976.

28) Mikami, I.: Orthotropic Plates under Varying Compression, Jour. Of Structural Engineering, ASCE, Vol.109, No.1, 1983.

29) Nakazawa, M., Iwakuma, T. and Kuranishi, S.: Elastic Buckling Strength and Postbuckling Behavior of a Panel under Unequal Bending and Shear, Structural Eng./Earthquake Eng., JSCE, Vol.8, No.1, 1991.

30) Tuda, H., Yonezawa, H. and Dogaki, M.: Ultimate Strength of Plate Girder under Unequal End Moments, Annual Meeting of JSCE, I-4, 1992.

31) Hancock, G. J.: Local Distorsional and Lateral Buckling of I-Beams, ASCE J. Struct. Div., Vol.104, No.ST11, 1978.

32) Galambos, T. V.: Inelastic Lateral Buckling of Beams, ASCE J. Struct. Div., Vol.89, No.ST5, 1963.

33) Linder, J.: Influence of Residual Stresses on the Load-Carrying Capacity of I-Beams, Stahlbau, Vol.43, 1974(in German).

34) Fukumoto, Y., Itoh, Y. and Kubo, M.: Strength Variation of Laterally Unsupported Beams, ASCE J. Struct. Div., Vol.106, No.ST1, 1980.

35) Fukumoto, Y. and Itoh, Y.: Statistical Study of Experiments on Welded Beams, ASCE J. Struct. Div. Vol.107, No.ST1, 1981.

36) Nakazawa, M. and Kuranishi, S.: An Ultimate Interactive Strength Formula of Web Plates in Plate Girder under Combined shear and Bending, Journal of Structural Engineering, Vol.37A, 1991.

37) Hughes, O. and Ma, M.: Lateral Distorsional Buckling of Monosymmetric Beams under Point Load, Journal of Engineering Mechanics, ASCE, Vol.122, No.10, 1996.

38) Plum, C. M. and Svensson, E.: Simple Method to Stabilize I-Beams against Lateral Buckling, Journal of Structural Engineering, ASCE, Vol.119, No.10, 1993.

39) Kounadis, A. N. and Ioannidis, G. I.: Lateral Postbuckling Analysis of Beam Columns, Journal of Engineering Mechanics, ASCE, Vol.120, No.4, 1994.

40) Kemp, A. R. : Inelastic Local and Lateral Buckling in Design Codes, Journal of Structural Engineering, ASCE, Vol.122, No.4, 1996.

41) Pi, Y. L. and Trahair, N. S. : Inelastic Bending and Torsion of Steel I-Beams, Journal of Structural Engineering, Vol.120, No.12, 1994.

42) Cheung, K. F.: Cross Section Distortion and Mode-Switching in Distortional Buckling of Beams with Very Slender Webs, Proceedings of the 5th international colloquium on Stability and Ductility of Steel Structures, Vol. 1, 1997.

43) Trahair, N. S.: Multiple Design Curves for Beam Lateral Buckling, Proceedings of the 5th international colloquium on Stability and Ductility of Steel Structures, Vol. 1, 1997.

44) Hotta, T., Naito, J. and Nsshimura, N.: Lateral-Torsional Buckling Strength of Steel Twin Girder Bridges under Erection, Journal of JSCE, No.612/ I -46, pp.287-296, 1999(in Japanese).

45) Ohgaki, K., Yabe, J., Nakazono, A., Nakamura, H. and Nagai, M.: Rational Design and Construction Methods of A Continuous Composite Two-I-Girder Bridge with PC Slabs, Journal of JSCE, No.679/VI-51, pp.65-80, 2001(in Japanese).

46) Nogami, K., Fukaya, M., Yamasawa, T. and Iwasaki, H.: Overall Lateral Buckling of Rational 2-Girder Bridges under Erection, Journal of Structural Engineering, Vol.49A, JSCE, 2003(in Japanese).

Chapter 3

Flexural buckling of multi-stiffened web plates

3.1 General description

In recent years, the construction of long-span steel bridges is remarkable. Two types of girder-bridges can be economically used for the long-span bridges: the first type is composed of main box-girders and orthotropic steel deck, and the second type consists of two main I-girders and orthotropic steel deck. The box-girder bridges have been built since about 1950, and the double I-girder bridges since about 1960. These types of bridges become longer year-by-year. Consequently, the main girders are large and deep, and then those web plates have multiple longitudinal and transverse stiffeners. Because it is supposed that such multi-stiffened webs will be used in for the future, the ultimate strength and behavior of such webs should be discussed.

Richmond[1] solved the elastic buckling of rectangular plates orthogonally stiffened under bending and combined bending and compression by using the orthotropic plate theory. Afterwards, this solution was also derived by Giencke.[2] A design procedure based on these research works was built up and the alternative design procedure based on the strength of plate panels bounded by the longitudinal and transverse stiffeners, and the column strength of both those stiffeners was proposed in several specifications. One of them is BS5400.[3] However, The Japanese Specifications for Highway Bridges does not explicitly contain any design provision applicable to the multi-stiffened webs.[4]

The failure tests on the box-girders with multi-stiffened webs have been reported by Dowling[5,6] and Dibley[7]. In Japan, a plate girder with many longitudinal stiffeners has been tested,[8] and the experiments on the ultimate strength of the plate girders and box girders with multi-stiffened webs have been carried out.[9-12]

The methods for theoretically predicting the strength of plate girders subjected to bending has been much proposed.[13] In these theories, only Rockey's theory is applicable to multi-stiffened webs.[14] Other theories cannot be applied to the plate girders with multi-stiffened web after expansion except Fujii's theory.[15] Therefore, a theory easily employable in predicting the bending strength of plate girders whose web has the multiple stiffeners is desirable.

3.2 Various rigidities of multi-stiffened web plates

When the orthotropic plate theory is applied to the plate girders with multiple longitudinal and transverse stiffeners, the determination of equivalent rigidities is of importance. The web of most plate girders has unequally spaced longitudinal and equally spaced transverse stiffeners. However, it is seen that the work on the equivalent rigidities of unequally spaced stiffeners is few.

In the case of the web plate with unequally spaced longitudinal stiffeners under bending, Richmond[1] proposed that it can be transposed by an orthotropic plate with constant rigidity which is equal to the rigidity at the center of compressive region. But the determination of equivalent torsional rigidity was made no mention of. So, the equivalent rigidity in Ref. 16) will be applied.

A web plate that has flexural rigidity D and thickness h is reinforced by s

longitudinal stiffeners arranged unequally and r transverse stiffeners arranged equally as shown in Fig.2.1. The longitudinal and transverse stiffeners have the same cross section, respectively. The flexural and torsional rigidity of a longitudinal stiffener are EI_s and GJ_s, respectively and those of a transverse stiffener are EI_r and GJ_r, respectively. It is assumed that an orthotropic plate has constant rigidity. The flexural rigidity D_x and D_y and effective torsional rigidity H can be determined by equalizing the strain energy of the orthotropic plate with that of the stiffened plate.

The equivalent rigidities given by Ref.16) are shown as follows:

a) Flexural rigidity in the longitudinal direction

$$D_x = D\left[1 + \frac{1}{0.6352}\sum_{i=1}^{s}\left(\sin\pi\eta_i + 0.52\sin 2\pi\eta_i\right)^2 \gamma_s\right] \tag{3.1}$$

where $\gamma_s = EI_s / bD$

b) Flexural rigidity in the transverse direction

$$D_y = D\left[1 + (r+1)\gamma_r\right] \tag{3.2}$$

where $\gamma_r = EI_r / aD$

c) Effective torsional rigidity

$$H = D\left[1 + \frac{1}{2.08}\sum_{i=1}^{s}(\cos\pi\eta_i + 1.04\cos 2\pi\eta_i)^2\psi_s + \frac{r-1}{2}\psi_r\right] \tag{3.3}$$

where $\psi_s = GJ_s / bD$ and $\psi_r = GJ_r / aD$

Now, the buckling stresses of an orthotropic plate obtained by applying these rigidities are compared with those obtained as a stiffened plate. The results will be summarized by using buckling coefficient $k(= \sigma_0 b^2 h / \pi^2 D)$.

The examples chosen are the simply supported web plate with two or seven longitudinal stiffeners. The position of stiffeners is decided as shown in Fig.2.2 according to Ref.4) and the cross sectional area of them is not considered. The number of transverse stiffeners is zero or four.
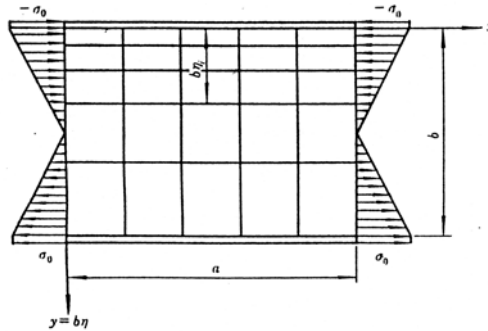
Fig.2.1 Multi-stiffened plate girder under bending.

48
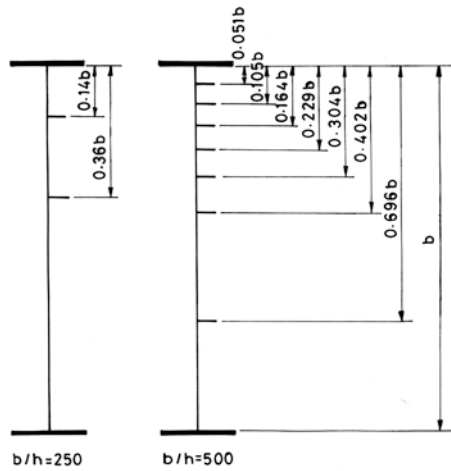
Fig.2.2 Plate girders for example.

The computed results of the web plate that has longitudinal stiffeners only are shown in Figs.2.3 and 2.4. The solid line indicates the result obtained as a stiffened plate and the broken line indicates the result regarded as an orthotropic plate. In Fig.2.3, a change that appears in solid line in the region of $a/b = 0.2$ means the occurrence of the local buckling at the panel between longitudinal stiffeners. This change cannot be detected in the broken line. However, it is seen that good agreement between two curves is obtained in the case that the stiffened plate buckles globally. In the case of seven longitudinal stiffeners (Fig.2.4), it is supposed that the application of the equivalent rigidity gives conservative buckling coefficients in a small range of a/b, but the minimum value of buckling coefficients is properly estimated.
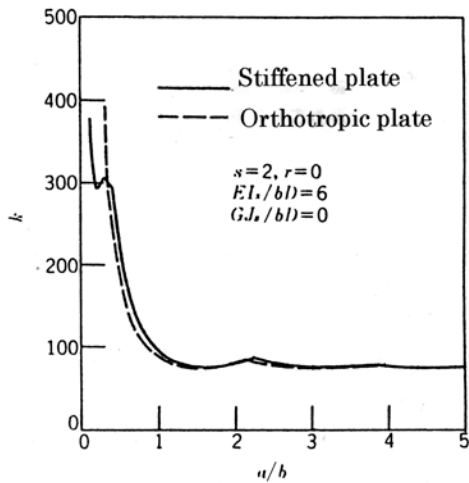
Fig.2.3 Buckling curves.
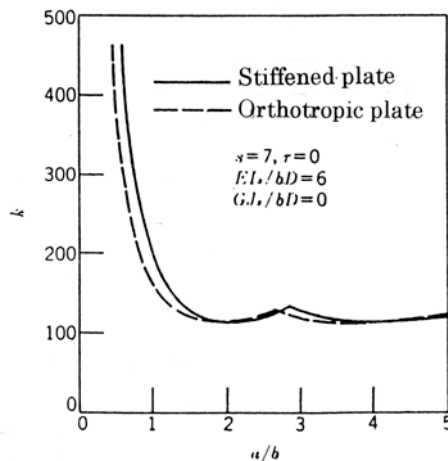
Fig.2.4 Buckling curves.

The computed results of the web plates with both longitudinal and transverse stiffeners are shown in Figs.2.5 to 2.7. Generally as shown in these figures, it is seen that the buckling coefficients computed by the orthotropic plate theory agree

49

comparatively well with those obtained as the stiffened plate. In Fig.2.5, when a / b is larger than 0.9, local buckling occurs between transverse stiffeners. In Fig.2.6, the torsional rigidity of the longitudinal and transverse stiffeners is taken into consideration. But in the region of $a / b > 1$ which the local buckling between transverse stiffeners, the torsional rigidity cannot be reflected in the solution obtained as the orthotropic plate. At the buckling curve using the orthotropic plate theory in Fig.2.7, the mode of $m=3$ does not appear. This fact is based on the reason why the solution using the orthotropic theory is smaller than that of the stiffened plate on the local buckling between transverse stiffeners. In the case that because the rigidity of the longitudinal stiffener is great the local buckling occurs between the transverse stiffeners, the use of the equivalent rigidity gives conservative values. However, it is presumed that in these cases owing to the occurrence of the inelastic buckling the error will be small. Therefore, as long as the flexural rigidity and space of stiffeners based upon Ref.4) are insured it is supposed that these equivalent rigidity will produce the results within acceptable accuracy.
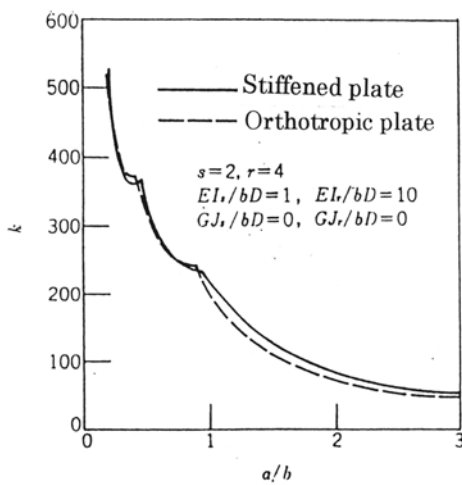
Fig.2.5 Buckling curves.
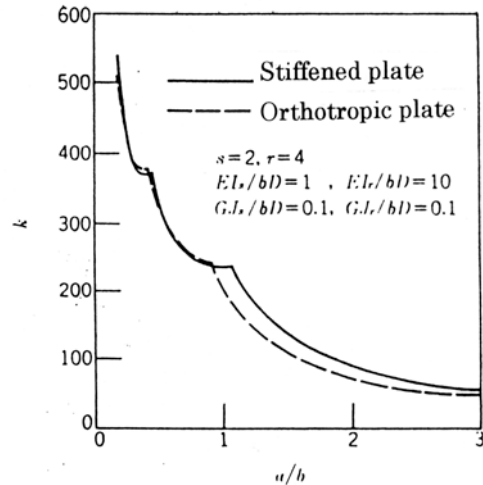
Fig.2.6 Buckling curves.
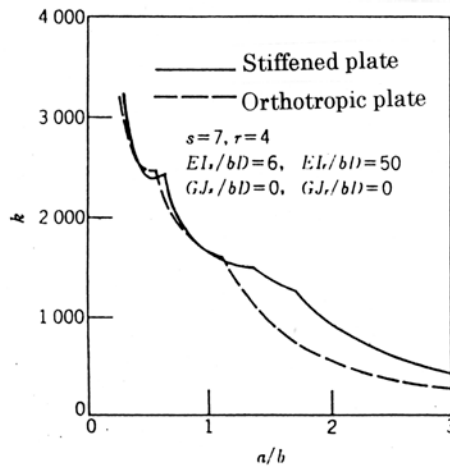
Fig.2.7 Buckling curves.

50

3.3 Approximate buckling analysis

An approximate calculation method for bending strength of multi-stiffened plate girders is developed hereafter.[17]

3.3.1 Elastic buckling stress of compression flange

It is assumed that a flange has rectangular cross section of width c and thickness t. If there is no vertical buckling of the compression flange and the lateral buckling can be regarded as column buckling, the elastic buckling stress is as follows:

$$\sigma_{cr}{}^{e} = \pi^2 E / 12(a/c)^2$$

where E is elastic modulus.

Moreover, if the torsional buckling is considered to be the buckling of a plate with three simply supported edges and one free edge under compression, the elastic buckling stress is as follows:

$$\sigma_{cr}{}^{e} = k_f \frac{\pi^2 E}{3(1-\nu^2)} \left(\frac{t}{c}\right)^2$$

where ν is Poisson's ratio. And the buckling coefficient k_f is given by the following expression.[18]

$$k_f = \left(\frac{c}{2a}\right)^2 + \frac{6(1-\nu)}{\pi^2}$$

3.3.2 Elastic buckling stress of web plate

By considering a stiffened web as an orthotropic plate, the elastic buckling stress of the web can be obtained as follows:

$$\sigma_{cr}{}^{e} = k_w \frac{\pi^2 \sqrt{D_x D_y}}{b^2 h}$$

The buckling coefficient k_w is estimated by the simplification of Giencke's approximate solution.[2]

$$k_w = \frac{9\pi^2}{32} \sqrt{\frac{R_1 R_2}{1 + (27/25)^2 R_1 / R_3}}$$

R_n (n=1,2,3) in this expression can be given by extending Giencke's formula[2] which is applied to all simply supported edges to the case of the plate with one free edge and three simply supported edges. Comparing with the results of the precise calculation,[17] R_n is obtained as follows:

$$\alpha^* < 2/3 \sqrt[4]{q} : R_n = (1/\alpha^*)^2 + pn^2\kappa + qn^4(\alpha^*)^2$$
$$\alpha^* \geq 2/3 \sqrt[4]{q} : R_n = 9\sqrt{q}/4 + pn^2\kappa + 4\sqrt{q}n^4/9$$

where

$$\left. \begin{array}{l} p = 2.48 - 0.48/(1+0.019\varphi) \\ q = 3.86 - 2.86/(1+0.0535\varphi) \end{array} \right\}$$

$$\varphi = (\pi b / a)^2 C_f / b D_y$$

C_f : the torsional rigidity of compression flange

The comparisons of the approximate solution with the exact solution are shown in Figs.3.1 and 3.2 for the case of $\kappa = 0$ and 1. Though it is seen that the approximate solution gives relatively conservative values in the case of $5 < \varphi < 50$, it will be satisfactory enough for design.
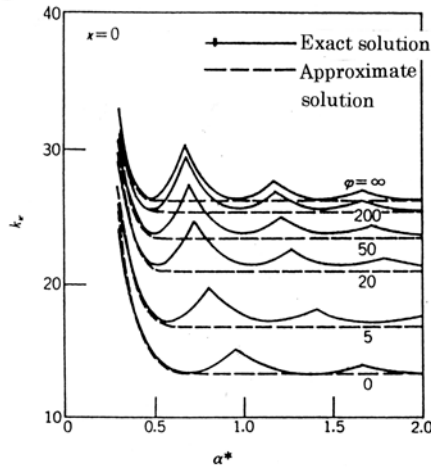
Fig.3.1 Buckling coefficient.
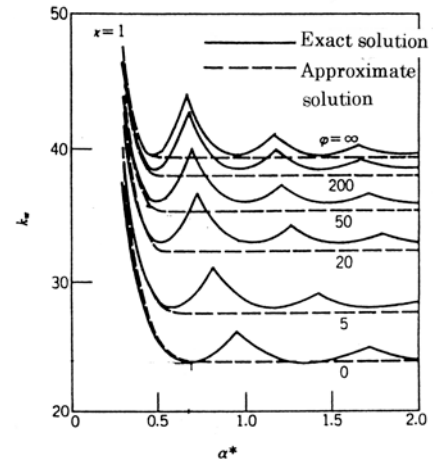
Fig.3.2 Buckling coefficient.

3.3.3 Inelastic buckling stress of compression flange

In order to estimate inelastic buckling stresses, the reduction method of elastic buckling stresses will be used.

For the lateral buckling of compression flange the following reduction curves[4] are adopted at present.

$$\left.\begin{array}{l} \lambda \le 0.2 : \sigma_{cr} / \sigma_Y = 1 \\ 0.2 < \lambda : \sigma_{cr} / \sigma_Y = 1 - 0.412(\lambda - 0.2) \end{array}\right\}$$

where $\lambda = \sqrt{\sigma_Y / \sigma_{cr}^{e}}$

For the torsional buckling of compression flange the next curves are used.[19]

$$\left.\begin{array}{l} \lambda \le 0.45 : \sigma_{cr} / \sigma_Y = 1 \\ 0.45 < \lambda : \sigma_{cr} / \sigma_Y = 1 - 0.53(\lambda - 0.45)^{1.36} \end{array}\right\}$$

3.3.4 Inelastic buckling stress of stiffened web

Various reduction curves have been proposed. As it is supposed that the effect of the residual stress at horizontal and vertical stiffeners on buckling stresses may be not a little, the following equation which predict the lowest limit among the experimental results for the plate girders with stiffened web is adopted.[20]

$$\sigma_{cr} / \sigma_Y = 1 / (1 + \lambda^2)$$

3.3.5 Strength of plate girders under bending

The smaller value between lateral buckling and torsional buckling stresses is adopted as the buckling stress of a compression flange. If the buckling of the compression flange antecedently occurs, it is considered to be a limit state. On the other hand in the case that the buckling of the web precedes, it may be assumed that only the flanges can support the increase in load after buckling without anymore increase in web stress. If the flange is subjected to be constant stress, the strength under bending can be calculated making use of the following expression on condition that σ_{crf} and σ_{crw} are the inelastic buckling stresses of flange and web, respectively.

If $\sigma_{crf} < \sigma_{crw}$, the ultimate moment M_u results in the following expression:

$$M_u = \frac{b^2 h}{6}\left(\sigma_{crw} + 6\frac{A_f}{bh}\sigma_{crf}\right)$$

where A_f is the cross sectional area of a compression flange.

The above expression can be rewritten by means of the yield moment M_Y and the yield stress σ_{Yf} of a compression flange as follows:

$$\frac{M_u}{M_Y} = \frac{\sigma_{crf}}{\sigma_{Yf}}\left(1 - \frac{1 - \sigma_{crw}/\sigma_{crf}}{1 + 6A_f/bh}\right)$$

If $\sigma_{crf} \leq \sigma_{crw}$, M_u can be estimated by the use of the following expression.

$$M_u/M_Y = \sigma_{crf}/\sigma_{Yf}$$

3.3.6 Stiffener rigidity

In the present method, buckling strength is calculated on basis of linear buckling theory. It has been considered questionable from many experimental results whether the required stiffener rigidity ratio γ^* according to linear buckling theory is valid. Test results suggest that the stiffener rigidity ratio γ have to take a value m several times as much as γ^* in order that the stiffeners are effective as rigid stiffeners. Subsequently, the linear buckling theory can be applied by using the effective rigidity γ/m.

Now, $m(=4)$ is used for both longitudinal and transverse stiffeners. In application of Eqs.3.1 to 3.3, $\gamma_s/4$, $\gamma_r/4$, $\phi_s/4$ and $\phi_r/4$ are used.

3.3.7 Comparison of experimental results with calculated results

The validity of the approximate calculation method to predict the bending strength is examined. The experimental results M_{max}/M_Y^* and the theoretical results M_u/M_Y are shown in Table4.1. M_Y^* indicates the yield moment of compression flange in consideration of horizontal stiffeners. A few theoretical values lower than the test results are seen in this table. However on the whole, it is found that the theoretically predicted results except for the above mentioned cases give not only safety evaluation but also satisfactory accuracy.

Table 4.1 Comparison of test results with predicted values.

References	Girder	No. of longitudinal stiffener	No. of transverse stiffener	① M_{max}/M_Y^*	Lateral buckling stress of compression flange (MPa)	Torsional buckling stress of compression flange (MPa)	Flexural buckling stress of stiffened web (MPa)	② M_u/M_Y	①/②
21)	C	1	2	0.841	215.3	294.2	215.1	0.732	1.15
22)	B-25-1	1	0	1.016	242.6	224.4	186.3	0.898	1.13
	B-25-5	1	0	1.061	242.6	224.4	253.3	0.925	1.15
	B-35-1	1	0	0.932	234.6	224.0	127.5	0.835	1.16
	B-35-1A	1	0	1.039	234.6	224.0	128.0	0.836	1.24
	B-35-1E	1	0	0.905	234.6	224.0	128.4	0.836	1.08
	B-35-5	1	0	0.975	234.6	224.0	202.4	0.904	1.08
23)	B-3	1	0	1.097	494.4	475.9	355.6	0.910	1.21
	B-4	1	0	1.007	488.6	474.9	305.8	0.876	1.15
	B-5	*1	0	1.008	479.4	474.4	263.6	0.838	1.20
	B-6	1	0	1.192	503.3	498.9	356.1	0.928	1.28
	B-7	1	0	1.258	492.8	498.7	302.0	0.884	1.42
	B-8	1	0	1.096	482.1	498.5	265.1	0.833	1.32
24)	UA-1	1	1	0.822	297.7	344.0	182.8	0.764	1.08
	UA-2	1	1	0.756	297.7	344.0	192.0	0.772	0.98
	UB-1	1	2	0.694	284.4	344.0	180.0	0.682	1.02
	UB-2	1	2	0.739	284.4	344.0	191.0	0..744	0.99
25)	BL-3	1	0	1.010	693.6	660.0	200.5	0.745	1.36
8)	-	7	0	0.823	443.8	456.2	152.7	0.892	0.92

3.3.8 Conclusions

1) In order to replace a multi-stiffened web with an orthotropic plate having constant rigidities, an expression for equivalent rigidities was proposed. After the investigation on the validity, it became clear that the formula was sufficiently available on condition that the stiffeners on the web had the flexural rigidity and space defined by Ref.4).

2) An approximate calculation method to predict the bending strength of multi-stiffened plate girders was presented making use of the linear buckling theory and the reduction curve and assuming the stress distribution at ultimate state.

3) The comparison of the predicted values with the existing test results on bending strength is in good agreement. Accordingly, it is considered that this estimation is sufficiently available as an approximate calculation method.

3.4 Coupled inelastic flexural buckling of web plates and flange plates

In the former article, an approximate calculation method for predicting the ultimate static strength of plate girders with multiple longitudinal and transverse stiffeners under bending was introduced. Also the comparison with several test results was done.

In this article, the inelastic buckling of plate girders whose web has multiple longitudinal and transverse stiffeners is investigated under bending. Namely, the multi-stiffened web plate is regarded as an orthotropic rectangular plate, and the load of the coupled buckling between the flanges and the stiffened web plate is numerically calculated as an estimation of the load carrying capacity of such plate girders by using the finite difference method. It is examined how the support condition of the stiffened web plate by compression flange, and the flexural and torsional rigidities, the aspect ratio, and depth-to-thickness ratio of the web plates have the effect on the coupled buckling load.

3.4.1 Inelastic buckling of plate girders with orthotropic web plate under bending

A plate girder subjected to bending has the web plate of length a, depth b, and thickness h, and with multiple longitudinal and transverse stiffeners as shown in Fig. 4.1. The stiffened web plate is regarded as an orthotropic rectangular plate of flexural rigidities in the x- and y-directions D_x and D_y, rigidity with respect to the transverse contraction D_1, and torsional rigidity $2D_{xy}$. It is assumed that the orthotropic plate is simply supported along both the edges x=0 and x=a, and that its top and bottom edges (y=0 and b) are elastically supported and elastically restrained by the compressive and tensile flanges of flexural rigidity B_b, torsional rigidity C_b, warping rigidity C_w, cross-sectional area F, and polar moment of inertia about the centroid themself I_0. It is also assumed that each cross-section of the girder, originally plane, remains plane, and that the strain of the flange is equal to the extreme fiber strain of the web plate.

The differential equation of the deflection surface for the buckled orthotropic plate with varying rigidities is [26]

$$
D_x \frac{\partial^4 w}{\partial x^4} + 2(D_1 + 2D_{xy}) \frac{\partial^4 w}{\partial x^2 \partial y^2} + D_y \frac{\partial^4 w}{\partial y^4} + 2\left[\frac{\partial D_x}{\partial x} \frac{\partial^3 w}{\partial x^3} \right.
$$
$$
\left. + \left(\frac{\partial D_1}{\partial y} + 2\frac{\partial D_{xy}}{\partial y} \right) \frac{\partial^3 w}{\partial x^2 \partial y} + \left(\frac{\partial D_1}{\partial x} + 2\frac{\partial D_{xy}}{\partial x} \right) \frac{\partial^3 w}{\partial x \partial y^2} + \frac{\partial D_y}{\partial y} \frac{\partial^3 w}{\partial y^3} \right]
$$
$$
+ \left(\frac{\partial^2 D_x}{\partial x^2} + \frac{\partial^2 D_1}{\partial y^2} \right) \frac{\partial^2 w}{\partial x^2} + 4\frac{\partial^2 D_{xy}}{\partial x \partial y} \frac{\partial^2 w}{\partial x \partial y} + \left(\frac{\partial^2 Dy}{\partial y^2} + \frac{\partial^2 D_1}{\partial x^2} \right) \frac{\partial^2 w}{\partial y^2}
$$
$$
= h\sigma_x \frac{\partial^2 w}{\partial x^2}, \tag{4.1}
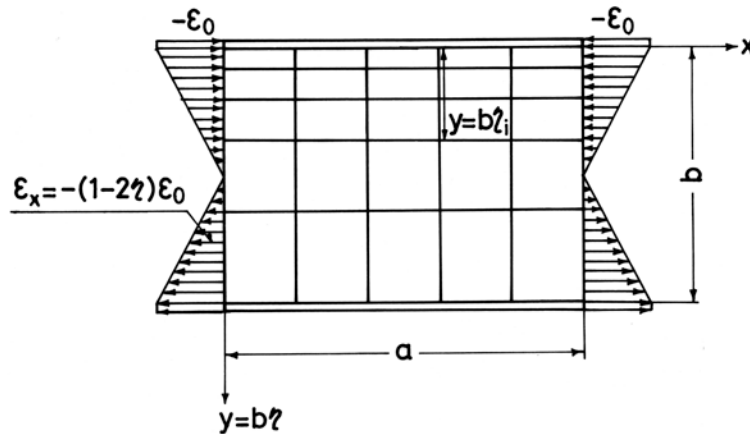$$

where σ_x is the normal stress parallel to the x-axis.

Fig.4.1 A multi-stiffened plate girder under bending.

The differential equations of the deflection curve become

$$\frac{d^2}{dx^2}\left(B_b \frac{d^2 w_0}{dx^2}\right) - \frac{d}{dx}\left[F(\sigma_x)_{y=0} \frac{dw_0}{dx}\right] = -\left[\frac{\partial}{\partial y}\left(D_y \frac{\partial^2 w}{\partial y^2} + D_1 \frac{\partial^2 w}{\partial x^2}\right)\right.$$

$$\left. + 2\frac{\partial}{\partial x}\left(2D_{xy} \frac{\partial^2 w}{\partial x \partial y}\right)\right]_{y=0}, \tag{4.2}$$

$$\frac{d^2}{dx^2}\left(C_w \frac{d^2 \varphi_0}{dx^2}\right) - \frac{d}{dx}\left(C_b \frac{d\varphi_0}{dx}\right) - I_0 (\sigma_x)_{y=0} \frac{d^2 \varphi_0}{dx^2} = \left[D_y \frac{\partial^2 w}{\partial y^2} + D_1 \frac{\partial^2 w}{\partial x^2}\right]_{y=0} \tag{4.3}$$

for the top flange, and

$$\frac{d^2}{dx^2}\left(B_b \frac{d^2 w_b}{dx^2}\right) - \frac{d}{dx}\left[F(\sigma_x)_{y=b} \frac{dw_b}{dx}\right] = \left[\frac{\partial}{\partial y}\left(D_y \frac{\partial^2 w}{\partial y^2} + D_1 \frac{\partial^2 w}{\partial x^2}\right)\right.$$

$$\left. + 2\frac{\partial}{\partial x}\left(2D_{xy} \frac{\partial^2 w}{\partial x \partial y}\right)\right]_{y=b}, \tag{4.4}$$

$$\frac{d^2}{dx^2}\left(C_w \frac{d^2 \varphi_b}{dx^2}\right) - \frac{d}{dx}\left(C_b \frac{d\varphi_b}{dx}\right) - I_0 (\sigma_x)_{y=b} \frac{d^2 \varphi_b}{dx^2} = -\left[D_y \frac{\partial^2 w}{\partial y^2} + D_1 \frac{\partial^2 w}{\partial x^2}\right]_{y=b} \tag{4.5}$$

for the bottom flange, where w_0 and φ_0 are the horizontal deflection and the angle of twist for the top flange, in compression, respectively; further w_b and φ_b are the horizontal deflection and the angle of twist for the bottom flange, in tension, respectively.

In the inelastic range, the rigidities $D_x, D_y, D_{xy}, D_1, B_b, C_b$ and C_w should be read for $D_x', D_y', D_{xy}', D_1', B_b', C_b'$ and C_w', respectively. By introducing the reduced coefficients

$$\tau_x = D_x'/D_x, \tau_y = D_y'/D_y, \tau_{xy} = D_{xy}'/D_{xy}, \tau_1 = D_1'/D_1, \tau_{bb} = B_b'/B_b, \tau_{cb} = C_b'/C_b$$

and $\tau_{cw} = C_w'/C_w$, and assuming that the stress is constant along the x-axis, Eq. 4.1 becomes

$$D_x \tau_x \frac{\partial^4 w}{\partial x^4} + 2(D_1 \tau_1 + 2D_{xy} \tau_{xy}) \frac{\partial^4 w}{\partial x^2 \partial y^2} + D_y \tau_y \frac{\partial^4 w}{\partial y^4} + 2\left(D_1 \frac{d\tau_1}{dy}\right.$$

$$\left. + 2D_{xy} \frac{d\tau_{xy}}{dy}\right) \frac{\partial^3 w}{\partial x^2 \partial y} + 2D_y \frac{d\tau_y}{dy} \frac{\partial^3 w}{\partial y^3} + D_1 \frac{d^2 \tau_1}{dy^2} \frac{\partial^2 w}{\partial x^2} + D_y \frac{d^2 \tau_y}{dy^2} \frac{\partial^2 w}{\partial y^2}$$

$$= h\sigma_x \frac{\partial^2 w}{\partial x^2} \tag{4.6}$$

The solutions that satisfy the boundary conditions along the simply supported edges $x = 0$ and $x = a$ may be assumed as follows:

$$w = b \sum_{m=1}^{\infty} f_m(\eta) \sin(m\pi x / a), \tag{4.7}$$

$$w_0 = b \sum_{m=1}^{\infty} A_{m1} \sin(m\pi x / a), \quad \varphi_0 = b \sum_{m=1}^{\infty} A_{m2} \sin(m\pi x / a), \tag{4.8}$$

$$w_b = b \sum_{m=1}^{\infty} A_{m3} \sin(m\pi x / a), \quad \varphi_b = b \sum_{m=1}^{\infty} A_{m4} \sin(m\pi x / a), \tag{4.9}$$

where $\eta = y / b$; and A_{m1} to A_{m4} are constants.

The continuous conditions at $y=0$ and $y=b$ with respect to the horizontal deflection and angle of twist give the following relations:

$$A_{m1} = (f_m)_{\eta=0}, A_{m2} = (df_m / d\eta)_{\eta=0}, A_{m3} = (f_m)_{\eta=1}, A_{m4} = (df_m / d\eta)_{\eta=1}. \tag{4.10}$$

Thus Eq. 4.6 becomes

$$K_y \tau_y \frac{d^4 f}{d\eta^4} + 2K_y \frac{d\tau_y}{d\eta} \frac{d^3 f}{d\eta^3} + \left[K_y \frac{d^2 \tau_y}{d\eta^2} - 2K_1 \tau_1 - 2K_{xy} \tau_{xy} \right] \frac{d^2 f}{d\eta^2}$$

$$- 2 \left[K_1 \frac{d\tau_1}{d\eta} + K_{xy} \frac{d\tau_{xy}}{d\eta} \right] \frac{df}{d\eta} + \left[K_x \tau_x - K_1 \frac{d^2 \tau_1}{d\eta^2} + \overline{\sigma}_x \mu_m \right] f = 0, \tag{4.11}$$

where $K_x = \varphi_m{}^2 D_x/D$; $K_y = D_y/D$; $K_{xy} = 2\varphi_m D_{xy}/D$; $K_I = \varphi_m D_l/D$; $\mu_m = \varphi_m E\varepsilon_0 hb^2/D$; $\varphi_m = (m\pi b / a)^2$; $\overline{\sigma}_x = \sigma_x /E\varepsilon_0$; D is the flexural rigidity of the web plate; E is Young's modulus; and $-\varepsilon_0$ is the strain of the compressive flange.

Consequently, substituting Equations 4.7-4.10 into Equations 4.2-4.5 yields

$$\left[K_y \tau_y \frac{d^3 f}{d\eta^3} + K_y \frac{d\tau_y}{d\eta} \frac{d^2 f}{d\eta^2} - (2K_{xy} \tau_{xy} + K_1 \tau_1) \frac{df}{d\eta} \right.$$

$$\left. - (K_1 \frac{d\tau_1}{d\eta} - M_b \tau_{bb} - M_f \overline{\sigma}_x \mu_m) f \right]_{\eta=0} = 0, \tag{4.12}$$

$$\left[K_y \tau_y \frac{d^3 f}{d\eta^3} - (N_w \tau_{cw} + N_b \tau_{cb} + N_I \overline{\sigma}_x \mu_m) \frac{df}{d\eta} - K_1 \tau_1 f \right]_{\eta=0} = 0, \tag{4.13}$$

$$\left[K_y \tau_y \frac{d^3 f}{d\eta^3} + K_y \frac{d\tau_y}{d\eta} \frac{d^2 f}{d\eta^2} - (2K_{xy}\tau_{xy} + K_1\tau_1)\frac{df}{d\eta} \right.$$

$$\left. - (K_1 \frac{d\tau_1}{d\eta} + M_b\tau_{bb} + M_f\overline{\sigma}_x\mu_m)f \right]_{\eta=1} = 0, \tag{4.14}$$

$$\left[K_y \tau_y \frac{d^2 f}{d\eta^2} + (N_w\tau_{cw} + N_b\tau_{cb} + N_I\overline{\sigma}_x\mu_m)\frac{df}{d\eta} - K_1\tau_1 f \right]_{\eta=1} = 0, \tag{4.15}$$

where $M_b = \varphi_m^2 B_b / bD$; $M_f = F / bh$; $N_b = \varphi_m C_b / bD$; $N_w = \varphi_m^2 C_w / b^3 D$; and

$N_I = I_0 / b^3 h$.

It is impossible to solve Eq.4.11 together with Eqs.4.12-4.15 for the inelastic buckling, and thus the finite difference method is used. The web depth b is divided into n_s equal parts and the values of the function f_m at the pivotal points are indicated by $f_{m0}, f_{m1}, \cdots, f_{mn}$, where f_{m0} and f_{mn} are the values at $y=0$ and $y=b$, respectively. By expressing Eq.4.11 together with Eqs.4.12-4.15 in the finite difference form, the following set of linear equations is obtained:

$$[A]\{f_m\} = \mu_m [B]\{f_m\}. \tag{4.16}$$

The least eigenvalue μ_m of Eq.4.16 gives the critical load.

3.4.2 Critical moment

1) Inelastic stress-strain relationship

Various stress-strain relationships have been presented by Bleich[27], Hsu-Bertels[28], Ramberg-Osgood[29], Bettern[30], and Richard-Blacklock[31]. The following expression proposed by Richard-Blacklock is adopted for both the tensile and compressive regions:

$$\sigma = E\varepsilon / \left[1 + \left|E\varepsilon / \sigma_Y\right|^n\right]^{1/n} \tag{4.17}$$

where σ is the stress; ε is the strain; σ_Y is the yield point stress; n is the nonlinear parameter. This relationship does not include the effect of strain hardening and is compared with Bleich's relationship in Fig. 4.2, where ε_Y is the yield strain; and σ_p is the proportional limit stress. Because of a double symmetrical plate girder the strain in each fiber is

$$\varepsilon_x = -(1 - 2\eta)\varepsilon_0, \tag{4.18}$$

the non-dimensional stress in the fiber is given as follows:

$$\overline{\sigma}_x = -(1 - 2\eta) / \left[1 + \left|(1 - 2\eta)E\varepsilon_0 / \sigma_Y\right|^n\right]^{1/n}, \tag{4.19}$$

where σ_Y is read for σ_{YW} or σ_{YF} at the web or flange, respectively.

The ratio of the tangent modulus E_t to Young's modulus E, $\tau = E_t/E$, may be determined from Eq.4.17; the ratios for the web, τ_w, and the flange, τ_f, are represented by

$$\tau_w = 1/\left[1 + \left|(1-2\eta)E\varepsilon_0/\sigma_{YW}\right|^n\right]^{(n+1)/n},$$ (4.20a)

$$\tau_f = 1/\left[1 + \left|E\varepsilon_0/\sigma_{YF}\right|^n\right]^{(n+1)/n},$$ (4.20b)
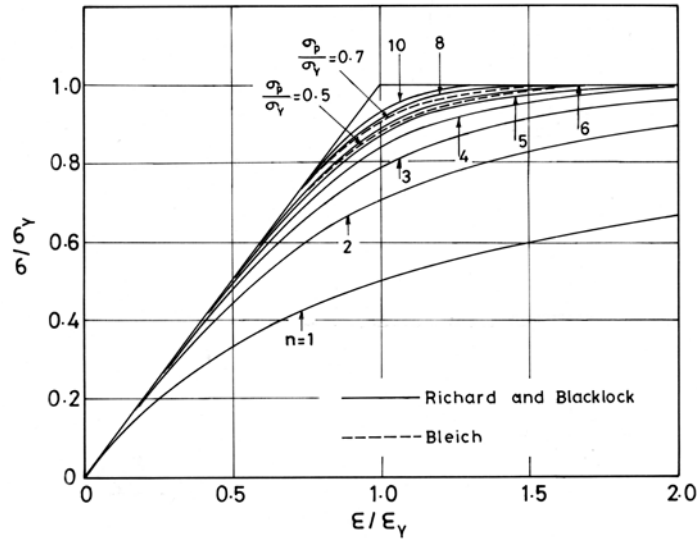
Fig.4.2 Stress-strain relationships.

2) Reduced coefficients of rigidities

The various reduced coefficients for the rigidities of isotropic plates in the inelastic region have been proposed[31]. If it is considered that only the stress in the x-direction is applied to the orthotropic plate, the following Bleich's approximation for the isotropic plate may be adapted:

$$\tau_x = \tau_w, \tau_y = 1, \tau_{xy} = \sqrt{\tau_w}, \tau_1 = \sqrt{\tau_w}, \tau_{bb} = \tau_{cw} = \tau_f, \tau_{cb} = \sqrt{\tau_f}.$$ (4.21)

4) Rigidities as orthotropic plates

The various methods for calculating the equivalent rigidity of the web plate with multiple stiffeners as an orthotropic plate have been proposed in regard to the case of equally spaced stiffeners. However, the web plates are usually reinforced by equally spaced transverse stiffeners and unequally spaced longitudinal stiffeners. The approximation at the former article is used too.

Critical Moment. - The critical moment M_{cr} can be calculated by

$$\frac{M_{cr}}{M_Y} = \frac{6}{1+6F/bh}\left[-\frac{F}{bh}(\overline{\sigma}_x)_{\eta=0} - \int_0^{0.5}\overline{\sigma}_x(1-2\eta)d\eta\right]\frac{E\varepsilon_0}{\sigma_{YF}},$$ (4.22)

where M_Y is the so-called flange yield moment given as

$$M_Y = \sigma_{Yf}(b^2 h/6)(1 + 6F/bh),\qquad\qquad (4.23)$$

In the preceding discussion, it was assumed that the neutral axis remains unmoved. Nevertheless, the present theory can be expanded for the case that the neutral axis is movable.

3.4.3 Numerical results and considerations

For the case of SM570 steel, taking $\sigma_{YW}= \sigma_{YF}$ =460.9MPa and the nonlinear parameter n=5, the numerical computations were carried out by using a mesh, n_s=40.

The effects of the rigidities of the orthotropic plate D_x, D_y, and $2D_{xy}$, the aspect ratio a/b and depth-to thickness ratio b/h of the web plate on the coupled buckling moment are examined. If the cross section of the flanges is rectangular, width c and thickness t, there are two independent parameters: the width-to-thickness ratio of flange c/t and the ratio between the cross-sectional areas of flange and web plate F/bh.

1) Coupled buckling loads

The critical moments are plotted versus a/b in Fig. 4.3. It is obvious from this figure that the critical moment is affected significantly by the value of a/b. The buckling modes are shown in Fig. 4.4, from which it is found that the torsional buckling of compressive flange and the bending buckling of web plate are coupled for the small value of a/b, curve ①, while the lateral buckling of compressive flange is dominant for the large value of a/b, curve ③.
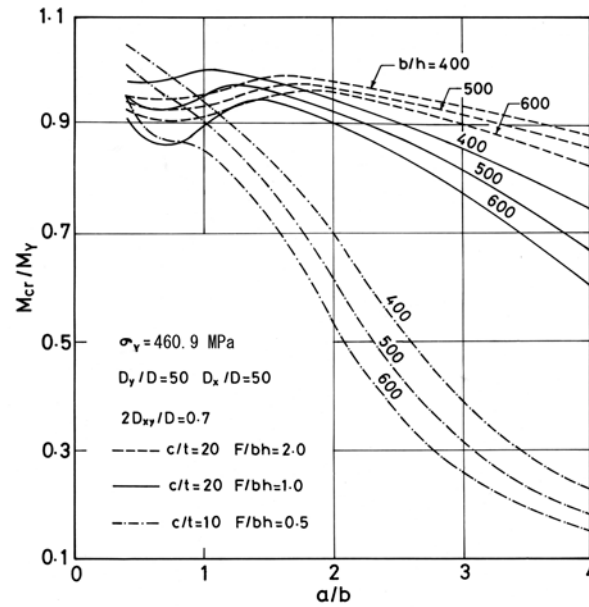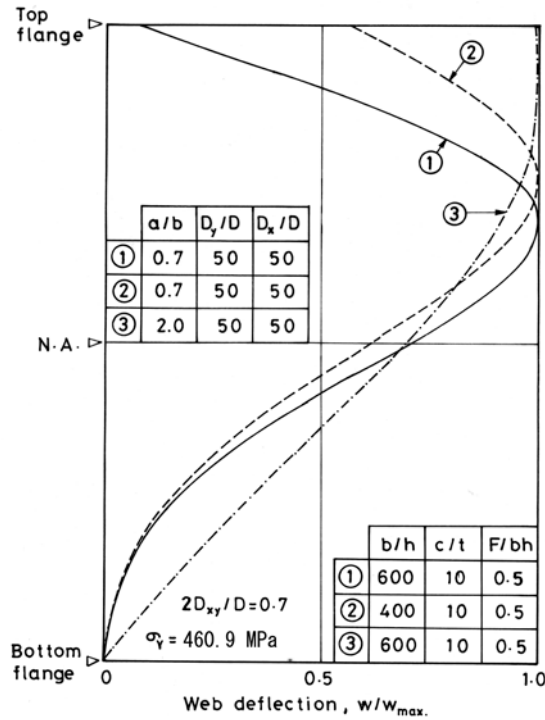

Fig.4.3 Buckling moment curves.

Fig.4.4 Buckling modes.

It is also seen from Fig. 4.3 that the critical moment decreases as the value of b/h increases, and from the comparison of curve ① with curve ② in Fig. 4.4 it becomes clear that the deformation of thin web plate grows.

The relation between the flange rigidity and the girder critical moment is shown for the web plates of $a/b=1$ and 2 in Figs. 4.5 and 4.6, respectively. The theoretical buckling modes for several cases are plotted in Fig. 4.7. It may be seen from Figs. 4.5 and 4.6 that the critical moment increases according to the increase of either D_x or D_y, or both, and however if the values of D_x and D_y exceed each limiting value the critical moment is almost constant.

These limiting values may be estimated from Fig. 4.5 as follows: in the case of the flange with the smallest flexural rigidity, plotted by the dot-dash-line, the buckling load does not remarkably increase as the increase of D_y if the value of D_x/D lies between 150 to 200, and however the large rigidity of D_x makes the critical moment increase gradually. It is obvious from comparison of curve ① with curve ② in Fig. 4.7, that if the longitudinal stiffeners have large rigidity, the deformation of the web plate is restricted and the bending strength of girders can be almost determined by the lateral buckling.

In the case of the flange with the intermediate flexural rigidity, plotted by the solid line in Fig. 4.5, if the rigid transverse stiffeners of D_y/D=500 are attached, the longitudinal stiffeners with the comparatively small rigidity of D_x can be adopted, while the limiting value of D_x increases considerably according to the decrease of rigidity D_y. In the last case of the flange with the largest flexural rigidity, plotted by the broken line, if the value of D_y/D is over 500, the limiting value of D_x becomes very

small. However, as the value of D_y decreases, the limiting value of D_x increases rapidly, and thus it seems that the suitable rigidity of transverse stiffeners must be chosen.

This fact is evident from the comparison between the two buckling modes ③ and ④ in Fig. 4.7.

Consequently, it is found that the limiting values of D_x and D_y are influenced by the web aspect ratio, a/b, the web depth-to-thickness ratio, b/h, and the flange flexural rigidity, B_b, and then according as these values the suitable combination of D_x and D_y must be chosen. For example, in the case that $a/b=1$
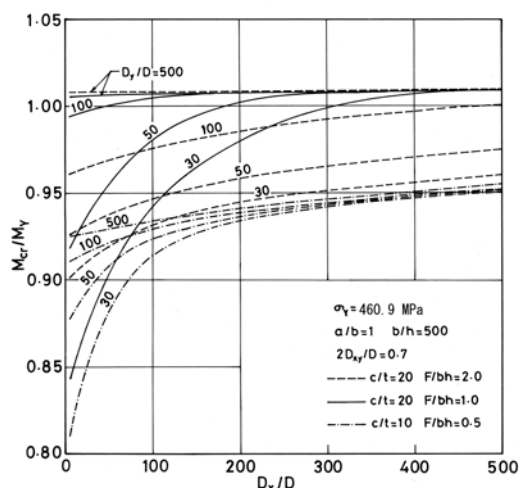
Fig.4.5 Effect of flexural rigidity of stiffeners on buckling moment.
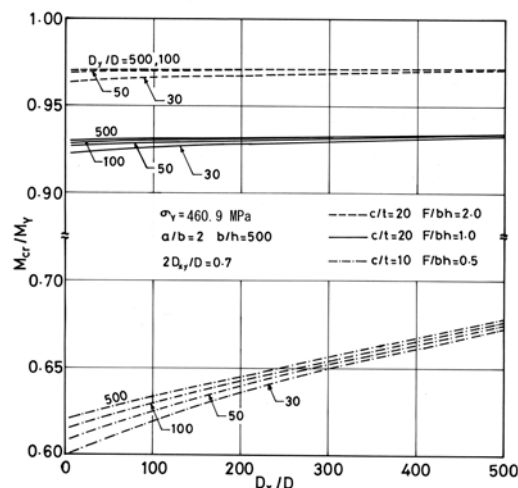
Fig.4.6 Effect of flexural rigidity of stiffeners on buckling moment.

And $b/h=500$, there is the limiting value of D_y/D from 200 between 300 for $D_x/D>50$. When the flexural rigidity of the flange is large, the considerable large value of D_y is required in order to maximize the bending strength of the girder.

2) Torsional rigidity of stiffeners

The influence of the torsional rigidity of stiffeners $2D_{xy}/D$ on the buckling load was numerically discussed: for example, in the case of $a/b=0.4$, the relation between $2D_{xy}/D$ and M_{cr}/M_Y is shown in Fig. 4.8. In the case of $D_y/D=30$ and $D_x/D=5$, the critical moment M_{cr}/M_Y increases slightly, about 1.0 to 1.6%, according as the value of $2D_{xy}/D$ increases. Moreover, it is found that there is no difference between the theoretical buckling modes for two cases of $2D_{xy}/D=1.0$ and 0.7. The buckling loads of the girder with $D_x/D=50$ and $D_y/D=50$ is hardly influenced by the torsional rigidity of stiffeners. Therefore, it seems that the torsional rigidity of ordinarily used stiffeners can be ignored.

Fig.4.7 Buckling modes.

Fig.4.8 Effect of torsional rigidity of stiffeners on buckling moment.

3) Buckling loads of web plate alone

The bending strength of the stiffened web plates of box girders will be discussed herein: the critical moment* of the web plate alone, of which the compressive edge is simply supported or fixed and the tensile edge is simply supported, was calculated as

63

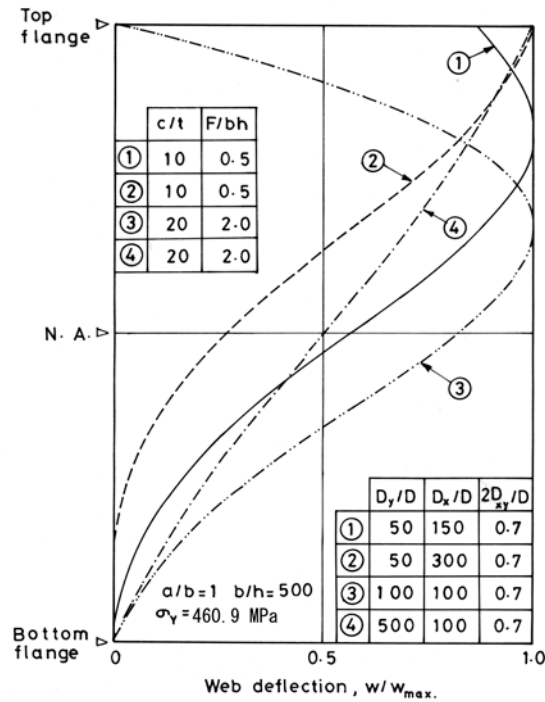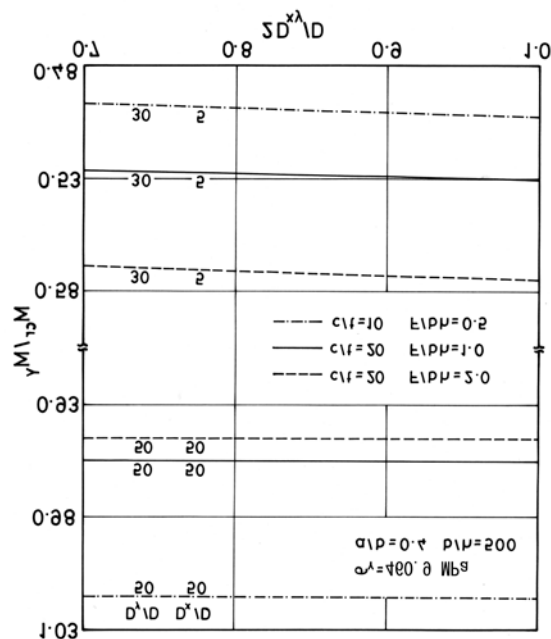shown in Figs. 4.9 to 4.11. From Fig. 4.9 it is seen that as the web depth-to-thickness ratio b/h increases, the minimum critical moment decreases and the influence of the restraining condition by the compressive flange becomes large.

Figure 4.10 shows the relation between the rigidities of longitudinal and transverse stiffeners and the minimum critical moment of web plate alone. The critical moment increases considerably according as the increase of the rigidity of stiffeners, in particular, of the longitudinal stiffeners in the case of the fixed compressive edge.

Let us estimate the limiting value of D_x. In the case of the fixed compressive edge, the limiting value of D_x/D seems to be 150 to 200. In the case of the simply supported edge, the limiting value of D_x is affected by the value of D_y and becomes very large for the small value of D_y.

Figure 4.11 shows how the minimum critical moment of stiffened plates varies with the values of D_x and D_y. As the plate becomes thin, the limiting value of D_x increases considerably, and is not influenced by the ratio b/h for the large value of D_y. Consequently, it is necessary to consider on the proper combination of D_x and D_y according to the value of b/h.

[* In Eqs.4.22 and 4.23, taking F=0]
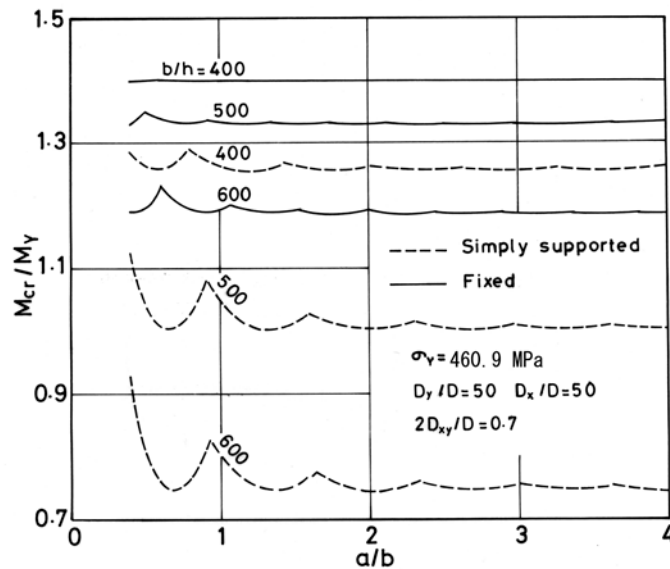
Fig.4.9 Buckling moment curves for stiffened web plates.
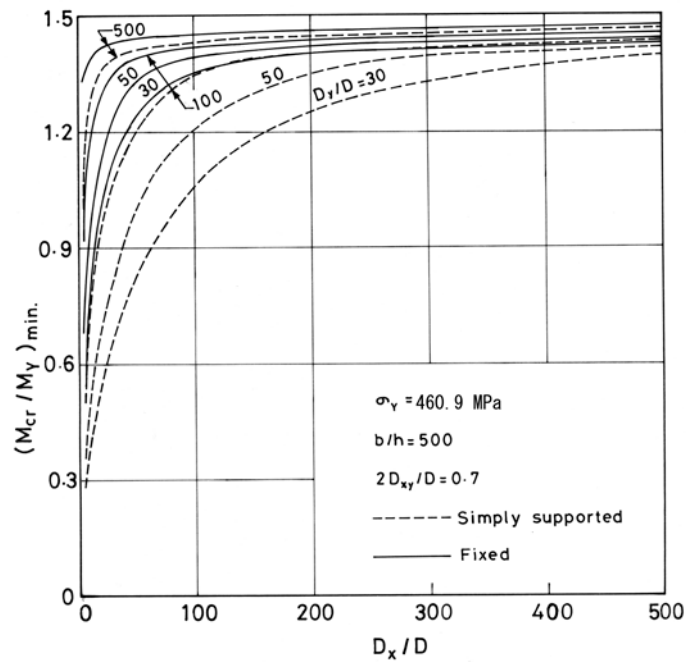
Fig.4.10 Effect of flexural rigidity of stiffeners on buckling moment.
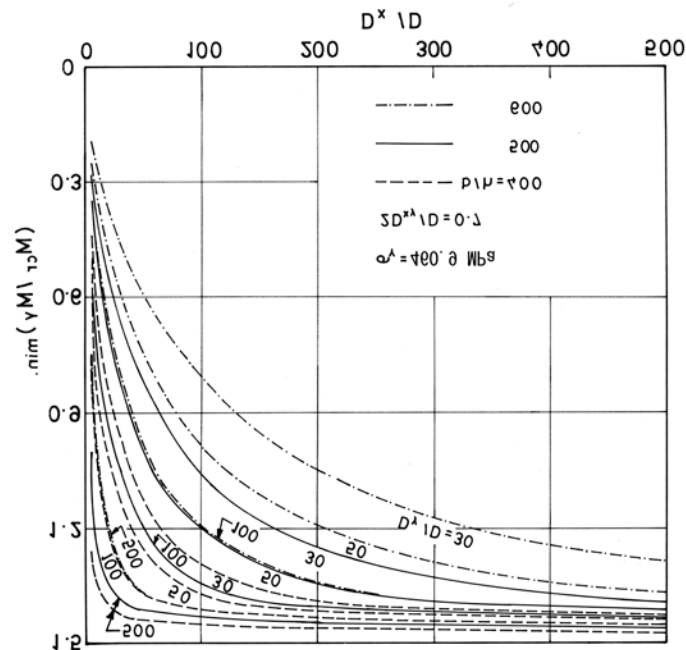
Fig.4.11 Effect of width-to-thickness ratio of web plate on buckling moment.

3.4.4 Comparison of numerical results with test data

In order to evaluate the present theory, the failure test result for a girder model whose web has the multiple longitudinal stiffeners[8] is referred to. As shown in Fig. 4.12, the model has the compressive flange reinforced by two corner plates and the web plate stiffened by seven longitudinal stiffeners with L-section. This model collapsed at the maximum moment 3,106 kN・m.

The compressive flange with the corner plates is converted into a rectangular flange with the same torsional and flexural rigidities. The stiffened web plate is replaced by an orthotropic rectangular plate with the equivalent rigidities.

The theoretical critical moment is obtained as 3,550 kN・m, which is about 14.3% larger than the experimental one. The overestimation seems to be due to the disregard for the yielding of the corner plates occurring at the moment of 2,402 kN・m. The theoretical buckling mode is shown in Fig. 4.13, and agrees well with the observed mode in the test.
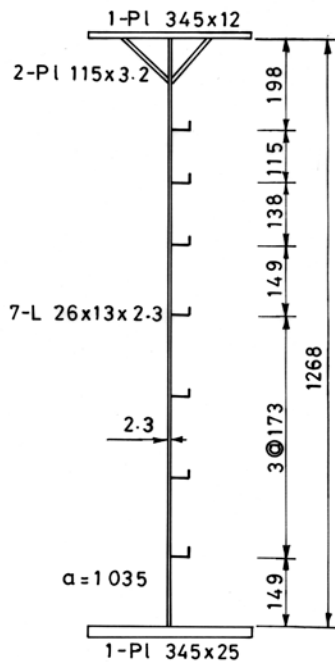
Fig.4.12 Dimensions of a girder tested by Yuhki et al.
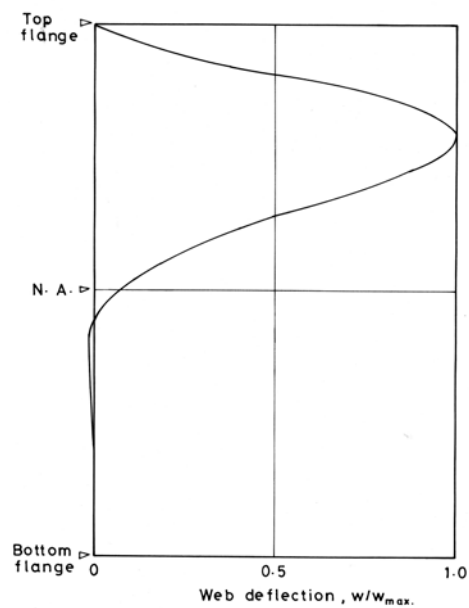
Fig.4.13 Theoretical buckling mode.

3.4.5 Conclusions

The bending strength of plate girders with web plate stiffened by multiple stiffeners has been analyzed as the inelastic coupled buckling of the compressive flange and web plate by using the orthotropic plate theory. The stiffened web plate was regarded as an orthotropic plate and the buckling moment was obtained by means of the finite difference method. The nonlinear stress-strain relationship by Richard-Blacklock was adopted and the reduced coefficients for the rigidities in the inelastic region by Bleich were adapted.

The influence of various parameters on the coupled buckling moment and the buckling mode were discussed as follows:

1) Although the buckling load increases according as the flexural rigidities of the longitudinal and transverse stiffeners increase, a limiting value of the rigidities can be found.

2) The limiting rigidity depends on the flange flexural rigidity, the web aspect ratio, and the web depth-to-thickness ratio.

66

3) The torsional rigidity of stiffeners has little effect on the buckling moment.

The bending strength of the stiffened web plates of box girders was also discussed. The effect of the flexural rigidity of stiffeners and the depth-to-thickness ratio of web plate on the buckling moment of stiffened web alone was examined.

The theoretical critical moment was compared with a failure test result on the girder model with multiple longitudinal stiffeners, and a sufficient agreement between both the values was observed.

3.5 Discussions

In order to realize long-span girder-bridges, web plates need multiple longitudinal and transverse stiffeners. Such multi-stiffened webs were investigated in this chapter.

The obtained results are as follows:
1) An expression for the equivalent rigidities to replace such multi-stiffened web with an orthotropic plate was given. And the usefulness of it was verified.
2) An approximate calculation method to predict the bending strength of multi-stiffened plate girders was presented. It was clarified that this estimation was simple and useful method.
3) The bending strength of plate girders with multiple-stiffened web plates was analyzed as the inelastic coupled buckling of the compressive flange and web plate by using the orthotropic plate theory. The effect of various parameters on the coupled buckling moment and the buckling mode were investigated.

The following subjects must be settled as future studies.
1) It is supposed that approximate prediction method on the bending strength of multi-stiffened plate girders is plain and proper. But the applicability of this method must be taken notice of. Consequently, it is considered that the further comparison of the calculated results with the experimental results is required.
2) The reduced coefficients for the rigidities in the inelastic region by Bleich were used for the calculation on the bending strength of plate girders. Hereafter, the validity of these reduced coefficients should be confirmed by means of some way, for example, finite element method.

3.6 References

1) Richmond, B.: Approximate buckling criteria for multi-stiffened rectangular plates under bending and compression, Proc. ICE, Vol.20, pp.141-150, 1961.
2) Giencke, E.: Uber die Berechnung regelmassiger Konstruktionen als Kontinuum, Stahlbau, Jg.33, 1964. H.1, s.1～6, und H.2, s.39-48.
3) Draft BS5400: Steel, Concrete and Composite Bridges, Part 3: Code of Practice for Design of Steel Bridges, British Standard Institution, London, 1979.
4) Specifications for Highway Bridges, Japan Road Association, 1994.
5) Dowling, P. J. et al.: Experimental and predicted collapse behaviour of rectangular steel box girders, Steel Box Girder Bridges, ICE, London, pp.77-94, 1973.
6) Dowling, P. J. et al.: The effect of shear lag on the ultimate strength of box girders, Steel plated Structures, ed. By P. J. Dowling, J. E. Harding and P. A. Frieze, Crosby Lockwood Staples, pp. 108-141, 1977.

7) Dibley, J. E. et al.: Experimental behaviour of a two-span continuous box girder, Steel Box Girder Bridges, ICE, London, pp.119-130, 1973

8) Yuhki, K., Matsusita, S., Ando, K. and Kawai, Y. ：A test on ultimate strength of plate girder with longitudinal stiffeners, Preliminary Reports of 27th Annual meeting, JSCE, Oct., 1972(in Japanese).

9) Mikami, I. et al.: Inelastic coupled buckling of steel box girders under bending, Proc. of JSCE, No.301, pp.23-36, 1980(in Japanese).

10) Mikami, I., Dogaki, M. and Yonezawa, H.: Ultimate load tests on multi-stiffened steel box girders, Technology Report of Kansai Univ., No.21, pp.157-169, 1980.

11) Niwa, Y., Watanabe, E. and Nishigome, A.: A study on shear ultimate capacity of box girder webs with multi-stiffeners, Preliminary Report of Annual Meeting, Kansai Branch of JSCE, June, 1979.

12) Mikami, I. et al.: A test on ultimate strength of multi-stiffened plate girders in bending, Technology Reports of Kansai Univ., No.22, pp.149-161, 1981.

13) Galambos, T. V.: Guide to Stability Design Criteria for Metal Structures, 4th ed., John Wiley & Sons, 1988.

14) Owen, R. et al.: Ultimate load behaviour of longitudinally reinforced webplates subjected to pure bending, Publ. IABSE, Vol.30-I, pp.113-148, 1970.

15) Fujii, T. and Akita, Y.: Minimum weight design of structures based on buckling strength and plastic collapse (2nd report), Jour. of Society of Naval Architects of Japan, No.120, pp.22-48, 1966(in Japanese).

16) Mikami, I. Dogaki, M. and Takeda, H. ：An approximate method for ultimate strength of steel box girders, Proc. of JSCE, No.298, 1980 (in Japanese).

17) Konishi, I., Yonezawa, H. and Mikami, I.: Elastic Buckling of Plate Girders under Pure Bending, Proc. JSCE, No.143, 1967 (in Japanese).

18) Gerard, G. et al.: Handbook of Structural Stability, Part I-Buckling of Flat Plates, NACA Technical Note 3781, 1957.

19) Basler, K. et al.: Strength of Plate girders in bending, Proc. ASCE, Vol.87, No.ST6, pp.153-181, 1961.

20) Fukumoto, Y. et al.: An experimental review of lateral buckling of beams and girders, International Colloquium on Stability of Steel Structures, Washington, D. C., May, 17-19, 1977.

21) Mikami, I.: A study on buckling of thin-walled girders under bending, thesis presented to Nagoya University, in 1972, in partial fulfillment of the requirements for the degree of Doctor of Engineering (in Japanese).

22) Hasegawa, A., Nishino, F. and Okumura, T.: Static tests on longitudinally stiffened plate girders in bending, Proc. of JSCE, No.234, 1975(in Japanese).

23) Maeda, Y.: Ultimate static strength and fatigue behaviour of longitudinally stiffened plate girders in bending, Proc. Of Colloqium on Design of Plate and Box Girders for Ultimate Strength, IABSE, Report, Vol.11, March 1971.

24) Fukumoto, Y. et al: Ultimate strength of longitudinally stiffened plate girder due to lateral buckling, Proc. of JSCE, No.220, 1973(in Japanese).

25) Lew, H. S. et al.: Static tests on hybrid plate girders, Welding Journal, Vol.48, No.2, 1969.

26) Mikami, I. and Yonezawa, H.: Inelastic buckling of plate girders with transverse

stiffeners under bending, Technology Reports of Kansai Univ., No.24, 1983.

26) Bleich, F.: Buckling Strength of Metal Structures, McGraw-Hill, New York, 1952.

27) Hsu, T. R. et al.: Improved approximation of constitutive elastoplastic stress-strain relationship for finite element analysis, Jour. AIAA, Vol.12, No.10, 1974.

28) Ramberg, W., et al.: Description of stress-strain curves by three parameters , NACA TN, 1943.

29) Betten, J.: Zum Traglastverfahren bei nichtlinearem Stoffgesetz, Ing. Arch., Vol.44, No.3, 1975.

30) Richard, R. M., et al.: Finite element analysis of inelastic structures, Jour. Of AIAA, Vol.7, No.3, 1969.

31) Column Research Committee of Japan: Handbook of Structural Stability, Corona Publishing Company, Tokyo, 1971.

Chapter 4

Load-carrying capacity of girders in shear

4.1 General description

It has been proved that the load-carrying behavior of a plate girder in shear consists of three components of response.[9] The load owing to the beam-action of the girder can be evaluated from the shear buckling stress of the web panel. After the shear buckling the behavior in the post-buckling range of the web panel is characterized by the diagonal tension field action. The load-carrying capacity due to the tension field in this stage may be remarkable in the case of the girders with a thin web plate. Basler is a pioneer in the study on the shear strength of plate girders[5),13)]. His ultimate shear model has involved the assumption that the flanges of most plate girders may be unserviceable as an anchorage for the tension field because of poor rigidity. After his formulation many tension field theories have been developed. Most of them take account of the effect of the flexural rigidity of the flange. Namely, the tension field in the plate girder with slender webs and transverse stiffeners is anchored by the flanges and stiffeners. Accordingly, the tension field is influenced by the flexural stiffness of the flanges. If the stiffness of the flanges is large, the yielded zone of the web extends over the entire panel. A frame mechanism with plastic hinges is formed. The additional shear loads are supported by this frame action.

The loading tests on the ultimate shear strength of plate girders have been considerably conducted. And various ultimate strength models have been verified experimentally. The comparisons of predicted shear strengths with the test results have been much reported.

Some numerical analyses for the load-carrying behavior of plate girders in shear by means of a finite element method have been conducted with the development of digital computers.[14)-18)] Especially, Nakazawa et al. have presented the results in detail on the shear strength behavior of girder panels by elasto-plastic finite element displacement analysis.[16),17)] In such numerical analyses the modeling of a structural subject is extremely important.

Plate girders are used not only in equal web depth but also in tapered web depth. The works for the ultimate strength of the panels with variable depth are required.[9] However, there are a few ultimate strength investigations on such girders. Falby and Mandal et al. have examined the shear strength of the plate girders with tapered web panel theoretically and experimentally[6),7),19)].

In this chapter, the load carrying capacity and behavior of girder panels subjected in shear will be investigated experimentally and theoretically. The results obtained by the modal analyses, elasto-plastic finite element displacement analyses and experimental works will be given in respect to the girder with equal web depth. Further, the results obtained by the modal analyses and tests will be presented as regards the girder with linearly varying web depth.

4.2 Load-carrying capacity of girders with uniform depth in shear

4.2.1 Experiments on girders in shear

(1) Introduction

There have been many experimental studies on the ultimate strength of plate girders subjected to shear force.[9] Various models to predict the shear strength of plate girders have been also formulated.[9] Although these methods can estimate the ultimate shear strength of plate girders, the process of the post-buckling behavior cannot be known. In order to utilize effectively the post-buckling strength in design, the post-buckling behavior should be considered in detail. The post-buckling strength can be realized by the tension field action and the frame mechanism. It is supposed that the stiffness of these boundary members affects the post-buckling behavior. Therefore the relationship between the post-buckling behavior of the flanges and the shear strength should be sufficiently clarified.

In this article the post-buckling behavior of plate girders in shear are examined experimentally. In particular the influences of the rigidity with these boundary members on the post-buckling behavior is investigated. Furthermore, the characteristics in several proposed collapse models to predict the ultimate shear strength are discussed on basis of the experimental results.

(2) Description of tests

  (2.1) Models

Four models (Models US-1, US-2, US-3 and US-4) were tested. All models were made of SS400 steel.

The point of load application is indicated by a thick arrow in Fig.2.1. The shadowed portion in Fig.2.1 is testing panel and the web panel on the other side was properly stiffened to prevent it from failing earlier than the failure of the testing panel. The cross section of the web and flanges was the same through the length of each girder. The actual girder dimensions on the testing panel were measured. These measurements are summarized in Table 2.1. All girders were designed to have equal web aspect ratio. The thickness to depth ratio of the web panel for Models US-1 and US-2 was designed to be identical and Models US-3 and US-4 similar. All models were designed to have equal breadth of flanges. The flange thickness for Models US-1 and US-3 was designed to be identical and Models US-2 and US-4 similar.
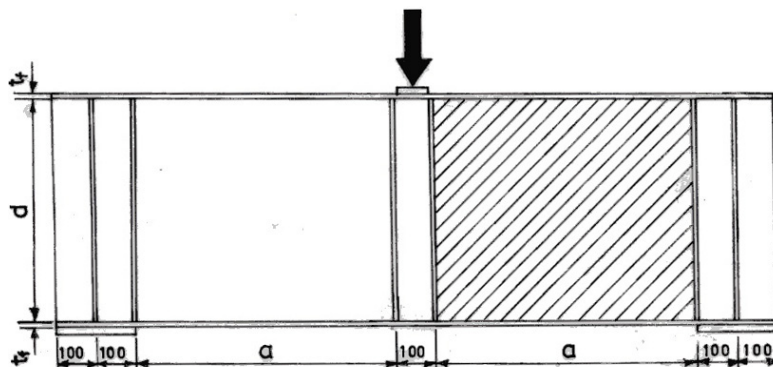

Fig. 2.1 Girder model.

Table 2.1 Measured dimensions of girders.

Model	US-1	US-2	US-3	US-4
Web length, a (mm)	627.6	649.0	393.8	393.6
Web depth, d (mm)	548.2	550.6	361.3	343.2
Web thickness, t (mm)	1.55	1.51	2.18	2.19
d/t	354	365	166	157
Flange width, b (mm)	90.7	89.8	90.7	89.8
Flange thickness, t_f (mm)	12.1	18.6	12.1	19.4

(2.2) Coupon tests

Coupon plates were cut from the same length of girder components to obtain tensile test coupons. The results of the coupon tests are shown in Table 2.2.

Table 2.2 Yield stress obtained by coupon tests.

Model		US-1	US-2	US-3	US-4
Yield stress, σ_Y (MPa)	Flange	284.4	225.4	284.4	225.4
	Web	290.3	290.3	278.9	278.9

(2.3) Test setup

Each girder was tested in the simply supported condition with roller supports at the ends. A concentrated load was applied to the girder at mid-span using an oil jack of the capacity of 294kN. To prevent any horizontal movement of the girders, the lateral supports were provided at mid-span. These supports consisted of a roller attached to a rigid frame bolted to the laboratory floor. Also the wings were attached to the bearing stiffeners to prevent the distortion of the girder.

(2.4) Instrumentation

Dial gauges and electrical displacement transducers were used to observe the deflection on each girder. To measure the out-of-plane deflection of the web plate relative to the boundaries, a frame that was clamped to the bearing stiffeners was used. Dial gauges were mounted underneath the tension flange to observe the vertical girder deflection. The horizontal and vertical deflections of the top flange were observed by cathetometers.

Electrical resistance strain gauges, with uni-axial and rosette types, were used on each girder. Measurements of the strains were taken on both faces of the girder components. Namely, by placing identical strain gauges opposite each other (at each side of the web, flange and stiffener), it was possible to separate membrane and bending strain.

(2.5) Testing procedure

After each model was set up, the eccentricity of the load application point was adjusted and initial out-of-plane deflection of web plates were measured. The maximum initial deflection on web for each model is shown in Table 2.3. The value of the maximum initial deflection Model US-1 is large.

Table 2.3 Maximum initial deflection of testing panel.

Model	US-1	US-2	US-3	US-4
$w_{0,max}$ (mm)	6	3	3	2

The step-by-step loading procedure was used in each girder test. After the attainment of ultimate load the removal of load was conducted.

(3) Experimental results and considerations

  (3.1) Collapse mode at failure of girders

    All models after test are shown in Fig.2.2. The development of the tension field in the web panel and the formation of the plastic hinges in the compression and tension flange were observed. The capacity of the oil jack, 294kN, was not sufficient for the final failure of Model US-4.

US-1
        US-2
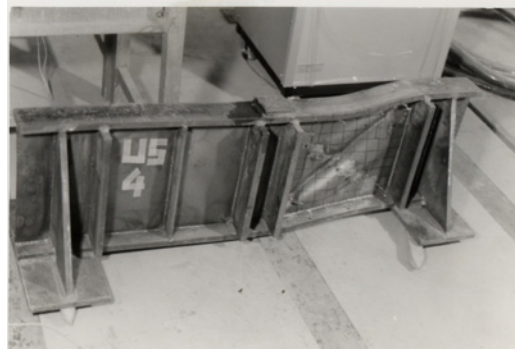
US-3
        US-4

Fig.2.2 Girders after tests.

  (3.2) Out-of-plane deflections of web panels

    The relative deflections of the web panels were measured at several points on each girder. The observed and theoretical buckling loads under shear are shown in Table 2.4. For the case in which the longitudinal edges of the web panel are fixed and the transverse edges of it are simply supported, the theoretical values agree well with the experimental results. The contour lines of the residual deflection in the web panel are illustrated in Fig.2.3. The inclination of the tension band in the web panel may be estimated from these figures.

Table 2.4 Shear buckling loads (kN).

Model		US-1	US-2	US-3	US-4
Experiment		22.6	27.5	125.5	126.5
Theory	S.S.	20.6	19.6	93.2	96.1
	Fixed	29.4	27.5	127.5	128.5

S.S.　：All edges are simply supported.

Fixed：Two edges are fixed.

Model US-1

Model US-2

Model US-3

Model US-4
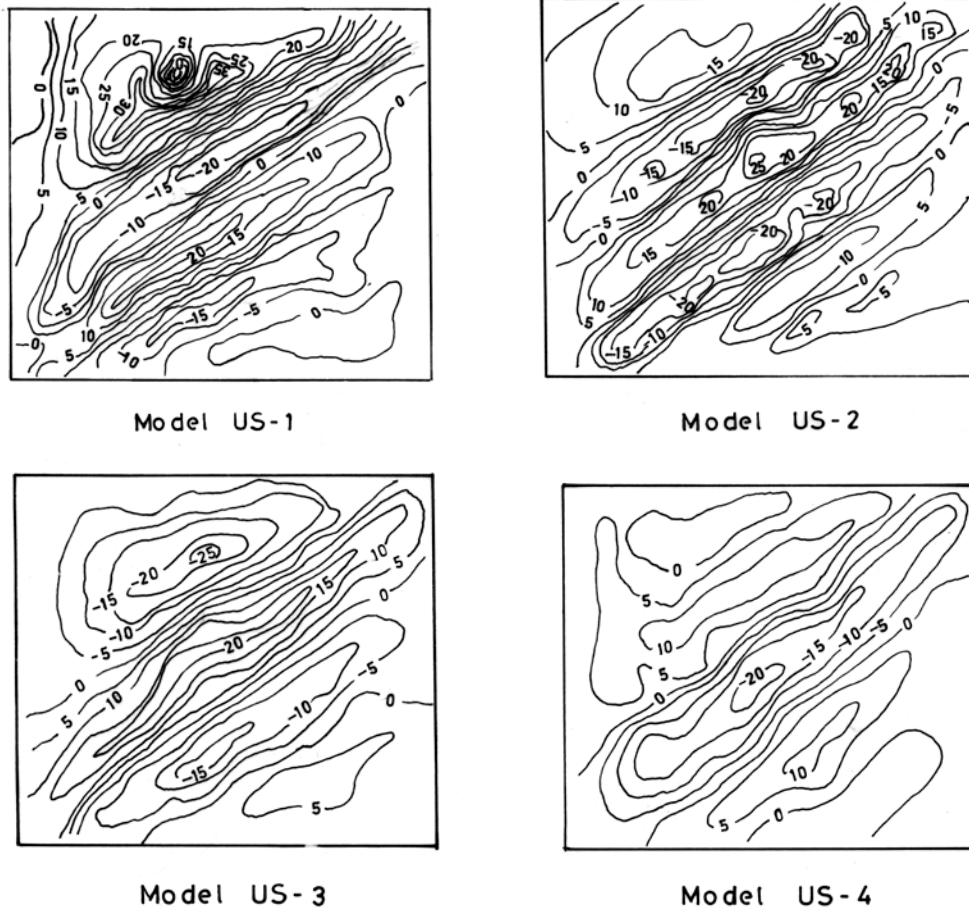
Fig.2.3 Residual web deflection (mm).

(3.3) Girder deflection

The central deflections of every girder are plotted with respect to applied loads in Fig.2.4. The load-central deflection relationship is linear up to about 80% of the collapse load for Models US-1 and US-3. In the case of Models US-2 and US-4, the load-central deflection relationship becomes nonlinear earlier and the deflection increases gradually for a while as the load increases. As the failure draws near the deflection shows a rapid rate of increase.
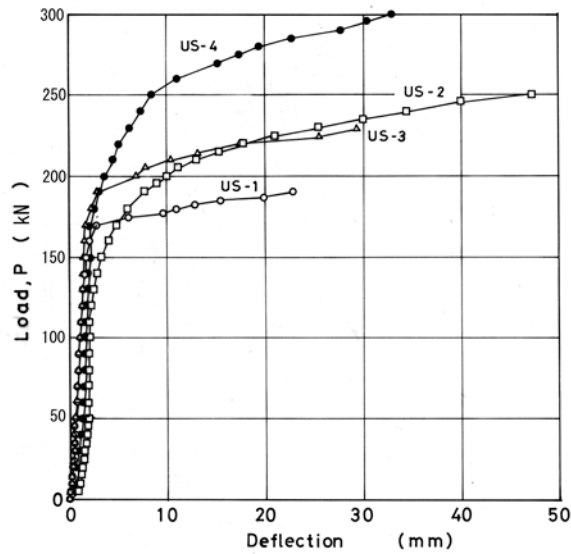
Fig.2.4 Central deflection.

(3.4) Vertical displacement of top flange

The relationship of load against vertical displacement of the top flange is shown in Fig.2.5. These observations were obtained by reading the movements of the marks on the top flange using cathetometers. The influence of web buckling on the vertical deflection of the flange may be observed in these figures for Models US-3 and US-4. It is found that from the comparison of the load-central deflection curve in Fig.2.4 with the load-vertical deflection curve of the flange in Fig.2.5 a similar tendency is shown for each girder. Therefore it is supposed that the dent of the top flange affects definitely on the girder behavior.
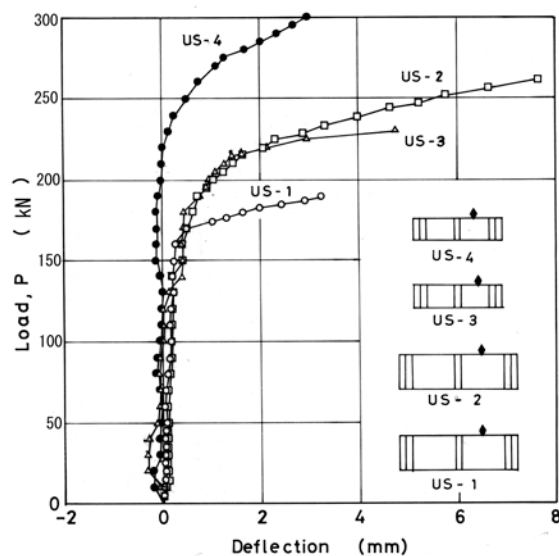
Fig.2.5 Vertical displacement of top flange.

76

(3.5) Strains of top flange

The bending strains and the longitudinal strains of the top flange have been plotted against various loads to form Figs.2.6 and 2.7, respectively. It should be noted that from the comparison of Fig.2.5 with Fig.2.6 when the maximum bending strain exceeds the yield strain of the flange material the dent of the top flange begins. Also it is found that from the comparison of Fig.2.5 with Fig.2.7 when the maximum longitudinal strain approaches the yield strain of the flange material the top flange is rapidly bended inward and the plastic hinge is formed. The collapse load is soon reached. But the longitudinal strains except for ones near the position of the plastic hinge have relatively small values and are almost uniformly distributed even when the collapse load is reached.
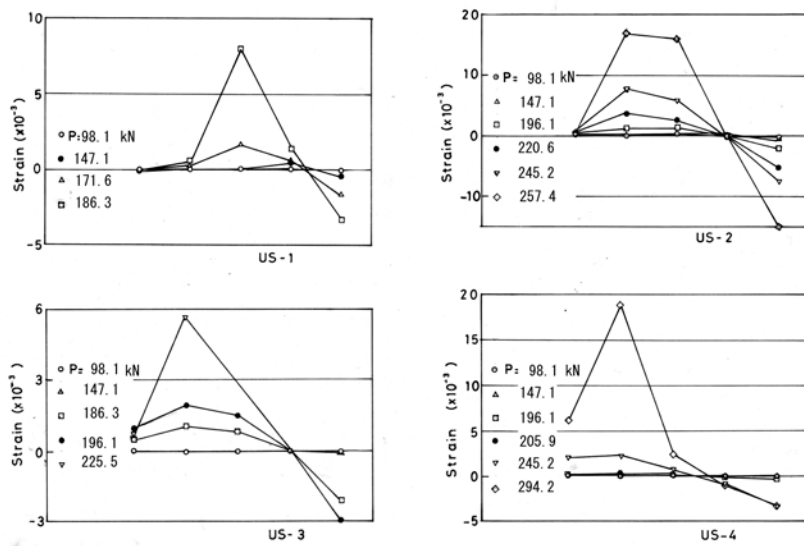
Fig.2.6 Bending strains of top flange.
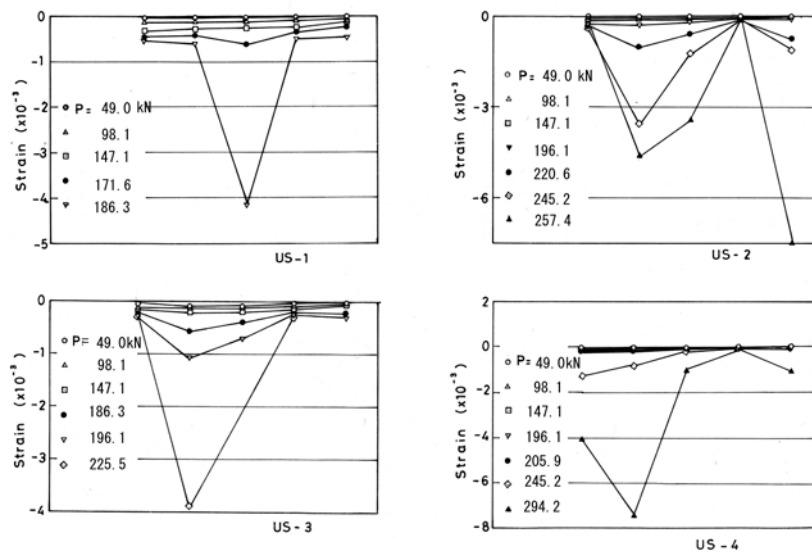
Fig.2.7 Longitudinal strains of top flange.

(3.6) Strains across tension band

The variation of the tensile strains acting at right angles across the diagonal AB of the web panel measured by the rosette gauges are shown against several applied loads in Fig.2.8. From this figure, the width of the tension band can be approximately estimated. It can be seen that from comparison Fig.2.5 with Fig.2.8 the maximum tensile strain almost reaches 10,000 micro strains when the dent of the top flange begins.
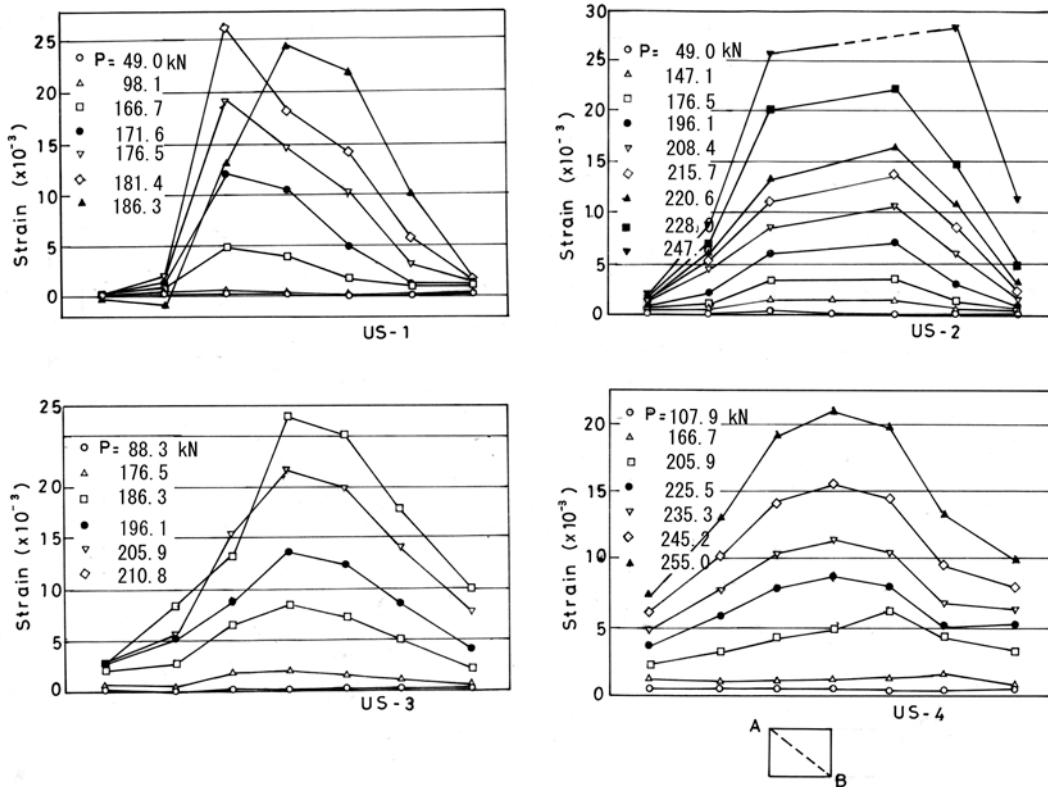
Fig.2.8 Strains across tension band.

(3.7) Distribution of principal stress

The distribution of the principal stresses of the web panel is shown in Fig.2.9 for each girder, where the numerical value is expressed as elastic body. It can be seen that the diagonal tension field develops with increasing load.

Fig.2.9 Principal stress distribution in web panel.

79

（3.8）Ultimate strength

The maximum shear loads, $P_{ult,}$ observed are shown in Table 2.5. Also in this table the value of V_{ult}/V_p for each girder is given, where V_{ult} is one half of P_{ult} and V_p is the full plastic shear force. As seen from this table and Fig.2.4, it is supposed that the increase of the flange stiffness raises certainly the ultimate shear strength due to the frame action.
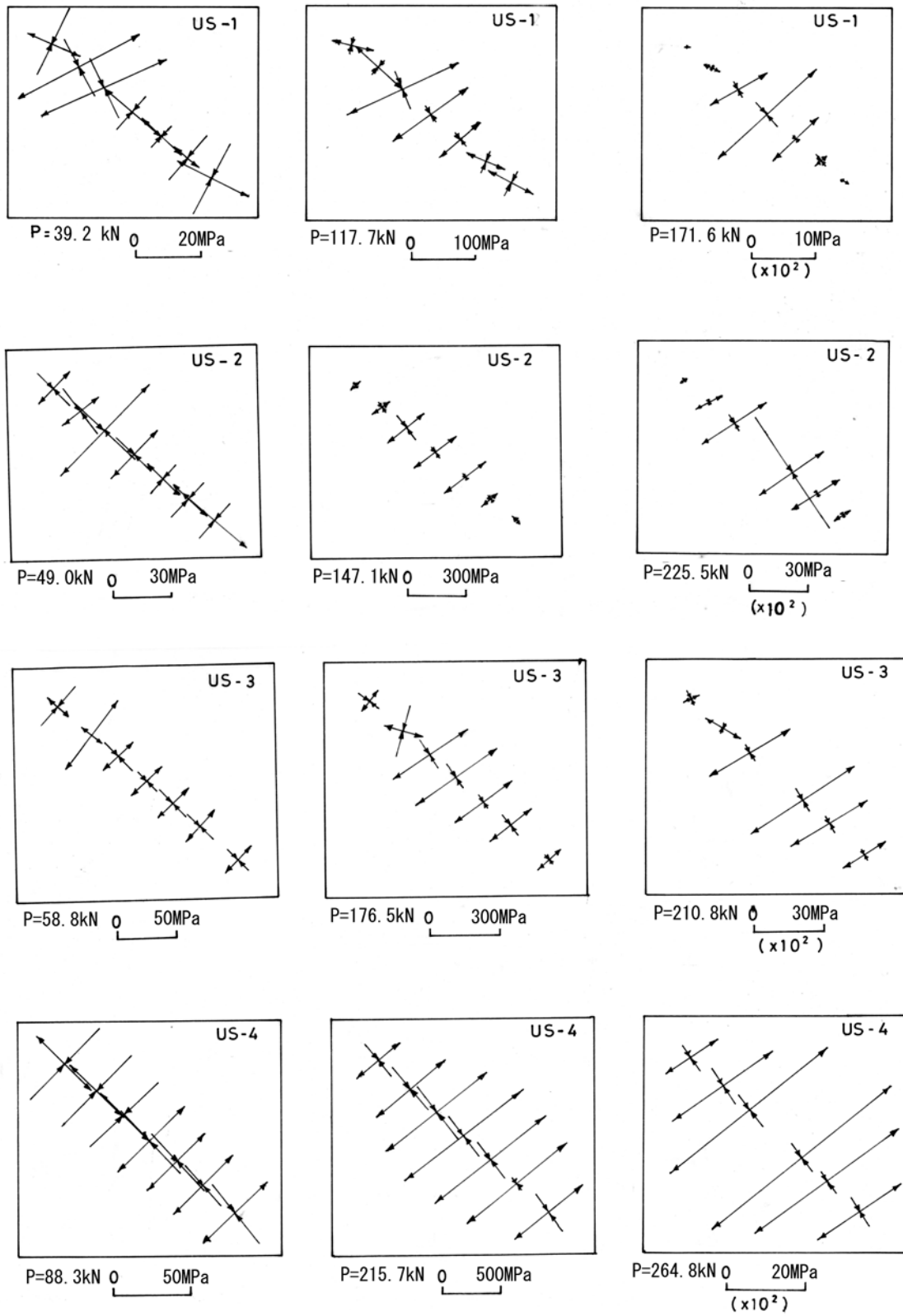
Table 2.5 Ultimate strength by tests.

Model	US-1	US-2	US-3	US-4
P_{ult} (kN)	186.3	257.9	229.5	above 294.2
V_{ult} / V_p	0.654	0.926	0.905	above 1.22

（4）Comparison of test results with estimated values

（4.1）Static limit state

It is extremely important how the static limit state is determined in the design of plate girders. The flanges must support a lateral loading from the tension field as it develops. According to the considerations in previous chapter, as soon as the maximum bending strain of the top flange exceeds the yield strain the dent of the top flange begins and the load-girder deflection relationship becomes nonlinear. At the same time the yielded zone spreads in the web extensively. If in the design of plate girders the yielding of web plate is permitted the arrival at the yield strain of the bending strain in the top flange may be considered as a static limit state.

（4.2）Prediction of shear strength

Many methods are presented which are capable of predicting the collapse load of plate girders in shear.[9] In this chapter three typical methods proposed by Basler[5], Rockey et al.[4] and Ostapenko et al.[10] are dealt with.

Gaylord discovered the mistake in Basler's formula and the correct formula was given later.[2] Basler's formula is surely mistaken and Basler assumed that the post-buckling strength was supported by only the web plate. Hasegawa et al. pointed out that the contribution to the post-buckling strength by the flanges was also contained in Basler's formula. [3] Therefore it is considered that the formula can take flange rigidity into consideration. It is supposed that in Basler's solution the equilibrium condition is applied before the deformation of the flanges becomes remarkable.

Rockey et al. assumed the formation of the plastic hinges in the flanges. Therefore it is supposed that in their solution the collapse model is formulated after the local deformation of the flanges becomes pronounced. A remarkable feature of Ostapenko's formula lies in its assumption on the diagonal tension band. The frame action contribution to the ultimate strength is also taken into consideration in this formula.

It must be considered that there are some differences among these theories in the estimation of the inelastic shear buckling stress. The comparison of the shear buckling stresses between Basler's and Rockey's methods is shown in Fig.2.10. As seen from Fig. 2.10, the values of the shear buckling stress in the inelastic range estimated by Basler's formula are higher than that by Rockey's formula. Ostapenko et al. assume that the web is fixed at the flanges and simply supported at the transverse stiffeners.

Table 2.6 gives comparisons of predicted shear loads with results of this test. The theoretical values estimated by Rockey's and Ostapenko's methods agree well with the experimental values for Models US-1 and US-3. It is supposed that Basler's formula gives the conservative results due to the collapse model as mentioned above for Models US-1 and US-3. For Models US-2 and US-4 having thick flanges, these formulas tend to considerably underestimate the shear strength. Besides it is insufficient that Rockey's formula cannot obtain the solution for Model US-4.

As stated above, a static limit state may be considered. It can be seen that on referring Fig.2.5 the shear strengths estimated by Basler's formula agree approximately with the shear forces that initiate at first the dent of the top flange. Therefore Basler's formula may be able to determine the static limit state as defined above.

Table 2.6 Comparison of experimental results with predicted ultimate loads (kN).

Models		US-1	US-2	US-3	US-4
Experiment		186.3	257.9	229.5	Above 294.2
Theory	Basler[5]	176.5	168.7	203.0	195.1
	Porter-Rockey-Evans[8]	180.4	201.0	227.5	—
	Ostapenko-Chern[10]	178.5	181.4	223.6	237.3
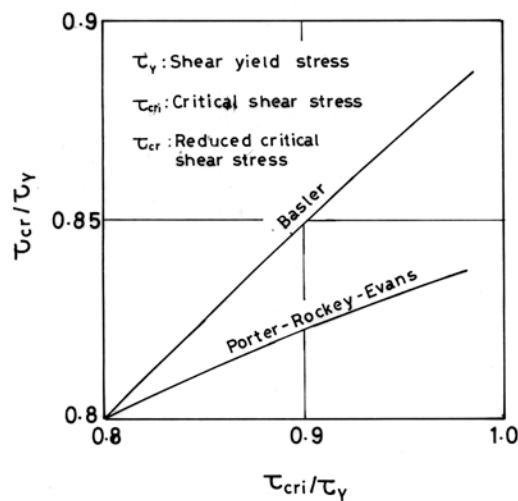
Fig.2.10 Buckling stress in inelastic range.

(4.3) Design of flanges

In order to examine the effect of flange rigidity upon the ultimate shear strength, the relationship between the ultimate shear stress at failure and the $I/a^3 t$ is given in Fig.2.11, where I=the flexural rigidity of the flange and the ultimate shear strength of Model US-4 is approximately regarded as 147 kN. The broken line in Fig.2.11 shows the experimental curves obtained from the tests carried out by Rockey et al. As the yielded region of the web spreads, the ultimate shear stress of the girders increases. But then the deformation of the flanges and the web becomes remarkable. Accordingly

although the large flange rigidity contributes to the increase of the ultimate shear strength of the girder, considering the limit state on the deformation as stated above it is supposed that the excessive increase of the flange rigidity is useless. However it is necessary that the flanges act sufficiently as the anchors of the tension field.

Fig.2.11 Variation of ultimate shear stress with flange stiffness.
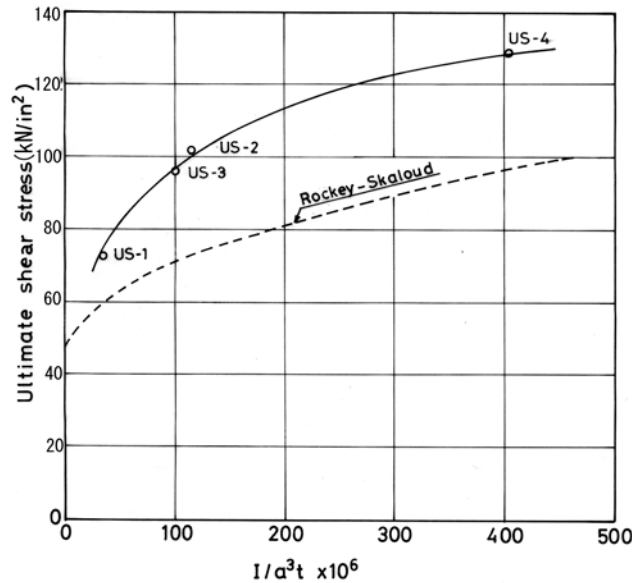
(5) Conclusions
Four models were tested to examine the ultimate strength and behavior of plate girders in shear. Subsequently the test results were compared with the ultimate shear strength estimated by several formulas.
Obtained results are as follows.
1) The flanges having the proper rigidity act as the anchors of the tension field.
2) When the maximum bending strain of the top flange exceeds the yield strain of the material the dent of the top flange begins and the load-girder deflection curve becomes nonlinear rapidly. Therefore it may be considered as a static limit state if the yielding of the web is permitted.
3) In the case of large flange rigidity the shear load increases relatively from the initiation of the dent of the flange to the failure of the girder. But the deformations of the flanges and web become considerable.
4) The shear strength predicted by Basler's formula gives the conservative value. But it is supposed that Basler's formula gives the value that corresponds to the static limit state as stated above.
5) Basler's formula comparatively underestimates the ultimate shear strength in the case of the girder with large flange rigidity. Also Rockey's and Ostapenko's formulas underestimate it and in some cases the solution cannot be obtained on Rockey's formula.

4.2.2 Elasto-plastic finite displacement analysis

(1) Introduction

The research on the static load-carrying capacity of the girder panel subjected to shear force has been carried out by various approaches.[9] The theoretical research can be divided into two methods. First, it is a method for predicting the load carrying capacity using plastic analysis model based on the assumption of the ultimate state. Another method is the elasto-plastic finite displacement analysis using means such as the finite element method by the development of digital computers. The material and geometric non-linearity must be considered, if a girder panel composed of thin plates is calculated by this method. This analysis is very complicated. As a leading research, that by Sawada et al.[14] is mentioned. Afterwards, Marsh[20], Nakazawa et al.[16),17)] and Lee et al.[21] carried out the elasto-plastic finite displacement analysis on the ultimate shear behavior of the plate girder panel using the finite element method considering both non-linearity, and the model for predicting the load carrying capacity was presented.   From the analytical result, Nakazawa et al.[16),17)] indicated that the flange did not bent and the plastic hinge did not occur in the ultimate state. This result is different from the existing experimental result and the assumption in modeling based on it. In addition, they asserted that the tension field is supported by gusset plate action due to the high biaxial stress state in the panel corner and it is formed without the anchor action by flange and stiffener. Recently, Lee et al.[21] indicated that the effect by bending owing to out-of-plane deformation on the yield condition was not considered, from the analytical result by Nastran programme. In addition, it is assumed that the shear strength is obtained as a sum of the buckling strength and the post-buckling strength, and he pointed out that there was almost no influence on the post-buckling strength due to flange rigidity and only buckling strength was different. And he tested for the verification of the theory.

In this article, the elasto-plastic finite element displacement analysis is carried out on a girder panel with equal depth under shear. As an analytical result, the ultimate shear strength and the behavior to the ultimate state of a girder panel are examined in detail.

(2) Analytical method (FEM)

In the analysis, the elasto-plastic finite element analysis that Komatsu et al.[22] developed was expanded so that it may be able to be applied to the girder panel.   A triangular finite element with 5 degrees of freedom on one node was used.
(2.1) Assumption on material
It is assumed that materials are as follows:
1) They are isotropic and homogeneous.
2) The yield condition by von Mises is followed.
3) The plastic flow rule by Prandtl-Reuss is followed.
4) The strain hardening is not considered.
(2.2) Assumption on displacement
Assumptions on the displacement are as follows:
1) The line element that is perpendicular to the neutral surface of a plate before

deformation is also similar after deformation.

2) In the beginning of each increment, the initial deflection composed of plane triangular element is given as initial shape.

(3) Analytical model

From a plate girder with vertical stiffeners, one panel surrounded by stiffeners and flanges is taken up. This panel is modeled for the analysis. As a result of examining beforehand convergence of a solution, eight divisions were adopted for a square panel in both directions. For a rectangular panel, number of subdivisions is made to increase in proportion to the aspect ratio. On the flange, the division in the longitudinal direction was made to be as well as the web, and the number of subdivisions in the direction of the width was taken as two. As the number of subdivisions in the direction of the thickness, eight divisions were adopted.

As an initial deflection of the web, sine half wave was assumed in both directions of length and width, and the maximum value was supposed to have 10% of the thickness. The residual stress is not considered. On the effect which initial deflection and residual stress give at shear strength, the experimental study by Fujino[23] is reported. That result shows that there is no effect as a difference.

The boundary condition was assumed as following. Though a separated panel must agree with the behavior of an actual girder as much as possible, it is difficult to realize this in the single panel only. Therefore, two kinds of modeling shown in Fig.2.12 were carried out. On the out-of-plane boundary condition, the simple support along all edges was assumed in both models. The in-plane boundary condition was assumed as following. As shown in Fig.2.12 (a), the displacement in the longitudinal direction is
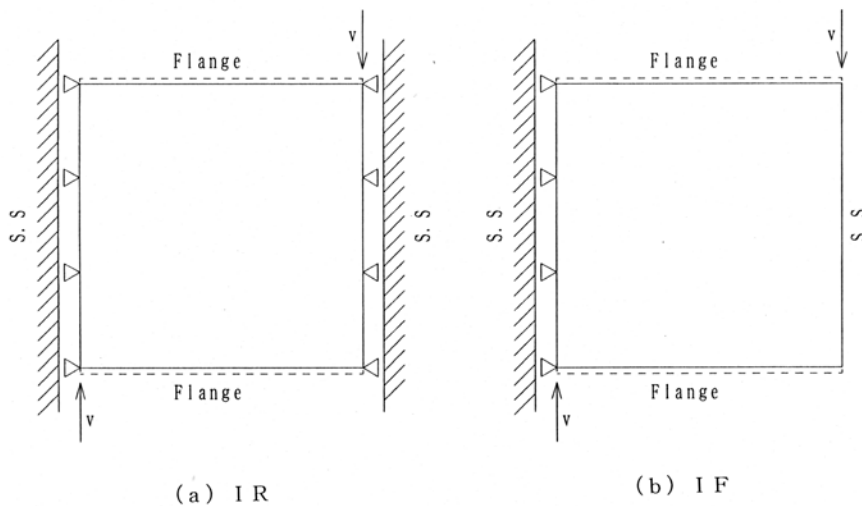

Fig.2.12 Analytical models.

restricted at the right and left edges of Model 1. This model will be called IR since then. In such model, it is supposed that the behavior is similar to that in the panel held between the adjacent panels. However, it is estimated that the longitudinal tension works owing to the restraint in the right end. In the case of this model, it seems to be

possible that the right and left edges work as anchors for the tension field. In the meantime, the in-plane displacement on the right edge for Model 2 is free as shown in Fig.2.12 (b). In this case, additional bending moments will occur in the left edge. This model will be called IF. The loading is given by the increment of displacement along the right and left edges as shown in Fig.2.12. Young's modulus E, Poisson's ratio v and yield point stress σ_Y are taken as 206GPa, 0.3, 235MPa, respectively. Shear yield point stress τ_Y is made to be $\sigma_Y/\sqrt{3}$. The following is chosen as parameters on the analysis: panel aspect ratio α, panel width-to-thickness ratio β and flange rigidity. Values of α are 1.0 or 1.6, and values of β are 100,150 or 200. On the flange rigidity, six types were set, and the above parameters were combined.

(4) Analytical results
.　 The value of each parameter for two kinds of aspect ratio (α=1.0 and 1.6) is shown in Table 2.7, where t_w, b, t_f, C, t_s and C_s show web thickness, web height, flange thickness, flange width, stiffener thickness and stiffener width, respectively. Values of width-to-thickness ratio in the web plate are as follows as shown by this table: 150 in case of 1,4 and 6, 100 in case of 2 and 5, 200 in case of 3.

　　Though the analytical results on Model 1 are mainly shown, those on Model 2 are also included for the comparison. Model 1 has the problem described before. However, the results on Model 1 are primarily given as it is supposed that this model shows well the behavior in the middle panel under shear force.

Table 2.7 Dimensions of models.

Case	1	2	3	4	5	6
t_w (mm)	5.0	7.5	3.75	5.0	7.5	5.0
b/t_w	150	100	200	150	100	150
t_f (mm)	20	20	20	10	10	5
C (cm)	30	30	30	30	30	15
t_s (mm)	25	25	25	13	13	7
C_s (cm)	25	25	25	25	25	20

(4.1)　 In-plane displacement behavior
　　The relationship between shearing stress τ and vertical displacement v is shown by Fig.2.13 on the case in which it is α=1 for different boundary conditions. The type of this model is IR. In the case of β=100, the load carrying capacity at the condition of fixed support is larger a little than that at simple support. However, it is proven that there is similarly very much no difference between the load carrying capacity owing to the difference between both boundary conditions for each case of β. Also, in each case the linear relationship is kept, until the ultimate state is approached. And the good deformability is obtained. From these figures, the difference between the load carrying capacity for different flange rigidity hardly is seen when β has the same value. There is a difference a little between the deformations for the case of small rigidity.
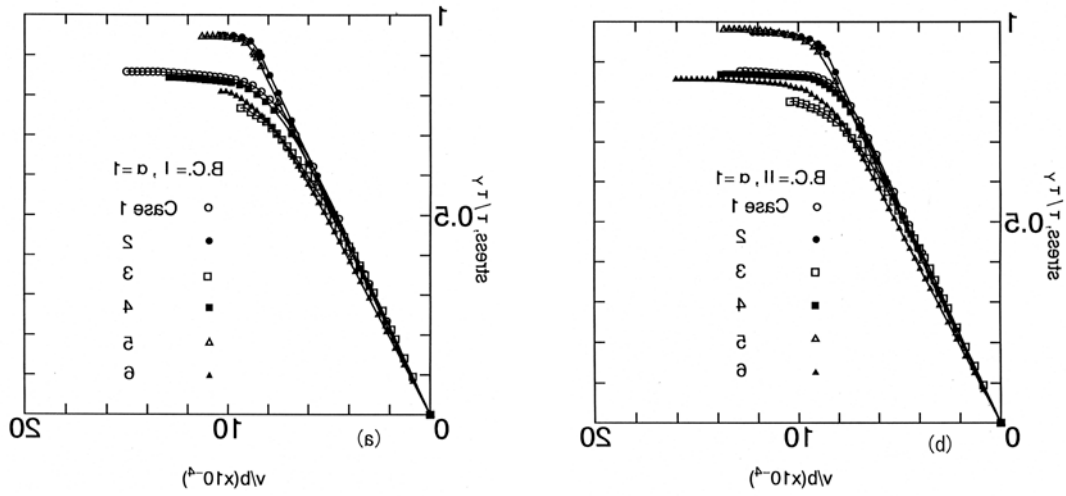
Fig.2.13 Vertical displacement vs. Shear stress.

The relationship between shearing stress and vertical displacement is shown in Fig.2.14 for the case of simply supported top and bottom edges when $\alpha=1.6$. In the case of $\beta=100$, there is hardly a difference between the behavior in both figures. However, the load carrying capacity for Model IF is low a little in the case of $\beta=200$ or 150 and low flange rigidity. Also, in the displacement there is a little difference. This seems to be a reason for describing in latter section.
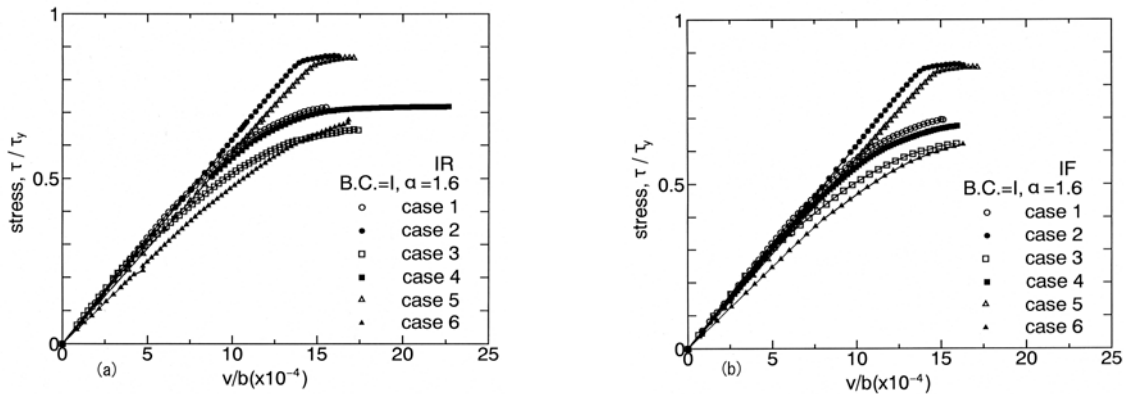
Fig.2.14 Vertical displacement vs. Shear stress.

The deformed shape of the outer frame in the maximum load is shown in Fig.2.15 for the case that $\alpha=1.6$, model type is IR, top and bottom edges are simply supported and the case number is 6. Though the flange thickness is relatively thin with 5mm, the deformation of the top and bottom edges is not conspicuous. As a deformation behavior of the panel, the shape of the parallelogram has been kept after the deformation as a whole.

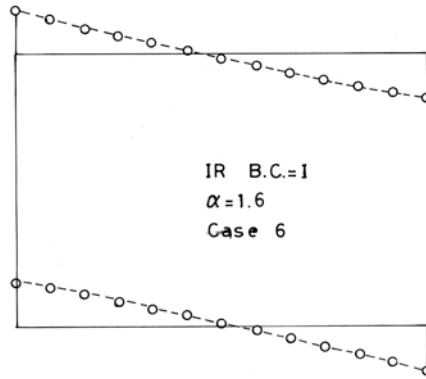Fig.2.15 In-plane deformation of web panel.

(4.2)   Out-of-plane deflection behavior

The relationship between shearing stress and out-of-plane deflection is given by Fig.2.16 for the case of the model type IR and α=1, where w_0, w and $(w+w_0)$ are initial deflection, additional deflection and totally out-of-plane deflection, respectively. When β=100, it is seen that the generation of tension field is not recognized and the ultimate state begins immediately after shear buckling as shown in this figure. However, it is proven that the load carrying capacity is greatly raised by the work of tension field after the occurrence of shear buckling, when β=150 and 200. In addition, it is noticed that there is very much no difference between the ultimate shear strength, though there is large difference between the shear buckling stress, by comparing the curve of B.C.=I with that of B.C.=II. It seems that this is because the development of the tension field after shear buckling differs. On the effect caused by the difference between the flange rigidity, there is very much no difference for the behavior, when the web panel has same width-to-thickness ratio.
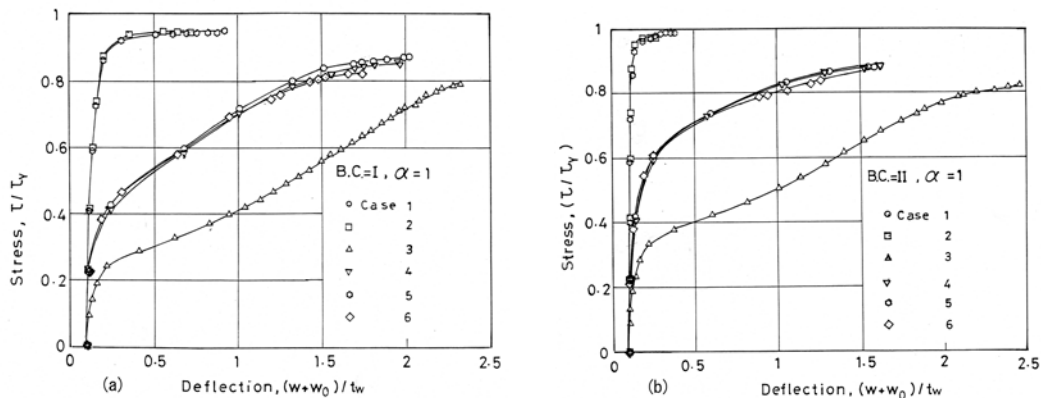

Fig.2.16 Out-of-plane deflection vs. Shear stress.

The effect in which the difference between IR and IF gives for the case of α=1.6 and the simply supported top and bottom edges is compared in Fig.2.17. On each corresponding case, there is very much no difference between the results of IF and

those of IR. The deflection for the case of model type IF is larger than that for the case of IR at the same shearing stress, as the degree of the restraint differs. In the case of model type IF, the effect due to flange rigidity is seen when $\beta=150$. It is considered that this is caused by the bending effect.
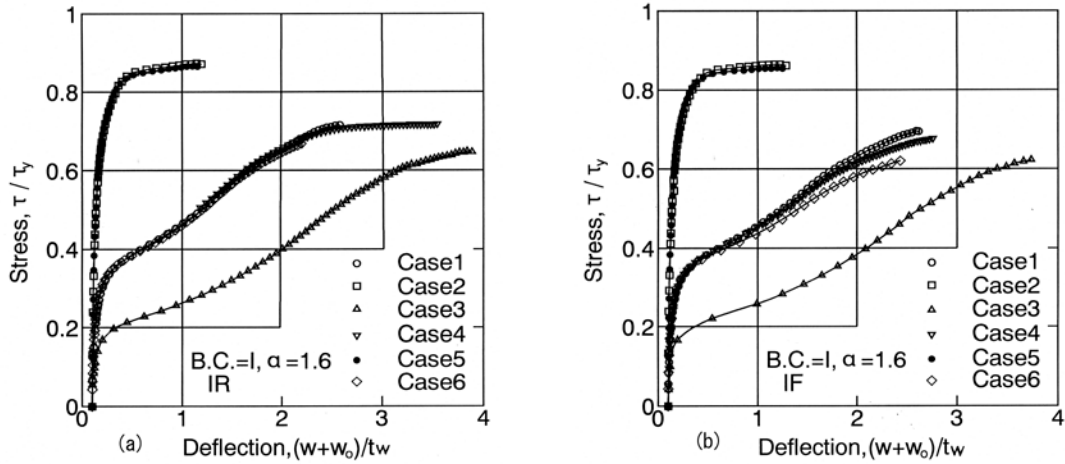

Fig.2.17 Out-of plane deflection vs. Shear stress.

Examples of out-of-plane deformation behavior of the web plate panel in the case of $\alpha=1$ are shown in Figs.2.18 to 2.20. Each first figure (a) shows the deformation immediately after shear buckling occurs, and each second figure (b) shows the deformation immediately before the ultimate strength is reached. In each case of 1 and 3, it is proven that the deflection band due to the progress of the tension field occurs. In the case of 2 in which web plate width-to-thickness ratio is 100, the band caused by the tension field is not viewed, though the value of the deflection increases. In addition, there is no very difference between the shape of (a) and (b), and the shape after buckling has been kept.
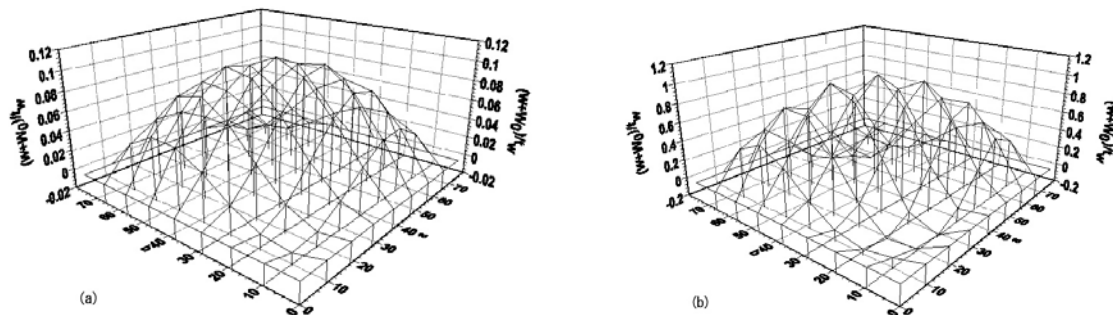

Fig.2.18 Out-of deformation of web panel (IR, B.C.=1, $\alpha=1$, Case 1).

88
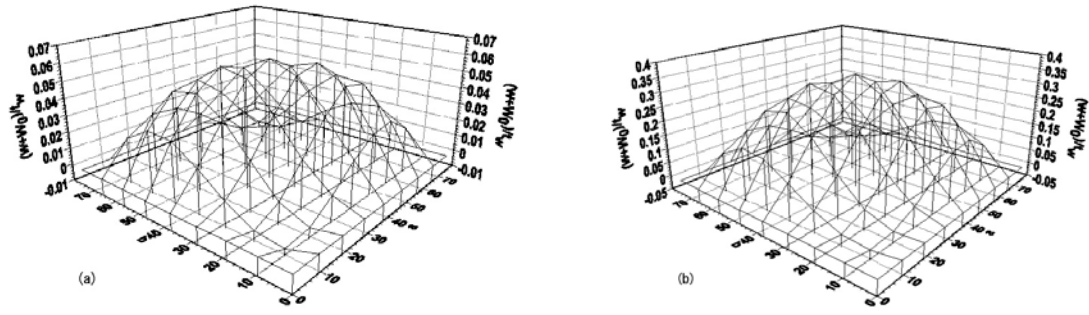
Fig.2.19 Out-of deformation of web panel (IR, B.C.=1, α=1, Case 2).
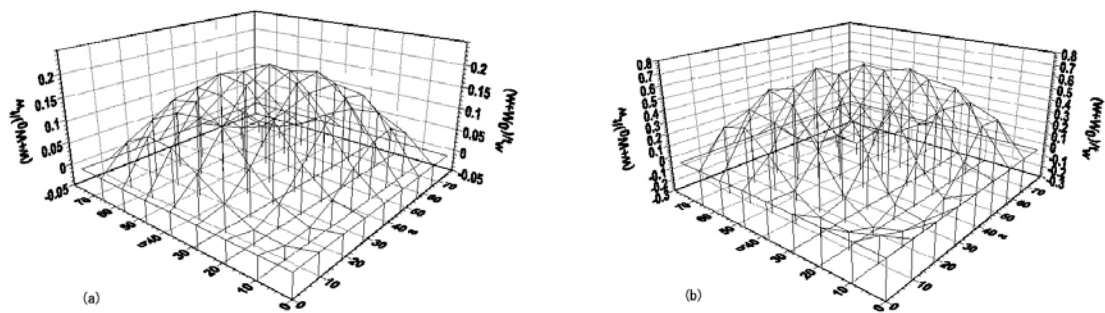
Fig.2.20 Out-of deformation of web panel (IR, B.C.=1, α=1, Case 3).

Out-of-plane deflection behavior of the panel in the case of α=1.6 is shown by Fig.2.21, similarly. The waveform immediately after the generation of shear buckling generation is shown in (a). As shown in (b), due to the increase in panel aspect ratio, it is seen that the deflection surface that shows the tension field becomes higher and narrower in the width than that for the case of (a). From this result, it seems that the lowering of the load carrying capacity is caused by the generation of large bending moment in the panel.

Fig.2.21 Out-of deformation of web panel (IR, B.C.=1, α=1.6, Case 3).

(4.3)   Proportion of tension field

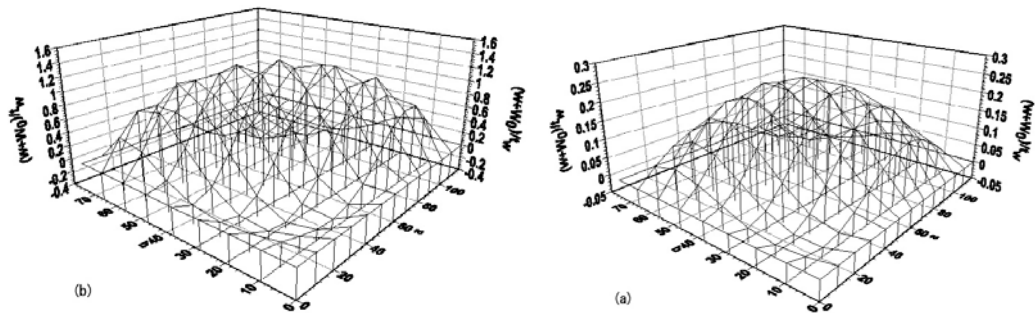   In many modal analyses, the shear strength is assumed calculating by the sum between the strength by the beam action and the strength by the tension field action. Now, the ratio of the beam action and the tension field action is examined based on the assumption of the superscription. The strength by frame action is not included. The proportion in which the beam action and the tension field action calculated from Figs.2.16 and 2.17 occupy in the strength is arranged in Tables 2.8 and 2.9. Though the shear buckling stress must be calculated in order to obtain the value by the beam action, it is hard to be required for the initial deflection. Then, the buckling stress is estimated using the inflection point that appeared in the figure first, and it is used as the value supported by the beam action. The value by the tension field action is calculated by deducting the value by the beam action from the value by the ultimate strength. On the case of α=1, Table 2.8 examines the effect of the boundary condition on the top and bottom edge on that ratio.   On the case in which α=1.6 and the top and bottom edges are simply supported, Table 2.9 examines the effect of the difference of the modeling on the ratio.

Table 2.8 Ratio of beam action and tension field action.
(a) α=1.0, B.C.= I , IR

Case	Beam action (%)	Tension field action (%)
1	46.0	54.0
2	99.0	1.0
3	29.0	71.0
4	47.0	53.0
5	99.0	1.0
6	48.5	51.5

(b) α=1.0, B.C.= II , IR

Case	Beam action (%)	Tension field action (%)
1	74.0	26.0
2	96.0	4.0
3	44.0	56.0
4	74.0	26.0
5	96.0	4.0
6	75.0	25.0

Table 2.9 Ratio of beam action and tension field action.
(a) α=1.6, B.C.= I , IR

Case	Beam action (%)	Tension field action (%)
1	47.0	53.0
2	98.5	1.5
3	29.0	71.0
4	47.0	53.0
5	98.5	1.5
6	50.0	50.0

(b) α=1.6, B.C.= I , IF

Case	Beam action (%)	Tension field action (%)
1	50.0	50.0
2	98.0	2.0
3	29.0	71.0
4	51.5	48.5
5	98.0	2.0
6	57.5	42.5

It is proven that the ratio in Table 2.8 considerably differs by the width-to-thickness ratio of the web plate panel. When the width-to-thickness ratio is 100, the ultimate strength depends on buckling strength without the development of the tension field, as it was mentioned earlier. In the case of β=150, from Table 2.8(a), the proportion is almost half-and-half, even if there is a little difference for the ratio of both actions by the difference between the flange rigidity. In the case of fixed top and bottom edges on Table 2.8(b), the proportion by the beam action exceeds 70%. Also, in the case of β=200, though the proportion in Table 2.8(b) which the beam action occupies is bigger than that in Table 2.8(a), it is not as the case which is β=150.

Also, in the case of β=200, though it is bigger of Case IF than Case IR for the proportion based on the beam action, it is not as the case of β=150. It seems that this reason is because shear buckling is generated in the elastic range in the case of β=200. Like this, the ratio that both actions occupy in the shear strength is different by the boundary condition of the top and bottom edges. However, it is noticed that the value of the ultimate strength is not very much affected, as it was mentioned earlier. By elasto-plastic finite displacement analysis using finite element method, Lee et al.[21] examined the relation of both actions for the case of the panel with comparatively large width-to-thickness ratio. They concluded that the strength after the buckling was almost 40% of the difference between plastic shear strength and shear buckling strength except for the small number of exception. New buckling coefficient for the support condition between the middle of simple support and fixed support is used taking the ratio of web plate thickness and flange thickness as the parameter, when the buckling strength is obtained. The post buckling strength is estimated considerably low, when this method is applied to the calculation for the square panel of the 3rd case in the present analysis. As the result, the ultimate strength by the method of Lee et al.[21] on the 3rd case is merely almost 80% of the value by present method. Though this is a safe side, it seems to too have underestimated the post-buckling strength. Further, though they explain that the post-buckling strength is not affected by the flange rigidity, it is different from the result obtained by this analysis.

In Table 2.9, the effect of the difference between Case IR and Case IF on the ratio of both actions in the case of α=1.6 is examined. From this table, it is seen that the difference of the modeling does not influence the ratio of both actions very much. It is one method to obtain the strength as a sum of beam action and tension field action, when the shear strength is estimated. However, the estimated value is influenced by the boundary condition of the top and bottom edge, when the shear buckling strength is obtained by this prediction method.
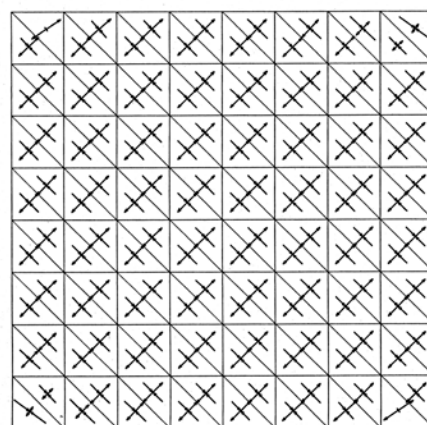
(4.4)   The distribution of the principal stress

The distribution of the principal stress in a panel at the load that is approximate to the ultimate state is shown by Fig.2.22. In this figure, the length of the arrow shows the magnitude of the stress, and corresponding to the arrow that is directed outward or inward, tension and compression of the stress are expressed, respectively. As the angle ϕ which shows the principal stress direction, the angle ϕ which principal stress σ_1 makes with the horizontal axis is used.   In case 2 which is $\beta=100$, it is seen that ϕ is approximated to 45 degrees of the diagonal line direction and the magnitude of both principal stresses are also equal except for a part of turbulence in the corner estimated with the result of the error in the calculation, In the whole panel, it seems to be almost similar to the pure shear.

In case 1 which is $\beta=150$, ϕ is smaller generally a little than 45 degrees. Then, the magnitude of σ_1 begins to be more distinguished than that of σ_2 in diagonal tension band in the panel central. The width of the tension band widens in the case of $\beta=200$, and the magnitude of σ_1 is very superior to that of σ_2.
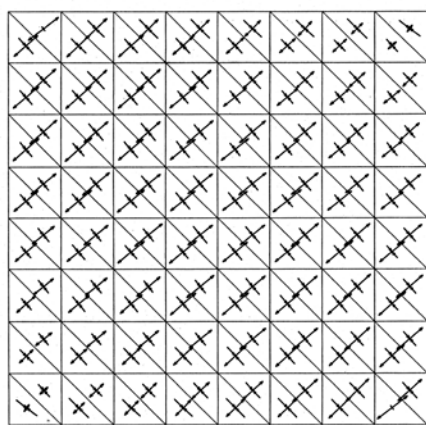
α =1. 0, B. C= I , IR, case1, step14

α =1. 0, B. C= I , IR, case2, step10
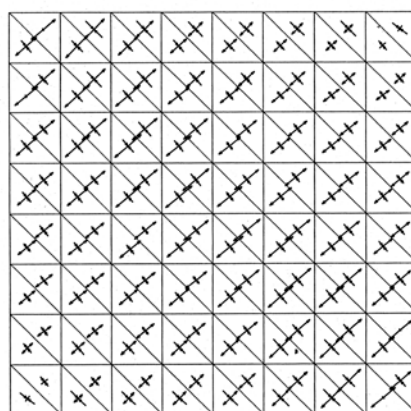
α =1. 0, B. C= I , IR, case3, step26

Fig.2.22 Principal stress distribution.

(4.5)　　Direction of principal stress

　　On each case of Fig.2.22, the angle　$\theta_1(=\phi)$ of the principal stress　σ_1 in the center point of the panel is plotted with　respect to the increase of the load, as shown in Fig.2.23(a). Where, S is shear force, and S_p is the plastic shear force. On the case in which the boundary condition except for B.C.=Ⅱ is same, the relation equal to Fig.2.23(a) is also shown by Fig.2.23(b). With the increase of the load, the angle gradually decreases as seen from Fig.2.23(a). The effect on θ_1 by the difference between web plate width-to-thickness ratio　β is clearly observed, when the angle is compared for the load near the ultimate state in each case. It is supposed, when Fig.2.23(b) is compared with Fig.2.23(a), so that there may be no the great difference on the angle at the load which is approximate to the ultimate state between both, though the route is different a little.
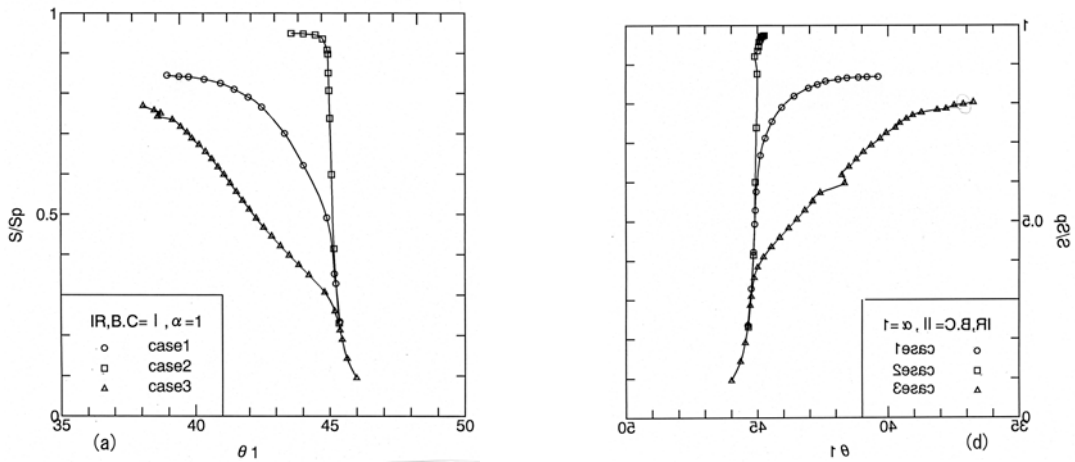

Fig.2.23 Direction of principal stress.

(4.6)　　The ratio between principal stresses

　　Fig.2.24 shows how the ratio of principal stress　σ_1 and　σ_2 in the panel center point changes with the increase of the load. Fig.2.24(a) and Fig.2.24(b) are respectively corresponding to the case that B.C.=Ⅰ and B.C.=Ⅱ. From the comparison of both figures, it is proven that both ratios in the same value of S/S_p are different and the value of S/S_p in which the ratio begins to increase from 1.0 considerably differs. It seems that this reason is because the load for the beginning of the post-buckling strength differs, as the deflection is suppressed owing to the fixed top and bottom edges in the case that B.C.=Ⅱ. It should be noticed that the effect by the flange rigidity on the ratio is very small in both cases that B.C.=Ⅰ and Ⅱ almost either, if the value of β is identical.
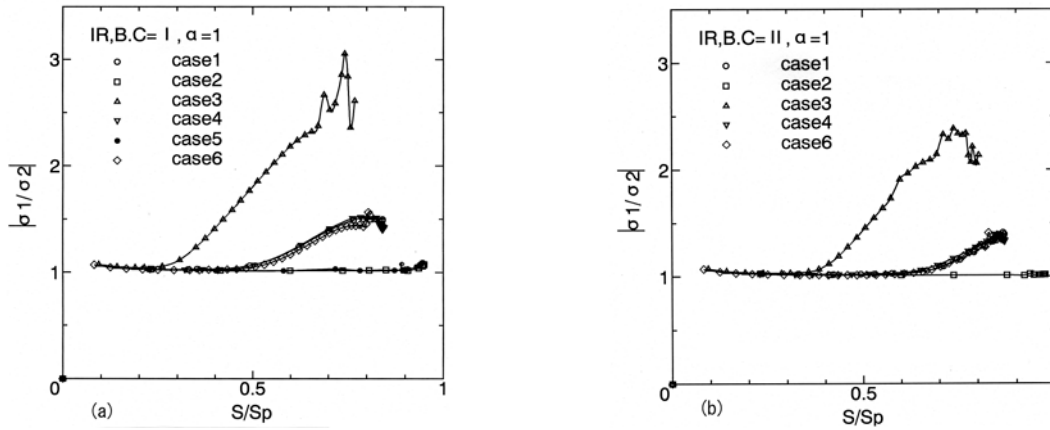
Fig.2.24 Ratio between both principal stresses.

(4.7)　Difference in principal stresses

　　The distribution on the difference between σ_1 and σ_2 in the web center plane is shown by Fig.2.25 for each case 1 to 3. In the case of 2, the difference is almost constant over the whole panel, though the turbulence caused by the numerical error is seen in the corner points. However, the value of the difference at each point in the panel varies considerably in the case of 3. In the case of 1, there is in the middle condition between two cases. The relationship on the difference between principal stresses and the distance from the lower end on the cross sections ② and ③ which Fig.2.26 shows is illustrated in Fig.2.27. Abscissa d is the distance from the lower end. From this figure, it is proven that the variation of the difference on the distance in the case 3 is remarkable and that also changes near the edge in the case 1.
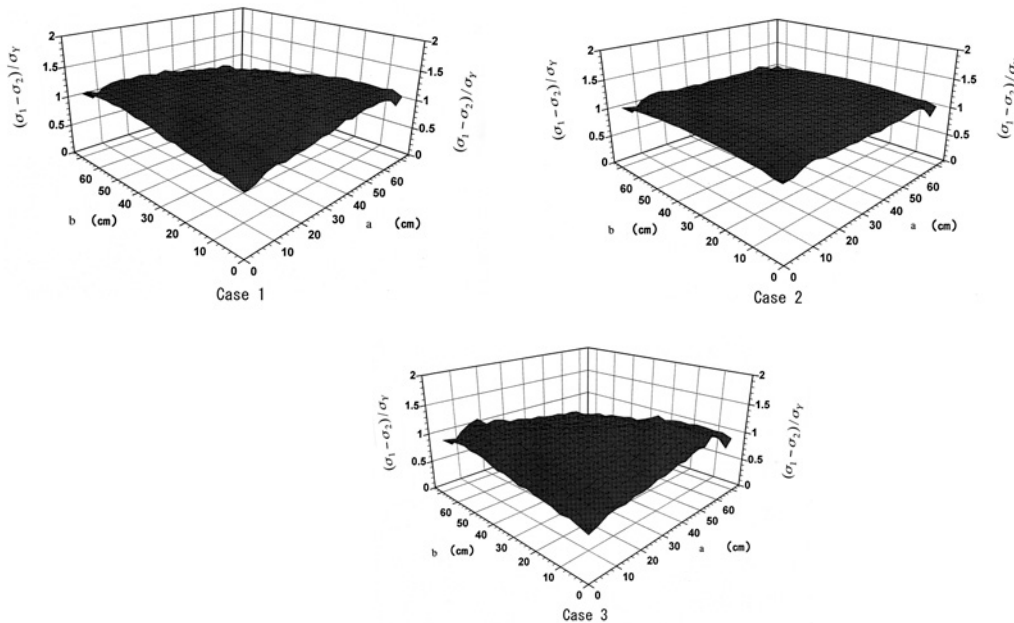

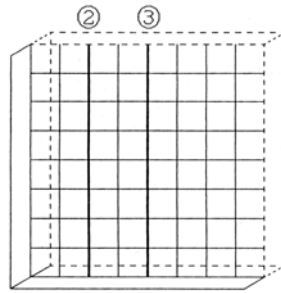Fig.2.25 Distribution on difference of principal stress.
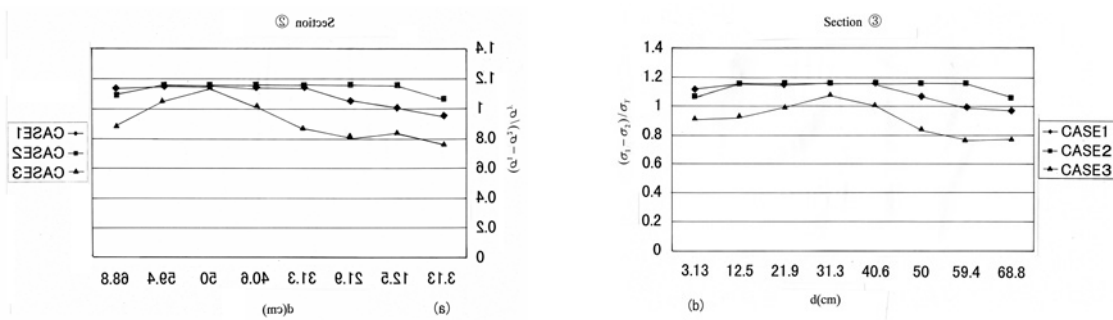
94

Fig.2.26 Location of section.

Fig.2.27 Difference of principal stresses.

(4.8)   Formula for estimation of ϕ and $(\sigma_1 - \sigma_2)$

From the result obtained until now, it is known that the influence of the flange rigidity on the load carrying behavior is not big. Therefore, panel aspect ratio and panel width-to-thickness ratio are chosen as parameters, and how the angle of principal stress direction and the difference of principal stresses are expressed by the value of α and β is investigated. These are necessary, when the prediction expression of the load carrying capacity is constructed. For the induction of the equation, the least squares method was applied. As a result of the regression analysis, the following approximation was obtained. Where, the parameters are applicable in the following range.

$$0.6 \leq \alpha \leq 1.6 \text{ and } 100 \leq \beta \leq 200$$

$$
\begin{aligned}
\phi = {} & 40.1825 + 10.4125\alpha + 0.0808\beta - 0.1443\alpha\beta \\
& + 7.3320\alpha - 3..2470 \times 10^{-4}\beta^2 - 0.1042\alpha^2\beta \\
& + 3.5580 \times 10^{-4}\alpha\beta^2 + 2.4995 \times 10^{-4}\alpha^2\beta^2
\end{aligned}
\tag{2.1}
$$

$$
\begin{aligned}
(\sigma_1 - \sigma_2)/\sigma_Y = {} & 1.0107 - 0.0264\alpha \\
& + 2.3750 \times 10^{-3}\beta + 4.370 \times 10^{-4}\alpha\beta \\
& - 0.0027 \times \alpha^2 - 9.3401 \times 10^{-6}\beta^2 \\
& + 1.723 \times 10^{-4}\alpha^2\beta - 1.660 \times 10^{-6}\alpha\beta^2 \\
& - 1.5052 \times 10^{-6}\alpha^2\beta^2
\end{aligned}
\tag{2.2}
$$

95

For 3 kinds of values of β, the relationship between ϕ and α in Eq.2.1 has been illustrated graphically in Fig.2.28. Though ϕ is decreased with the increase in the value of α, the degree of the decrease is related to the value of β and the degree of the decrease is bigger, as β is bigger. From this figure, it is proven that the difference between the curves by the value of β increases, when α exceeds 0.5.

The relationship between $(\sigma_1 - \sigma_2)/\sigma_Y$ and α in Eq.2.2 is shown by Fig.2.29 for 3 kinds of β. In the case of $\beta=200$, the difference between principal stresses decreases with the increase of α. In addition, it is proven that the value of the difference between principal stresses in this case is small without relating to the value of α in comparison with other cases.
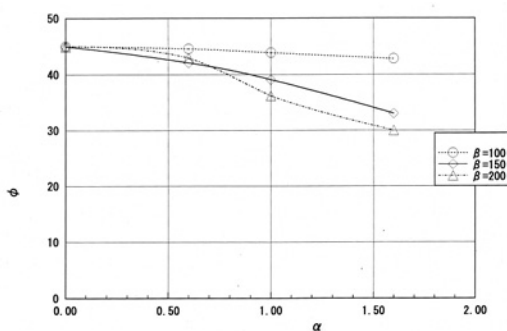

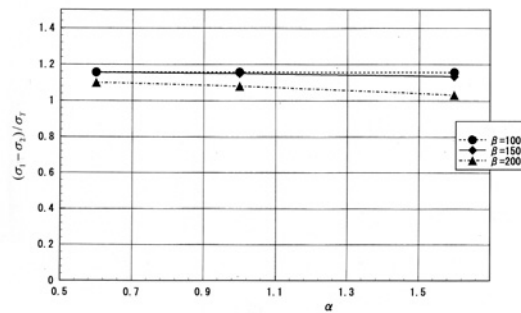Fig.2.28 Direction of principal stress
Vs. aspect ratio.

Fig.2.29 Difference of principal stress
Vs. aspect ratio.

(4.9)   Conclusions
Obtained results are as follows:
1) The girder panel shows the in-plane deformability that is stable to the ultimate strength.
2) Though the proportion for the ultimate strength of the strength supported by the tension field action is different according to the panel width-to-thickness ratio, the effect by the flange rigidity is not very much related.
3) The boundary condition of the top and bottom edges has influence on the proportion of the strength supported by the tension field action in the ultimate strength. In the case of the simple support, the ratio for the tension field action relatively increases, as the buckling strength is estimated making use of low buckling coefficient.
   However, the value of the ultimate strength is not affected very much by the boundary condition, and almost resembled value is shown.
4) It becomes a cause of the strength degradation that the bending moment owing to large out-of-plane deformation arises in the panel with large width-to-thickness ratio.
5) Corresponding to the value of the panel width-to-thickness ratio, the principal stress distribution is considerably different. With the increase of the panel width-to-thickness ratio, the angle where the principal stress direction associates with the horizontal axis decreases.
6) The ratio between both principal stresses increases, when the panel

96

width-to-thickness ratio is large.

7) With the increase in the panel width-to-thickness ratio, it is noticed that the difference of both principal stresses decreases.

8) The difference between both principal stresses in the height direction of the panel increases, as the panel width-to-thickness ratio increases.

9) Using the numerical calculation results, the regression analysis equation for obtaining the principal stress direction and the difference between the both principal stresses that took the aspect ratio and the width-to-thickness ratio as the parameters was proposed.

10) It is seen on the appearance that the load carrying capacity under shear can be estimated as a sum of the strength supported by the beam action and tension field action, as a panel takes the behavior shown in Figs.2.16 and 2.17.

4.3 Load-carrying capacity of girders with linearly varying depth in shear

4.3.1 Analytical methods

(1) Introduction

Plate girders with webs tapered in depth are used widely in bridges. But there is little ultimate shear strength investigation on such girders. Falby[19] has proposed a calculation method to predict shear strength by means of plastic analysis in Basler's style[5]. Also, Mandal et al.[6],[7] have given a predicting method extending the theory of Porter et al.[8]. So far, it has been assumed in many modal analyses that the shear strength on webs after shear buckling can be obtained as the sum of the shear buckling strength of webs and the strength caused by the vertical components of a diagonal tension field[9]. Then, this assumption will be used too fundamentally.

The shear buckling load on a trapezoidal web panel are calculated on the condition that flange edges are simply supported or fixed and other two edges are simply supported making use of a finite element method. Then, the calculated results are compared with the case of rectangular web panels. It is supposed that the stress distribution on the diagonal tension field that develops in the trapezoidal panel can be determined based upon Ostapenko's model[10]. Then, by applying equilibrium conditions to the panel the shear strength owing to the tension field and the axial forces on flanges can be estimated. In regard to the girder reinforced by transverse stiffeners, it is assumed that diagonal tension fields develop independently in adjacent two panels. And the axial stiffener force can be estimated according to the equilibrium condition.

(2) Buckling loads of trapezoidal web plates

In order to calculate shear buckling loads of web panels, a trapezoidal plate subjected to the force along each edge in a state of plane stresses shown in Fig.3.1 is chosen. In this figure, a, d_m and β denote web length, mean panel depth and the angle of a inclined flange, respectively. It is assumed that the plate is simply supported along $Y=0$ and a, and simply supported or fixed along other edges in regard to out-of-plane deflection. Really, it is suggested that the boundary condition in which two edges are simply supported and other edges are fixed is proper for shear buckling analysis in rectangular plates[11]. Stress analysis will be carried out by using the FEM with

constant strain triangles. In buckling analysis the FEM with triangular elements in which the deflections at three apexes and the rotation along three sides constitute the degree of freedom will be used[12]. And an extrapolation method will be adapted to obtain converged values[24]. Three kinds of β ($5°, 10°$ and $15°$) are selected. Buckling coefficients, k_τ, can be obtained from the mean value of shearing stresses on the panel and the mean width-to-thickness ratio. The relation between k_τ and the mean aspect ratio , $\overline{\alpha}(= a/d_m)$, is shown in Fig.3.2. It is seen from this figure that k_τ varies with the value of β and the boundary conditions.
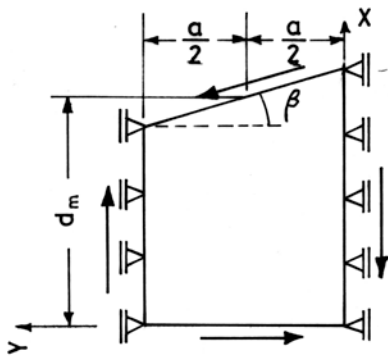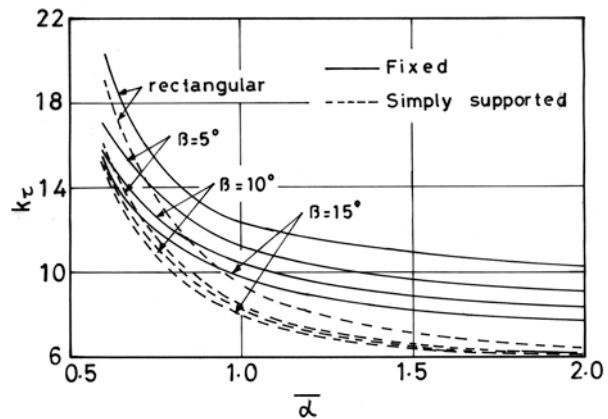
Fig.3.1 Trapezoidal panel.   Fig.3.2 Buckling load curves.

(3) Model of diagonal tension field

As it is supposed that the tension field develops slightly in the upper part of a trapezoidal panel, the assumption on the tension field distribution by Oatapenko[10] is adapted to the rectangular part of the panel illustrated in Fig.3.3. Namely, so far as the distribution of the tension field the model in which an inclined flange holds the position AA may be assumed. As shown in Fig.3.3, the web panel is cut along a section $t-t$ close the intermediate stiffener in the panel nearest to supports that the collapse is expected. By applying the equilibrium condition to this free body panel, the action of shear forces can be obtained as follows:

Fig.3.3 Equilibrium conditions applied to web panel.

$$\frac{P}{2} = \frac{\sigma_t t}{d_h \cos\beta - e\sin\beta}\left[s\left(s\sin\beta/2 + d_h\cos\beta\sin\phi\right)\right.$$
$$\left. + \rho a\sin\phi\left\{(s + a\sin\phi/2)\sin\beta + d_h\cos\beta\sin\phi\right\}\right]$$

(4.1)

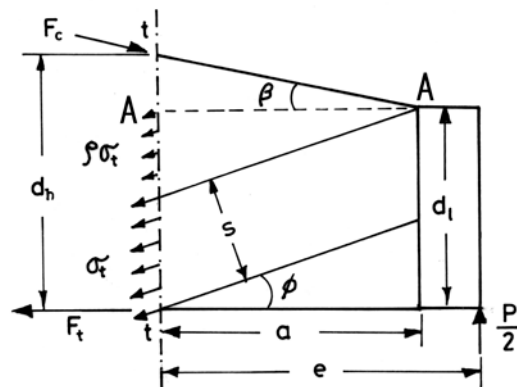where σ_t, t, d_h, ϕ, e, ρ and s are the tension field stress, the web thickness, the maximum panel depth, the inclination angle of tension field, the length from section t-t to the loading point, the coefficient of equivalent tension field stresses and the width of tension field, respectively. When the minimum panel depth is represented by d_l,

$s = d_l\cos\phi - a\sin\phi$.

At the estimation of σ_t, if both cases of the approximate yield condition by Basler[5] and the exact yield condition by von Mises are adopted, ϕ can be determined on condition that $P/2$ takes the maximum value as follows:

a) In the case of approximate yield condition

$$\tan 2\phi = \frac{2d_l d_h\cos\beta - 2(1-\rho)ad_l\sin\beta}{d_l^2\sin\beta - a^2(1-\rho)\sin\beta + 2(1-\rho)ad_h\cos\beta}$$

(4.2)

b) In the case of exact yield condition

$$\left\{(1-\rho)ad_h\cos\beta + d_l^2\sin\beta/2 - a^2(1-\rho)\sin\beta/2\right\}\tan 2\phi =$$
$$d_l d_h\cos\beta - (1-\rho)ad_l\sin\beta - 3(\tau_{cr}/\sigma_Y)\left[s(s\sin\beta/2 + \right.$$
$$d_h\cos\beta\sin\phi + \rho a\sin\phi\left\{(s + a\sin\phi/2)\sin\beta + \right.$$
$$\left. d_h\cos\beta\sin\phi\right\}\right]/\sqrt{1 + (\tau_{cr}/\sigma_Y)^2\left\{\left[1.5\sin 2\phi\right]^2 - 3\right\}}$$

(4.3)

where σ_Y and τ_{cr} are the yield stress and the shear buckling stress, respectively.

(4) Force acting on intermediate stiffener

As seen in Fig.3.4, it is assumed that each tension field is formed independently on the adjacent panels subjected to shearing forces. By applying the equilibrium condition to the panel after cutting, the acting force on the intermediate stiffener F_s can be obtained as follows:

$$F_s = \left[\sigma_{t2}t_{s2}\sin(\phi_2 + \beta) - \sigma_{t1}t_{s1}\sin(\phi_1 + \beta)\right.$$
$$\left. + 2\rho_2\sigma_{t2}ta_2\sin\phi_2\sin(\phi_2 + \beta)\right]/\cos\beta$$

(4.4)

where the subscripts 1 and 2 correspond to the panels Ⅰ and Ⅱ, respectively.
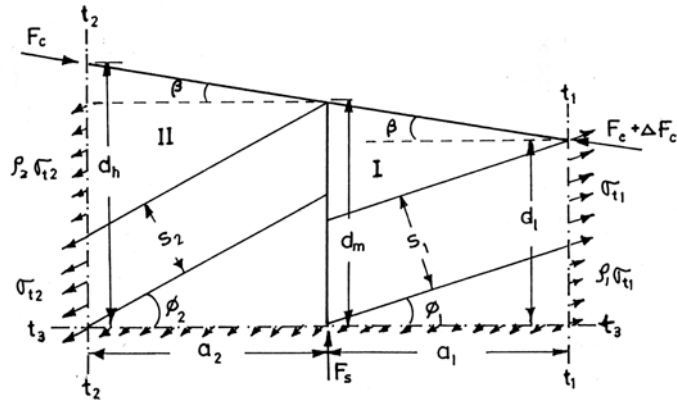
Fig.3.4 Equilibrium conditions applied adjacent web panels.

An example of the relation between the maximum value of F_s and β obtained by using Eq.(4.4) is shown in Fig.3.5. As β increases the maximum value of F_s shows approximately a linear increase. Also in this figure, the maximum force acting on the intermediate stiffener obtained by Basler's expression is given in a broken line. On this occasion, the trapezoidal web panel is converted into the rectangular panel with mean panel depth.
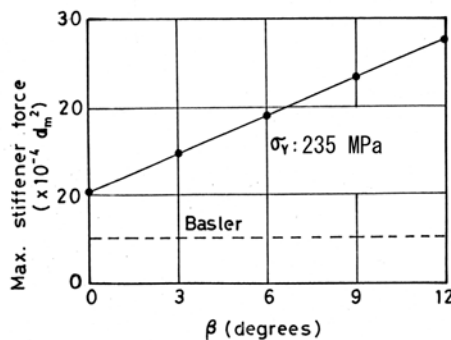
Fig.3.5 Relation between maximum stiffener force and β.

(5) Conclusions

The expression to predict the load carrying capacity of tapered girders was proposed by calculating shear buckling load curves of trapezoidal panels and assuming a model of tension fields. And the estimation of the force applied on intermediate stiffeners was done.

Obtained results on the theoretical study are as follows.
1) Shear buckling loads of trapezoidal web panels are fairly affected by the inclination angle of flanges.
2) The expression using the approximate yield condition is considerably simple because of no iteration.
3) The relation between the inclination angle of flanges and the maximum stiffener force was considered.

100

4.3.2 Experiments on girders with linearly varying depth in shear

(1) Introduction

There is little ultimate shear strength investigation of girders with webs tapered in depth even on experimental works. Davis and Mandal have presented the test results for tapered plate girders in shear[6),7)]. But the flanges in these girders were formed from hollow sections and the girders had not intermediate transverse stiffeners.

In this article, the ultimate shear strength and the behavior for tapered girders will be discussed. Eight model girders with straight varying depth are tested under shearing force and four of them have intermediate transverse stiffeners. The flanges in these girders are formed from rectangular solid sections dissimilar to the test by Mandal et al. The effects of the failure of web plates, flanges and stiffeners upon the ultimate strength and the collapse behavior are examined experimentally, and the properties of tapered plate girders are investigated in detail.

(2) Description of tests

 (2.1) Models

Eight models of tapered plate girders were tested. Four models (Models TS-1, TS-2, TS-3 and TS-4) with no intermediate transverse stiffeners are called as the series I and other four girders (Models TS-T-1, TS-T-2, TS-T-3 and TS-T-4) with them as the series II. A parallel flange girder (Model US-1) was also tested with the purpose of comparison.

As shown in Fig.3.6, the shadowed portion is the testing panel and the arrow indicates the point of load application. Intermediate transverse and bearing stiffeners at the point load application and at ends were used in pairs. The web plate opposite to the testing panel relative to the girder center was suitably reinforced by stiffeners to ensure that it should not fail before the testing panel.

(a) Series I

a = 650 (TS-1·TS-2·TS-3) 586(TS-4)
D_l = 550(TS-1·TS-3) 450(TS-2) 496(TS-4)
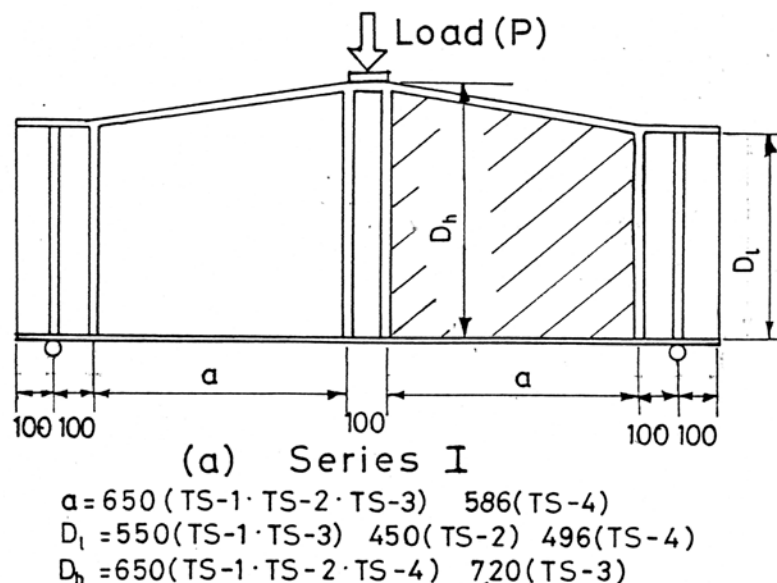D_h = 650(TS-1·TS-2·TS-4) 720(TS-3)

Fig.3.6 Tapered girders.
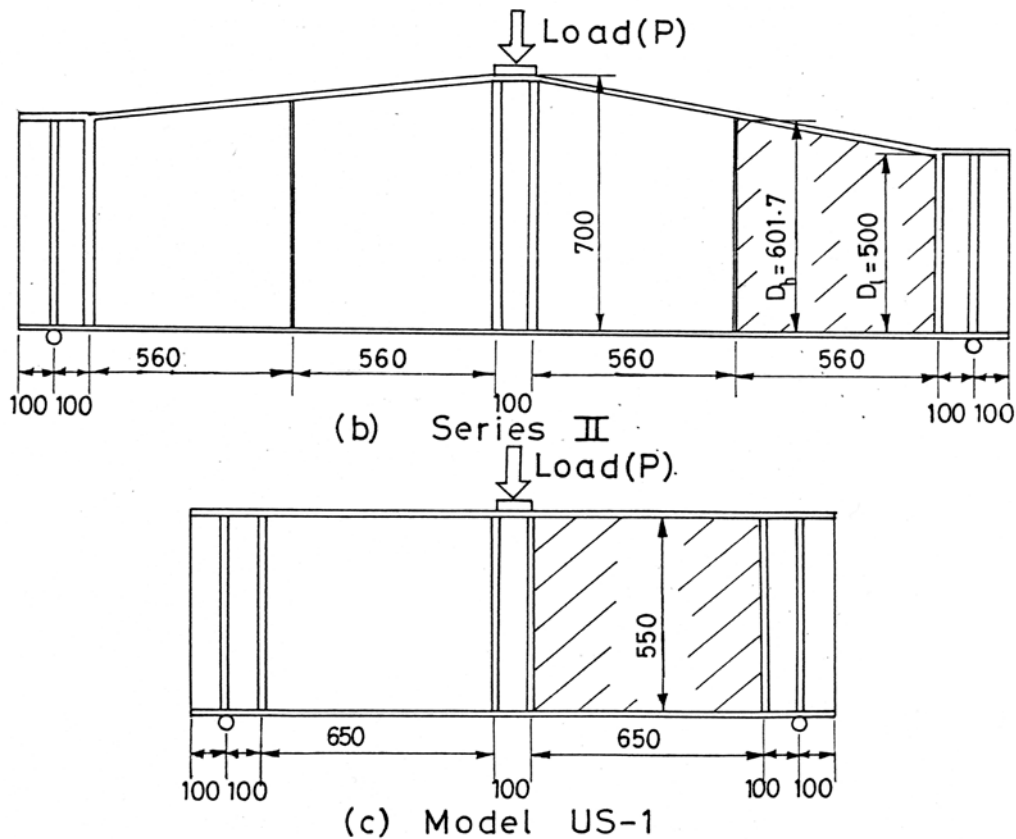
Fig.3.6 Tapered girders (Continued).

The cross section of the web and flange was the same throughout the length of the girder. The web and flange plate with 1.6mm and 12mm thickness in the plan, respectively were chosen. Models TS-1 and TS-2 were designed so as to have the same maximum web depth and Models TS-1 and TS-3 the same minimum web depth. Each inclination angle of the compression flange for Models TS-3 and TS-4 is identical. In the series II, each girder was designed to be identical except for the dimensions of the intermediate stiffeners. The actual girder dimensions on the testing panel were measured. These measurements are summarized in Table 3.1. The flexural rigidity of the intermediate stiffener on Model TS-T-2 is nearly equal to that of Model TS-T-3. The stiffener rigidities of Models TS-T-1 and TS-T-4 are about 13 and 2 times as large as that of Model TS-T-2, respectively.

All models were made of SS400 steel. Coupon plates were cut from the same length of girder components to obtain tensile test coupons. The results of the coupon tests are given in Table 3.2.

Table 3.1 Measured dimensions of girders.

Model	Series I				Series II				
	TS-1	TS-2	TS-3	TS-4	TS-T-1	TS-T-2	TS-T-3	TS-T-4	US-1
Web length a (mm)	654	652	640	579	559	560	561	560	647
Min. web depth D_l (mm)	549	449	549	491	505	505	503	504	548
Max. web depth D_h (mm)	649	646	719	633	700	698	697	699	548
Web thickness t (mm)	1.57	1.59	1.50	1.51	1.62	1.58	1.70	1.69	1.55
Flange width b (mm)	89.1	89.3	90.8	89.4	160	160	162	160	90.7
Flange thickness t_f (mm)	11.8	11.9	12.1	12.1	11.3	11.3	11.6	11.6	12.1
Panel length l / D_l	1.16	1.42	1.13	1.14	1.09	1.09	1.10	1.09	1.14
D_l / t	350	283	366	325	313	320	297	298	354
θ (degree)	8.7	17.1	14.7	14.7	10.1	10.1	10.1	10.1	0
b_s (mm)	-	-	-	-	32.8	13.5	17.8	21.0	-
t_s (mm)	-	-	-	-	2.97	3.01	1.65	1.68	-

θ: Inclination angle of flange b_s: Width of intermediate stiffener

t_s: Thickness of intermediate stiffener

Table 3.2 Coupon test results.

Model		Series I				Series II				
		TS-1	TS-2	TS-3	TS-4	TS-T-1	TS-T-2	TS-T-3	TS-T-4	US-1
Yield stress σ_Y (MPa)	Flange	282.2	282.2	284.4	284.4	216.1	216.1	286.3	286.3	284.4
	Web	286.9	323.3	290.3	290.3	280.8	280.8	281.4	281.4	290.3
	Stiffener	-	-	-	-	371.6	371.6	318.7	318.7	-
Young's modulus E X10⁵ (MPa)	Flange	-	-	2.05	2.05	1.95	1.952.	2.03	2.03	2.05
	Web	-	-	1.99	1.99	2.12	2.12	2.13	2.13	1.99
	Stiffener	-	-	-	-	2.10	2.10	2.06	2.06	-
Poisson's ratio ν	Web	-	-	0.275	0.275	0.269	0.269	0/326	0.326	0.275

(2.2) Test setup

Each girder was tested in the simply supported condition with roller supports at the ends and a concentrated load was applied to the girder at mid-span using an oil jack of the capacity of 294 kN. To prevent any horizontal movement of the girders, the lateral supports were provided at mid-span. These supports consisted of a roller attached to a rigid frame bolted to the laboratory floor.

(2.3) Instrumentation

Dial gauges and electrical displacement transducers were used to observe the deflection on each girder. To measure the out-of plane deflections of the web plate relative to the boundaries, a frame that was clamped to the bearing stiffeners was used. Dial gauges were mounted underneath the tension flange to observe the vertical girder deflections. The horizontal and vertical deflections of the inclined (compression) flange were observed by cathetometers.

Electrical resistance strain gauges, with uni-axial and rosette types, were used on each girder. Measurements of the strains were taken on both faces of the girder components. Namely, by placing identical strain gauges opposite each other (at each side of the web, flange and stiffeners), it was possible to separate membrane and bending strain.

(2.4) Testing procedure

Before testing, the initial deflections of web plates were measured. As an example, the distribution of initial deflection of the web for model TS-2 is shown in Fig.3.7. The

maximum initial deflections of the webs for each model were obtained as shown in Table 3.3. As seen in this table, the value of each maximum initial deflection is relatively large owing to the use of thin plate.

The step-by-step loading procedure was used in each girder test. After the attainment of ultimate load, the removal of load was conducted.

Table 3.3 Maximum initial deflection of testing panel.

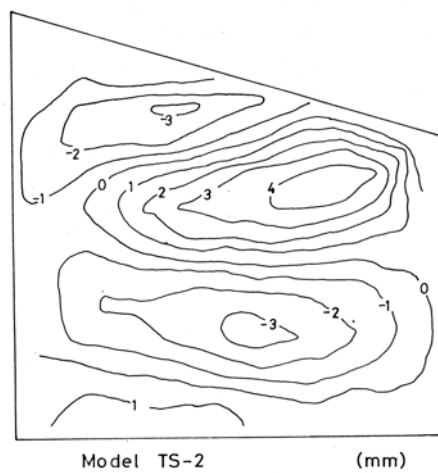| Model	Series I				Series II				
	TS-1	TS-2	TS-3	TS-4	TS-T-1	TS-T-2	TS-T-3	TS-T-4	US-1
$w0, max$ (mm)	4	4	6	6	4	5	6	4	6

Model TS-2   (mm)

Fig.3.7 Initial deflection of web panel.

(3) Experimental results and considerations

(3.1) Collapse mode of failure of girders

All tapered girders failed with the development of the tension field in the web panel and the formation of the plastic hinges in the compression and tension flanges. As examples, Models TS-1 and TS-T-1 collapsed are shown in Fig.3.8 and Fig.3.9, respectively. The plastic hinges formed are clearly visible in these photographs.
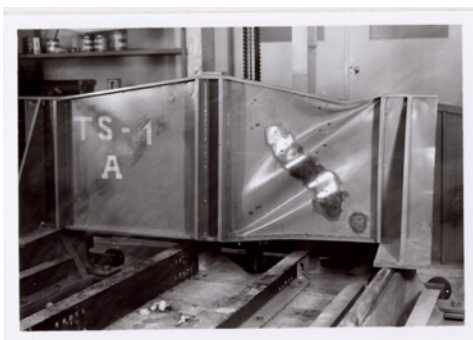

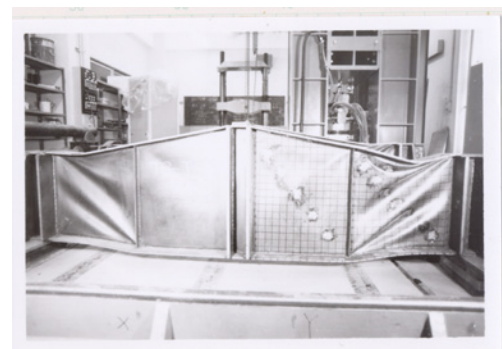Fig.3.8 Collapsed girder (TS-1).

Fig.3.9 Collapsed girder (TS-T-1).

(3.2) Out-of plane deflections of web panels
    The relative deflections of the web panels were measured at several points on each
girder. The relative deflections have been plotted against the applied load to form
Figs.3.10 and 3.11. In Fig.3.12 the deflections of various points of the web panel are
shown at the five different loads. As seen from Figs.3.10 and 3.11, it is difficult to
estimate the shear buckling load of the web panel due to the initial web imperfections.
It can be seen from Fig.3.12 that the tension field develops with the increase of load on
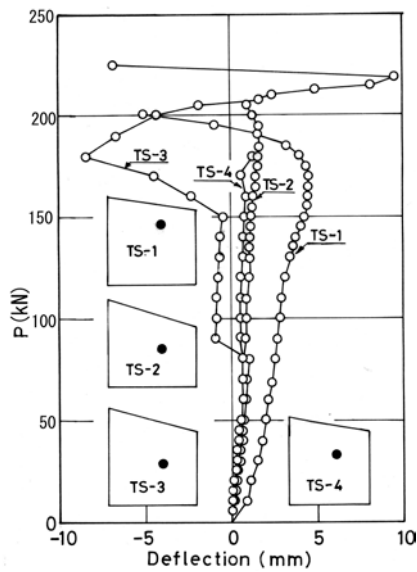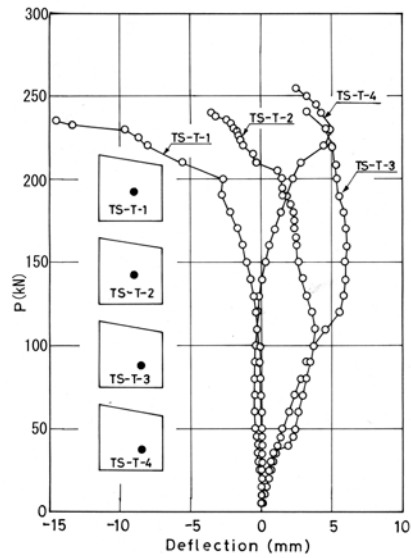the panel.

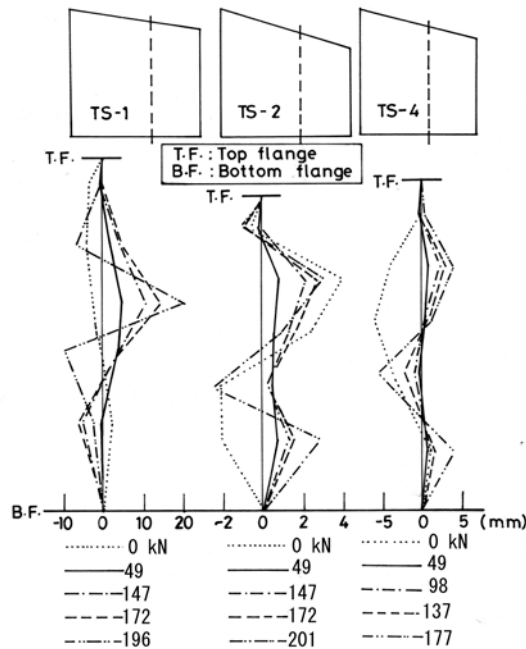Fig.3.10 Relative web deflection.   Fig.3.11 Relative web deflection.

Fig.3.12 Deflected web profile.

105

The contour lines of the residual deflection are illustrated in Figs.3.13 and 3.14. Also the result of Model US-1 is shown in Fig.3.13. Each model of the series I girders showed the similar distribution of residual deflections. It is found from Fig.3.13 that the inclination of the tension band, which may be estimated from the residual deflection, is similar in both models. But in the series II girders, the distribution of residual deflections were affected considerably by the rigidity of the intermediate transverse stiffeners. As the rigidity of the intermediate transverse stiffeners decreases (see Table 3.1), the diagonal tension fields extend over the adjacent panel to the testing one. Namely, it is evident that two adjacent web panels tend to function as a single web panel. The intermediate transverse stiffener on Model TS-T-1 deflected hardly in the lateral direction.
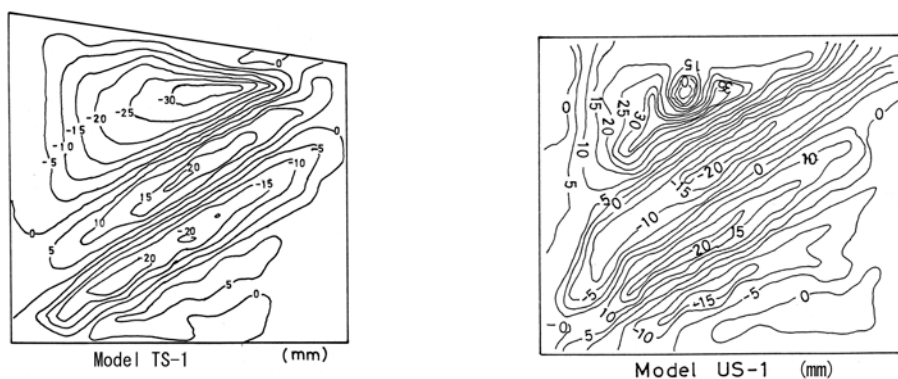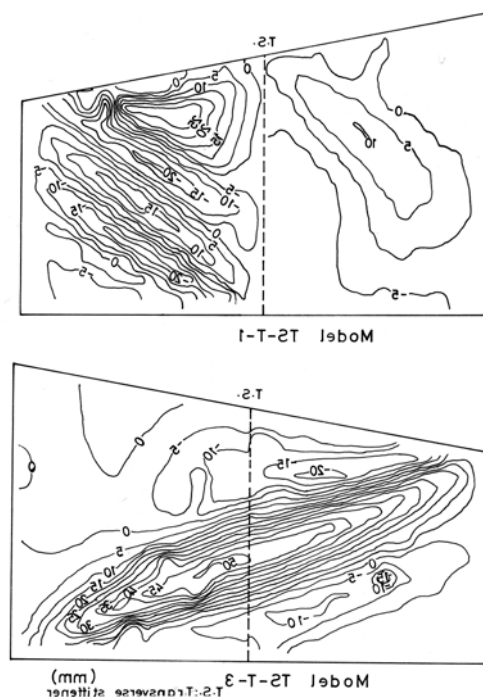

Fig.3.13 Residual web deflection.

Fig.3.14 Residual web deflection.

106

(3.3) Girder deflection

The central deflections of every model are plotted with respect to applied loads in Figs.3.15 and 3.16. Each load-central deflection relationship is linear up to, at least, approximately 85% of the collapse load except for TS-2. In the case of Model TS-2, the load-central deflection relationship becomes nonlinear at approximately 80% of the collapse load. When the load-central deflection relationship becomes nonlinear at first, the value of the ratio of the central deflection to the overall span is in the range 1/700-1/1000 except for Model TS-4. On Model TS-4 the ratio is about 1/450. The deflection shows a rapid rate of increase as the load approaches that of the failure.
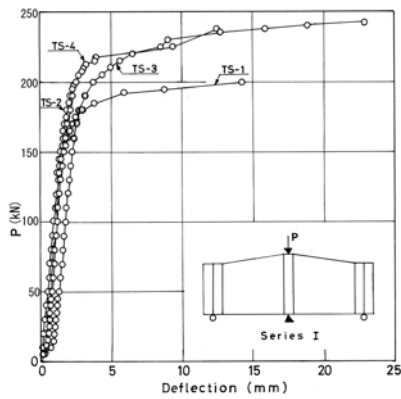
Fig.3.15 Central deflection.   Fig.3.16 Central deflection.
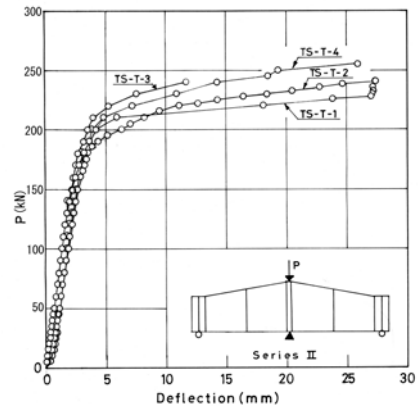
(3.4) Vertical displacement of inclined flange

A plot of load against vertical displacement of the inclined flange similar to that shown in Fig.3.17 was obtained. These observations were obtained by reading the movements of the marks on the inclined flange using cathtometers. It can be seen that in the case of Fig.3.17 the curve is linear up to approximately 90% of the collapse load.
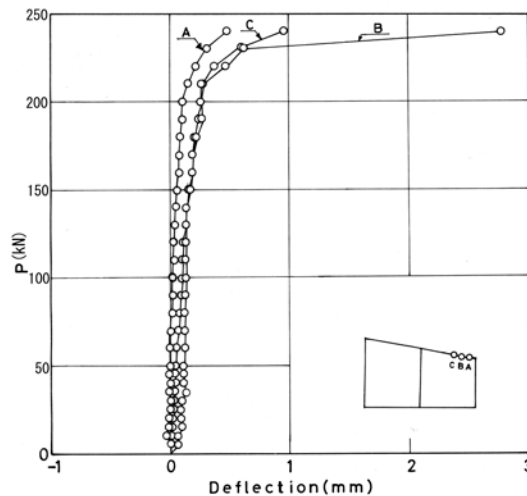
Fig.3.17 Vertical displacement of inclined flange.

107

(3.5) Strain of flange

For Girder TS-1, the longitudinal strains of the compression flange have been plotted against various loads to form Fig.3.18. In this figure, it should be noted that the strains near the position of the plastic hinge increase rapidly with the approach to the collapse load and subsequently are beyond the yield strain of the material at about 90% of the collapse load. But the strains that were caused on other positions have relatively small values and are almost uniformly distributed even when the collapse load is reached.
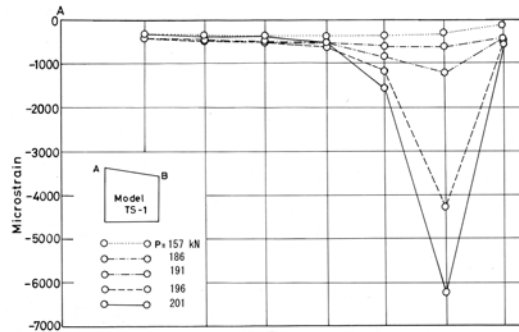
Fig.3.18 Longitudinal strains of inclined flange.

In Fig.3.19, the variations of the surface strains on the inclined flange are shown against several applied loads. From this figure, it is seen that the strains near the center of the flange develop gradually owing to the tensile stresses of the web with increasing load.
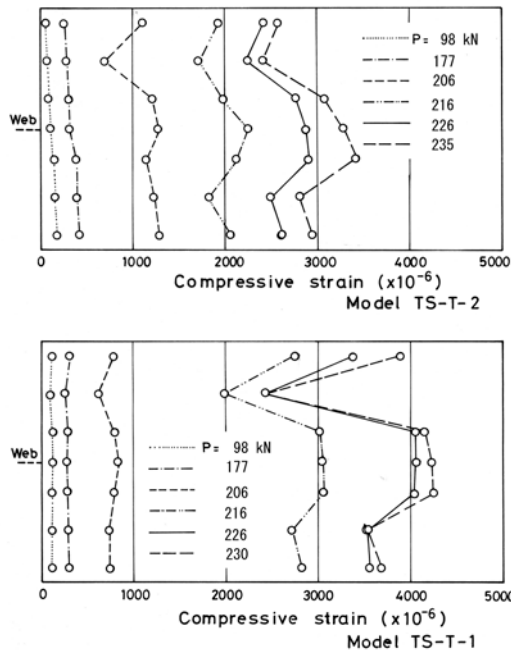
Fig.3.19 Distribution of strains on inclined flange surface.

(3.6) Strains across tension band

The variations of the diagonal tensile strains acting at right angles across the diagonal AB of web panel measured by the rosette gauges are shown against several applied loads in Fig.3.20 for Girder TS-4. Also the result of Model US-1 is indicated in the same figure. From this figure, the width and inclination of the tension band can be estimated. It can be seen that the strains at the points across the tension band have mostly exceeded yield point. Further, it is of interest to note that the distribution of the strains across the tension band has been unsymmetrical about the center of the diagonal and the extent of the development has been remarkable in the tensile zone. While, such distribution on Model US-1 is more symmetrical than that of Model TS-4.
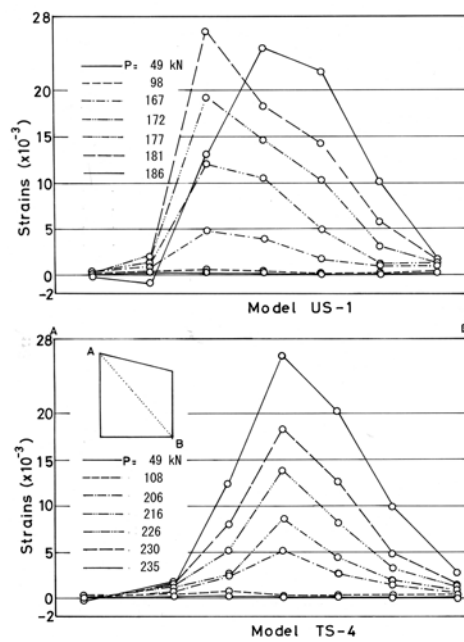
Fig.3.20 Strains across tension band.

(3.7) Distribution of principal stress

As an example, the distribution of the elastic principal stresses is shown in Fig.3.21. From this figure, it can be seen that the diagonal tension field develops widely and rapidly with increasing load. Besides it should be noted that these membrane stresses have been undeveloped in the upper triangular part and around the part. This fact is similar for other models and compatible with the foregoing assumption at 4.3.1 (3).
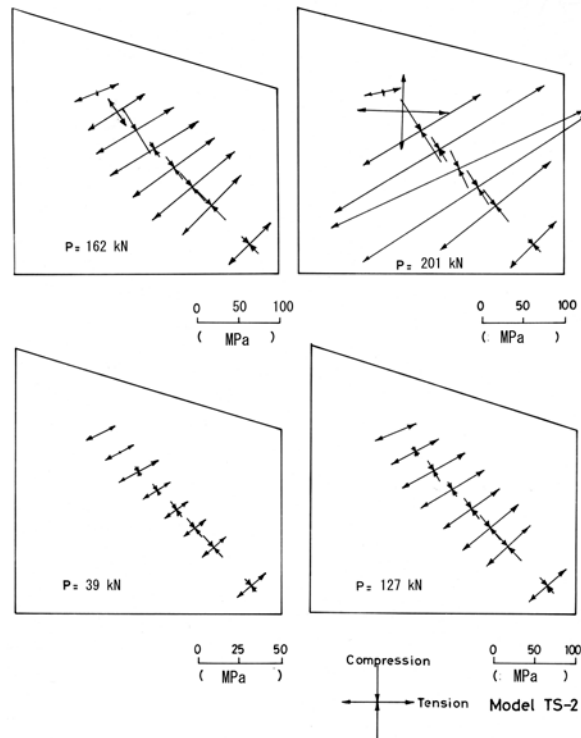
Fig.3.21 Principal stress distribution in web.

(3.8) Equivalent stress

For Model TS-4, the equivalent stresses in the middle plane of the web panel are plotted against the load in Fig.3.22. It will be seen that the equivalent stresses at the ends of the tension band grow gradually up to the neighborhood of the collapse load. But the values are large near the center of the panel on account of the unrestricted condition by boundaries. Namely, as the web deformation in the vicinity of the tension band is large the large membrane stresses grow owing to the deformation.

It is founded from this figure, Fig.3.17 and Fig.3.18 that after the web part just under the inclined flange yields the flange begins to dent considerably. Therefore, it is presumed that the large deformation of the flange occurs in the rather final stage of loading. Furthermore, it may be supposed that from this figure, Fig.3.15 and Fig.3.16 even if the rigidities are reduced by the spread of yielded areas on webs owing to the large web deformation, the behavior on deformation of girders has not been seriously influenced.
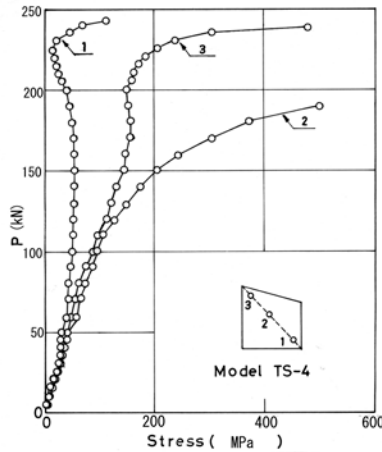
Fig.3.22 Equivalent stress in web.

(3.9) Strains of intermediate stiffener

Fig.3.23 shows how the axial strains varied along the length of the intermediate transverse stiffeners against various applied loads. Fig3.24 gives the positions of the strain gauges on the intermediate stiffeners. It seems that Fig.3.22 shows the similar distribution pattern. It is seen that in every models the distribution of the axial strains along the length of the stiffener is unsymmetrical. But for Model TS-T-1 the values of compressive strains are smaller than those for other models when failure occurs.

Fig.3.25 shows how the strains due to lateral bending grew along the length of the intermediate stiffeners against various applied loads. From these figures, it can be noticed that the strains on Model TS-T-1 for which the rigidity of the intermediate stiffeners is large (see Table 3.1) have been comparatively small. It is evident that the intermediate stiffener of Model TS-T-1 was effectively subdividing the web into two panels. While on other three models in the series II the out-of plane deflection which extended over the adjacent panels was developed.
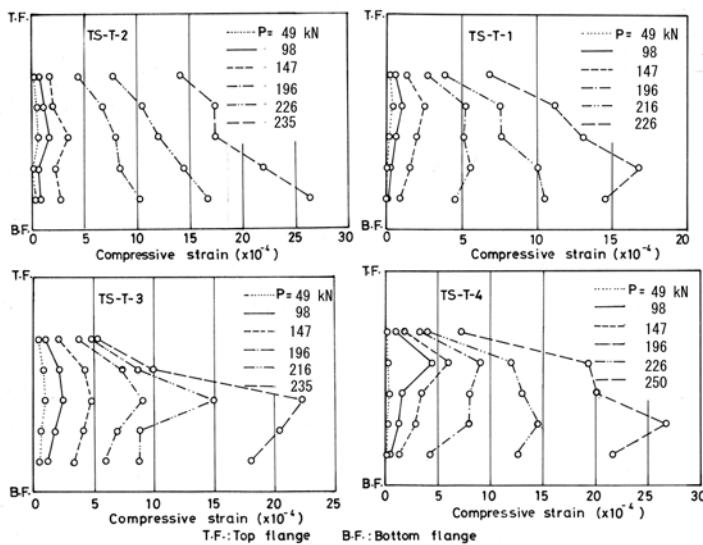
Fig.3.23 Longitudinal strains in transverse stiffener.
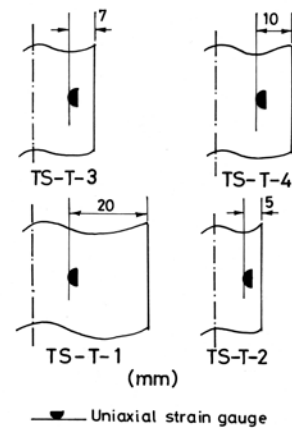
Fig.3.24 Location of strain gauges.
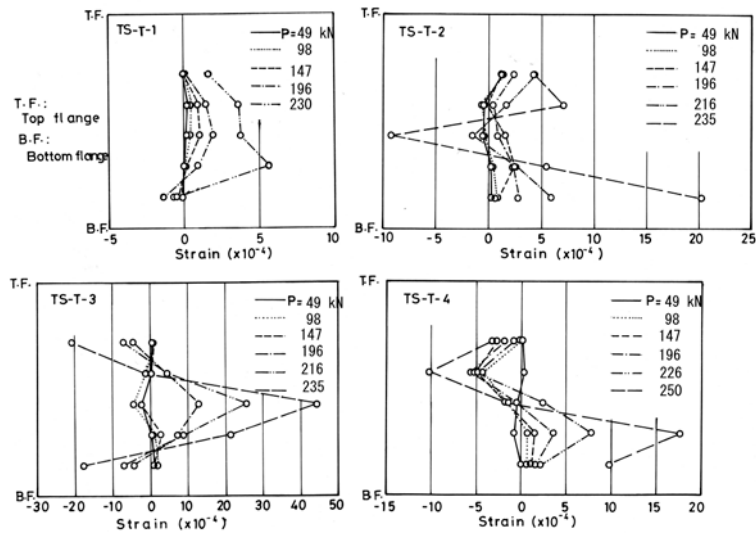
Fig.3.25 Strains in transverse stiffener due to lateral bending.

(3.10) Ultimate strength

Table 3.4 shows the maximum shear loads, P_{ult}, observed. Also in this table the ratios $V_{ult}/V_{p,m}$, $V_{ult}/V_{p,t}$ and $V_{ult}/V_{p,h}$ are given, where V_{ult} is one half of P_{ult} and $V_{p,m}$ is the full plastic shear force which is obtained by assuming the girder depth to be the mean depth of the trapezoidal testing panel. Similarly, $V_{p,t}$ and $V_{p,h}$ are the full plastic shear force in the case for which the minimum depth and the maximum depth of the testing panel are taken as the girder depth, respectively.

On comparing the values of $V_{ult}/V_{p,t}$ for Models US-1, TS-1 and TS-3, when the panel length and the minimum girder depth of a tapered panel are constant the collapse load will increase with the increase of the maximum girder depth. But by making a comparison between Models TS-1 and TS-2 that have the same panel length and the same maximum girder depth, it is assumed that there may be a certain inclination angle of the flange that allows the collapse load to become a maximum.

Though Models TS-1 and TS-4 have the same maximum girder depth and the same ratio of the panel length to the minimum girder depth and the inclination angle of the flange for Model TS-4 is greater than that for Model TS-1, Model TS-4 gives the collapse load greater than that of Model TS-1.

112

Table 3.4 Collapse loads.

Model	Series I				Series II				
	TS-1	TS-2	TS-3	TS-4	TS-T1	TS-T2	TS-T3	TS-T4	US-1
P_{ult} (kN)	201.5	220.6	243.2	237.9	230.4	236.8	235.8	254.5	186.3
V_{ult} / $V_{p,m}$	0.647	0.680	0.763	0.836	0.794	0.835	0.776	0.839	0.654
V_{ult} / $V_{p,l}$	0.706	0.829	0.882	0.957	0.871	0.915	0.851	0.921	0.654
V_{ult} / $V_{p,h}$	0.598	0.577	0.673	0.743	0.730	0.768	0.714	0.771	0.654

It is supposed that these results are due to the action of the vertical component of the axial force in the inclined flange.

With regard to the results of the series II, the collapse load of Model TS-T-1 is smaller than that of Models TS-T-2 and TS-T-4 in spite of the high rigidity of the intermediate transverse stiffener. To investigate the cause, the relationship between the load and the diagonal strains at the middle plane of the web panel is shown in Fig.3.26 on Models TS-T-1 and TS-T-2.
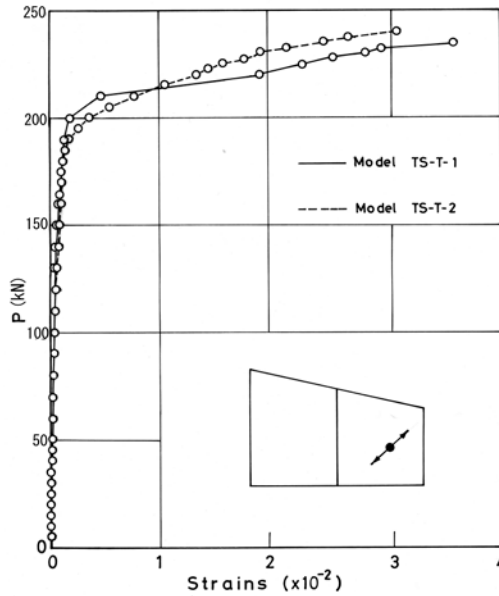
Fig.3.26 Diagonal strain in web.

The variations of the bending strains along the inclined flange for Models TS-T-1 and TS-T-2 are also shown in Fig.3.27 against various loads. From Fig.3.26, it is seen that the tensile strains of the web panel for Model TS-T-1 have been developed remarkably and rapidly. Therefore as shown in Fig.3.27, it is considered that because the inclined flange had been deformed abruptly the maximum load was reached. As the intermediate stiffener with the small rigidity develops large deformation and strains, the use of that is undesirable.
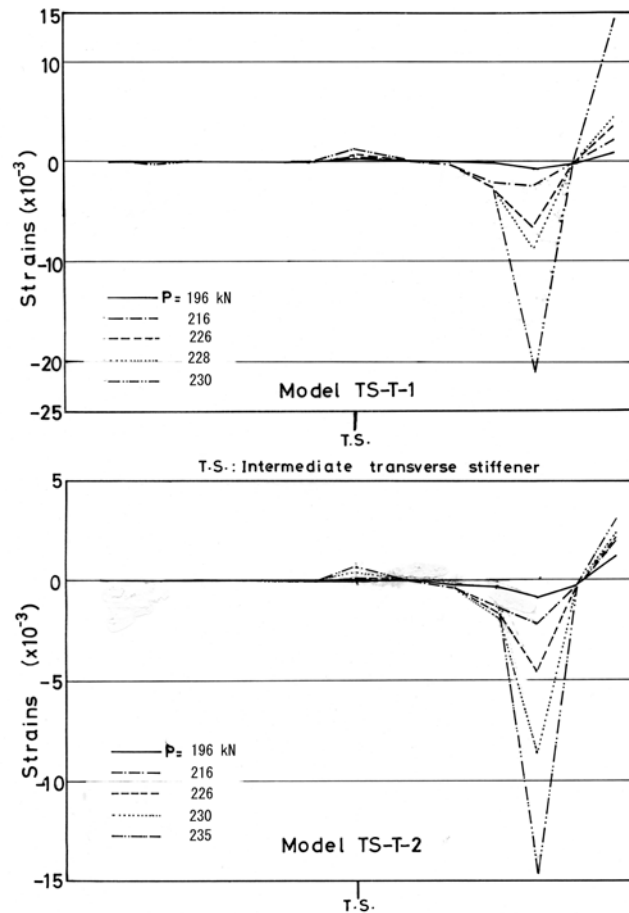
Fig.3.27 Bending strain in inclined flange.

(3.11) Comparison of experimental results with theories

(1) Ultimate strength

In most modal analyses, the assumption that the ultimate shear strength, V_{ult}, may be expressed as the sum of the shear buckling stress, V_{cr}, and the shear strength due to tension fields, V_t or with addition to the strength, V_f, caused by frame actions has been used. Here, it is assumed that the ultimate shearing force is expressed by the following form: $V_{ult}=V_{cr}+V_t$. It is considered that the equilibrium is kept in immediately before the final frame action.

It has been often said that the boundary condition for fixed upper and lower edges and simply supported other edges is really suitable in order to obtain shear buckling stresses of rectangular web plates. Also, it is assumed that this condition holds good for trapezoidal web plates.

By using Fig.3.2 the shear buckling strength for trapezoidal web plates can be calculated. From these results and the results obtained by applying Eq.(4.2) or Eq.(4.3) to Eq.(4.1), the ultimate loads can be estimated. Then, the computed results for the loading tests on the tapered plate girders are given in Table 3.5. In these calculations the value of ρ is assumed to be 0.5. In this table, the predicted values by means of the calculation methods proposed by Davis et al.[6],[7] and Falby[19] are similarly presented.

114

Table 3.5 Comparison of tests with various theories (kN).

Theory \ Girder		TS-1	TS-2	TS-3	TS-4	10A	20A	60A	70A	$\dfrac{Theory}{Exp._{mean}}$	Standard Deviation
Present	Approx.	197.2	222.3	223.8	197.8	125.2	174.2	164.8	254.2	0.98	0.11
	Exact	201.1	227.3	227.2	201.7	129.5	179.9	171.0	266.9	1.01	0.12
Davis-Mandal		225.5	248.1	231.4	214.8	127.0	154.0	175.0	233.0	1.00	0.09
Falby		105.1	89.2	102.0	94.0	37.1	38.8	51.8	71.6	0.36	0.09
Experiment		201.5	220.6	243.2	237.9	125.0	144.0	189.9	252.0	–	–

The present values predicted by applying the approximate yield condition, Eq.(4.2), agree well comparatively with the test results. Likewise, the present values predicted by applying the exact yield condition, Eq.(4.3), and the values given by using the expression of Davis et al.[6),7)] agree well relatively with the experimental results. The method by means of the approximate yield condition without iterations is exceedingly simple. The values obtained by the application of Falby's method[19)] are far apart from the experimental results.

(2) Required area for intermediate stiffener

Many suggestions have been proposed with respect to the required rigidity and area of intermediate stiffeners[6)]. The force acting on intermediate stiffeners of tapered plate girders may be obtained by applying Eq.(4.4). In Table 4.6, the ratios of the areas of intermediate stiffeners obtained from the measured dimensions in the test series II, A_s, to the required areas of intermediate stiffeners estimated on basis of this equation, $A_{s,req}$, are shown. It seems that these results coincide enough with the above-mentioned collapse modes. The above values for $A_{s,req}$ almost agree with the results obtained by applying Cooper's expression presented for uniform depth girders[25)] to the tapered girders of which trapezoidal web plates are converted into the rectangular web plates with the mean depth.

Table 3.6 Area of transverse stiffener.

Girder	TS-T-1	TS-T-2	TS-T-3	TS-T-4
$A_s / A_{s,req}$	0.79	0.34	0.20	0.24
$\gamma = EI / D_m D$	321	27	26	44
$\delta = A_s / D_m t$	0.200	0.085	0.056	0.070

$$D_m = (D_h + D_l)/2 \qquad D = Et^3 / 12(1 - v^2)$$

I: moment of inertia of area for stiffener

(3) Conclusions

The loading test results on the tapered girders with linearly varying depth loaded in shear were presented. Eight models were tested. Four models of them have intermediate transverse stiffeners. The present experimental works has clarified the failure mechanism of the tapered girders.

The results obtained by tests are as follows.

1) The development of the diagonal tension field is insufficient in the triangular part of

the trapezoidal panel.

2) In the case of the tapered girders with intermediate stiffener, the deflected surface of the web panel depends on the rigidity of intermediate stiffener.

3) Though the small rigidity of intermediate stiffener does not result in the girder collapse, the large deformation of web is undesirable.

The validity of the expression to predict the load carrying capacity was examined by comparing some experimental results with the predicted collapse loads.

4) The expression using the approximate yield condition predicts fairly well the ultimate strength.

A formula to estimate the force applied on intermediate stiffeners was introduced.

5) The investigation on the required area of intermediate stiffeners was tried by using above results.

4.3.3 Rigidity of intermediate vertical stiffener

(1) Introduction

There is little in the study of plate girders with webs tapered in depth. The test results on the ultimate shear strength of tapered plate girders with straight varying depth having intermediate vertical stiffeners and some theoretical considerations are presented. After the first testing panels that had been once tested in Article 4.3.2 were stiffened, the other side panels were used as the second testing panels in these experiments. The variation of the axial force along intermediate stiffeners is theoretically estimated and it is compared with the axial strain obtained by the test. On the basis of these results, how the properties of intermediate stiffeners effect on the ultimate strength and the failure mode of girders are discussed.

(2) Description of tests

(2.1) Models

Four models were tested. The models that had been used in the study at Article 4.3.2. were once applied. The theoretical collapse load of the first testing panels in the previous experiment is lower than that of the second testing panels in this experiment. The collapsed panels were reinforced by welding angles over top and bottom flanges. Typical stiffened panels are shown in Fig.3.28.

Each girder is designed to be identical in size except for intermediate stiffeners. The outlines of these dimensions are shown in Fig.3.29. Intermediate transverse stiffeners are used in pairs. The actual dimensions of intermediate stiffeners are shown in Table 3.7. The symbol "S" which is contained in some girder numbers is used to denote the present testing panels.
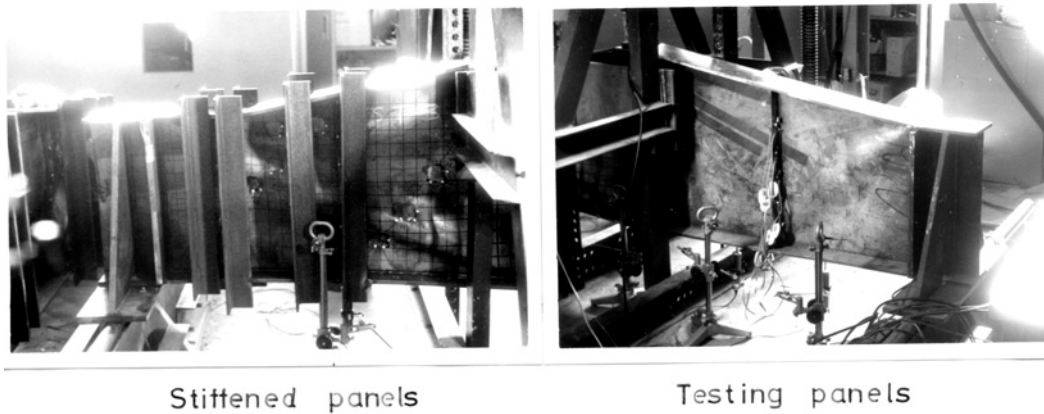
Fig.3.28 Girder before test.
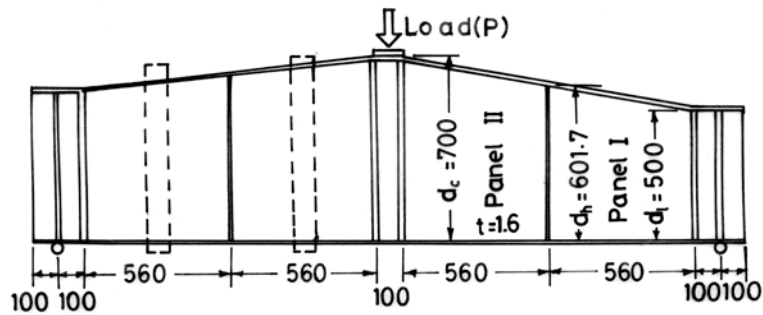
Fig.3.29 Outlines of test girders.

Table 3.7 Measured dimensions of intermediate stiffeners.

Model	TS-T-1(S)	TS-T-2(S)	TS-T-3(S)	TS-T-4(S)	TS-T-1	TS-T-2	TS-T-3	TS-T-4
l_s (mm)	598	599	599	598	602	602	602	602
b_s (mm)	41.0	40.4	40.5	40.2	32.8	13.5	17.8	21.0
t_s (mm)	4.3	4.2	3.1	3.1	2.97	3.01	1.65	1.68

l_s: Length of intermediate stiffener b_s: Width of intermediate stiffener
t_s: Thickness of intermediate stiffener

(2.2) Coupon tests

All models were made of SS41 steel. The results of the coupon tests are shown in Table. 3.8.

Table 3.8 Coupon test results.

Model		TS-T-1(S)	TS-T-2(S)	TS-T-3(S)	TS-T-4(S)	TS-T-1	TS-T-2	TS-T-3	TS-T-4
Yield stress	F	216.1	216.1	286.3	286.3	216.1	216.1	286.3	286.3
σ_Y (MPa)	W	280.8	280.8	281.4	281.4	280.8	280.8	281.4	281.4
	S	253.6	253.6	318.7	318.7	371.6	371.6	281.4	281.4
Young's	F	1.95	1.95	2.13	2.13	1.96	1.96	2.13	2.13
Modulus E	W	2.12	2.12	2.13	2.13	2.12	2.12	2.13	2.13
X10⁵ (MPa)	S	2.15	2.15	2.06	2.06	2.10	2.10	2.13	2.13
Poisson's ratio ν	W	0.269	0.269	0.326	0.326	0.269	0.269	0.326	0.326

F: Flange   W: Web   S: Stiffener

117

(2.3) Initial deflections

The initial deflections of the flanges and the web over the present testing panels were not small owing to the effects of the previous load application. But the deformation of intermediate stiffeners on the present testing panels was very small.

(3) Experimental results and considerations

(3.1) Failure mode

The collapsed panels after the tests are shown in Fig.3.30. It is found that the outside panel (Panel I) of each girder developed sufficient shear mechanism. The inside panel (Panel II) of each girder was subjected to the combination of bending moment and shearing force. Then, it is seen that the development of the tension field was not enough in Panel II.
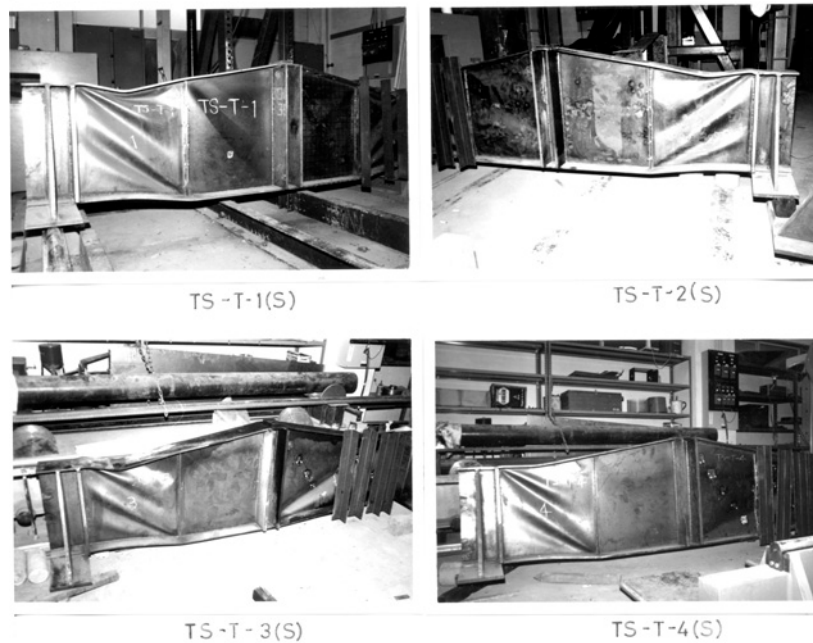
Fig.3.30 Collapsed girders.

(3.2) Girder deflection

The central deflections are plotted with respect to applied loads in Fig.3.31. Each curve is linear up to about 90% of the collapse load. When the load-central deflection relationship begins to be nonlinear, the ratio of the central deflection to the overall span is in the region of 1/500～1/700. Subsequently the deflection shows a gradual rate of increase for a while. However, it increases rapidly as the failure approaches.

(3.3) Vertical displacement of inclined flange

The relationship of load against vertical displacement of the inclined flange is shown in Fig.3.32. It is seen that from the comparison of Fig.3.31 with Fig.3.32 the load-central deflection curve closely corresponds to the load-vertical displacement curve of the top flange. Namely, it is supposed that the dent of the top flange has a serious effect on the failure of the girder.
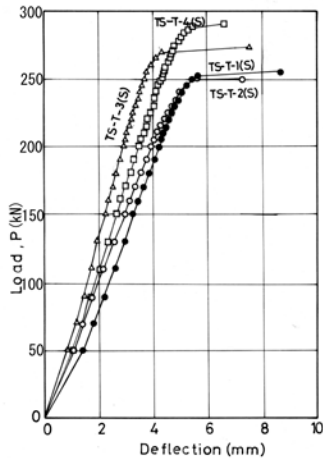
Fig.3.31 Central deflection.　　　Fig.3.32 Vertical displacement of inclined flange.
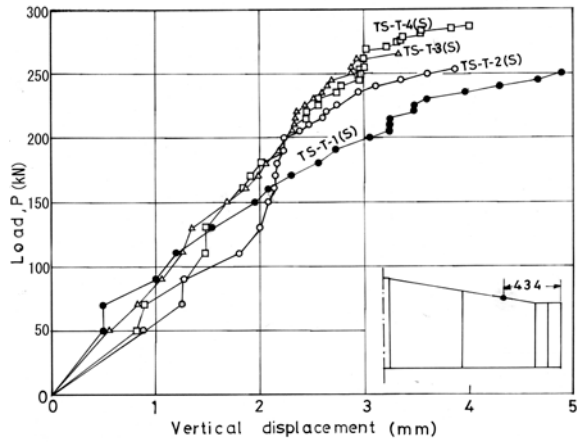
(3.4) Strains of intermediate stiffener

　　Fig.3.33 shows how the axial strain varies along the length of the intermediate transverse stiffener against various applied loads. Fig.3.34 gives the positions of the strain gauges on the intermediate stiffener. Each girder shows the similar distribution of strains and the maximum compressive strain 500～600 micro-strain in the order of magnitude. Though these distributions are similar to the distribution for Model TS-T-1 in form, the magnitude of the maximum strain in Fig.3.33 is considerably smaller than that for Model TS-T-1 owing to the difference in size of those stiffeners. In Fig.3.35, the variation of the bending strain along the intermediate stiffener at various loads is shown. The maximum value of the strains for each girder is under 20% in comparison with that for Model TS-T-1. Therefore, it is evident that the function of each intermediate stiffener was satisfactorily effective at the failure of the girder and the panels buckled individually.

Fig.3.33 Axial strain along vertical stiffener.　　　Fig.3.34 Position of strain gauges.

119
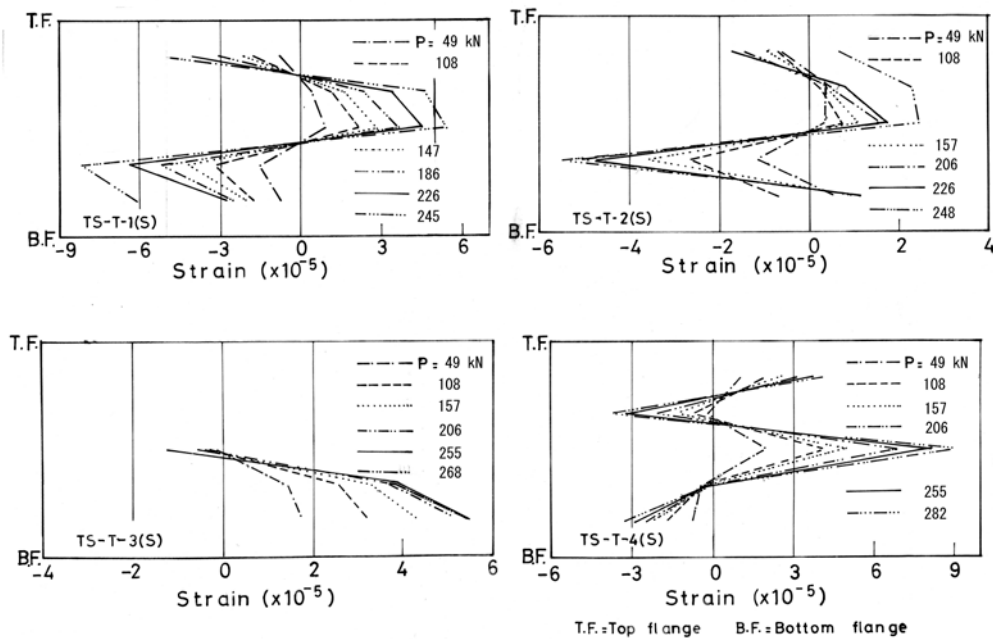
Fig.3.35 Bending strain along vertical stiffener.

(3.5) Ultimate strength

The collapse loads, P_{ult}, observed are shown in Table 3.9. In this table, the results obtained by the previous experiment are also shown. In each girder, the value for the present testing panel is slightly exceeding that for the first testing panel. It seems that the reason is due to the restrict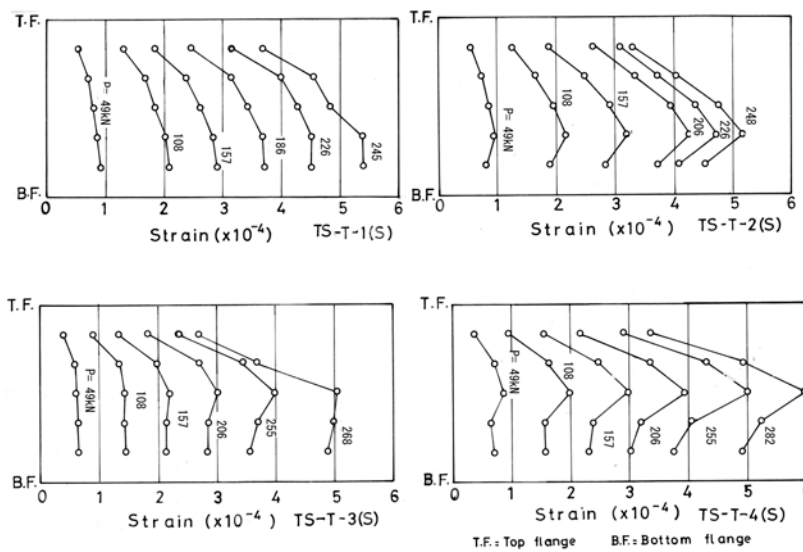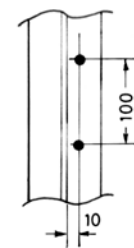ion of deformation by the stiffened panels. It is supposed that the reason why the collapse load for Models TS-T-3(S) and TS-T-4(S) are higher than that for Models TS-T-1(S) and TS-T-2(S), respectively, is reduced to the difference in the yielding stress of flanges. Since every intermediate stiffener was effective when the failure of the girder took place, it can be considered that there is no effect of the difference in size of intermediate stiffeners on the ultimate strength of the present test.

Table 3.9 Collapsed loads.

Model	TS-T-1(S)	TS-T-2(S)	TS-T-3(S)	TS-T-4(S)	TS-T-1	TS-T-2	TS-T-3	TS-T-4
P_{ult} (kN)	245	248	269	282	230	237	236	255

(4) Loads on intermediate stiffener

A method predicting the collapse load of tapered plate girders in shear has been proposed at 4.3.1. Further, in the article the axial force acting on the intermediate stiffener has been given by Eq.(4.4). This method can be extended as shown hereunder.

 (4.1) As shown in Fig.3.4, it is assumed that two adjacent panels loaded in shear develop independent membrane stress fields. When failure occurs earlier in Panel I, the inclination of the diagonal tension field for Panel I, ϕ_1, can be determined. The axial force acting on the intermediate stiffener at any section, $F_{s,n}$, can be obtained by considering the equilibrium of the force acting on the free body as follows:

120

$$F_{s,n} = \tan\beta \left(\sigma_{t2}\, t\, s_2 \cos\phi_2 + 2\rho_2\, \sigma_{t2}\, t\, a_2 \sin\phi_2 \cos\phi_2 - \sigma_{t1}\, t\, s_1 \cos\phi_1 \right) + A_{\mathrm{I}} + A_{\mathrm{II}}$$

$$(4.5)$$

in which A_I and A_{II} are the vertical components of the forces acting along the boundaries of Panel I and II, respectively, and the loads applied by buckling stress fields to the intermediate stiffener are neglected for simplification. Then the variation of the axial force along the intermediate stiffener on the testing panel is obtained as shown in Fig.3.36 if the nominal dimensions of the girder are employed in the calculation. The ratio of the maximum value of $F_{s,n}$ to F_s is about 1.2.
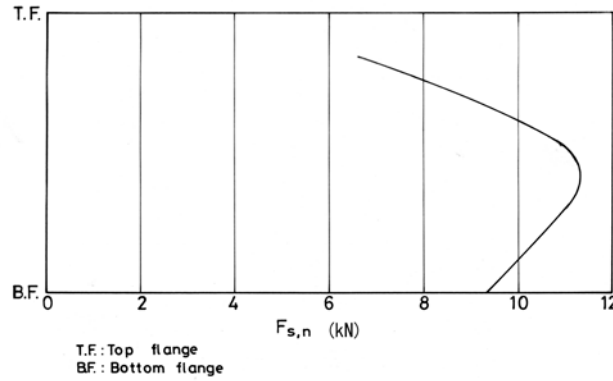
Fig.3.36 Predicted axial load carried by vertical stiffener.

(4.2) Comparison of calculated values with experimental results

It is seen that the curve at the maximum load in Fig.3.4 and the curve in Fig.3.36 resemble closely in form. It is assumed that the required area of intermediate stiffeners. $A_{s,req}'$, can be estimated from the maximum value of $F_{s,n}$. The ratio of the effective cross-sectional area of the intermediate stiffener, A_s', between $A_{s,req}'$ is shown in Table 3.10.

Table 3.10 Required cross-sectional area of intermediate stiffener.

Model	TS-T-1(S)	TS-T-2(S)	TS-T-3(S)	TS-T-4(S)	TS-T-1	TS-T-2	TS-T-3	TS-T-4
$A_S' / A_{S,req}'$	1.04	1.00	1.05	1.04	1.04	0.61	0.43	0.46
$\gamma = E_S I_S / d_h D$	934	895	642	623	321	27	26	44
$\delta = A_S / d_h t$	0.362	0.355	0.264	0.260	0.200	0.085	0.058	0.070
Collapse mode	S	S	S	S	S	W	W	W

A_S': Effective cross-sectional area of intermediate stiffener.

A_S: Cross-sectional area of intermediate stiffener.

E_S: Young's modulus of intermediate stiffener.

E_W: Young's modulus of web plate.

I_S: Moment of inertia of area for intermediate stiffener.

$D = E_W t^3 / 12(1 - \nu^2)$

S: Stiffener effective 　　W: Stiffener failed

A_s´must contain an effective part of the web plate. A width of 40t[12] is assumed to act with the stiffener in the calculation of this table. In this table, the results applied to the previous testing panels are also shown. It has been assumed in the theoretical analysis that the individual shear mechanism is formed in the adjacent panels. In the experiment, Panel I developed independently and sufficiently the tension field in comparison with Panel II subjected to the combination of bending moment and shearing force. Then, it should be noted that A_s´$/ A_{s,req}$' is closely related to the collapse mode as shown in Table 3.10. Therefore, it is considered that the required area of intermediate stiffeners must be incorporated in design. Since in tapered plate girders the vertical component of the inclined flange force acts on the intermediate stiffener, it is still more necessary. It is obtained that $A_{s,req}$' may be an approach to the design of intermediate stiffeners, nevertheless the width of he web plate acting with the stiffener is obscure.

(5) Conclusions

In order to investigate the ultimate strength and the behavior of the tapered plate girders with varying depth loaded in shear, four model girders having intermediate transverse stiffeners were tested. The strains on the intermediate stiffener were measured and the variation of the axial force along it was theoretically estimated.

Obtained results are as follows.
1) The dent of the top flange has a serious effect on the failure of the girder.
2) The property of the intermediate stiffener influences the formation of shear mechanism definitely.
3) The magnitude of the ultimate strength of tapered plate girders in shear is not much reduced owing to the slightly insufficient rigidity of intermediate stiffeners.
4) It is considered that the variation of the predicted axial force along the intermediate stiffener is proper comparing the strains obtained by the tests.
5) There was a suggestion on the required cross-sectional area of intermediate stiffeners. It corresponds quite to the collapse mode of the panels.

4.4 Discussions

The researches on the static load carrying capacity of the steel plate girders under shear have been much carried out experimentally and theoretically. However, it seems to be necessary to carry out the research like the following hereafter.

Longitudinally stiffened web panel should be researched by the elasto-plastic finite displacement analysis using means such as the finite element method. Then, simple and accurate design methods, for example any plastic analysis, for such stiffened panel need to be developed.

On the ultimate strength of girders with varying depth in shear, the study of the inelastic behavior for such tapered panel is required. The research on such problem seems to be almost lacking. On the required stiffness of intermediate stiffeners, further examination is necessary.

In the future, further discussions will be necessary concerning not only viewpoint of the strength but also the serviceability. Besides, it is supposed to be necessary that proper girders are used in proportion to various purposes.

4.5 References

1) Johnston, B. G.: Guide to Stability Design Criteria for Metal Structures, 3rd ed. (John Wiley & Sons, 1976).

2) Gaylord E H Discussion of "Strength of plate girders In shear" by Basler K. Transactions of ASC.E, Vol. 128, Part II, 1963.

3) Hasegawa, A., F. Nishino and T. Okumura : Ultimate strength of longitudinally stiffened plate girders in shear, Proceedings of JSCE, No. 235, March, IQ. 75 (in Japanese).

4) Rockey, K. C. and M. Skaloud : The ultimate load behavior of plate girders in shear, Struct. Engr., Vol. 50, No. 1, Jan., 1972.

5) Basler,K. : Strength of Plate Girders in Shear, Journal of the Structural Division, ASCE, Vol.87,No.ST7, pp.151-180., 1961.

6) Davis,G. and Mandal,S.N. : The collapse Behaviour of Tapered Plate Girders Loaded within the Tip, Proc. Instn. Civ. Engrs., Part2, Vol.67,pp.65-80,1979.

7) Davis,G. and Mandal,S.N. : Tapered Steel Beams Loaded within Tip, Journal of the Structural Division, ASCE, Vol.105,No.ST3,pp.589-599,1979.

8) Porter,D.M., Rockey,K.C. and Evans,H.R. : The collapse behaviour of plate girders loaded in shear, Structural Engineer, Vol.53,No.8,pp.313-325,1975.

9) Galambos,T.V. (ed.), Guide to Stability Design Criteria for Metal Structures, 4th ed., John Wiley & Sons, New York, 1988.

10) Ostapenko,A. and Chern,C. : Ultimate Strength of Plate Girders under Shear, Fritz Eng. Laboratory Report, No.328.7,Lehigh Univ., 1969.

11) Vasarhelyi,D.D. et al. : Tests of Riveted Plate Girder with a Thin Web, Proc. of ASCE., No.ST10, 1960.

12) Tani,S. : Analysis of Plated Structures, Gihodo, 1969 (in Japanese).

13) Basler,K., Yen,B.T., Muller,J.A. and Thürlimann,B. : Web Buckling Testson Welded Plate Girders, Weld. Res. Counc. Bull., No.64, 1960.

14) Sawada,Y., Lee.G.C. and Ito,M. : FINITE ELEMENT ANALYSIS OF TRANSVERSELY STIFFENED PLATE GIRDERS IN SHEAR, Stability of Steel Structures, Second International Colloquium of IABSE, 1977.

15) Cescotto,S., Maquoi,R. and Massonnet,Ch. : Simulation sur ordinateur du comportement ⬜ la ruine des poutres ⬜ ⬜me pleine cisaill⬜⬜s ou fl⬜chies, Construction Metallique, No.2, pp.27-40, 1981.

16) Kuranishi,S., Nakazawa,M. and Iwakuma,T. : On the tension field action and collapse mechanism of a panel under shear, structural Eng./earthquake Eng., JSCE, Vol.5,No.1,pp.161s-171s, 1988.

17) Kuranishi,S., Nakazawa,M. and Iwakuma,T. : A new formula to predict the ultimate shear strength of a plate girder, Structural Eng./Earthquake Eng., JSCE, Vol.6,No.2, pp.239s-250s, 1989.

18) Nara,S. and Komatsu,S. : A study on the ultimate strength of steel plate under pure shear stress, Proc. of 38th Annual Conference of JSCE, I-88, pp175-176, 1983 (in Japanese).

19) Falby,W.E. and Lee,G.C. : Tension-Field Design of Tapered Webs, AISC,

Engineering　Journal, Vol.13, No.1, pp.11-17, 1976.

20) Marsh C., Ajam W. and Ha H.: Finite Element Analysis of Postbuckled Shear Webs, Journal of Structural Engineering, ASCE, Vol.114, No. 7, pp.1571-1586, 1988.

21) Lee, S. C., and Yoo, C. H.: Strength of Plate Girder Web Panels under Pure Shear, Journal of Structural Engineering, ASCE, Vol.125, No.8, 1999

22) Komatsu,S., Kitada,T. and Miyazaki,S. : Elastic-Plastic Analysis of Compressed Plate with Residual Stress and Initial Deflection,proceedings of JSCE,No.244, pp.1-14, 1975.

23) Moriwaki,Y. and Fujino,M.: Experimental Study on Shear Strength of Plate Girders with Initial Imperfections, Proceedings of JSCE, No.249, PP.41-54, 1976.

24) Mikami,I. And Yonezawa,H. ：Extrapolation Technique for Finite Difference and Finite Element Solutions, Proc. Of the Japan national congress for Applied Mechanics, Vol.25,Univ. of TOKYO Press, 1975.

25) Cooper,P.B. ：Strength of longitudinally stiffened plate girders, Journal of the Structural Division, ASCE, Vol.93,No.ST2, pp.419-451, 1967.

26) Rockey,K.C.,Valtinat,G. and Tang,K.H. ：The design of transverse stiffeners on webs　loaded in shear-an ultimate load approach, Proc. Instn. Civ. Engrs., Part 2, Vol.71,　pp.1069-1099, 1981.

Chapter 5

Load-carrying capacity of girders under combined bending and shears

5.1 General description

Many studies on a plate panel subjected simultaneously to bending moments and shear forces in its plane have been carried out and the interaction curves have been proposed.[1)-4)] The boundary conditions of all four edges simply supported have been applied in these analyses. For a plate simply supported on four edges, under bending, compression and shear, an approximate evaluation of the critical combined load has been obtained[5)]. Most of the panels in plate girders are subjected to the combined loading of varying bending moments in longitudinal direction and uniform shearing stress. Accordingly, a plate panel under the combined action of unequal end moments and shear forces must be chosen as the study model. In the part 2.5 of this thesis, the elastic buckling of a rectangular plate panel under unequal end moments and shear forces was treated and the interaction expressions was presented.

A panel of plate girders has four edges. Therefore, the effects of these frame members, flanges and stiffeners, should be considered in an analysis. In the article 2.3 of this thesis, the elastic buckling of plate girders loaded with the unequal end moments through some panels was investigated.

The studies on the post-buckling strength of plate panels under the combined action of bending moments and shear forces are relatively fewer.[6),7)] The investigations on the interaction of girder panels in inelastic range under combined loading have been proposed.[8)-10)] These theories have been based on the assumption of the analytical modeling.

The plate girders with tapered web in depth have been often used. However, the investigation on the buckling strength of such tapered web panels under the combined action of bending moments and shear forces is few. The works of general design procedures for the ultimate strength of panels with variable depth are required.[11)]

In this chapter, the interaction for buckling strength of plate panels under the combined action of bending moments and shear forces will be presented. To begin with, the existing studies on the interaction for buckling strength of rectangular plate panels will be introduced. Subsequently, the theoretical and experimental investigations on the buckling strength of tapered panels under the combined action of bending moments and shear forces will be given.

5.2 Girders with uniform depth under combined bending and shear

A web panel of plate girders is surrounded by frame members, flanges and stiffeners. The bending capacity of plate girders depends principally on the ultimate strength of the flanges. Supposing that these flanges are excluded from the contribution for the shear capacity of the web, the shear force is independent of the moment in the panel if the bending moment is less than M_{Yf}, which is the moment that produces yield in the flanges. If the contribution caused by flanges to shear strength is taken into consideration, the shear force depends on the moment due to the influence of the flange axial force on the flange plastic moment. If M_u indicates the ultimate

bending moment, for values of the bending moments $M_{Yf} \le M \le M_u$, the shear force V must be less than V_u, which represents the ultimate shear force.

Basler suggests that the shear force in a girder may be supported only by the web. Accordingly, his proposal on the interaction diagram between bending moment and shear force is shown in Fig.2.1.[8] The vertically straight line applies to the girder with thin webs in which M exceeds the yield moment M_Y.
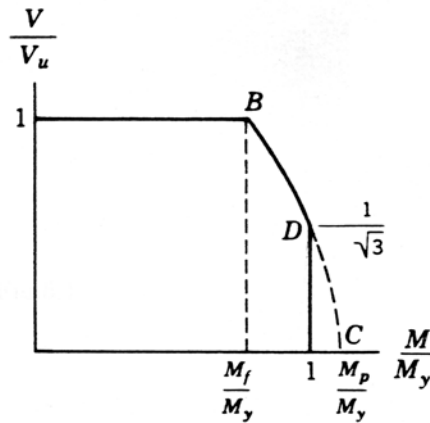

Fig.2.1 Shear-moment interaction diagrams.

When the flange rigidity is taken into account in the shear capacity, the reduction in the shear capacity due to coexisting bending moment becomes a problem. Rockey's model[10] assumes the inclusion of the following factors: (1) the reduction in the buckling stress of the web due to the presence of a bending stress or a direct stress, (2) the influence of the in-plane bending stresses upon the value of the diagonal tensile membrane stress which is developed in the diagonal strip, (3) the reduction in the magnitude of the plastic modulus of the flanges due to the presence of the axial compressive and tensile stresses. For the case of the combined action of shear forces and bending moments, the buckling stress reduction can be calculated from the interaction curve in the shape of an arc.

Rockey et al. have proposed the interaction diagram between the shear and bending as shown in Fig.2.2[12]. In this figure, C represents the position at which the mode of failure changes from the shear mechanism mode to the flange failure mode. The shear at S' is equal to the pure shear at S and the bending moment M_s' is assumed to be the maximum bending moment in the end panel of a simply supported girder.
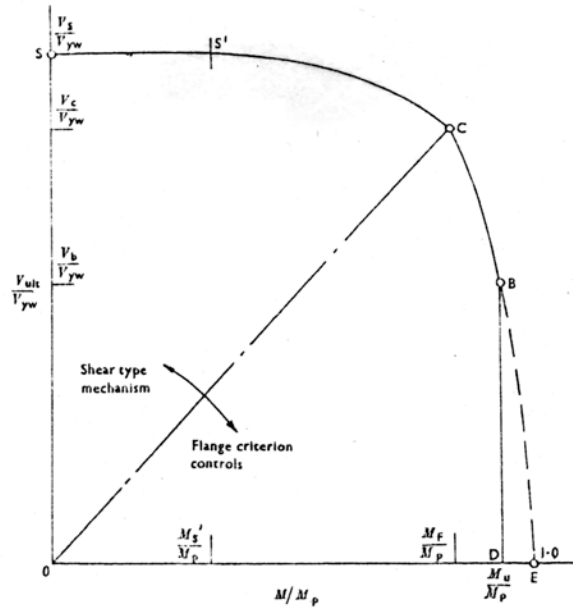
Fig.2.2 Shear-moment interaction diagrams.

Chern and Ostapenko[9] suppose that the failure of a girder panel subjected to the combined action of shear and bending moment may be due to the failure of the web, buckling of the compression flange or yielding of the tension flange. The proposed interaction curve is shown in Fig.2.3. At point Q_1, the panel is under pure shear. Q_2 is the point in which the stress in the compression flange due to the ultimate shear strength under combined loads is equal to the buckling stress of the compression flange. In the region under the control of web failure, the buckling stress of a panel subjected to combined shear and bending is calculated by the interaction equation that is represented elliptically in shape. At points Q_3 and Q_5, the panel is under pure bending. At point Q_4, the stress in the tension flange due to the ultimate web shear strength under combined loads is equal to the tension flange yield stress.
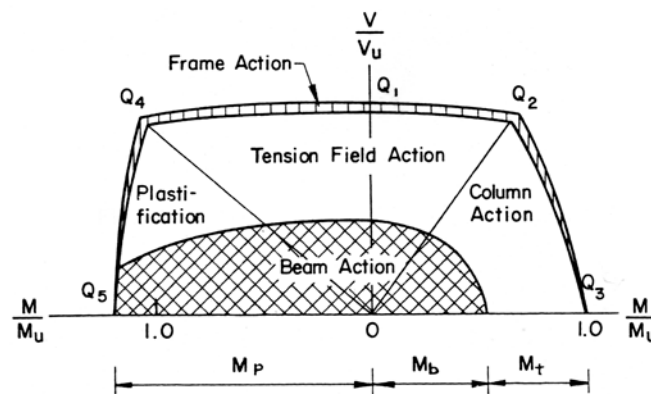

Fig.2.3 Shear-moment interaction diagrams.

127

5.3 Girders with linearly varying depth under combined bending and shear
5.3.1 Analytical methods

(1) Introduction

A large number of studies on the ultimate strength of plate girders under combined loads have been done.[1)-4)] The design methods of the girders with parallel flanges have been considerably established. On the one hand, the girders with varying depth are also often used. Two types are available for varying web depth: 1) the application of a curved line, 2) the application of a straight line. However, the researches on the strength of such girders with varying depth under the combined action of bending and shear are few. The girder panel under such state applies to the panel near the intermediate supports of continuous girders. The design method on the strength of these panels with varying depth is undoubtedly necessary.[11)]

In this article, for the case in which a trapezoidal panel of plate girders with linearly varying web depth is subjected to the combined action of bending moments and shear forces, the elastic buckling loads are calculated by using a finite element method, and an interaction equation for the combined loading is obtained. In order for the interaction equation to be easily used, the buckling loads of the trapezoidal panels may be estimated by the conversion from the buckling coefficients of rectangular plates. Furthermore, a method to predict the ultimate strength is also proposed. In this case for which a simple modal analysis is introduced, it is assumed that the ultimate strength can be obtained as the sum of the buckling strength under the combined loads and the strength supported by the tension field. Also, it is assumed in this analysis that the local and lateral buckling of flanges do not occur until the ultimate strength is attained. It will be found that this simple estimation can predict relatively well the ultimate strength of the girder panel. Therefore, it may be found that this estimation method is useful for the design of the plate girder with non-uniform sections.

(2) Analysis on strength of panel under combined load
(2.1) Interaction curves

In order to predict the ultimate strength of the panel, the estimation by means of a modal analysis is adopted because of its simplicity. At first, the buckling strength of the trapezoidal panel under the combined action of bending moments and shear forces is calculated. From the numerically computed results by a finite element method, the interaction curves under the combined load can be obtained.

So as to estimate the elastic buckling loads of the trapezoidal web panel under the combined action of bending and shear, a trapezoidal panel in the condition of plane stress is assumed as shown in Fig.3.1. As the boundary condition of lateral deflections, it is assumed that the plate is simply supported at $Y = 0$ and $Y = a$, and simply supported or fixed at other two edges. Stress analysis is carried out by using a finite element method with constant strain triangles. In buckling analysis a finite element method with triangular elements in which the deflections at three apexes and the rotations along three sides constitute the degree of freedom is used.[13)] The calculations about three kinds of $\beta (5°, 10° \text{and} 15°)$ are executed. An extrapolation method is adapted to predict the converged values from numerically computed results.[14)] By considering

the equilibrium among forces acting on the panel shown in Fig.3.1, the relationship among these forces can be obtained. By calculating mean shearing stress, τ *, among all elements in consideration of the area of each element and assuming that the bending moment in the panel varies linearly, the edge fiber stress at the middle of the panel length, $\sigma_m = \{\sigma_1(d_1/d_m)^2 + \sigma_h(d_h/d_m)^2\}/2$, is taken as the representative value of normal stresses, σ *. By using τ *, σ * and the average value of panel depth-to-thickness ratio, d_m/t , k_τ* and k_σ* which are buckling coefficients can be estimated, on condition that t is the thickness of the web panel.
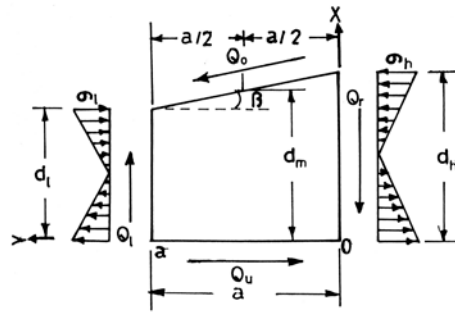

Fig.3.1 Trapezoidal panel.

In order to obtain the interaction curve on the buckling under the combined action of bending and shear, the flexural buckling coefficient, k_σ, of the trapezoidal panel in which only normal stress is in equilibrium is calculated by means of the stress, σ, at the middle of the panel. As a result of numerical computations the buckling curves were obtained as shown in Fig.3.2. Namely, it is suitable to understand that the shear forces shown in Fig.3.1 appear if the equilibrium in Fig.3.2 breaks. Besides, the in-plane displacement is restricted in the direction of x and y at the middle point of the left side and in the direction of x at the middle point of the right side. Generally, it is the purpose of this analysis to get at the behavior in average of the panel. In Fig.3.2, $\overline{\alpha}$ denotes the mean aspect ratio of the panel. It is seen that as β increases buckling coefficients decrease.
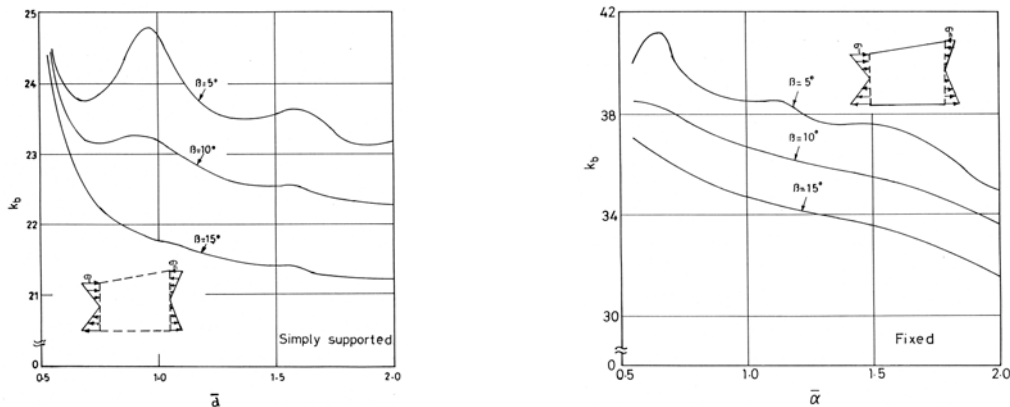
(a) Simply supported.　　　　　　　　(b) Fixed.

Fig.3.2 Buckling load curves.

The shear buckling curves that are necessary to obtain the interaction curves under the combined loads are shown in Fig.3.3 too. The shearing stress that corresponds to the buckling coefficient under shear, k_τ, is represented by τ.
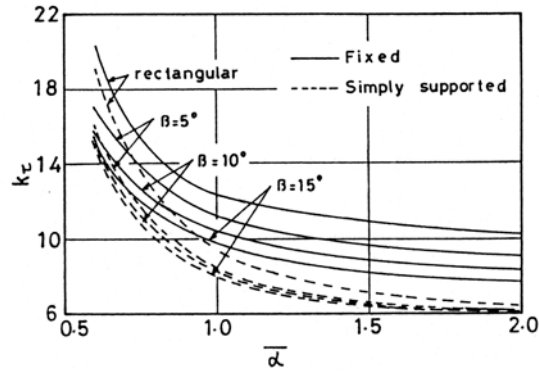

Fig.3.3 Buckling load curves.

From the computed results, the interactive buckling curves under combined loads of the panel in the case that $\beta=10°$ are shown in Fig.3.4. In these figures, κ denotes the ratio of the moment acting on the left side, M_l, with that acting on the right side, M_r, and it can be expressed as $\kappa = M_l / M_r = (\sigma_l / \sigma_r) \cdot (d_l / d_r)^2$. It is evident from these figures that slight differences in the shape of the curves depend on the value of κ in every case of $\bar{\alpha}$. The curves corresponding to $\kappa = 0.9$ are held in the inner position. Even if the value of $\bar{\alpha}$ changes from 0.6 to 1.2, the curve corresponding to each κ shows a similar tendency. Comparing the interaction curves corresponding to simply supported and fixed conditions for $\bar{\alpha}=1$ in order to examine the difference between the boundary conditions, it is seen that they have a similar tendency.
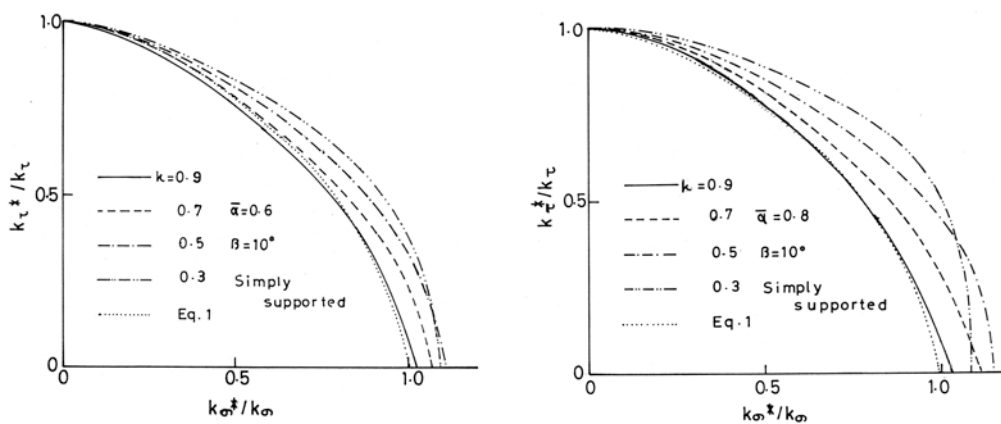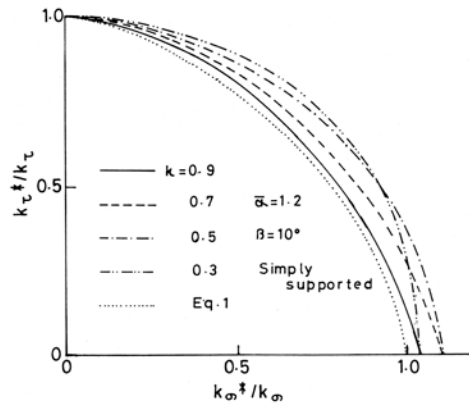

(a) $\bar{\alpha} = 0.6$ (Simply supported)   (b) $\bar{\alpha} = 0.8$ (Simply supported)
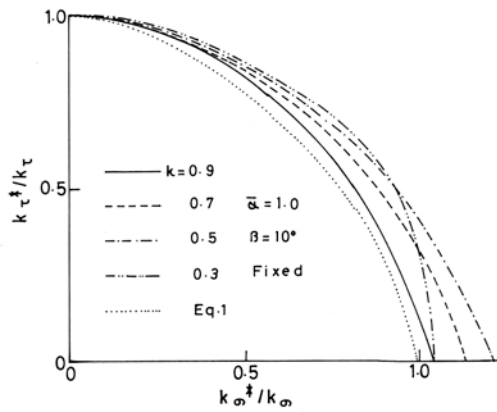
Fig.3.4 Interaction curves.
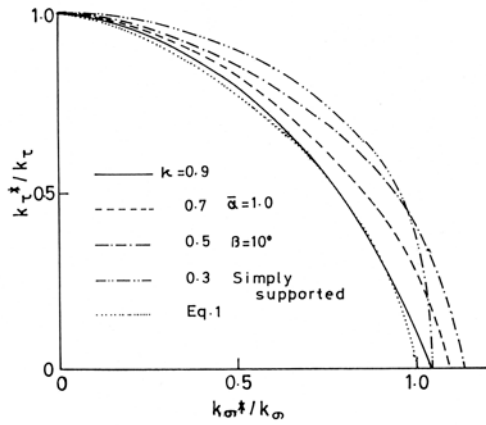
(c) $\overline{\alpha} = 1.0$ (Simply supported)   (d) $\overline{\alpha} = 1.2$ (Simply supported)

(e) $\overline{\alpha} = 1.0$ (Fixed)

Fig.3.4 Interaction curves (Continued).

An interaction curve for the trapezoidal panel is assumed to be the following form: $(\sigma^*/\sigma)^j + (\tau^*/\tau)^j = 1$. Each dotted line corresponds to the case in which j takes the value of 1.6 in the above equation. Each curve is located almost within the curve in which κ equals to 0.9. Though it is also fairly conservative compared with the case in which κ takes small values, owing to the convenience of design this curve is adopted as the interaction curve. Namely, the interaction equation becomes as follows:

$$\left(\sigma^*/\sigma\right)^{1.6} + \left(\tau^*/\tau\right)^{1.6} = 1 \tag{5.1}$$

In order to facilitate the calculation of the buckling load under the combined action, the coordinate, ξ, where the buckling load of trapezoidal panels is equivalent to that of rectangular panels is estimated as conversion positions and is related to $\overline{\alpha}$ as shown in Fig.3.5.

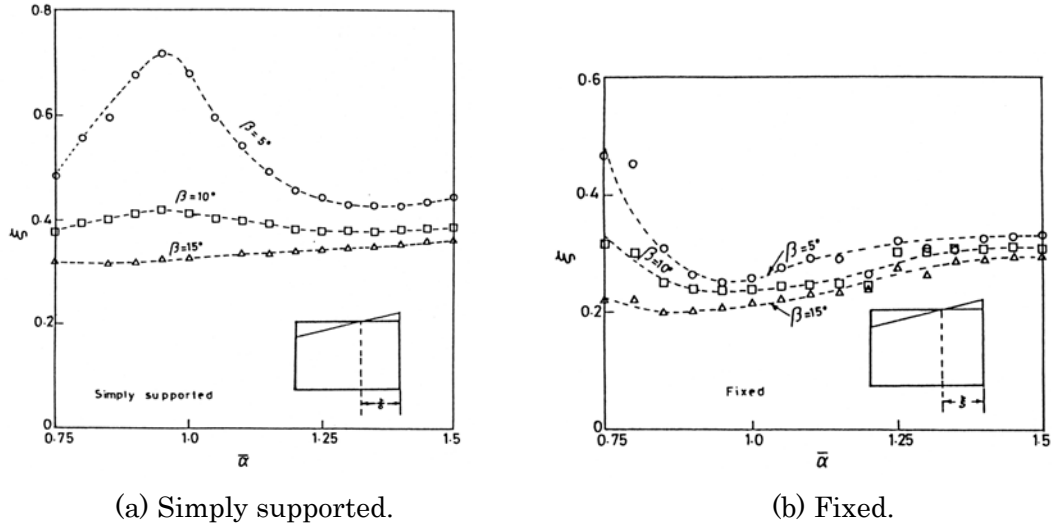(a) Simply supported.   (b) Fixed.

Fig.3.5 Conversion into rectangular panel.

Furthermore, the regression equations about these curves are shown as follows:

Simply supported:

$$\beta = 5^0 : \xi = -0.409 + 1.19\bar{\alpha} \qquad\qquad (\bar{\alpha} \leq 0.95)$$

$$\xi = 3.816 - 4.98\bar{\alpha} + 1.83\bar{\alpha}^2 \qquad (\bar{\alpha} > 0.95)$$

$$\beta = 10^0 : \xi = 0.226 + 0.206\bar{\alpha} \qquad\qquad (\bar{\alpha} \leq 0.95)$$

$$\xi = 0.905 - 0.795\bar{\alpha} + 0.3\bar{\alpha}^2 \qquad (\bar{\alpha} > 0.95)$$

$$\beta = 15^0 : \xi = 0.225 + 0.068\bar{\alpha}$$

$$(5.2)$$

Fixed:

$$\beta = 5^0 : \xi = 4.36 - 8.32\bar{\alpha} + 4.2\bar{\alpha}^2 \qquad\qquad (\bar{\alpha} \leq 1.1)$$

$$\xi = 0.32 - 0.148\bar{\alpha} + 0.105\bar{\alpha}^2 \qquad (\bar{\alpha} > 1.1)$$

$$\beta = 10^0 : \xi = 1.76 - 3.1\bar{\alpha} + 1.57\bar{\alpha}^2 \qquad\qquad (\bar{\alpha} \leq 1.1)$$

$$\xi = -0.96 + 1.74\bar{\alpha} - 0.6\bar{\alpha}^2 \qquad (\bar{\alpha} > 1.1)$$

$$\beta = 15^0 : \xi = 0.80 - 1.31\bar{\alpha} + 0.722\bar{\alpha}^2 \qquad (\bar{\alpha} \leq 1.1)$$

$$\xi = -0.49 + 0.989\bar{\alpha} - 0.309\bar{\alpha}^2 \quad (\bar{\alpha} > 1.1)$$

$$(5.3)$$

From the regression analysis of the shear buckling curves shown in Fig.3.3, the following expressions can be obtained.

Simply supported:

$$\beta = 5^0 \ : k_\tau = 7.12 - 5.34/\overline{\alpha} + 6.60/\overline{\alpha}^2$$

$$\beta = 10^0 : k_\tau = 6.84 - 3.30/\overline{\alpha} + 4.78/\overline{\alpha}^2 \qquad (5.4)$$

$$\beta = 15^0 : k_\tau = 6.78 - 4.09/\overline{\alpha} + 5.21/\overline{\alpha}^2$$

Fixed:

$$\beta = 5^0 \ : k_\tau = 8.86 - 1.54/\overline{\alpha} + 3.84/\overline{\alpha}^2$$

$$\beta = 10^0 : k_\tau = 7.58 + 0.083/\overline{\alpha} + 2.85/\overline{\alpha}^2 \qquad (5.5)$$

$$\beta = 15^0 : k_\tau = 7.38 - 1.28/\overline{\alpha} + 3.56/\overline{\alpha}^2$$

Determining the position, ξ, by means of Eq.(5.2) or (5.3) and estimating the aspect ratio of the corresponding rectangular plate, the value of σ can be obtained. By determining the value of τ from Eq.(5.4) or (5.5) and substituting these values into Eq.(5.1), the buckling loads of trapezoidal panels under the combined action of bending moments and shear forces can be easily obtained. The intermediate values of β can be approximated with linear interpolation.

(2.2) Ultimate strength

The ultimate strength of girder panels after buckling is estimated by applying the method of a plastic analysis. It is assumed that the strength can be obtained as the sum of the buckling strength of webs under the combined loads and the strength supported by the tension field. However, the effect of frame action on the panel strength is excluded in this case. The assumption on the diagonal tension field of the trapezoidal panel is used in the analogous form to the model for parallel flange girders proposed by Ostapenko.[9] Since the upper part of the trapezoidal panel is small and the tension field develops slightly from the test results at 4.3.2, the distribution of the tension field may be assumed as shown in Fig.3.6. Besides, the distribution of normal stresses is also simplified as seen in Fig.3.6. If the equilibrium condition is applied to the collapsed panel that is cut off at the section near an intermediate stiffener, the shear force supported by the tension field can be obtained as follows:
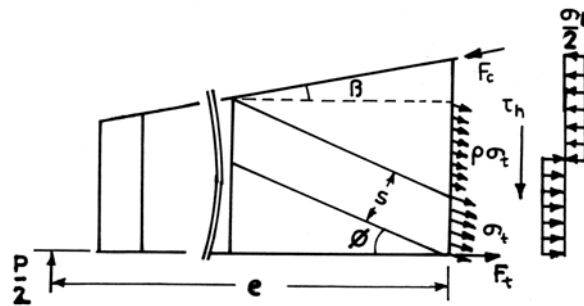

Fig.3.6 Applied forces on web panel.

$$\frac{P}{2} = \frac{\sigma_t t}{d_h \cos\beta - e\sin\beta}\left[s\left(\frac{s}{2}\sin\beta + d_h\cos\beta\sin\phi\right)\right.$$

$$\left. + \rho\, a\sin\phi\left\{\left(s + \frac{a}{2}\sin\phi\right)\sin\beta + d_h\cos\beta\sin\phi\right\}\right]$$

<div align="right">(5.6)</div>

where t, a, d_h, ϕ, β, e and ρ are the web thickness, the panel length, the highest panel depth, the inclination of the tension field, the inclination of the flange, the length from the cut section to the point of load application and the coefficient of equivalent tension field stresses, respectively. Furthermore, s is the width of the tension field and if d_l denotes the lowest panel depth, $s = d_l \cos\phi$ - $a \sin\phi$. The value of ϕ can be decided so as to obtain the maximum shear force. σ_t which denotes the tension field stress becomes as follows:

$$\sigma_t = -\left[\frac{\sigma_h}{8} + \frac{3}{2}\left(\frac{\sigma_h}{4}\cos 2\phi + \tau_h\sin 2\phi\right)\right] + \sqrt{A - B}$$

$$A = \frac{3}{8}\sigma_h\left(\frac{\sigma_h}{4}\cos 2\phi + \tau_h\sin 2\phi\right) + \sigma_Y^2$$

$$B = \frac{3}{4}\left(\frac{\sigma_h^2}{8} + \tau_h^2\right) + \frac{9}{4}\left(\frac{\sigma_h}{4}\sin 2\phi - \tau_h\cos 2\phi\right)^2$$

<div align="right">(5.7)</div>

where σ_Y indicates the yield point stress of web plates.

The buckling load of the trapezoidal panel under the combined action of bending moments and shear forces is calculated by means of the method described at 4.3.1. The boundary condition at the upper and lower edges of the panel is assumed to be fixed considering the matching with the experimental results.

5.3.2 Experiments on girders with linearly varying depth under bending and shear

(1) Introduction

Loading tests of plate girder models with linearly varying depth are carried out. Four models are tested under bending and shear. Although the size at the tapered panels of each model is similar, the ratio of bending moments with shear forces acting on a testing panel is different. Test results are described about the ultimate strength of the girders and the collapse behavior on the components of a testing panel in full, and the correlation is investigated. Because three girders were collapsed due to flange failure after the buckling of a trapezoidal panel, they lost the load carrying capacity. One girder was collapsed due to the lateral-torsional buckling of an inclined flange after web buckling.

The ultimate strength obtained from the test results is compared with the predicted values by the above-mentioned method on basis of a simple failure model. As this simple method predicts relatively well the ultimate strength of girder panels under the combined loads, its availability will be confirmed.

(2) Description of tests
 (2.1) Models
　　Four model girders with tapered webs were tested. The outline plan of Models
CL-S-2 and CL-S-4 is shown in Fig.3.7. The dimension of Models CL-S-1 and CL-S-3 is
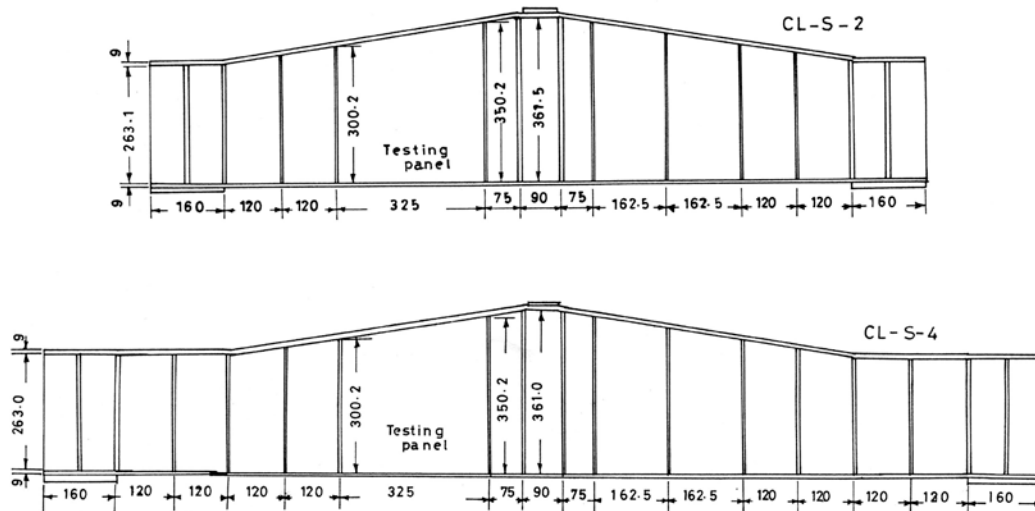

Fig.3.7 Tapered girders (Models 2 and 4).

obtained by eliminating, symmetrically, a trapezoidal panel and a rectangular panel of
which the length is 120mm from Models CL-S-2 and CL-S-4, respectively. A
concentrated load was applied to each girder at mid-span. Intermediate transverse and
bearing stiffeners were used in pairs. Each testing panel was designed so that its
dimension was identical. However, the span was designed so that the ratio of bending
moments with shear forces acting on the testing panel was different. M_m/d_mQ_m and κ
are shown in Table3.1, where d_m, M_m and Q_m denotes the depth, the moment and the
shear force at the middle of the testing panel, respectively. These testing panels were
designed so that the width-to-thickness ratio took about 150 and the aspect ratio was
about 1.0 in the case of using the mean panel depth. The actual girder dimensions on
the testing panel were measured. These measurements are summarized in Table 3.2.

Table 3.1 Ratio of moment to shearing force.

Models	CL-S-1	CL-S-2	CL-S-3	CL-S-4
M_m/d_mQ_m	1.12	1.50	1.87	2.24
κ	0.38	0.50	0.58	0.63

Table 3.2 Measured dimensions.

Models	CL-S-1	CL-S-2	CL-S-3	CL-S-4
Panel length a (mm)	320.4	321.5	319.8	325.3
Web thickness t (cm)	2.12	2.08	2.10	2.21
Min. panel depth d_l (mm)	298.0	298.0	295.9	297.0
Max. panel depth d_h (mm)	348.0	346.5	347.9	347.0
Flange thickness t_f (mm)	8.67	8.99	8.88	8.96
Flange width b (mm)	90.05	94.25	90.01	89.93
a/d_l, a/d_h	1.075,0.921	1.079,0.928	1.081,0.919	1.095,0.937
d_l/t, d_h/t	140.6,164.2	143.3,166.6	140.7,165.4	134.3,156.9
β (degree)	8.9	8.6	9.2	8.7
t_s (mm)	3.08	3.09	3.17	2.61
b_s (mm)	30.99	31.93	31.85	31.58

β: Inclination angle of flange b_s: Width of intermediate stiffener

t_s: Thickness of intermediate stiffener

All models were made of SS400 steel. The results of the coupon tests are given in Table 3.3. From this table it is seen that each model has a comparatively similar yield point stress.

Table 3.3 Coupon test results.

Models		CL-S-1	CL-S-2	CL-S-3	CL-S-4
Yield point stress σ_Y (MPa)	Web	282.4	271.6	282.4	274.1
	Flange	288.3	255.9	288.3	279.9
	Stiffener	287.3	235.3	287.3	236.8
Young's modulus E X10^5 (MPa)	Web	1.91	1.97	1.91	2.03
	Flange	1.69	2.30	1.69	2.11
	Stiffener	2.03	2.11	2.03	2.10
Poisson's ratio ν	Web	0.277	0.270	0.277	0.284

(2.2) Testing procedure

Before testing, initial deflections of web plates were measured. The initial deflection of each model was smaller than the following values:

 1.8mm for Model CL-S-1, 0.9mm for Model CL-S-2, 1.5mm for CL-S-3 and 1.5mm for Model CL-S-4.

Each girder was tested in the simply supported condition with roller supports. A concentrated load was applied to a sole plate at the mid-span of the girder. The step-by-step loading procedure was used and after the attainment of the ultimate load, the removal of the load was conducted. Electrical displacement transducers were used to observe out-of-plane deflections of the web plate relative to the boundaries and vertical girder deflections. Electrical resistance strain gauges of the uni-axial type were used for flanges and stiffeners, and those of the rosette type were used for web plates. Measurements of the strains were taken on both faces of the girder components.

(2.3) Experimental results and considerations

All girders after tests are illustrated in Fig.3.8. In the case of three girders except for Model CL-S-4, it is observed that the tension field developed in the testing panel, though some differences in the results appeared. Models CL-S-1 and CL-S-2 collapsed

after the dent of the inclined flange had occurred, however in the case of Model CL-S-3 such deformation was not so large. Model CL-S-4 collapsed owing to the flexural-torsional buckling of the inclined flange.
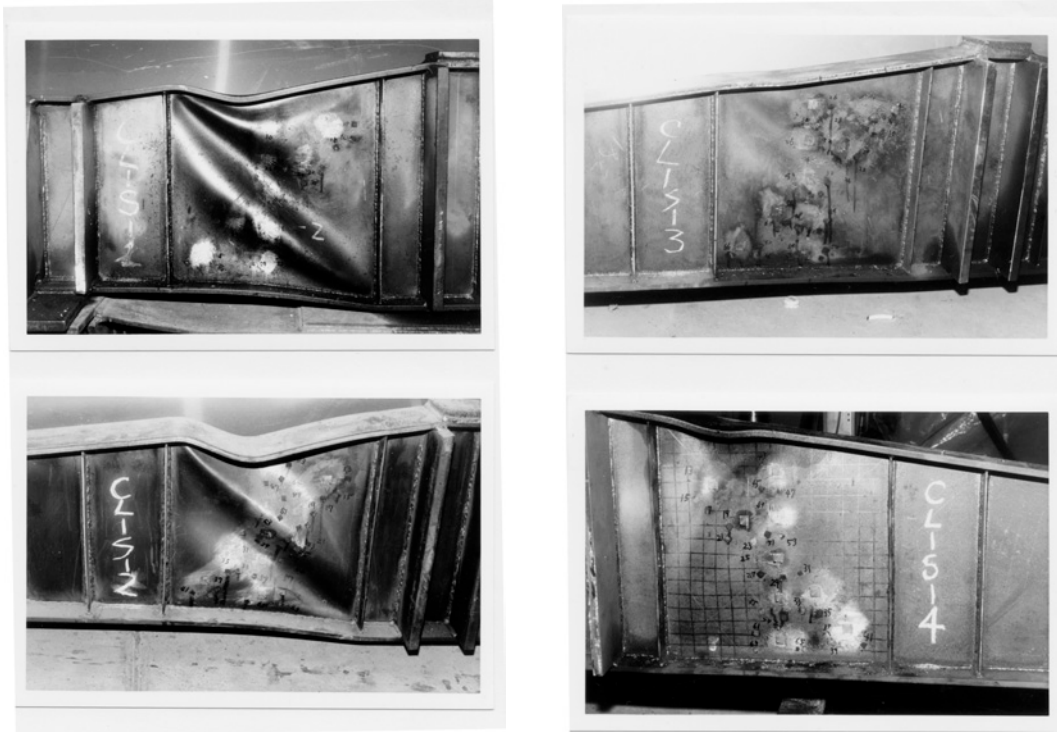

Fig.3.8 Collapsed girders.

The central deflections of each model girder are shown with respect to applied loads in Fig.3.9. Each load-central deflection relationship is linear up to about 70～80 % of the collapse load. After this stage, the deflection in Models CL-S-3 and CL-S-4 shows a rapid rate of increase. And in the case of the remaining two girders, although the increase after the break of the linear relation is not so much, the deflection shows a rapid rate of increase immediately before the collapse load.
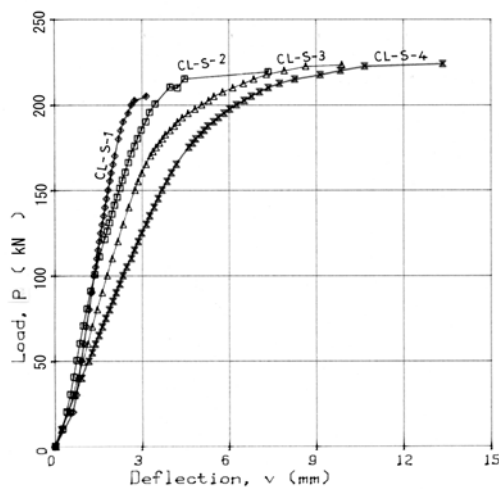

Fig.3.9 Central deflection.

The relative deflections of the web panels are plotted against the applied load to form Fig.3.10 as an example. Though it is difficult to estimate buckling loads of the web panel due to the small value of deflections and the initial web imperfections, the experimental buckling loads of the trapezoidal panel under the combined bending and shear were presumed with reference to such changes in deflections.
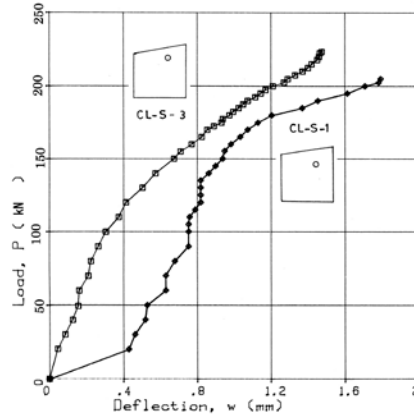

Fig.3.10 Relative web deflection.

The relationship between the bending strains of web panel in the horizontal direction and applied loads is exemplified for each girder in Fig.3.11. Similar relationship with respect to the vertical direction is illustrated in Fig.3.12.
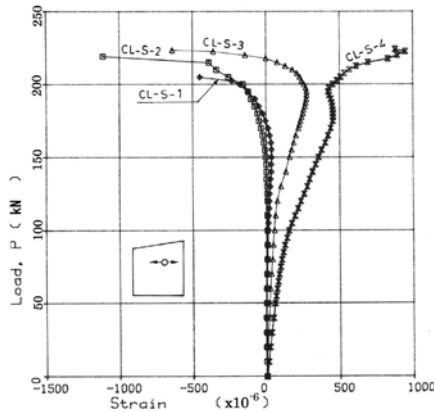

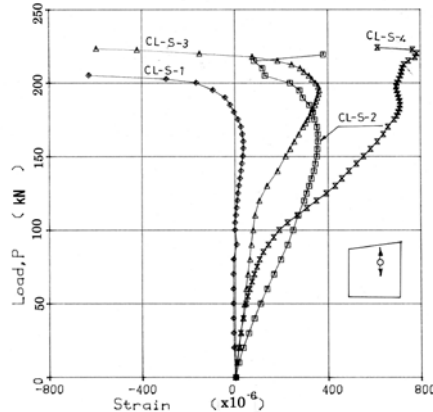Fig.3.11 Bending strains of web panel in horizontal direction.

Fig.3.12 Bending strains of web panel in vertical direction.

The experimental buckling loads of the web plate can be estimated from inflection points using such relation at several measured points and the results of the relative web deflections as before. It is seen from Figs.3.11 and 3.12 that there are first inflection point corresponding to the web buckling and second inflection point at about 196 kN. After this point, the value of strains increases rapidly and the collapse of the girder breaks out. It is considered that as a result of the successive deformation between the flange and web and the arrival at the ultimate state of the flange, the girder reaches the final failure stage.

138

For each girder, the longitudinal strains of the inclined flange have been plotted against several loads to form Fig.3.13. These values represent the average values of the strains that were measured on the inside and outside of the flange plate. From these figures, it is obvious that the strains in Models CL-S-1, CL-S-2 and CL-S-3 are kept at relatively uniform distribution up to the load near the ultimate one. However, owing to the influence of the diagonal tension field the variation of this distribution begins and the value of the strains around the center of the panel becomes to be remarkably large compared with other region getting close to the collapse state. It is considered that the reason is caused by the dent of the inclined flange in this region. When Mode CL-S-4 collapsed, the strain distribution was different compared with other girders and the value of the strains in the neighborhood of the end of the panel was considerably large. This fact coincides with the collapse mode in which local buckling occurred.

The vertical component of the axial force acting on the inclined flange can carry shear forces. Consequently, since the shear force acting on the web decreases in comparison with that of parallel flange girders, this becomes an advantage to the carrying load. On the other hand, it is considered that the application of such vertical force gives a strict condition to the inclined flange.

(a) Model CL-S-1

(c) Model CL-S-3

(b) Model CL-S-2

(d) Model CL-S-4
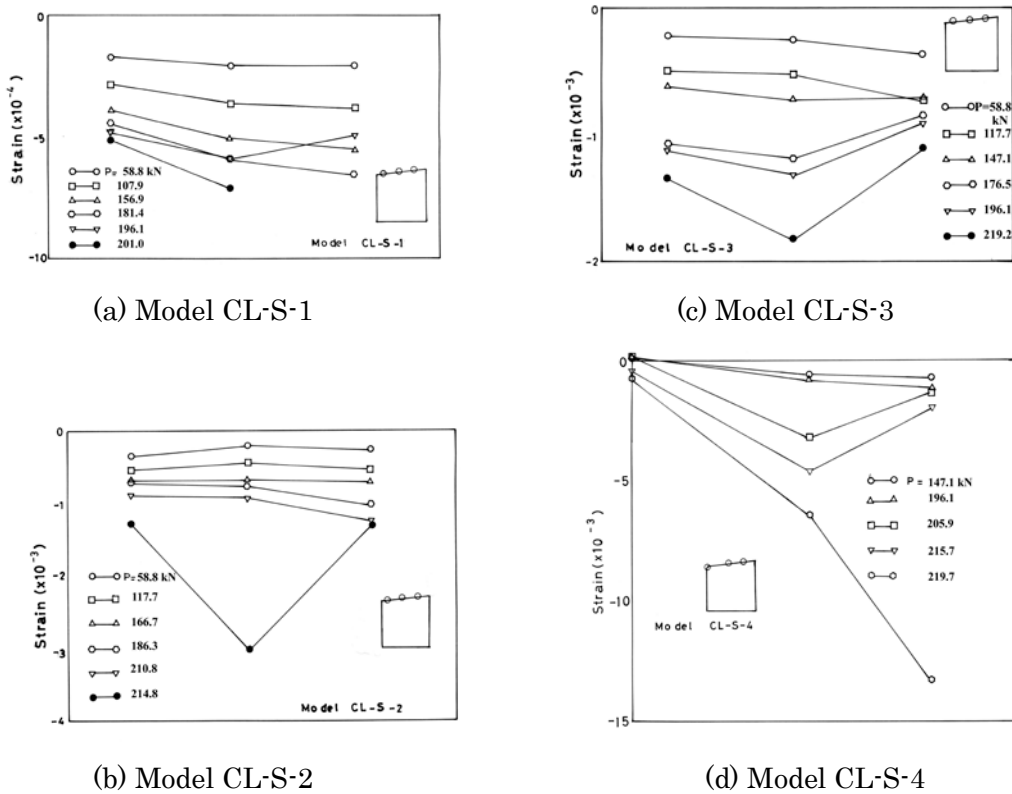
Fig.3.13 Longitudinal strains on inclined flange.

The distribution of the diagonal tensile strains acting at right angles across the diagonal line *AA'* drawn by a broken line is shown against several applied loads in Fig.3.14 for each girder. In this figure, the broken line *AA'* has been translated on the abscissa. It is seen that the diagonal tension field has grown quickly at an ultimate

stage approaching the collapse load in Models CL-S-1, CL-S-2 and CL-S-3. On the other hand, from this figure the development of the tension field in Model CL-S-4 cannot be found.

(a) Model CL-S-1

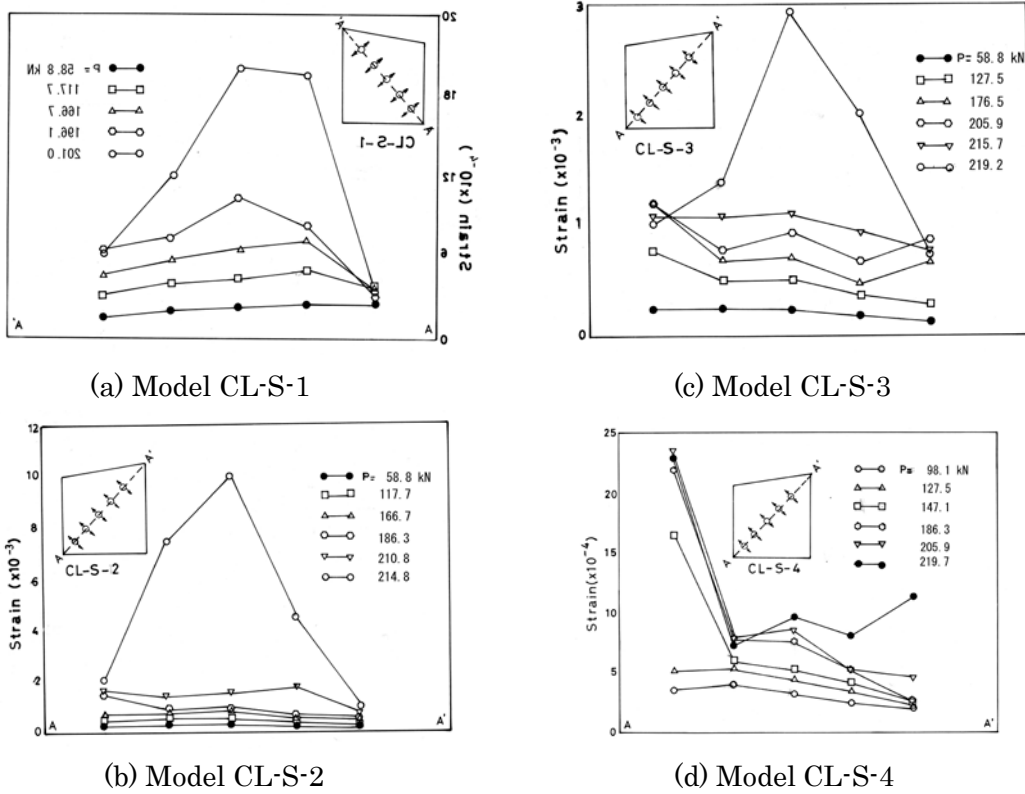(c) Model CL-S-3

(b) Model CL-S-2

(d) Model CL-S-4

Fig.3.14 Diagonal strains on web panel.

As examples, the distribution of principal strains of the testing panel in Models CL-S-2 and CL-S-4 is shown in Fig.3.15 for the case close to the collapse load. It is evident from this figure that principal tensile strains corresponding to the tension field develop over a comparatively wide range in Model CL-S-2. It was also observed in the case of CL-S-3 that principal tensile strains were highly developed in a relatively narrow range near the diagonal line. These three girders including Model CL-S-1 showed a similar distribution form, although the degree of development somewhat differed. In Model CL-S-4, because principal compression strains were outstanding at the upper part near to the higher edge of the panel, it is considered that this gave rise to local deformation of the flange. Model CL-S-4 is different from other three models in the collapse mode.
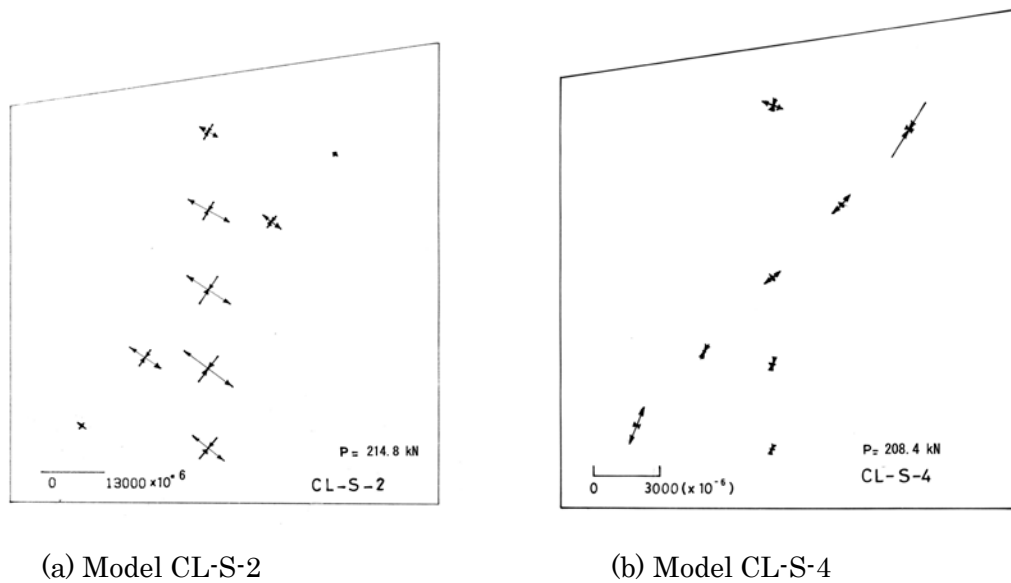
140

(a) Model CL-S-2   (b) Model CL-S-4

Fig.3.15 Principal strain distribution on web panel.

The buckling loads of the trapezoidal panel, $P_{cr,ex}$, and the collapse loads, P_{ex}, are shown in Table 3.4. In this table, M_{ex}, Q_{ex}, M_{fY}, Mp and Q_p denote the maximum bending moment by the experiment, the maximum shear force by the experiment, the yield moment of compression flanges, the full plastic moment and the full plastic shear force (supported by web), respectively. These have been estimated as the values at the middle of the testing panel. Q_{ex} contains the shear force that is supported by the inclined flange. The vertical component of the axial force at the case that the inclined flange stress arrives at the yield point stress is estimated and the sum of this value and Q_p is expressed by Q_p again. If Q_{ex} is divided by Q_p, those values are 0.689, 0.784, 0.747 and 0.748 in numerical order of the model girders, respectively.

Table 3.4 Results of web buckling and ultimate strength.

Models	$P_{cr,ex}$ (kN)	P_{ex} (kN)	M_{ex} (kN·m)	Q_{ex} (kN)	M_{fY} (kN·m)	M_p (kN·m)	Q_p (kN)	M_{ex}/M_{fY}	M_{ex}/M_p	Q_{ex}/Q_p
CL-S-1	128.5	201.0	36.48	101.0	73.74	89.82	111.7	0.494	0.406	0.904
CL-S-2	103.0	214.8	51.78	107.9	71.00	86.10	105.1	0.730	0.602	1.03
CL-S-3	106.9	219.2	65.99	109.8	75.21	91.10	110.2	0.878	0.725	0.994
CL-S-4	90.2	219.7	79.33	109.8	73.55	89.92	112.7	1.08	0.883	0.975

The interaction on the ultimate strength under the combined bending and shear obtained by the tests is shown in Fig.3.16. The symbols in this figure, 1～4, indicate the numbers of four models and the symbols "low, middle and high" are used to represent the minimum depth, the mean depth and the maximum depth as the panel depth, respectively. The value, Q_{ex}, includes the shear force loaded by the inclined flange. As these obtained results, it is seen that even if the ratio of bending moments increases, the shear strength does not so much decrease in this range.
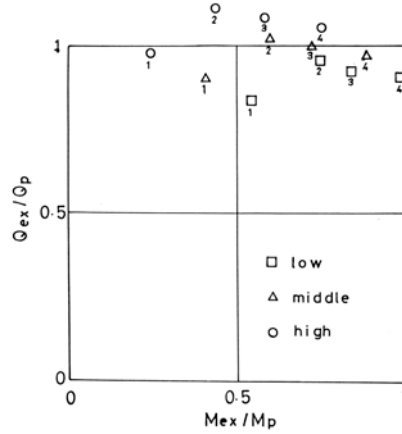
141

Fig.3.16 Test results.

(2.4) Comparison of test results with calculated results

The predicted value for the ultimate strength can be calculated by the sum of the shear buckling force P_{cr}, the value obtained from Eq.5.6 and the vertical component of the axial force acting on the inclined flange. The axial force acting on the inclined flange may be estimated according to the stress immediately before the formation of the tension field at the trapezoidal panel, that is, the value when the buckling of the panel occurs, which is conservative. And the value of ρ is assumed to be 0.5. The comparison of the predicted value, P_{th}, with the collapsed load observed in the experiment, P_{ex}, is shown in Table 3.5.

Table 3.5 Comparison of tests with theory.

Models	CL-S-1	CL-S-2	CL-S-3	CL-S-4
Present theory, P_{th} (kN)	204.0	200.0	219.7	—
Experimental value, P_{ex} (kN)	201.0	214.8	219.2	219.7
P_{th}/P_{ex}	1.01	0.93	1.00	—

Moreover, the value of three components in P_{th} described above is as follows for each girder:

Model CL-S-1: $P_{cr} = 102.0 kN$, $P_t = 87.3 kN$, $P_f = 15.7 kN$

Model CL-S-2: $P_{cr} = 97.1 kN$, $P_t = 84.3 kN$, $P_f = 19.6 kN$

Model CL-S-3: $P_{cr} = 94.1 kN$, $P_t = 101.0 kN$, $P_f = 25.5 kN$

Since Model CL-S-4 collapsed in the manner that was different from the supposition for the theoretical calculation, it is omitted from the subject of comparison. Although test girders are only four, it is supposed from this table that this method can fairly well predict the ultimate strength using comparatively simple calculation.

5.4 Discussions

The ultimate strength of plate girders with uniform web depth under the combined action of bending and shear was reviewed on a basis of existing works at first. The results obtained by Basler, Ostapenko and Rockey were introduced mainly. Subsequently, the girder with tapered webs was investigated. For the case in which the instability of flanges does not occur, a simple expression was introduced to predict the ultimate strength on the trapezoidal panel of plate girders with linearly varying web depth under the combined action of bending and shear and the test results were presented. At last, the theoretical and experimental results were compared.

In order to predict the ultimate strength, the estimation by means of a modal analysis was adopted. It was assumed that the ultimate strength of the panel consisted of the sum of the buckling strength under the combined bending and shear, the strength supported by the tension field and the vertical component of the force acting on the inclined flange. Furthermore, the analysis was carried out on the assumption that the panel has relatively large width-to-thickness ratio.

(1) Buckling curves for the trapezoidal panel subjected to bending moments vary fairly depending on the angle of inclination of the flange.

(2) The interaction curve on buckling for the trapezoidal panel under the combined bending and shear can be approximated conservatively and fairly well with Eq.5.1.

(3) Buckling loads estimated for the panel with fixed upper and lower edges with respect to the boundary conditions are close to obtained experimental results.

(4) Regarding the model of the tension field distribution, that of the case in which only shear force acted was extended.

The loading test was carried out preparing four girder models in such a way that the mean aspect ratio was about 1 and the mean width-to-thickness ratio approximately 150 at the middle of the trapezoidal panel. Three girders collapsed at the state in which shear forces were dominant and the flexural-torsional buckling of the flange occurred at the remaining girder. The collapsed behavior obtained from the test results is chiefly as follows:

(5) The tension field is formed in the state close to the collapse. And the final stage is caused by the dent of the inclined flange.

(6) Even if the ratio of bending moments increases, the strength does not decrease rapidly within the range of this experiment.

The predicted values of the ultimate strength were compared with the experimental results.

(7) It was found that the theory could simply and fairly well predict the ultimate strength. However, the elasto-plastic finite displacement analysis may have to be applied for the general application and for the verification of the obtained results.

5.5 References

1) Timoshenko, S. P.: The stability of the webs of plate girders, Engineering, Vol.138, pp.207-209, 1934.,

2) Stein, O.: die Stabilität der Blechträgerstehbleche im zweiachsigen Spannungszustand, Der Stahlbau, Heft 8, s.57-60, 1934.

3) Chwalla, E.: Beitrag zur Stabilitätstheorie des Stegbleches vollwandiger Träger,

Der Stahlbau, Heft 21/22, s.161-166, 1936.

4) Way, S.: Stability of rectangular plates under shear and bending forces, Journal of Applied Mechanics, Vol.3, No.4, pp. A 131-A 135, 1936.

5) Radulovic', B.: Beitrag zur Stabilit☐t einer Rechteckplatte, die einer in beiden Richtungen ☐ber die Plattenebene linear ver☐nderlichen Last unterworfen ist, bei Navierschen Randbedigungen, Der Stahlbau, 42, Jahrgang, Heft 7,S.199-205, Heft 12,S.384, 1973.

6) Tuda, H., Yonezawa, H. and Dogaki, M.: Ultimate Strength of Plate Girder under Unequal End Moments, Annual Meeting of JSCE, I-4, 1992.

7) Nakazawa, M., Iwakuma, T. and Kuranishi, S.: Elastic Buckling Strength and Post-buckling Behavior of A Panel under Unequal Bending and Shear, Structural Eng./Earthquake Eng., Vol.8, No.1, pp.29-38, 1991.

8) Basler, K.: Strength of Plate Girders under Combined Bending and Shear, Trans. Am. Soc. Civ. Eng., Vol.128, Part Ⅱ, p.720. 1963.

9) Chern, C. and Ostapenko, A.: Unsymmetrical Plate Girders under Shear and Moment, Fritz Eng. Lab. Rep., No.328.9, Lehigh Univ., Bethlehem, Pa., 1970.

10) Rockey, K. C.: An Ultimate Load Method for the Design of Plate Girders, IABSE Coll. Des. Plate Box Girders Ultimate Strength, London, 1971.

11) Galambos, T. V. (ed.): Guide to Stability Design Criteria for Metal Structures, 4th Edition, John Wiley & Sons, New York, 1988.

12) Rockey, K. C., Evans, H. R. and Porter, D. M.: A design method for predicting the collapse behaviour of plate girders, I.C.E., Vol.65, pp.85-112, 1978.

13) Tani,S. : Analysis of Plated Structures, Gihodo,1969.

14) Mikami,I. and Yonezawa,H.: Extrapolation Technique for Finite Difference and Finite Element Solutions, Proc. of the Japan national congress for Applied Mechanics, Vol.25, Univ. of TOKYO Press, 1975.

Chapter 6

Strength and deformability of girders under repetitive shear

6.1 General description

The behavior of girder structures under the cyclic loading even at low stress such as traffic loads is especially important as a fatigue problem. On the other hand, there is the problem of the cyclic loading for low cycle but high stress. In such type of the cyclic loading, the study on the inelastic behavior for girders and girder panels under shear or combined loads is also necessary. As a typical example, the case of strong earthquake load affects is mentioned. Furthermore, the cyclic behavior of end panel in the girder bridge constructed over a valley subjected to the strong wind from the downward can cause a serious problem.

Popov et al. have proceeded with a series of studies on the case in which shear links are subjected to cyclic shear loads.[1)-2)] In these studies, the width- to-thickness ratio of a web panel and the spacing of stiffeners are chosen as parameters and many load-displacement hysteretic diagrams have been described. From these results, shear links have been found to exhibit excellent energy absorption has been shown and its effectiveness has been discussed. Test girders are wide flange beams of which the web has comparatively small width-to-thickness ratio. Many loading tests have been conducted and the behavior up to the ultimate state has been clarified considerably in detail by Hjelmstad.[1)] Also in Japan, for an example, Suzuki et al. has studied inelastic behavior of beams under non-uniform moment.[3)]

In the Great Hanshin-Awaji earthquake of 1995, the phenomena of repetitive inelastic buckling were observed in many steel girders including horizontal girders of portal steel piers on elevated highways. The author has been interested in steel girders' ability of dissipating the hysteretic plastic strain energy due to such repetitive buckling of steel girders for earthquake-resistance design.

Utilizing the excellent energy absorption performance of the shear panel, the use as a damper system is being developed. Takahashi et al[4),5)] developed a hysteretic damper using eccentric brace system. The application of such panel has been examined[10)-12)] to the cross beam for steel bridge piers of two-story portal frame with box sections.

In this chapter, to begin with, the inelastic buckling behavior of the single panel under shearing force is examined analytically. The inelastic repetitive shear and flexural buckling of plate girders with multi-panel have been investigated experimentally and theoretically where the strength and ductility of steel girder panels are examined in detail.

6.2 Strength and ductility for single panel of plate girders under cyclic shear loading
6.2.1 Introduction

The investigations on the load-carrying capacity of plate girders under static shear loading were mentioned in Chapter 4. However, their ductility has not been mentioned.

As one approach for preventing the whole collapse of the structure, the excellent deformability must be ensured. The studies on the deformability for the bridge pier and

columns with large resisting force have been widely carried out by today.[6)-9),15)] The use of members with large resisting force is advantageous concerning the earthquake-resistance design, because large energy absorption can be attained even if the plastic deformation is small. However, when considerably big seismic force is applied, there is the possibility that causes the damage leading to the whole collapse of the structure.

On the other hand, there is an approach that prevents the whole collapse of the structure by concentrating the damage in the position where the shear force dominantly works.[10)-12)] Namely, the whole collapse is expected to be prevented through the dissipation of the energy by the large deformation of the position which concentrate the damage. In the field of the architecture, the damper element of the shear resisting type has been developed.[4),5)] The deformability of structures is evaluated by the hysteretic behavior in the post-buckling range. Therefore, the behavior after shear buckling must be clarified in order to effectively utilize the deformability of members or plate elements.

The studies on the applicability of the finite element method to the elasto-plastic finite displacement analysis are also carried out.[16)] The computation is carried out for the frame structure under cyclic loadings.

The coupled behavior between whole deformation and local deformation of the steel girders is important. However, at first, the ultimate strength and hysteretic behavior of the single girder panel subjected to the repetitive shear force are clarified numerically.

6.2.2 Method of numerical computations
(1) Analytical model and initial imperfection

A panel of bi-axial and symmetrical plate girder as shown in Fig.2.1 is analyzed. Where, a, b_f, t_f, b_w and t_w, refer to the panel length, flange width, flange thickness, web depth and web thickness, respectively. The elasto-plastic finite displacement behavior is clarified analytically on the case in which the shear force Q works gradually or repetitively in right and left edge of this panel.
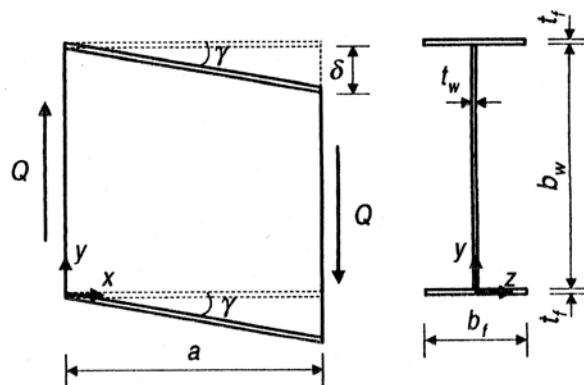

Fig.2.1 Steel girder in shear.

146

The initial deflection of web panel will be assumed as following (Fig.2.2(a)),

$$w_0 = C_w \frac{b_w}{250} \sin \frac{m\pi x}{a} \sin \frac{n\pi y}{b_w} \qquad (6.1)$$

where, C_w is a magnification for the limiting value of manufacturing error determined in Japanese specifications[13], and m and n are numbers of a half wave of the initial deflection in the direction of x and y, respectively. By assuming that the flange and web plate keep the vertical in the juncture, the initial deflection of the flange will be shown as following.

$$v_0 = \mp C_w \frac{n\pi}{250} z \sin \frac{m\pi x}{a} \qquad (6.2)$$

As a residual stress by welding, that of self balancing shown in Fig.2.2(b) is assumed. In this figure, σ_{rt} and σ_{rc} show the tensile and compressive residual stress, respectively.

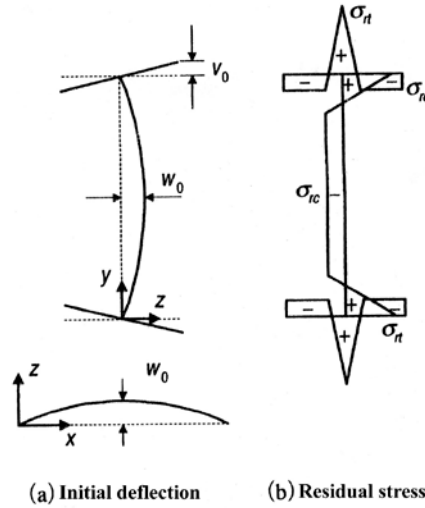(a) Initial deflection   (b) Residual stress

Fig.2.2 Initial imperfections.

The vertical displacement δ which corresponds to the shearing strain γ in Fig.2.1 is applied in order to cause shear forces in the panel. In this case, yielding shear force is expressed as

$$Q_Y = \tau_Y b_w t_w \qquad (6.3)$$

and the shear displacement in proportion to Q_Y is made to be

$$\delta_Y = \frac{aQ_Y}{Gb_w t_w} \qquad (6.4)$$

in which τ_Y is the shear yield point stress and G is the modulus of rigidity.

As loading pattern, the following two methods are adopted:

① An incremental loading method: this is the method in which the displacement always increases.

② A repetitive loading method: this is the method in which the maximum amplitude increases every cycle.
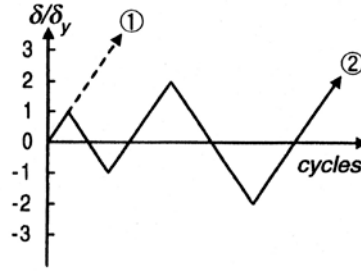
These loading patterns are illustrated in Fig.2.3

Fig.2.3 Loading sequence.

(2) Boundary condition

As a support condition in the boundary of the panel, the following assumptions are set:

1) The deformation between analyzed panel and adjacent panels continues. Therefore, the rigidity of vertical stiffeners is high and the straight line is always kept.

2) As to out-of-plane deformation, the web plate is simply supported on the vertical stiffeners.

The displacement in the direction of x, y, z axes, respectively, is called u, v, w and the rotation angle about z axis is called θ_z. The equivalent vertical displacement in shear force is made to be δ. At top and bottom flanges and web plate in $x = 0$ edge, the boundary conditions are assumed as follows:

$$u = v = w = 0 \tag{6.5}$$

In $x = a$ edge, the boundary condition at top and bottom flanges is assumed as follows:

$$w = 0 \tag{6.6}$$

Similarly, at web plate it is assumed as follows:

$$w = \theta_z = 0, \quad v = \delta \tag{6.7}$$

Actually, the boundary surface of web plate is assumed to be the rigid body region at $x = a$ edge in order to realize assumption 1).

(3) Numerical computation

General-purpose finite element analysis program "Marc-K6" was used in order to carry out the elasto-plastic finite displacement analysis on the panel. In this case, the finite element method formulated by up-dated Lagrangian technique for 4-node thick shell element was used. In addition, Newton-Raphson method and arc length incremental method were chosen in the solution method of nonlinear algebraic equation. The equivalent stress formula of von-Mises in the decision of the yield and the plastic flow rule of Prandtle-Reuss for the flow rule were used. And for the hardening rule, the following was used: Isotropic hardening rule and mixing hardening rule which used the kinematic hardening law jointly.

The convergence of nonlinear solution was judged in the following equation,

$$R_{\max} \langle \varepsilon \tag{6.8}$$

in which R is the residual un-equilibrium force, and ε is set at 10^{-4} in the allowable error for the convergence decision.

6.2.3 Results of the numerical analysis and considerations

The material property of steel plate is assumed being bi-linear type such as shown in Fig.2.4. It is assumed that yield point stress $\sigma_Y = 365MPa(t \leq 16mm)$, $\sigma_Y = 355MPa(t >16mm)$ elastic modulus $E = 206GPa$, strain hardening coefficient $E_p = E / 100$ and Poisson's ratio $\nu = 0.3$, respectively.
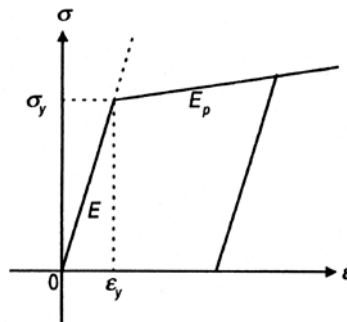
Fig.2.4 Stress-strain curve.

As to flange and web plate, the effect of divided element number on the convergence of solution was examined. The result showed that the solution with the good accuracy was obtained in respect of both plates, if in the x direction made each 14 divisions, in the y direction 6 and 14 divisions, respectively and each 9 divisions in the z direction.

(1) Comparison between present solution and past experimental value

In comparison with the solution by present finite element method and existing experimental value, the validity of the solution is verified. On the initial imperfection of the girder, measured values were adopted. And, the average of measured values on the residual stress, namely tensile residual stress $\sigma_{rt} / \sigma_Y = 1.0$, compressive residual stress $\sigma_{rc} / \sigma_Y = -0.12$, was assumed.

In comparison with test results and these analytical value of the ultimate strength on steel girders subjected to shear force, Fig.2.5 is obtained. In this figure, the ordinate and abscissa are respectively experimental value $(Q / Q_Y)_{exp}$ and analytical value $(Q / Q_Y)_{ana}$ for shear force made dimensionless in yield shear force Q_Y. The analytical values are almost being obtained at the accuracy within $\pm 10\%$ of the experimental values, as it is clear from this figure. According to present method, it seems to be able to estimate the appropriate solution.
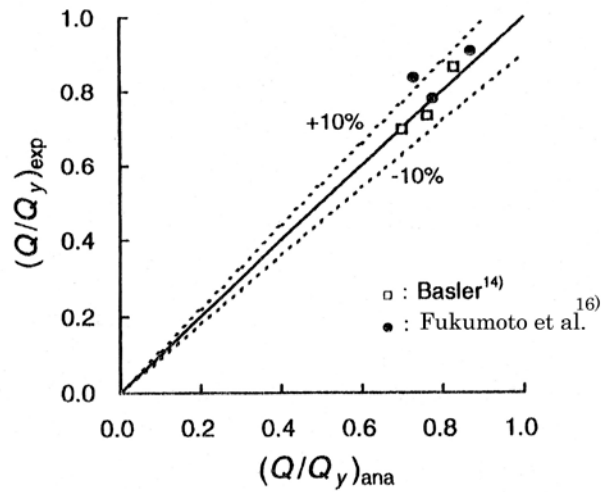
Fig.2.5 Comparison between present theory and experiments.

(2) Panel subjected to be monotonic loading

The ultimate shear strength and the deterioration characteristic of the panel under monotonic loading are investigated. In a web plate, the initial deflection of sine half wave with the 1/500 maximum value of web depth was assumed.

1) Aspect ratio of web panel

The relationships between shear force and shear displacement as aspect ratio a/b_w of web plate changes is shown in Fig.2.6. Aspect ratio a/b_w =0.5,1.0,2.0 is respectively correspondent to width-to-thickness ratio parameter R_w=0.82,1.35,1.64. In this figure, the ordinate and abscissa are expressed by the use of dimensionless shear force Q/Q_Y and shear displacement δ/δ_Y, respectively. Circles in this figure show the ultimate shear strength.

It is clear from this figure that the panel has the high shear strength, as aspect ratio of the panel decreases. In either case, the shear strength does not lower very much, after it reaches the maximum load. And the characteristic difference of the degradation is not remarkable.
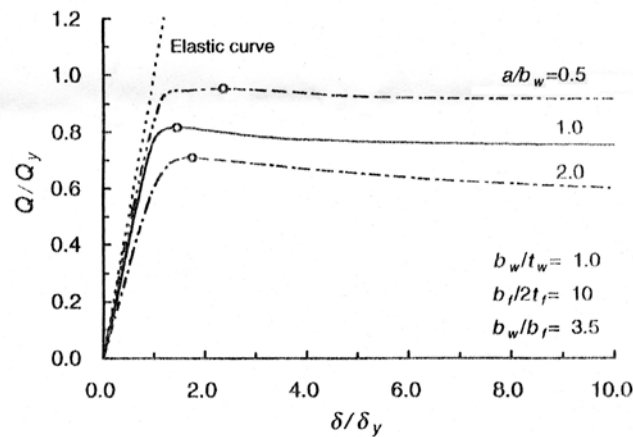

Fig.2.6 Influence of aspect ratio of web panel.

150

2) Width-to-thickness ratio

The relationships between shear force and shear displacement as web width-to-thickness ratio b_w/t_w changes with 91,123,200 has been given in Fig.2.7. Width-to-thickness ratio b_w/t_w=91,123,200 is respectively correspondent to R_w=1.00,1.35,2.20. It is clear from this figure that the ultimate shear strength increases, as width-to-thickness ratio of web plate is smaller. In either case, it tends to converge Q/Q_Y to the value of 0.7~0.8, after the shear force reaches the maximum load.

From this fact, the lowering of the strength is little with the increase of the width-to-thickness ratio of web plate, and it is not almost seen at b_w/t_w=200. Therefore, there is no inferiority on the deformability, when the width-to-thickness ratio of web plate is large even in.
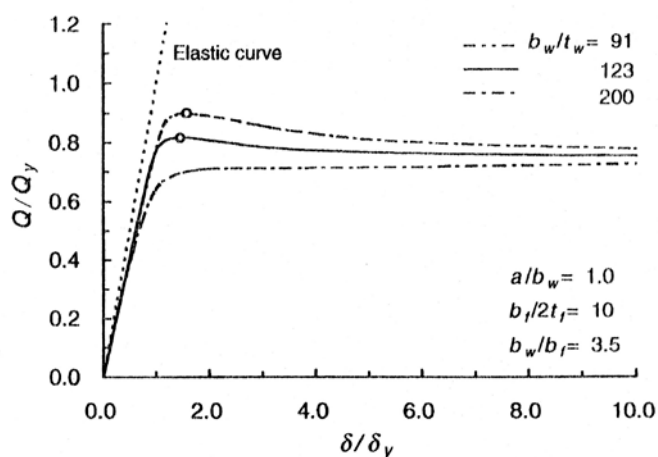
Fig.2.7 Influence of width-to-thickness ratio of web panel.

3) Ultimate shear strength of girder panel

From the results of Fig.2.6 and Fig.2.7, Fig.2.8 showing the relationship between the ultimate strength Q/Q_Y and width-to-thickness ratio parameter R_w of web plate is given. In the same figure, the results of load carrying capacity tests under shear of steel girder[14),17)-19)] and ultimate shear strength curve by Basler. Except for the test results by Rockey-Skaloud, there are present solution and test results for the good relation, as it is clear from this figure. Though at test girders that they used the shape of the web plate was identical, the flange is different at each girder. The dispersion of the strength in the test results by Rockey-Skaloud observed in Fig.2.8 seems to be caused by using R_w that cannot consider the effect of the restraint of the flange for the parameter. Therefore, it is necessary to use width-to-thickness ratio parameter that can consider the restraint of the flange in order to evaluate the ultimate strength of steel girder at the good accuracy.
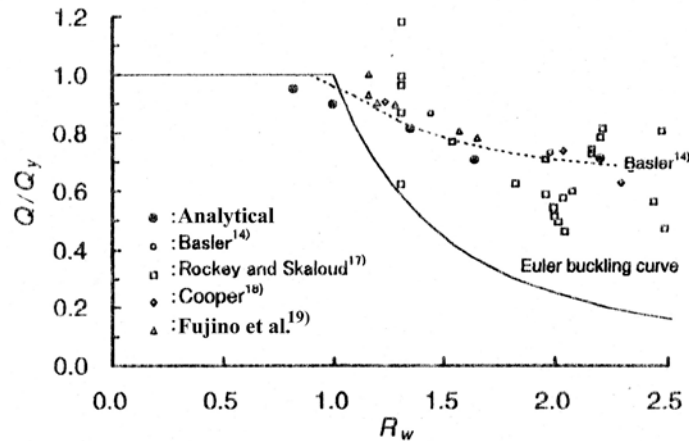
151

Fig.2.8 Ultimate shear strength of steel girders.

(3) Girder panel under cyclic shear load

1) Aspect ratio of web panel

The relationship between shear force and shear displacement of the steel girder which Fig.2.9 shows is obtained, when aspect ratio a/b_w of the web panel is 0.5, 1.0, 2.0. For the comparison, the relation between shear force and shear displacement in the case of the monotonic loading is also shown in the same figure, where b_w/b_f=3.5, $b_f/2t_f$=10, b_w/t_w=123.

As it is clear from this figure, at either aspect ratio, the maximum shear force in the every cycle tends to lower according to the increase of repetition number in comparison with the case of the monotonic loading. Because the diagonal tension field is formed after buckling, the remarkable strength degradation is not generated like the case of compression and bending and the hysteresis loop has comparatively been stabilized. In these hysteresis loops, features by the difference between aspect ratio have appeared well. That is to say, the load is temporarily decreasing sharply at the process in which the sign of shear force changes in the long panel. The snap-through phenomenon in which the buckling mode changes suddenly has appeared. However, the hysteresis loop approaches load-displacement curve in the case of the monotonic loading, when the pattern of buckling mode is determined and the tension field is formed again, and it shifts to the stable behavior.
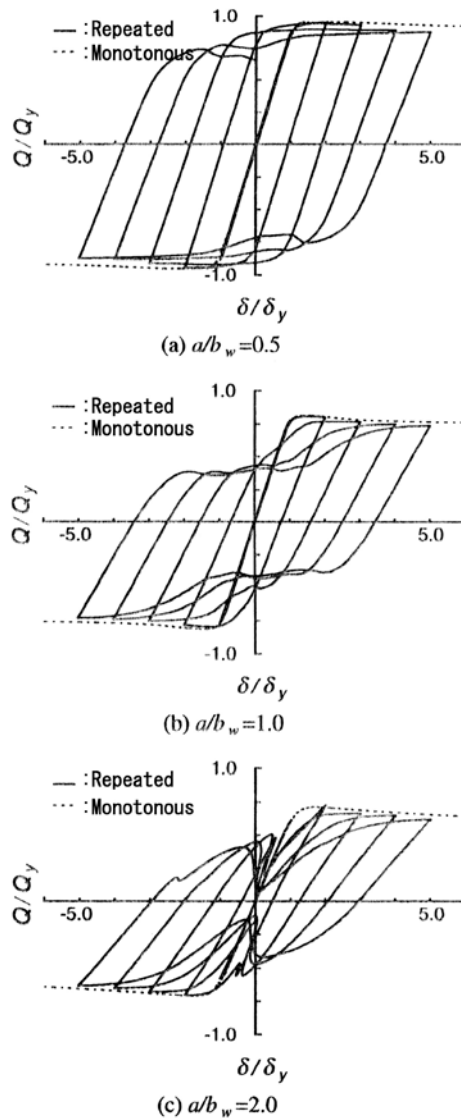
Fig.2.9 Hysteretic loop of relation between shear force and displacement.

The relationship between accumulation quantity of the energy and the number of cycle is shown in Fig.2.10. In this figure, the ordinate is the accumulation energy made dimensionless by $Q_Y \delta_Y$, and the abscissa shows the cycle number. The absorbed energy was obtained from the area of the region surrounded by the hysteretic loop at each cycle in the relationship between shear force-shear-displacement. The accumulated energy decreases, as aspect ratio a/b_w increases. It is seen that the degradation of the strength is little, even if the repetitive load is applied. Therefore, it seems to be useful for reduction of the weight and restoration in the early stage after earthquake disaster, if the member of whom energy dissipation is remarkable is used as subsidiary member.
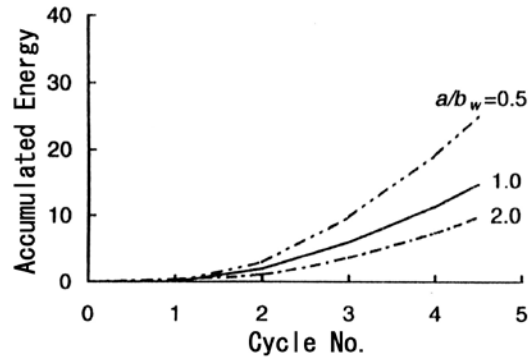
Fig.2.10 Accumulated energy.

2) Width-to-thickness ratio of web panel

The relation between the shear force and shear displacement of the girder panel is shown as Fig.2.11, when the width-to-thickness ratio b_w/t_w of the web plate is changed with 91, 123, 200. For the comparison, the relation between shear force and shear displacement in the case of the monotonic loading is shown by broken line. In this figure, each parameter is as follows: $b_w / b_f = 3.5$, $a / b_w = 1.0$, $b_f / 2t_f = 10$. As shown from this figure, the tension field formed before gradually disappears when the unloading begins by inverting shear force. As the result, the strength also lowers. Afterwards, the strength would rise again with the formation of the tension field to the reverse diagonal line direction. This phenomenon is remarkable as a web plate in which width-to-thickness ratio is large.

The relationship between the accumulation energy and the loading cycle is obtained as shown in Fig.2.12. In this figure, the ordinate is the accumulated energy made dimensionless by $Q_Y \delta_Y$ and the abscissa has shown the loading cycles. As before, when the member with the hysteretic behavior of the energy dissipation type can be built in the frame structure, the damage of the frame may be concentrated at this part. That is to say, it seems to be possible that a whole collapse of the structure is avoided, when the remarkable plastic deformation disperses the energy.
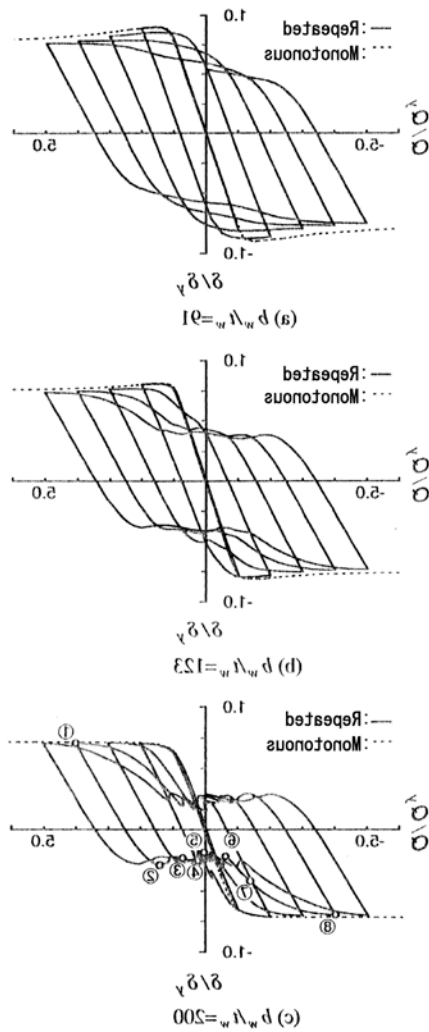
154

Fig.2.11 Hysteretic loop of relation between shear force and displacement.
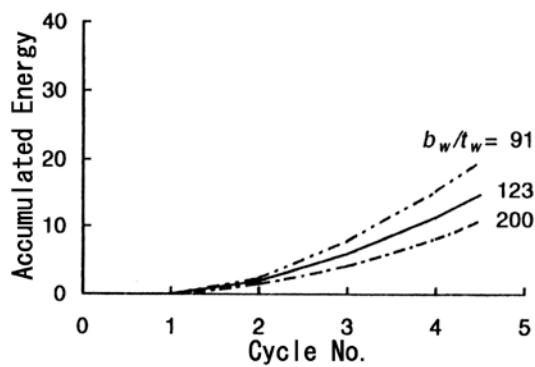
Fig.2.12 Accumulated energy.

3) Development of diagonal tension field

In the process in which the sign of the vertical displacement along the edge of the

155

girder panel changes, the snap-through buckling may occur. In the hysteretic behavior as shown in Fig.2.11, by noticing the case of Fig.2.11(c) with the lowering of which the strength is remarkable, when the load is inverted, deflection distribution of the web panel is examined. In this case, each parameter is as follows: $a / b_w = 1.0$, $b_f / 2t_f = 10$, $b_w / t_w = 200$, and $b_w / b_f = 3.5$. For several loading stages, out-of-plane deflection of the web panel is obtained as shown in Fig.2.13. The value in these figures is denoted by the out-of-plane deflection w/t_w made dimensionless using the web thickness t_w.

(1) $\delta/\delta_y = 4.00$ $Q/Q_y = 0.70$

(2) $\delta/\delta_y = 1.42$ $Q/Q_y = -0.30$

(3) $\delta/\delta_y = 0.71$ $Q/Q_y = -0.24$

(4) $\delta/\delta_y = 0.24$ $Q/Q_y = -0.26$

(5) $\delta/\delta_y = 0.06$ $Q/Q_y = -0.19$

(6) $\delta/\delta_y = -0.61$ $Q/Q_y = -0.22$

(7) $\delta/\delta_y = 1.39$ $Q/Q_y = -0.42$
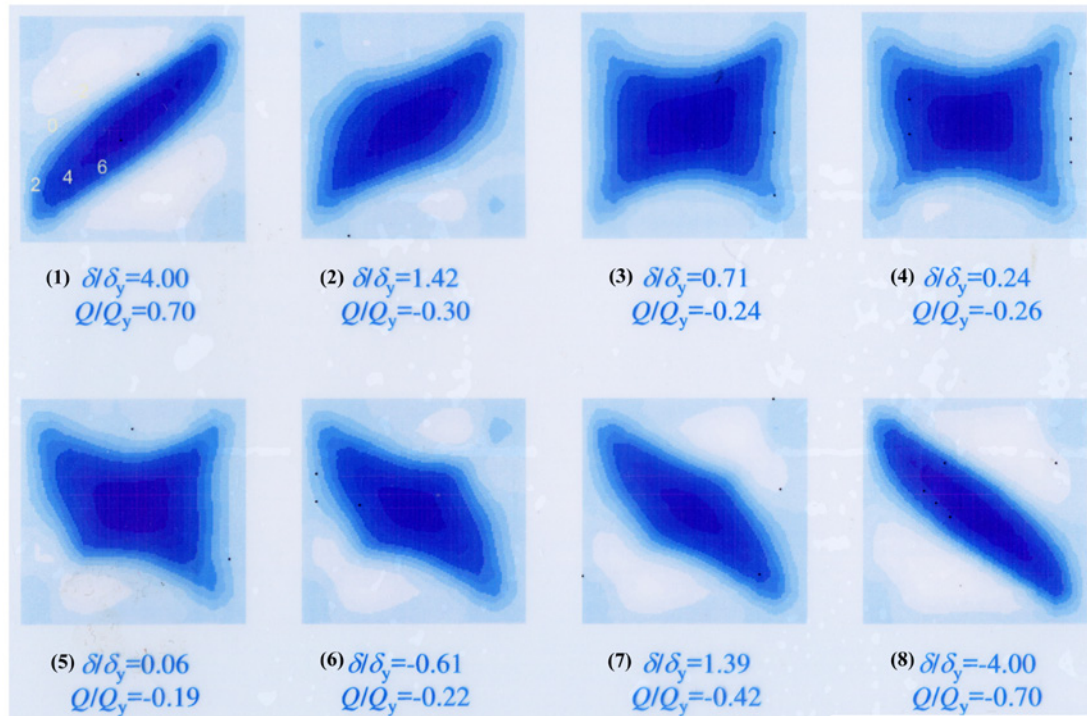
(8) $\delta/\delta_y = -4.00$ $Q/Q_y = -0.70$

Fig.2.13 Distribution of out-of-plane deformation on web panel.

As it is clear from this figure, in loading stages (1) and (2), the typical tension field seems to tend to gradually disappear with the unloading of the load. In the loading stages from (3) to (6), the tension field formed before then diffuses in the whole web panel, and simultaneously it would be newly formed along the other diagonal line direction.

The shear force is maintained in the low level in these stages. Afterwards, in the loading stages (7) and (8), the newly formed tension field is more clarified, and the shear strength rises due to this development. From these figures, the tension field seems to have smoothly been formed.

6.2.4 Conclusions

The ultimate strength and deformability were clarified on the girder panel gradually or repetitively subjected to the shear force by using elasto-plastic finite deflection analysis. A analyzed panel was assumed to be supported by sufficiently rigid

vertical stiffeners. The summary of the obtained results is as follows:

1) In the case in which the vertical stiffener has wide interval or the web plate is thin, the shear strength after the maximum load hardly fall unlike the case in which bending or compression acts.

2) The drop of the strength is caused by unloading after the inversion of the load, when the cyclic loading acts. But, the strength rises again. This phenomenon remarkably appears as a case that the vertical stiffener has wide interval and that the web plate is thin.

3) From the relationship between the accumulated energy and loading cycle, it is evident that such girder panel is excellent in the energy absorption performance.

4) If such hysteretic behavior is realized in framed structure, by the concentration of the plastic deformation in the girder panel with thin web plate, it is supposed to be possible to avoid a collapse of the whole frame.

6.3 Inelastic repetitive shear and flexural buckling of plate girders with multi-panel

6.3.1 Introduction

Many classical studies have been carried out experimentally and theoretically on isolated steel plate girder panels subjected to shear or the combined shear and bending. These studies include those by Galambos[21], Basler[14),20)], Ostapenko[22),23)] and Porter[24]. Theoretical methods based on the collapse mechanism are meant for efficient determination of the load-carrying capacity but not for analyzing the deformation process up to the ultimate strength. On the other hand, there exist such theoretical methods for the description of the load-carrying process up to the ultimate strength. Studies based on the latter methods have increased with the development of computers for example, such as by Marsh[25], Kuranishi[26] and Lee[27]. These analytical methods are quite limited to considering isolated panels but those considering also adjacent plate girders panels subjected to repetitive loading, in particular, are rather few.

For a single panel, the evaluation of strength and deformability of the steel girder under repetitive shear was carried out by Takeda.[28] On the other hand, although limited to shear link beams under cyclic loading, many loading tests have been conducted, and the behavior up to the ultimate state has been clarified considerably in detail by Hjelmstad[1]. Recently, Lubell showed that steel plate shear walls exhibit many desirable structural characteristics in the area of high seismic risk[29] and similarly, the use of shear links is proposed for the main tower of the new San Francisco-Oakland Bay self-anchored suspension bridge for its ability of dissipating the hysteretic plastic strain energy by making the links finally removable without causing difficulties from the rest of the main members after its significant inelastic deformation[30].

This article is focused on the theoretical and experimental study on the strength and ductility of steel plate girder panels under the repetitive inelastic buckling subjected to shear or the combined shear and bending. Eight model girders were tested in consideration of the combinations of two independent loading patterns, the flange thicknesses and the depth-to-thickness ratios of the web plate. In the finite element analyses using shell elements considering the material and geometrical

non-linearities in the repetitive inelastic buckling behavior of plate girders, only a half of the girder was analyzed considering the symmetry Good correlations were found between the results of tests and numerical computations.

6.3.2 Description of Tests

(1) Models

Fig.3.1 shows the dimensions and the tested models with one-point loadings at the span center as indicated by white and black arrows. The cross section of the web plate remains the same throughout the length of the girders. The actual girder dimensions such as the panel length, a; panel depth, b; web thickness, t; flange thickness, t_f; flange width, c of the testing panels, respectively were measured and the results are summarized in Table 3.1.
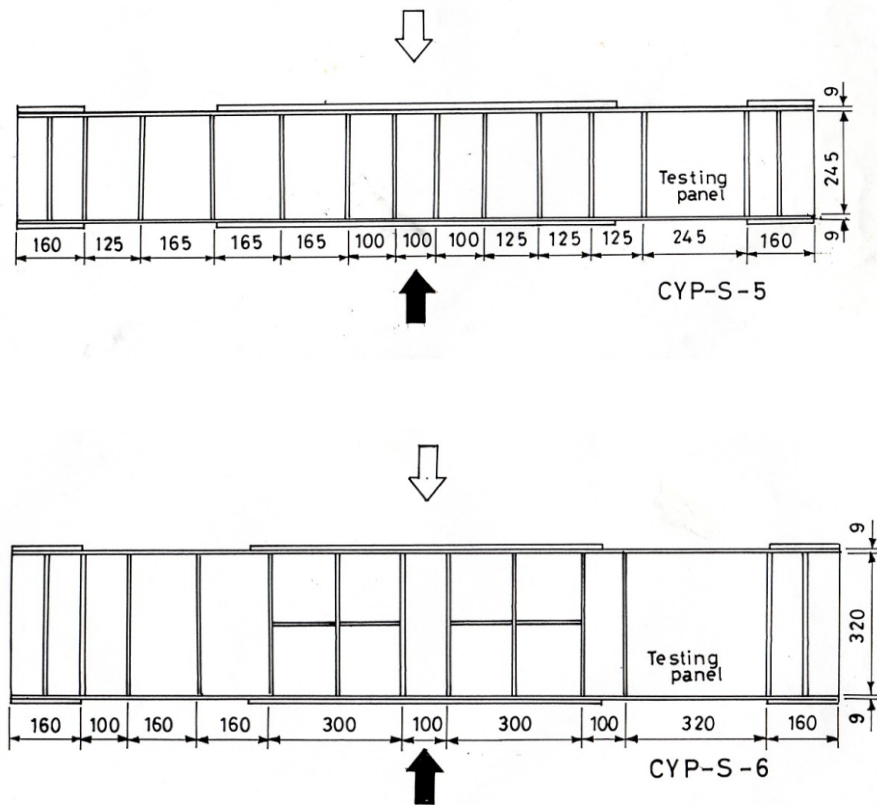

Fig.3.1. Experimental model girders.

All models are made of SS400 steel in accordance with the Japanese Industrial standard, JIS. The results of the yielding stresses obtained from the coupon tests are

158

shown in Table 3.2.

Table 3.1. Measured dimensions of models.

	CYP-S-3	CYP-S-4	CYP-S-5	CYP-S-6	CYP-S-7	CYP-S-8	CYP-S-9	CYP-S-10
Panel length, a (mm)	241	310	235	310	236	313	237	314
Panel depth, b (mm)	244	318	244	319	245	320	245	319
Web thickness, t (mm)	1.63	1.58	1.62	1.52	1.54	1.61	1.64	1.59
Flange thickness, t_f (mm)	16.1	16.1	8.9	8.9	8.7	8.9	16.0	16.1
Flange width, c (mm)	160.3	120.6	159.9	120.8	160.5	121.3	155.9	121.5
b/t	150	201	150	210	158	199	150	200
Loading sequence	A	A	A	A	B	B	B	B

Table 3.2. Yield point stress (MPa).

	CYP-S-3	CYP-S-4	CYP-S-5	CYP-S-6	CYP-S-7	CYP-S-8	CYP-S-9	CYP-S-10
Flange	296.2	296.2	275.6	278.5	275.6	291.3	271.6	286.8
Web	248.1	248.1	368.7	390.3	368.7	211.8	271.6	286.8

(2) Loading

The loading jig was manufactured in order to apply the alternating load, and the loading apparatus shown in Fig.3.2 was used. A servo-controlled hydraulic testing machine was used for the test. A concentrated point load was applied to the girder at mid-span so that the shear force acts predominantly on the testing panel and the girders were simply supported by using roller bearings under the displacement control. Two loading patterns: Type A and Type B are adopted. Type A corresponds to the case in which the amplitude of the displacement is increased linearly with respect to time at every cycle; while Type B corresponds to the case in which the amplitude of the displacement is kept constant but increased at every 3 cycles. The loading sequence in the test is schematically shown in Fig.3.3. The value of the maximum displacement d_0 at the first cycle was determined so that the predicted edge fiber stress at the mid-span reaches the yielding stress. On the other hand, the incremental value of Δd was determined a little higher than the corresponding value of d_0 considering the displacement capacity of the testing machine and the possible number of cycles to be 4.0mm for Models CYP-S-3, 5, 7, 9; but to be 5.0mm for Models CYP-S-4, 6, 8, 10. The loading type for each girder is described also in Table 1.
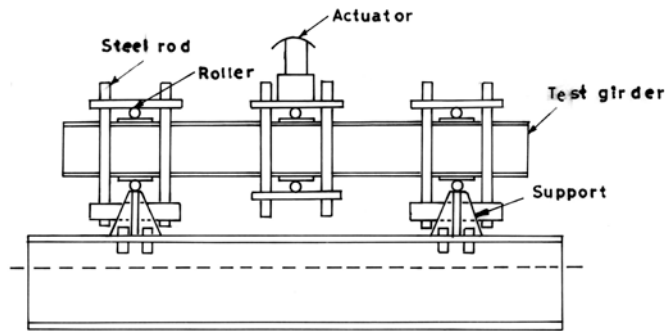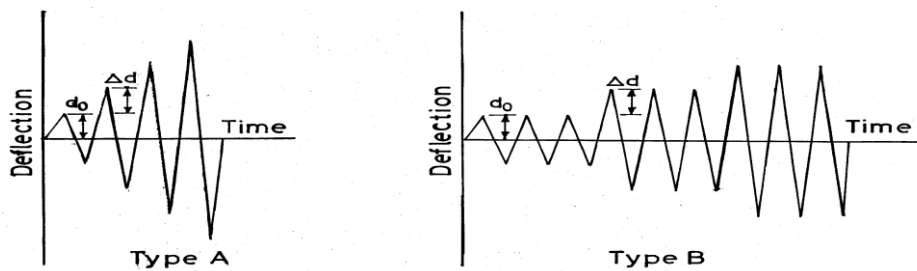
Fig.3.2 Loading apparatus.

Fig.3.3. Loading sequence.

6.3.3 Computer Analysis

(1) Analytical model

   In the analytical method, elasto-plastic finite displacement analysis was carried out using a general-purpose finite element analysis code ABAQUS. The analytical models and the meshes are shown in Fig.3.4. Obviously, not only the tested panel but also the other panels as shown in Fig.1 are divided into meshes, but only one half of the girder is considered assuming the symmetry with respect to the z-axis at the mid-span. Each of the adopted elements is a shell element with 4 nodes considering finite membrane strain. The number of partition is 16 for the web plate of the testing panel in the longitudinal and vertical directions. Also, there are 16 partitions in the longitudinal direction of the flange plate and 8 partitions in the direction perpendicular to the flange. The other part was also divided so that the local buckling mode could be evaluated with sufficient accuracy. The number of layers in the thickness direction of the shell is taken to be 5.

(2) Boundary conditions

   The boundary conditions are as shown in Fig.3.5. A small rigid body shell element is attached to the elastic element where the concentrated load is applied to satisfy the Kirchhoff's hypothesis that points on a plane remain plane after the deformation. As for the stress-strain relationship of steel, a nonlinear isotropic/kinematical hardening material model was used.

160

Analytical Model(CYP-S-3,5,7,9)   Analytical Model(CYP-S-4,6,8,10)
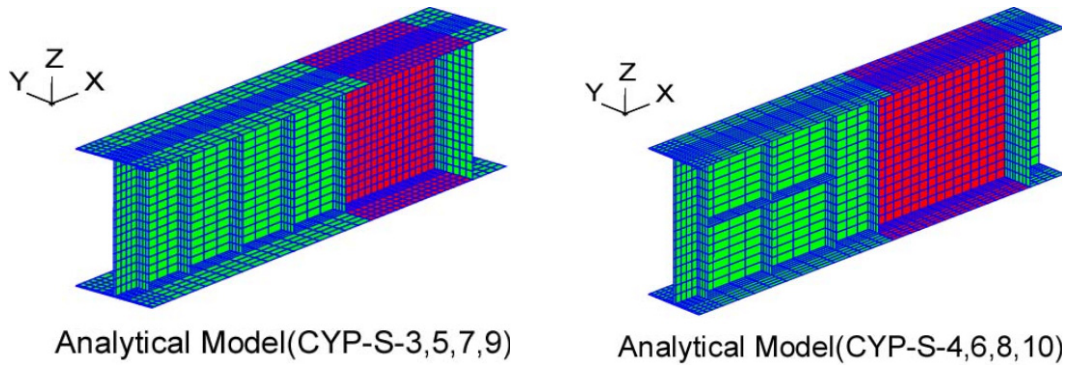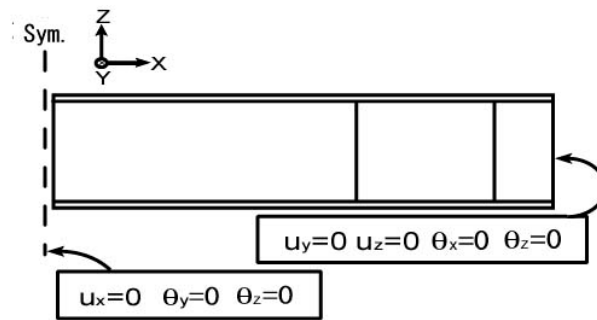
Fig.3.4 Analytical model.

Fig.3.5. Boundary conditions.

6.3.4. Collapse Mode of Panels and Equivalent Stress Distribution

Figs. 3.6 and 3.7 show the failure or the residual deformations of girders after collapse and the distributions of von Mises equivalent stress together with the collapse modes predicted from the computer analysis, respectively.

The flange deformation of Models CYP-S-3 and CYP-S-4 which have thicker flanges and subjected to loading pattern A but have different web depth-to-thickness ratios, b/t, is found to be relatively small. The out-of-plane deflection of the web, however, was large. In Model CY-P-S-3, there was a small initial crack in the vicinity where the tension fields crossed and at a corner of the testing panel, and no conspicuous fracture is observed in Model CYP-S-4. From the comparison of collapse modes, the analytical and experimental results are found to have good correlations.

Models CYP-S-5 and CYP-S-6 have a thinner flange subjected to the loading sequence A. A significantly large vertical dent of flange was observed for Model CYP-S-6 with a larger depth-to-thickness ratio of web plate, b/t, than that of Model CYP-S-5. Each of the web plates of the girders underwent significantly large out-of-plane deflections. Although cracks were observed in these specimens, these cracks did not greatly develop in the range of experimental repetitions. From the comparison of the test and computational results, the dent of flange at Model CYP-S-6 seems to be simulated very well. This dent makes the flange suddenly unable to carry flange forces and thus bringing about the abrupt reduction of the load-carrying capacity.

Next, the failure modes of Models CYP-S-7 and CYP-S-8 under the loading

161

sequence B are discussed. The crack in the web plate is apparently more significant than Model CYP-S-5 that is virtually the same as Model CYP-S-7, but the difference being only the matter of the loading sequence. For Model CYP-S-8 with a larger depth-to-thickness ratio, the web plate crack and the dent of the flange were severer. The computed result on the collapse mode for Model CYP-S-8 shows a very good correlation of large out-of-plane deformation of the web plate and the dent of the flange.

Both Models CYP-S-9 and CYP-S-10 showed large out-of-plane deformation in the web plate, and especially the generation of the crack is significant in Model CYP-S-10. Since a crack was generated at the joint of bearing stiffener and flange in Model CYP-S-10, the test had to be terminated immediately. The local deformation of the flange is not so large on each girder because of thicker flange. As a whole, the degree of the damage of Model CYP-S-9 with a smaller depth-to-thickness ratio is found smaller than that of Model CYP-S-10 with a larger depth-to-thickness ratio. The detailed description of the process of the crack initiation of web plate of Model CYP-S-9 is as follows: At eighth cycle, a small crack appeared near the corner in the supported edge of the panel. Afterwards, it began to generate the crack near the corner in the loaded edge of the panel. With the progress in the cycle, these cracks gradually developed. From the analytical results of the equivalent stress of von Mises for Models CYP-S-9 and CYP-S-10 in Fig.6, the deformation of the flange is small on both girders. The correlation of the results between the analysis and test is found to be very good for Model CYP-S-9.

| CYP-S-3 | CYP-S-4 |

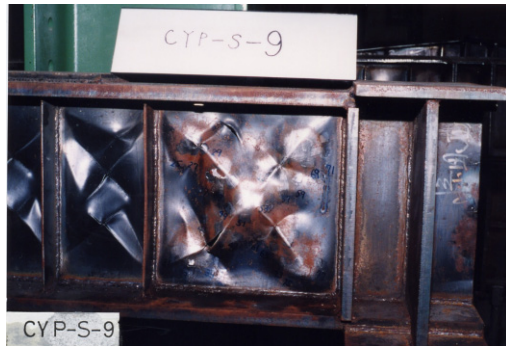| CYP-S-5 | CYP-S-6 |

Fig.3.6. Testing panels after test.

CYP-S-7   CYP-S-8

CYP-S-9   CYP-S-10

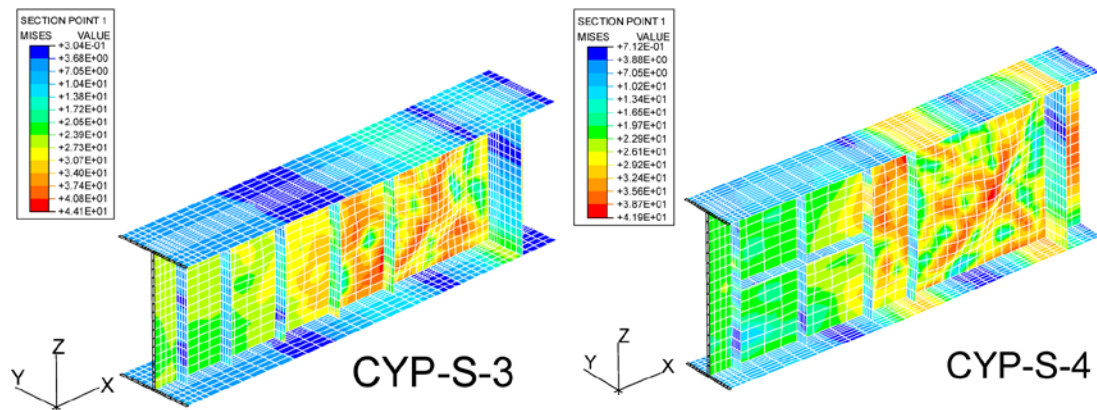Fig.3.6. Testing panels after test (Continued).
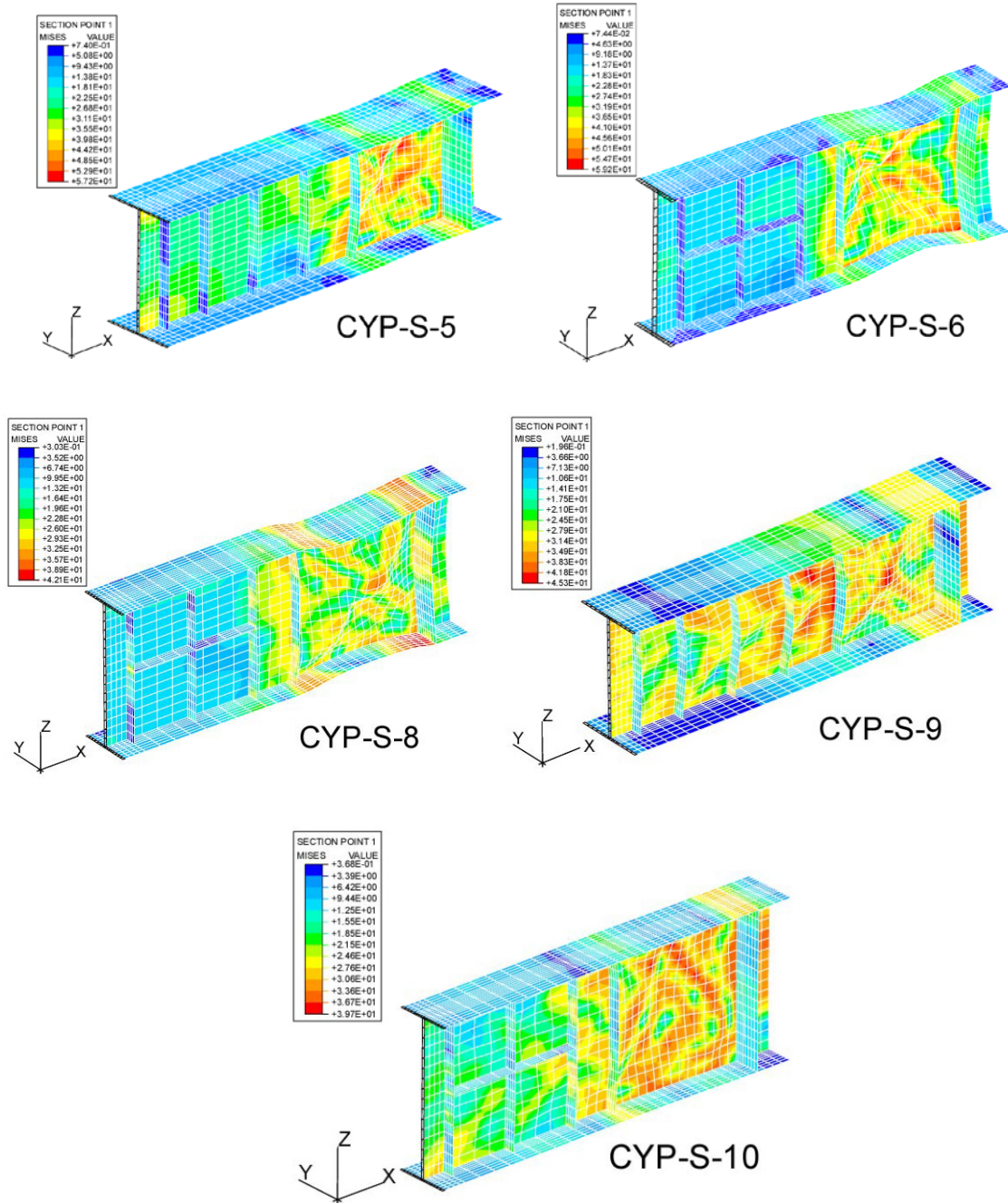

Fig.3.7. Von Mises equivalent stress.

Fig.3.7. Von Mises equivalent stress (Continued).

6.3.5. Comparison of Load-Displacement Envelope between Test and Analysis

The results of the analysis on the load-displacement envelope, the axial and the bending strain of the flange are compared with the experimental results.

(1) Load-displacement hysteretic loop

The hysteretic load-displacement diagrams from the tests are illustrated in Fig.3.8 for Models CYP-S-5, CYP-S-6, CYP-S-7 and CYP-S-8. For Model CYP-S-5, although the load drops temporarily owing to shear buckling of a web plate, the original loop is

restored afterwards and the tension field is formed alternatively with the change of the load direction. Consequently, within the number of repetitions the girder demonstrates a stable behavior. As the web plate of Model CYP-S-6 under the same loading type as that of Model CYP-S-5 has a larger depth-to-thickness ratio, the load-carrying capacity drops abruptly after the progress of several cycles. This might have a close relation with the occurrence of the vertical dent of the flanges. For Model CYP-S-7 of which the loading type is B and the dimensions remain the same as those of Model CYP-S-5, the cracks on the web grow under the increase of repeated numbers of cycles. This lead to the loss of the shear carrying capacity by the tension field and ultimately the abrupt deterioration of the load-carrying capacity occurs.   For Model CYP-S-8 of which the loading type is B and the depth-to-thickness ratio of the web plate is 200, the vertical dent of flanges occurs as in the case of Model CYP-S-6 and the crack of the web plate becomes significantly large. The deterioration of the load-carrying capacity is observed at an early stage of loading. In Models CYP-S-9 and CYP-S-10, since the crack in the web plate develops with the increase of the cycle, the hysteretic behavior that showed rapid deterioration was observed as in the case of Model CYP-S-7 in the Load Sequence B. In contrast, Models CYP-S-3 and CYP-S-4 which basically had the same cross sections as those of Models CYP-S-9 and CYP-S-10, respectively, displayed more stable hysteretic behavior in the Load Sequence A.
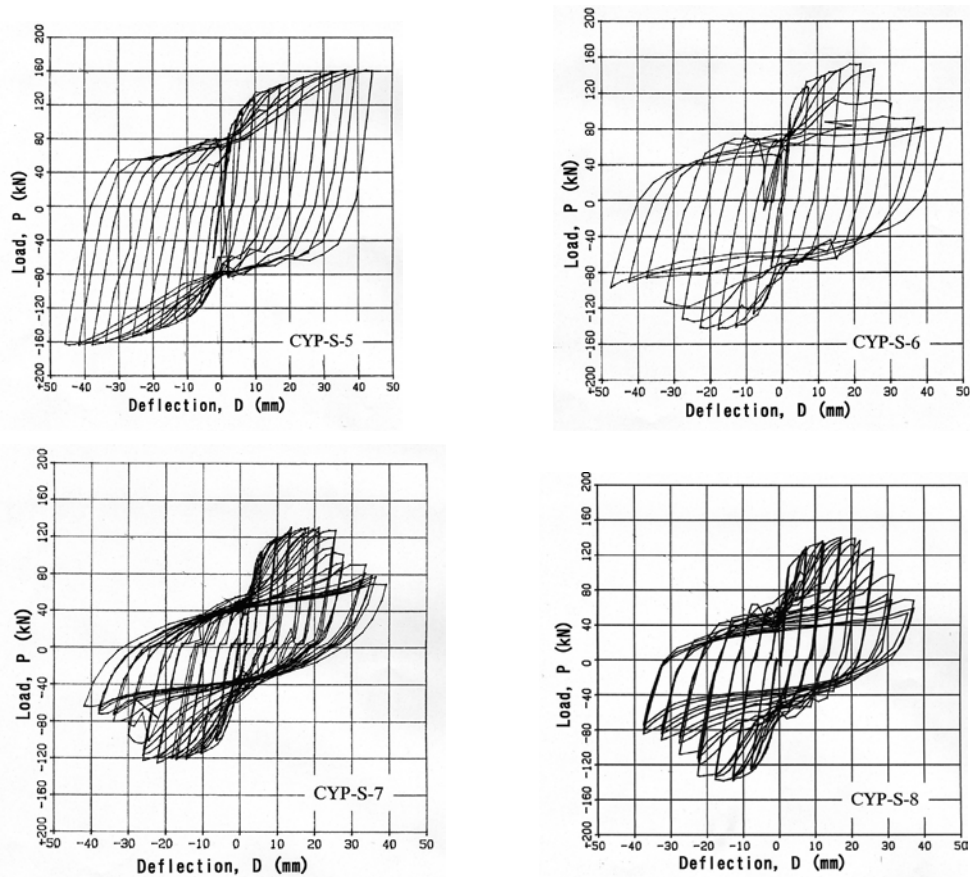
Fig.3.8. Hysteretic loop from test.

165

Similarly, the computed load-displacement hysteretic loops of Models CYP-S-5, CYP-S-6 and CYP-S-8 are shown in Fig.3.9. The shape of the curve of Model CYP-S-5 looks similar to those found experimentally. For Models CYP-S-6 and CYP-S-8, the deterioration of the load-carrying capacity after several cycles is not so apparent in the hysteretic loops because the progress of the web plate cracks is not considered in the analysis. From the comparison of experimental and analytical
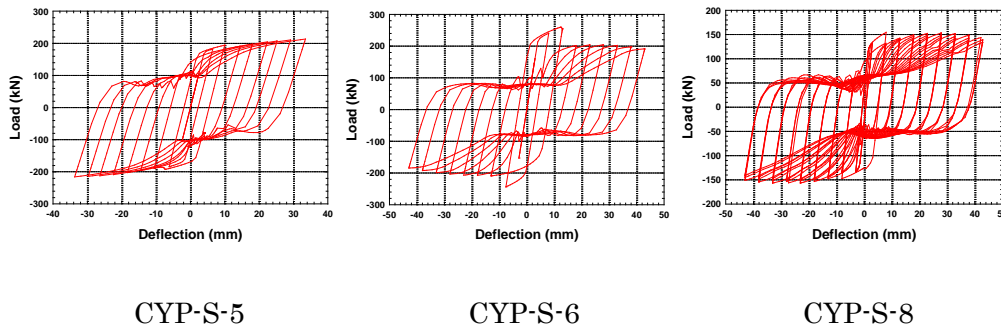

CYP-S-5   CYP-S-6   CYP-S-8

Fig.3.9. Computed hysteretic loop.

results, though there is a little difference of the load-carrying capacity, a good correlation can be seen between the test results and the analytical results.

(2) Axial strain of flange

Fig.3.10 shows the relationships between axial strains of Model CYP-S-8 at the flange center and the number of cycles from the test. A similar analytical result is shown in Fig.3.11. The experimental results may be seen to agree fairly well with the analytical results. From these figures, the dent of the flange is generated after the 3rd or the 4th loading cycle is over. This behavior is different from a stable one in a previous stage, and may reflect the decrement of the load-carrying capacity.
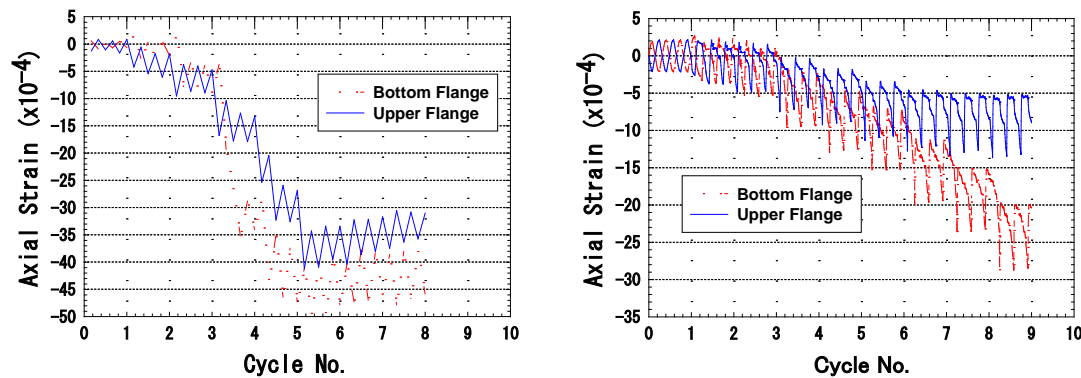

Fig.3.10. Experimental axial strain of flange. Fig.3.11. Analytical axial strain of flange.

(3) Load-displacement envelope

The envelope curves of Models CYP-S-3, CYP-S-4, CYP-S-5 and CYP-S-6 are shown in Figs.3.12 to 3.15, respectively. In each figure, the results from the tests and analysis are compared. From Figs.3.12 and 3.14, provided that the depth-to-thickness ratio of a girder web is a value of about 150, the load-carrying capacity and the deformability are in good condition because they are not so much influenced by the flange rigidity. The depth-to-thickness ratio of the web plate in the case of Figs.3.13 and 3.15 is larger than that in the case of Figs.3.12 and 3.14. Model CYP-S-4 with a larger flange rigidity shows a more stable behavior. On the other hand, the load-carrying capacity of Model CYP-S-6 with a smaller flange rigidity drops abruptly because of the occurrence of the dent at the flange. From the comparison of the results of the tests and analysis, it is found that a good agreement is obtained for Models CYP-S-3 and CYP-S-4, though the calculated values are a little higher. In the meantime, the difference of the curves from the analysis and the test is not small in Models CYP-S-5 and CYP-S-6. In the tensile test for these girders the yielding stress could have been possibly misread and thus overestimated as could be imagined by Table 3.2.

The envelope curve obtained from the test for Models CYP-S-7, CYP-S-8, CYP-S-9 and CYP-S-10 is shown respectively in Figs.3.16 to 3.19. The differences in the results may be due to the different loading processes. It is obvious that in Model CYP-S-7 as compared with Model CYP-S-5, since the out-of-plane deformation of the web plate is remarkable on account of the increase of repeated numbers with cracks developed notably. As a result of the decrease in the tension field action, only the edge frame of the web panel becomes effective for carrying load and the load-carrying capacity decreases at an early stage as shown in Fig.3.16. The load for each cycle makes little difference until the attainment of the maximum load. After which the strength deteriorates at every cycle for the repetition of the same amplitude. For Model CYP-S-8 having a depth-to-thickness ratio of 200 for the web plate, it is seen from Fig.3.17 that because the web plate was cracked and the flanges sank, the deterioration of this model was accelerated in comparison with Model CYP-S-6. As compared with Model CYP-S-6 of which the loading type is A, the deterioration of the deformability is noted. This tendency is evident in Model CYP-S-7, too. For Model CYP-S-10 having a large depth-to-thickness ratio of the web plate, it is seen that the non-linearity appeared at an early stage from Fig.18. It is noted from Figs.3.18 and 3.19 that as for deformability, both girders show a comparatively good tendency until the last stage.
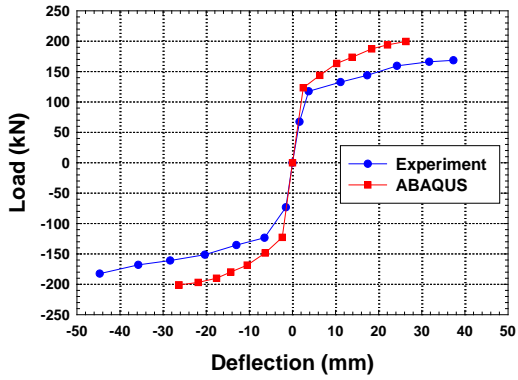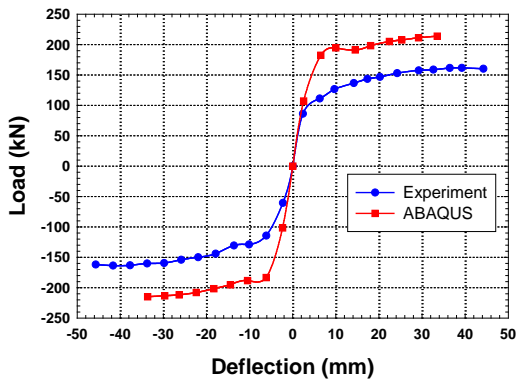
CYP-S-3
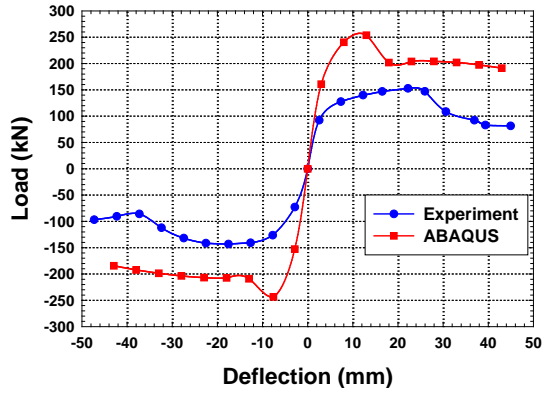
Fig.3.12. Envelope of load-deflection.
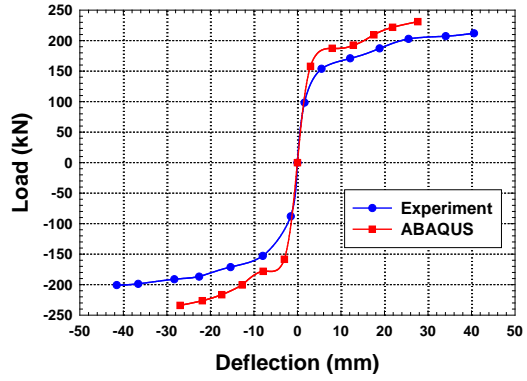
CYP-S-4

Fig.3.13. Envelope of load-deflection.
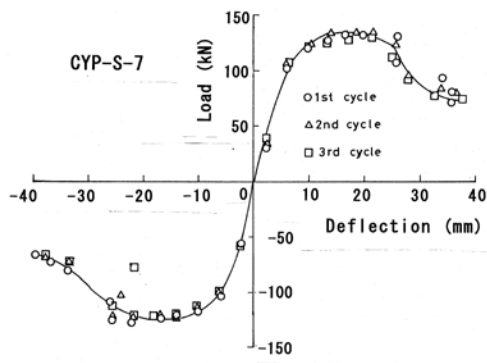

CYP-S-5

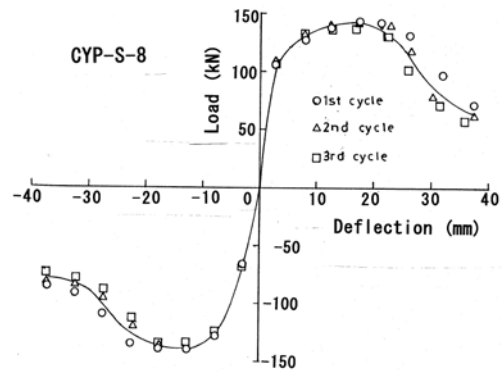Fig.3.14. Envelope of load-deflection.

CYP-S-6

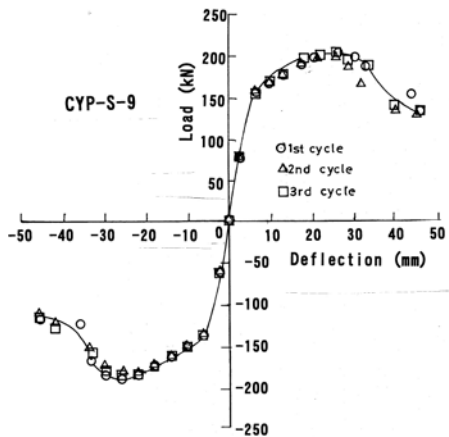Fig.3.15. Envelope of load-deflection.

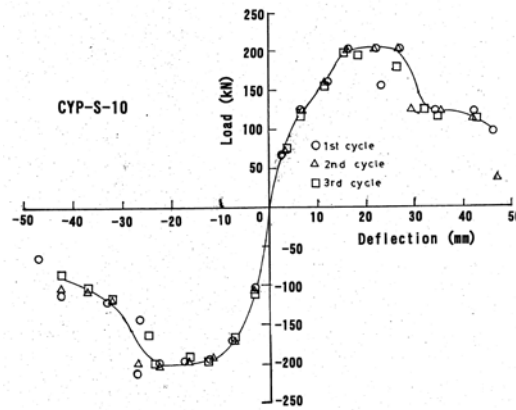CYP-S-7

Fig.3.16. Envelope of load-deflection.

CYP-S-8

Fig.3.17. Envelope of load-deflection.

CYP-S-9

Fig.3.18. Envelope of load-deflection.

CYP-S-10

Fig.3.19. Envelope of load-deflection.

6.3.6. Other Observations from Experimental Results

Except for the experimental results reported until now, the following results were obtained.

(1) Distribution of principal strains

Let us take Model CYP-S-6, for example, to see the distribution of principal strains. The principal strain distribution of the web panel is shown in Fig.3.20 when the maximum load is reached at each half cycle. It is evident that the tension field develops alternately and stably at the 3rd cycle. As a result of the effect caused by the flange dent, the flange ceases to work as an anchor of the tension field. This fact is shown by the figures in the 7th cycle, and the direction of principal strains greatly varies. Judging from the change of this direction, it can be predicted that the deterioration of the shear strength is caused. In Model CYP-S-5, as shown from the principal strain distribution at the 8th cycle in Fig.3.21, the direction of the tension field in its previous stage is maintained.
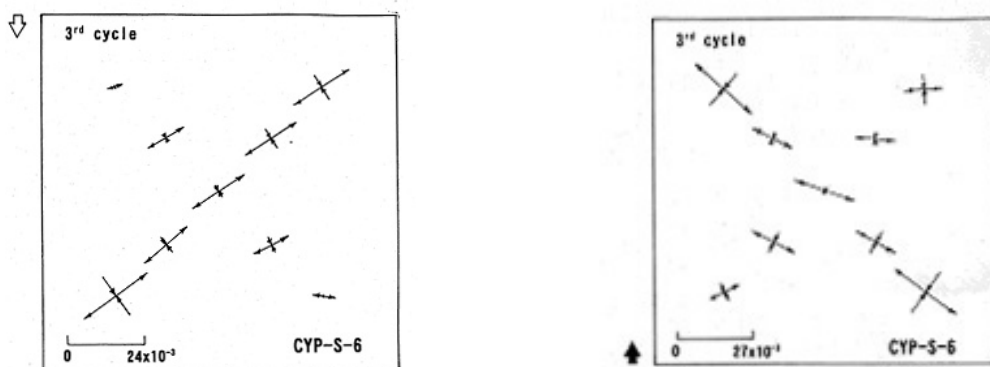

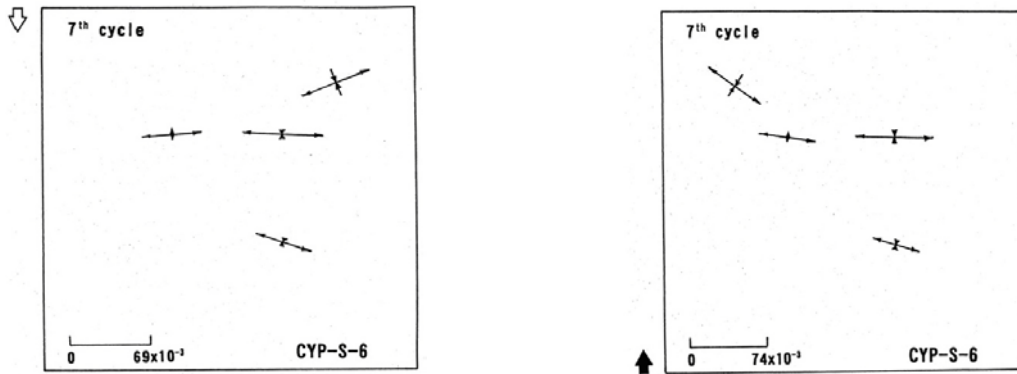Fig.3.20. Distribution of principal strains: CYP-S-6.

169

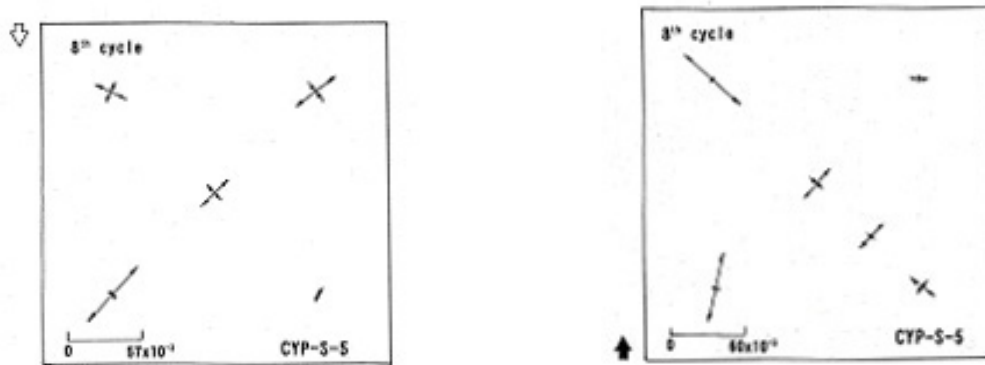Fig.3.20. Distribution of principal strains: CYP-S-6(Continued).

Fig.3.21. Distribution of principal strains: CYP-S-5.

(2) Load-Diagonal strain relationship

The variation in each every cycle of the strain at the panel diagonal direction is shown in Fig.3.22. It is proven that the strain in the direction that tensile stresses applied first has been almost tension strain throughout the whole cycle. In the case of Model CYP-S-6, the value of the strain suddenly drops after several cycle progress, and it increases afterwards. It seems that this fact is the effect by the dent of the flange. On the other hand, in the direction which compression stresses applied first the region of the compressive strains is also observed in the early cycles, though large tensile strains appeared finally by the repetitive generation of the tension field.

170
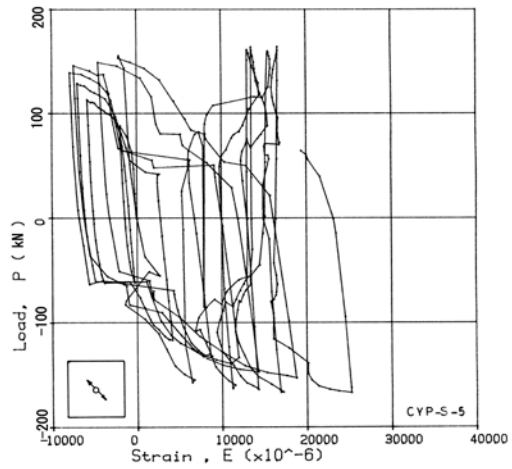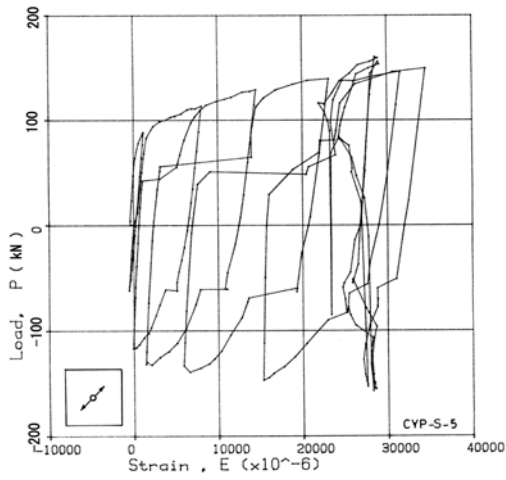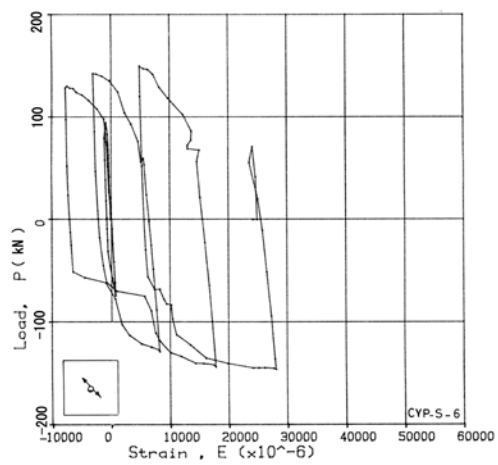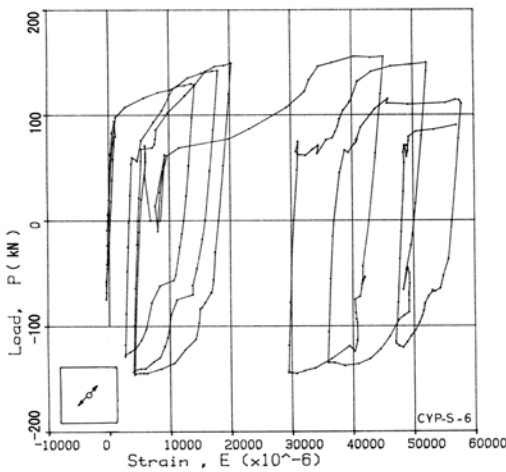
(a) Model CYP-S-5

(b) Model CYP-S-6

Fig.3.22 Load-Diagonal strain hysteretic loops.

(3) Relation between deflection and cycles

Fig.3.23 shows plots of the relation monitored by the actuator between the repetition number and the maximum deflection in each cycle of test for Model CYP-S-10. It is noted that although the linearity is disturbed at the 6th cycle which the dent of flanges are observed, this disturbance is improved and the good deformability is maintained until the last cycle at which a flange is broken. Similarly, the comparatively good deformability was also obtained for other models.

171

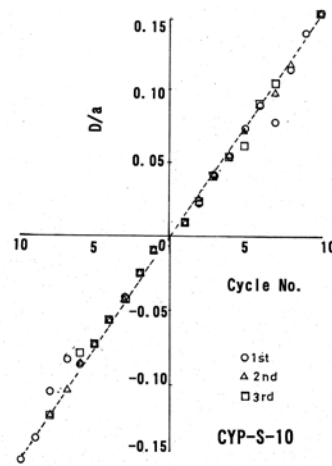Fig.3.23. Cycle vs. deflection relationship.

(4) Absorbed energy

The absorbed energy is shown to increase with the number of the loading cycle in Figs.3.24 and 3.25 for Models CYP-S-9 and CYP-S-10, respectively. Although the absorbed energy increases smoothly up to the development of web crack, then it decreases. However, in Model CYP-S-9 of which the flanges are in good condition, the absorbed energy increases again. It is seen from these figures that although the absorbed energy noticeably increases from the first to, the second and the third loading, it stays or drops significantly due to the growth of the deformation caused by the increase of loading cycles.
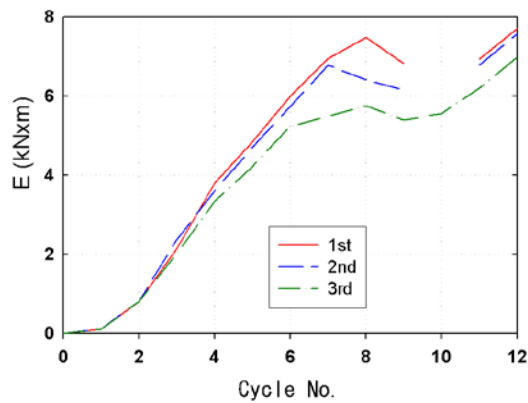
Fig.3,24. Absorbed energy: CYP-S-9.   Fig.3.25. Absorbed energy: CYP-S-10.
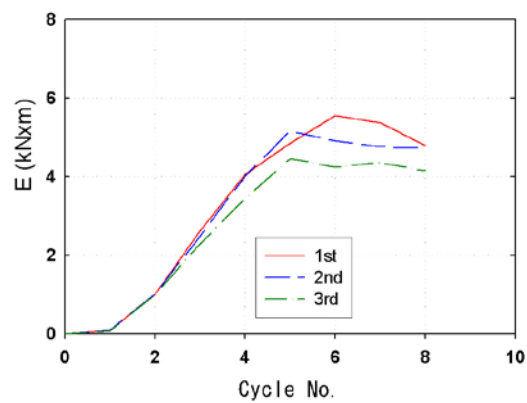
6.3.7. Conclusions

Particular emphasis is placed on the repetitive buckling behavior of steel plated girders under the inelastic shear or the combined shear and bending. Model girders were tested and the computer analysis was also carried out by finite element method. From the comparison between the experimental and analytical results, good correlations were found to exist in the repetitive inelastic behavior of girders. The following concluding remarks may be made:

1) On account of repetitive inelastic buckling under severely repeated shear force, remarkable out-of-plane deformation results in and the tension field is formed alternately in general. The strength is reduced owing to the crack in the web plate and the dent of the flange into the web plate in the case, where the web has

172

a large width-to-thickness ratio.

2) The deformability of the panel remains good until the maximum load is reached. Even if the dent occurs after that, the reduction of the deformability is only temporary and the recovery of the deformability is achieved.

3) In the case of loading Type A, and the depth-to-thickness ratio of a web plate is less than 150, stable behavior is expected. However, when the ratio exceeds 200 and the flange rigidity is not large, the strength is considerably reduced due to the vertical dent of the flange and the crack growth in the web plate.

4) In the case of loading Type B, as the web crack develops (due to large cycles of loading), the reduction of the strength may become significant even if the girder could be stable in Type A.

5) The direction of the principal strain in the web plate changes, when the dent of the flange occurs, even if the web crack is small. Consequently, the deterioration of the shear strength is brought about.

6) Absorbed energy increases smoothly until the development of the web crack. If flanges are in good condition, the cumulative energy grows well.

7) Since the out-of-plane deformation takes place in several panels as well as in the testing panel under the repeated load, it is not reasonable to assume the deformation only in the tested single panel.

8) In the buildings, steel shear panels have been already used as active hysteretic damper links. It is expected that the shear link can also be introduced into the steel bridge in order to be utilized as a hysteretic damper against earthquake loads. As it is mentioned above, the shear panel shows a stable elasto-plastic behavior generally, and the excellent deformability and energy dissipation capacity can be expected. By utilizing these characteristics, if the panel is effectively built as a link, the damage can be concentrated to these self-sacrificing shear panel members only so that the damage of primary members can be well protected from the action of the excessive earthquake load.

9) In this article, the panel with comparatively large value of the depth-to-thickness ratio was treated and the collapse over several panels was examined. The obtained results may give a basic and important insight to the introduction of this system to steel bridges in view of good displacement ductility capacity and stable hysteretic behavior with desirable energy dissipation characteristics in areas of high seismic risk utilizing shear links such as in the case of new San Francisco-Oakland Bay Bridge.

6.4 Discussions

The inelastic behavior of plate girders under cyclic loadings was discussed in this chapter. The ultimate strength and hysteretic behavior of the single girder panel subjected to the repetitive shear force are investigated numerically in 6.2. Article 6.3 is focused on the theoretical and experimental study on the strength and ductility of multi-panel under the repetitive inelastic buckling subjected to shear or the combined shear and bending. From the above results, it was proven that the examination over adjacently several panels is more desirable in order to take the interaction of panels into consideration.

The shear panel subjected to cyclic loadings shows not only relatively stable behavior and sufficient deformability, but also the energy dissipation capacity is found to be excellent. By utilizing such characteristics of the shear panel, the use as a damper system is noticed at present. This damper has been used in the buildings practically, and then the utilization should be also greatly promoted also in bridge structures. The use to new San Francisco-Oakland Bay Bridge is an example of the practical application.

Two-story portal frame is the type frequently used for the viaduct in the urban line. The application of the shear panel to the middle box-beam in two-story steel

portal frames is being investigated as a realistic application. The use of the low yield ratio steel may be recommended because of its excellent energy dissipation capacity. In addition, the panel may be desirably made demountable. By this damper, it is expected that the great damages of the important parts such as bases and corners of piers can be avoided or reduced.

6.5 References

1) Hjelmstad, K. D. and Popov, E. P.: Cyclic Behavior and Design of Link Beams, Journal of Structural Engineering, ASCE, Vol.109, No.10, pp. 2387-2402, 1983.
2) Kasai, K. and Popov, E. P.: Cyclic Web Buckling Control for Shear Link Beams, Journal of Structural Division, ASCE, Vol.112, N0.ST3, Mar. 1986.
3) Suzuki, T. and Ono, T.: An Experimental Study on Inelastic Behavior of Steel Members Subjected Repeated Loading, World Conf EE, No.6, pp.3163-3167, Jan., 1977.
4) Takahashi, Y. and Tanaka, K.: Development of Hysteretic Damper using Eccentrical Brace System, Steel Construction Engineering, Vol.4, No.14, pp. 39-52, 1997 (in Japanese).
5) Takahashi, Y. and Shinabe, Y.: Experimental Study on Restoring Force Characteristics of Shear Yielding Thin Steel Plate Elements, Journal of Structural and Construction Engineering(Transactions of AIJ), No.494, pp.107-114, 1997(in Japanese).
6) Usami, T. et al.: An Experimental Study on the Elasto-Plastic Cyclic Behavior of Stiffened Box Members, Journal of Structural Engineering, JSCE, Vol.38A, pp.105-117, 1992(in Japanese).
7) Suzuki, M. and Usami, T.: Estimating Formulas of Strength and Deformation Capacty of Steel Bridge Pier Model Under Cyclic Loading, Journal of Structural Mechanics and Earthquake Engineering, JSCE, No.519/I-32, pp.115-125, 1995(in Japanese).
8) Nshikawa, K. et al.: An Experimental Study on Improvement of Seismic Performance of Existing Steel Bridge Piers, Journal of Structural Engineering, JSCE, Vol.42A, pp975-986, 1996(in Japanese).
9) Sugiura, Y. et al.: Investigation into Seismic Upgrading of Frame-type Steel Pier Beam Webs by Bolted Stiffeners, Journal of Structural Engineering, JSCE, Vol.50A, pp.1447-1454, 2004(in Japanese).
10) Miki, T. and Yamada, O.: Inelastic Earthquake Response Analysis of Steel two-story Frames with Shear Collapse in Middle of Beam, Journal of Structural Engineering, JSCE, Vol.45A, pp.227-234, 1999(in Japanese).
11) Morishita, H. et al.: Experimental study on Strength and Ductility of a Rigid-Frame Steel Pier with Intermediate Cross Beam, Journal of Structural Engineering, JSCE, Vo.46A, pp.831-840, 2000(in Japanese).
12) Araki, T., Takeda, H. and Dogaki, M.: Cyclic Strength and Deformation Capacity for Steel Bridge Piers of Two-Story Portal Frame Type, Journal of Structural Engineering, JSCE, Vol.50A, pp1455-1465, 2004.
13) Specification for Highway Bridges, Japan Road Association, 1990.
14) Basler, K.: Strength of plate girders in shear, Journal of Structural Division, Proc. of ASCE, Vol.87, No.ST7, pp.151-180, 1961.
15) Yasunami, H. et al.: Evaluation of Seismic Capacity of Compact Section Steel Bridge Piers with A Few Stiffeners, Bridge and Foundation Engineering, Vol.32, No.4, pp.33-42, 1998(in Japanese).
16) Usami, T. et al.: Numerical Study on Cyclic Elasto-Plastic Behavior of Steel Bridge Piers of Pipe Sections without Stiffeners, Journal of Structural Mechanics and Earthquake Engineering, JSCE, No.577/I-41, pp.181-190, 1997(in Japanese).

17) Rockey, K. C. and Skaloud, M.: The ultimate load behaviour of plate girders loading in shear, The Structural Engineering, Vol.50, No.1, pp.29-48, 1972.

18) Cooper, P. B., Lew, H. S. and Yen, B. T.: Welded constructional alloy steel plate girders, Journal of Structural Division, Proc. Of ASCE, Vol.90, No.ST1, pp.1-36, 1972.

19) Moriwaki, Y. and Fujino, M.: Experimental Study on Shear Strength of Plate Girders with Initial Imperfections, Proceedings of JSCE, No.249, pp.41-54, 1976(in Japanese).

20) Basler, K.:Strength of Plate Girders under Combined Bending and Shear, Journal of the Structural Division, ASCE, Vol.87, No.ST7, pp. 181-197, 1961.

21) Galambos, T. V. ed.: *Guide to Stability Design Criteria for Metal Structures*, 5th ed., John Wiley & Sons, Inc., 1998.

22) Ostapenko, A. and Chern, C.: Strength of Plate Girders under Shear, Fritz Eng. Laboratory Report, No.328.7, Lehigh University, 1969.

23) Ostapenko, A., Chern, C. and Parsanejad, S.: Ultimate Strength Design of Plate Girders, Lehigh University Eng. Laboratory Report, No.328.12, 1971.

24) Porter, D. M., Rockey, K. C. and Evans, H. R.: The collapse behaviour of plate girders loaded in shear, Structural Engineer, Vol. 53, No. 8, pp. 313-325, 1975.

25) Marsh, C., Ajam, W. and Ha, H.: Finite Element Analysis of Postbuckled Shear Webs, Journal of Structural Engineering, ASCE, Vol.114, No. 7, pp.1571-1586, 1988.

26) Kuranishi, S., Nakazawa M. and Iwakuma, T.: On the Tension Field Action and Collapse Mechanism of a Panel under Shear, Structural Eng./Earthquake Eng., JSCE, 5(1), pp. 183-193, 1988.

27) Lee, S.C. and Yoo, C.H.: Strength of Plate Girder Web Panels under Pure Shear, Journal of Structural Engineering, ASCE, 124(2), pp. 184-194, 1998.

28) Takeda, H., Uchida, Y., Sasaki, D. and Dogaki, M.: Evaluation of Ultimate Strength and Ductility for Plate Girders under Cyclic Shear Loading, Journal of Constructional Steel, 8, pp. 33-40, 2000 (in Japanese).

29) Lubell, A. S., Prion, H. G. L. and Ventura, C. E.: Unstiffened Steel Plate Shear Wall Performance under Cyclic Loading, Journal of Structural Engineering, ASCE, Vol.126, No.4, pp.453-460, 2000.

30) McDaniel, C. C., Uang, Chia-Ming and Seible, F.: Cyclic Testing of Built-up Steel Shear Links for the New Bay Bridge, Journal of Structural Engineering, ASCE, Vol. 129, No. 6, pp. 801-809, 2003.

Chapter 7

Strength and deformability of steel box beams in repetitive shear

7.1 General description

In 1995, the Great Hanshin-Awaji earthquake arose. In this earthquake, the out-of plane deflection due to the shear buckling was also recognized at the web plate in the intermediate cross beam of two-story portal steel piers as well as the web plate in the steel girder under alternatively repetitive shear forces. Examples of the observed beam are shown in Fig.1[19]. From such fact, it seems to be considerably important to clarify the effect of the deformability of the member element subjected to be the primary action of the shear force on the strength and deformation of the whole structure. From the analysis of the damages in steel bridge piers for the above stated earthquake, the various improvements for the earthquake proof structural design of the bridge pier have been proposed. For examples, they are as follows:

① Improvement in the strength of steel bridge piers:
② Reinforcement for the corner connection of bridge piers:
③ Filling of concrete into the cross section of bridge piers:
④ Base-isolation for the elevated highways:

In the method of ①, it is considered that the increase of the energy absorption capacity owing to the raising on strength and rotation capacity as a result of using the thickened member brings about the improvement in the earthquake proofing.

On the other hand, a part in the member cross-section is intentionally weakened in order to damage earlier than other parts, and then the energy dissipation in its part is attempted. As the result, it is considered that the improvement in the earthquake proofing can be expected[1]-[4]. In this case, by utilizing the buckling in the early stage at the web plate near the center of the cross beam and afterwards diagonal tension field action the deformability is increased, and then it is intended that the whole collapse of the bridge pier can be prevented. For appropriate design in this purpose, it is required to sufficiently investigate the fundamental characteristics such as the strength and deformability on steel plates and member cross-sections subjected to repetitive shear forces.

The research on load carrying capacity of steel beams under shear has been much carried out theoretically and experimentally[5]-[8]. However, there are no many on the research on the deformability. The research on the shear strength and deformability for the central region of the intermediate beam in bridge piers of two-story portal steel frame has not been almost carried out[9] and there is only the research on the steel girder with single panel or several panels.

In this chapter, the intermediate beam in the bridge piers of two-story portal steel frame is noticed and for this modeled cross beam under repetitive shear forces, the elasto-plastic finite displacement analysis is carried out using the finite element method. Effect of energy dissipation due to the shear buckling deformation in the relatively thin web plate near the center of the crossbeam is clarified.

7.2. Analysis for steel beam in repetitive shear

7.2.1 Elasto-plastic finite displacement analysis
　(1) Modeling of steel beam

Fig.1 Shear buckling at box-beam in the Great Hanshin-Awaji earthquake

Analytical model is a box-section beam modeling an intermediately layered beam in the steel bridge pier of two-story portal frame as shown in Fig.2. This beam has length l, and it is divided by n diaphragms in interval a. The box-section is not stiffened, and the width and thickness of the flange and the width and thickness of the web are b_f, t_f, b_w and t_w, respectively.

Cross sectional parameters of the steel beam prepared for this analysis are as follows:
Slenderness ratio parameter λ of a steel beam is;
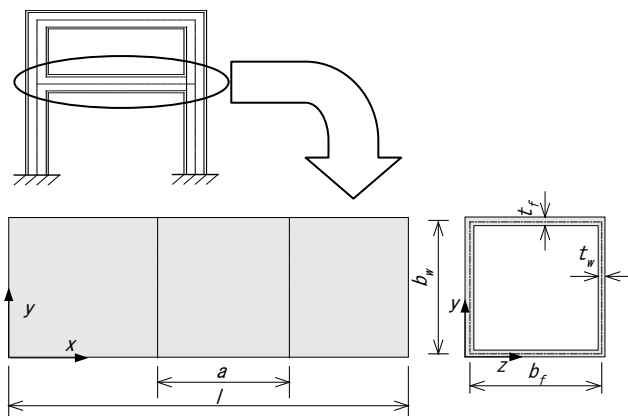
Fig.2 General view of steel box-beam

$$\lambda = \frac{l_e}{r}\frac{1}{\pi}\sqrt{\frac{\sigma_y}{E}} = 0.3 \tag{1}$$

Width-to-thickness ratio parameter R_f of the un-stiffened flange;

$$R_f = \frac{b_f}{t_f}\sqrt{\frac{\sigma_y}{E}\frac{12(1-v^2)}{\pi^2 k_{cr,comp}}} = 0.7, 1.5, 2.5 \tag{2}$$

Aspect ratio α and width-to-thickness ratio parameter R_w of the un-stiffened web plate;

$$\alpha = 1.0 \tag{3}$$

$$R_{tw} = \frac{b_w}{t_w}\sqrt{\frac{\sigma_y}{\sqrt{3}E}\frac{12(1-v^2)}{\pi^2 k_{cr,shear}}} = 0.3\sim0.5 \tag{4}$$

where l_e and r are the effective buckling length(=1.2) and the radius of gyration of the steel beam, respectively. $k_{cr,comp}$ is the elastic buckling coefficient(=4.0) of the simply supported compressive flange and $k_{cr,shear}$ is the elastic shear buckling coefficient of the simply supported web plate expressed as the following[15];

$$\alpha \leq 1 \quad : \quad k_{cr,shear} = 4.0 + \frac{5.34}{\alpha^2}$$

$$\alpha \geq 1 \quad : \quad k_{cr,shear} = 5.34 + \frac{4.0}{\alpha^2} \tag{5}$$

It is assumed that the steel beam is manufactured by the steel plate of Type SM490Y and the multi-linear type was adopted for the stress-strain relationship. The yield point stress is as follows:

σ_y=365Mpa ($t\leqq16$mm)
σ_y=355Mpa (16mm$<t\leqq$40mm)
σ_y=335Mpa (40mm$<t\leqq$75mm)
σ_y=325Mpa (75mm$<t$)

Young's modulus E and Poisson's ratio v equal to 206Gpa and 0.3, respectively.

(2) Application of elasto-plastic finite displacement analysis

The elasto-plastic finite displacement analysis was carried out using a general-purpose finite element analysis code MARC 2001. In this case, the finite element method by up-dated Lagrangian technique was used. In addition, the equivalent stress formula by von Mises in the decision of the yield and the plastic flow rule of Prandtle-Reuss for the flow rule were used. Newton-Raphson method and arc length incremental method were chosen in the solution method of nonlinear algebraic equation. And for the hardening rule, the following was used: Isotropic hardening rule and mixing hardening rule which used the kinematic hardening law jointly.

The convergence of nonlinear solution was judged in the following equation,

$R_{max} < \varepsilon$

In which R is the residual un-equilibrium force, and ε is set at 10^{-3} in the allowable error for the convergence decision.

(3) Analytical model for steel beam in bridge piers

In this research, the web plate near the center at the cross beam modeling the intermediately layered beam in the bridge piers of two-story portal steel frame under repetitive shear forces is noticed and the

Fig.3 Coupled element model

characteristics on its strength and hysteretic behavior is clarified analytically. Because it focuses on the central region of 3 panels divided by the diaphragm of 4 sheets as shown in Fig.3, for this region plate elements were used. Beam-column elements were used for both ends (=l-$3a$), and the coupled model as shown in Fig.3 was adopted. Considering the symmetry of the section, the half of the panels on the direction of z was analyzed.
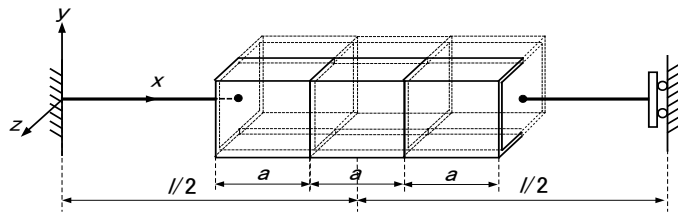
(4) Divisions in finite element method

4-node quadrilateral thick-shell element with 6 degrees of freedoms per node and beam-column element with 3 degrees of freedoms per node were applied for the plate region and for the bar region, respectively. The outline of the divisions is shown in Fig.4. The plate thickness of a central web panel within these three panels is more thinly set further than that of other panels, and

Fig.4 Divisions in three panels

the energy dissipation effect caused by the out-of-plane deformation in the early stage is examined. The central panel of which the shear deformation seems to be remarkable is divided into the axial direction of member using twelve elements in order to examine the aspect of the deformation as detailed as possible. The adjacent panels are divided into six elements. Since the cross section of the beam is assumed to be square, both the flange and web plate is divided into the perpendicular direction using twelve elements.

(5) Loading sequence and boundary conditions

As loading pattern, the following two methods are adopted as shown in Fig.5:

① An incremental loading method: this is the method in which the shear load always increases.
② A repetitive loading method: this is the method in which the maximum amplitude increases every cycle.

The equivalent vertical displacement is given so that the shear force may be made to apply in the steel beam. In this case, the vertical displacement is given so that the both ends of the beam-column element may not rotate. Namely, the displacement u in the direction x axis, the

Fig.5 Loading type

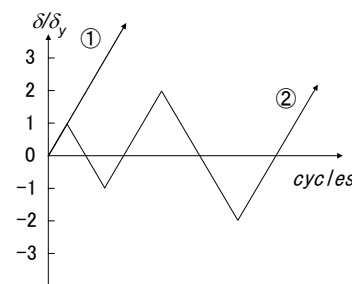displacement v in the direction y axis and the rotation angle ϕ about z axis were restricted in the left end of the coupled model as following:

$$u = v = \phi = 0 \tag{6}$$

The equivalent vertical displacement δ for shear force is given along the direction of y axis:

$$v = \delta \tag{7}$$

and the following condition is added.

$$\phi = 0 \tag{8}$$

The vertical displacement δ is given referring to the shear yield displacement δ_y corresponding to the shear yield load Q_y. Q_y and δ_y are expressed as following:

$$Q_y = 2\tau_y b_w t_w \tag{9}$$

$$\delta_y = \frac{aQ_y}{2Gb_w t_w} \tag{10}$$

where G is the elastic shear modulus.

 (6) Coupling method between elements and symmetrical conditions
    Conditions for continuity in the joint of the coupled model between beam-column element and plate element are as follows:
① Each cross section of the beam-column element and the plate element retains the perpendicularity to the member axis in the joint, therefore the continuity of the displacement between elements is guaranteed.
② Since the rigidity of the diaphragm between adjacent elements is very high, it restricts the out-of-plane deformation of the flange and web plate.
③ The flange and web plate in the region using plate elements are simply supported on the diaphragm.
    The above conditions are shown at the form of the equation in the following.

$$w = \theta_x = \theta_y = 0 : \text{on the flange in the joint.} \tag{11}$$

$$w = \theta_x = \theta_z = 0 : \text{on the web plate in the joint.} \tag{12}$$

In these equations, w is the displacement in the perpendicular direction to the member axis and θ_x, θ_y and θ_z are the rotation angles about x, y and z axes in the plate elements, respectively.
Furthermore, from the symmetry of the cross section, the following symmetrical condition along the centerline of the flange next is considered.

$$w = \theta_x = \theta_y = 0 \tag{13}$$

 (7) Initial imperfections
As an initial imperfection, the deflection was considered. The global buckling mode

was introduced into the beam-column element and the coupled buckling mode between the global buckling and local buckling was introduced into the plate element as shown in Fig.6.

At beam-column element:

$$v_0^{\ c} = v_{0\max}^{\ c}\ \frac{l}{1000}\cos\frac{n_c\pi}{l}x \qquad (14)$$

At the flange of the plate element:

$$v_0^{\ f} = y + v_{0\max}^{\ c}\ \frac{l}{1000}\cos\frac{n_c\pi}{l}x$$

$$\pm v_{0\max}^{\ f}\ \frac{b_f}{150}\sin\frac{n_x\pi}{a}x\cos\frac{n_z\pi}{b_f}z \qquad (15)$$
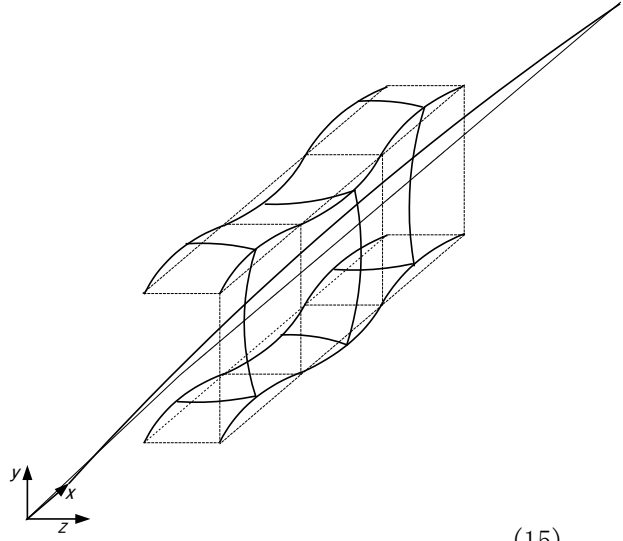
(15)

Fig.6 Initial imperfection mode

At the web plate:

$$v_0^{\ w} = y + v_{0\max}^{\ c}\ \frac{l}{1000}\frac{n_c\pi}{l}x \qquad (16)$$

$$w_0^{\ w} = z - w_{0\max}^{\ w}\ \frac{b_w}{150}\sin\frac{n_x\pi}{a}x\cos\frac{n_y\pi}{b_w}y \qquad (17)$$

In these equations, $v_{0max}^{\ c}$, $v_{0max}^{\ f}$ and $w_{0max}^{\ w}$ are magnifiers for the limiting values of manufacturing error allowed in the Japanese specifications[10]. n_c is half wave number in the axial direction of the initial deflection over the member. n_x, n_y and n_z are half wave number of the initial deflection for the plate element in the direction of x, y and z, respectively. On the double sign, the upper sign and the lower sign are applied to the upper flange and the bottom flange, respectively.

7.2.2 Numerical results and considerations

    The steel beam under the incremental shear force or repetitive shear load is analyzed, and the strength and deformability of the steel beam are examined.

 (1) Comparison between present solution and existing experimental results

    The validity on the analytical model and assumed conditions is examined before the extensive numerical calculation. Present solution is compared with the experimental result by Scheer-Pasternak-Ruga[11]. The relationship between shear force and vertical displacement in increment loading is shown in Fig.7. In this figure, the ordinate is the shear force Q/Q_y that is made dimensionless by the shear yield force Q_y, and the abscissa is the vertical displacement δ/δ_y that is made dimensionless by the shear yield displacement δ_y. The cross-sectional shape ratio b_w/b_f, the ratio between flange thickness and web plate thickness t_w/t_f, the width-to-thickness ratio parameter of flange plate R_f, the aspect ratio of web plate a/b_w, the width-to-thickness ratio of web plate

b_w/t_w and the width-to-thickness parameter R_w are 0.35, 0.094, 0.26, 1.0, 149 and 2.13, respectively.

As seen from this figure, both curves agree well until the arrival at the yield displacement. Afterwards, the difference occurred in both curves. The maximum load obtained by the present method shows a little higher value than the experimental value. It seems that this arose due to initial imperfections, mechanical property of steel members and the difference between the analytical and experimental conditions.
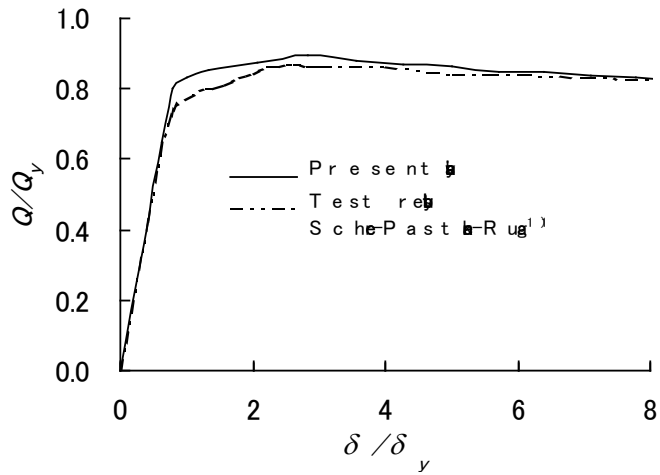
Fig.7 Comparison of present method with test result

(2) Strength and deformability of beam under incremental loading

The strength and deformability of girder in the monotonous loading are examined.

1) Influence of web width-to-thickness ratio on strength and deformability of girder

When the width-to-thickness ratio parameter of the flange R_f is 0.7, 1.5 or 2.5, the relationship between the shear force and vertical displacement of beam is shown in Fig.8 as the width-to-thickness ratio parameter of web plate variously changes. In these figures, the slenderness ratio parameter of the beam λ, the cross-sectional shape ratio b_w/b_f, and the aspect ratio of web plate a/b_w are 0.3, 1.0 and 1.0, respectively. The other parameters are shown in Table 1.

Table 1 Parameter of steel beam

| | Flange | Web plate | | | | |
| | | Center panel | | Adjacent panel | | |
	R_f	$R_{\tau w}$	b_w/t_w	$R_{\tau w}$	b_w/t_w	t_f/t_w
Fig.8(a)	0.7	0.4	37	0.3	28	0.86
		0.5	46			
		0.6	55			
Fig.8(b)	1.5	0.7	64	0.6	43	0.81
		0.9	83			
		1.1	101			
Fig.8(c)	2.5	1.5	138	1.0	92	0.80
		1.9	175			
		2.5	230			

As it is clear from these figures, the maximum load lowers with the increase of the width-to-thickness ratio parameter of web plate R_w and the degradation of the strength also occurs, after the maximum load is reached. However, the strength extremely does not lower owing to the tension field action after the buckling unlike the case of the thin plate under compressive force or bending moment.

Generally the use of the thickened members is effective, when the excellent earthquake proofing is expected in them. Though it is effective to make members thick for the rise in the strength, it becomes meanwhile difficult to be deformed. This is classified into an idea of earthquake-proof improvement in which the rise of the strength precedes. In the meantime, there is an idea in which to excessively require the strength of the member is avoided and the energy absorption capacity due to possible allowable deformation should be expected. This is an idea of the earthquake-proof guarantee taken seriously in the deformability. The improvement of the earthquake proofing by the latter method becomes actually, if the shear deformation due to the repetitive loading in the beam that is not directly related to the strength in the earthquake proceeds and it is possible to dissipate the seismic energy by the shear deformation of thin plate.

(a) R_f=0.7

(b) R_f=1.5

(c) R_f=2.5

Fig.8 Shear force and displacement

The effect of web plate thickness at the center of the beam on the strength and deformability of the steel beam is seen in Fig.8. With the research by Kasai et al.[9], the following results have been obtained when t_f/t_w is over 1.5: ① The action of the flange as an anchor of the tension field becomes more powerful. ② The rise of the shear
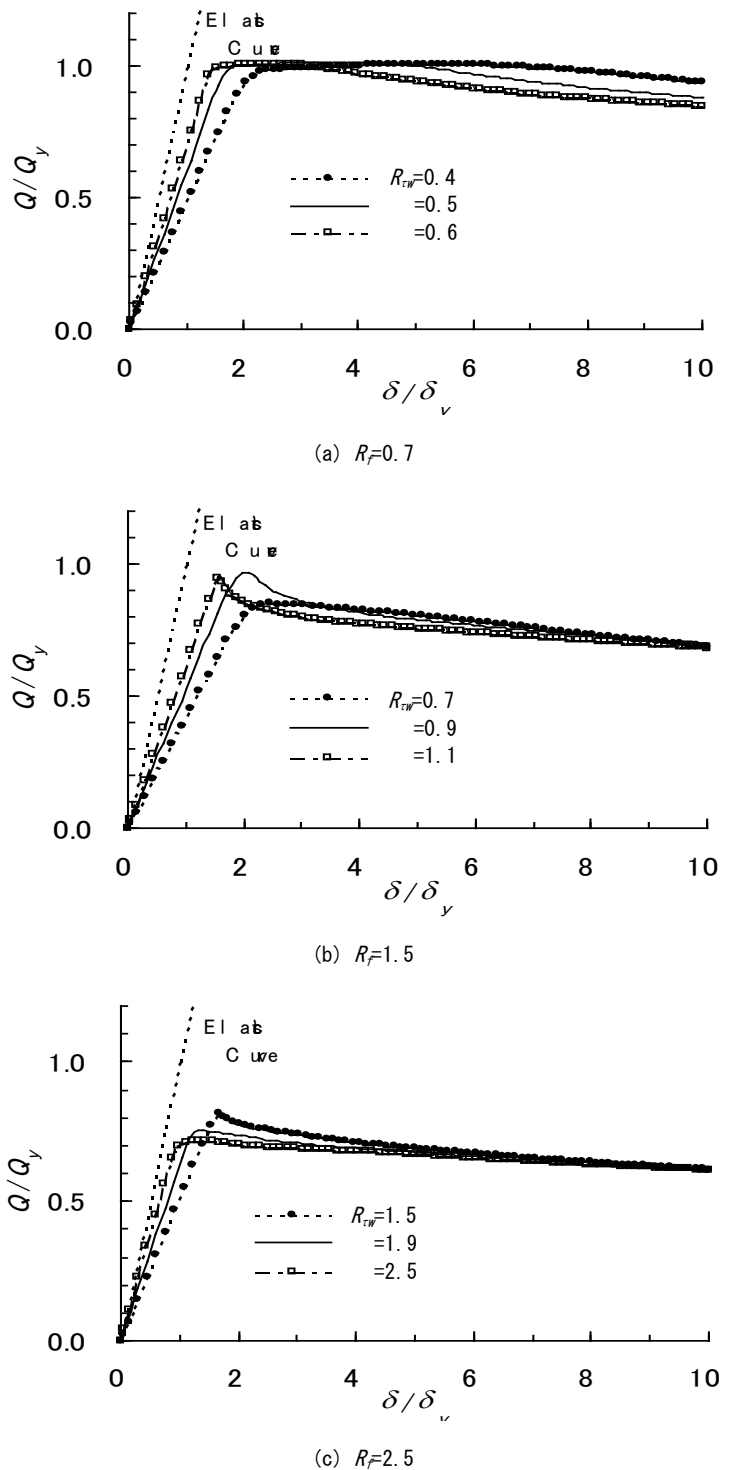
strength due to the strain hardening is generated after the yield. Here, the width-to-thickness ratio of the center flange panel was made to be larger value than it of the adjacent panels in order to utilize the deformability of the web plate without excessively expecting the increasing strength after the shear buckling of web plate.

2) Relationship between cross-sectional parameter at the center of beam and strength and deformability

In the case of steel box girder bridges, the role of the flange as an anchor of the diagonal tension field after the shear buckling of the stiffened web plate is less than that of the steel I girder because of ① a comparatively thin stiffened structure ② wide width between web plates. Here, the strength and deformability of the steel beam were examined changing variously the width-to-thickness ratio of web plate on each case that flange plate is thick or thin.

There is the investigation by Kasai et al.[9] on the actual steel portal piers for the elevated bridge in the urban area. According to this result, the plate thickness ratio t_f/t_w between flange and web plate in steel beam is almost from 1.0 to 1.5. Here, for the case that the value of t_f/t_w is 1.0, 1.5 or 3.0 and the width-to-thickness ratio parameter of the flange R_f is 0.7, 1.5 or 2.5 the steel beam under incremental loading was analyzed. The relationship between the shear force and the vertical displacement is shown in Fig.9. In this analysis, the slenderness ratio parameter of the steel beam λ, the cross-sectional shape parameter b_w/b_f, the aspect ratio of the web plate a/b_w, the width-to-thickness ratio of the web plate b_w/t_w and the width-to-thickness ratio parameter R_w are 0.3, 1.0, 1.0, 92 and 1.0, respectively.

There is the rise of the shear strength after the maximum load, when the flange is comparatively thick, as it is clear from this figure. In the box-sectional member which is simulated to be located in the center of a beam, Watanabe et al.[12] clarified that the strength rises on account of the strain hardening, if the beam with the thick flange is subjected to the shearing strain equal to that of the thin flange. In the researches by Takahasi et al.[13),14)], the case in which the shear strength reaches about 2.5 times of the   shear yielding force on account of the strain hardening has been shown, when the width-to-thickness ratio is small.
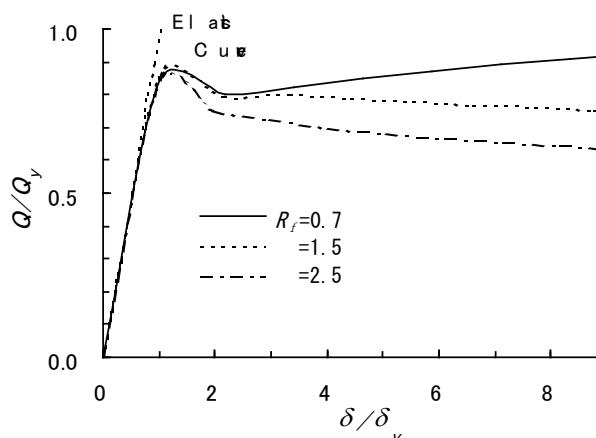

Fig.9 Effect of flange thickness

In the meantime, the degradation in the shear strength after the arrival at the maximum load is remarkable, when the flange is a comparative thin. The phenomenon of the strength degradation is more remarkable for the web plate with the large width-to-thickness ratio.

From the above-mentioned facts, it is proven that the effect of the ratio of flange thickness to web plate thickness on the shear strength and the energy absorption is also remarkable in the case of the box section. Therefore, it is effective to make flanges thick

for absorbing much energy. For the case that the thickness of the flanges and that of the web plate in the beam center are equalized, the relationship between shear force and vertical displacement with the change of the thickness has been obtained in Fig.10, where the slenderness ratio parameter of the beam λ =0.3, the ratio of the cross-sectional shape ratio b_w/b_f=1.0, the aspect ratio of the web plate a/b_w=1.0 and the width-to-thickness ratio parameter of the web plate $R_{\tau w}$= 0.6, 1.1, 2.5.

As shown in this figure, the lowering of the strength after the reach to the maximum load is distinctly observed, if the thickness of the flange is simultaneously thinned with the web plate thickness. In this case, the rise in the strength owing to the strain hardening is not observed. When the plate thickness is thin, the further degradation of the shear strength happens near δ / δ_y =10. This cause seems to be because the deformation that the flange is drawn in the web plate occurs with the growth of the buckling deformation in the web plate.

(3) Strength and deformability of steel beam under repetitive shear

The strength and deformability of the steel beam that is subjected to the repetitive shear are examined.

The relationship between the shear force and vertical displacement as the width-to-thickness ratio of the web plate at the center of the beam changes is shown in Fig.11, when the width-to-thickness ratio parameter of the flange R_f is 0.7. The similar figures for R_f=1.5 and 2.5 are shown in Fig.12 and 13, respectively. In these figures,
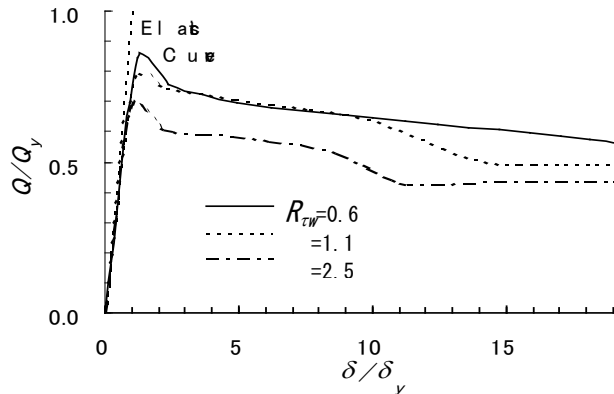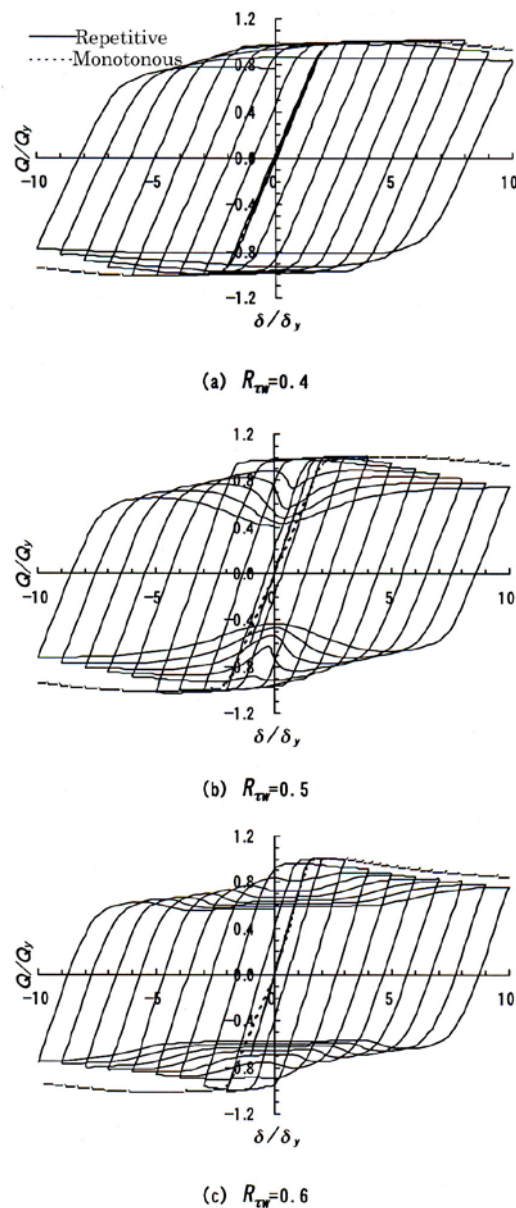

Fig.10 Effect of thin plate

(a) $R_{\tau w}$=0.4

(b) $R_{\tau w}$=0.5

(c) $R_{\tau w}$=0.6

Fig.11 Repetitive loading (R_f=0.7)

186

$\lambda=0.3$, $b_w/b_f=1.0$ and $a/b_w=1.0$. For the comparison, the results under the monotonous loading are also shown.

As seen from these figures, the shear force drops in comparison with that of the monotonous loading regardless the width-to-thickness ratio parameter of the flange plate according to the increase of the cyclic numbers and the displacement. However, the hysteretic loops show the comparatively stable loop without sudden strength degradation like the case of compression and bending, since after the shear buckling the diagonal tension field is formed. And, the shear strength tends to decrease as well as the case of the monotonous loading with the lowering of cross-sectional rigidity.

(a) $R_{\tau w}=0.7$

(b) $R_{\tau w}=0.9$

(c) $R_{\tau w}=1.1$
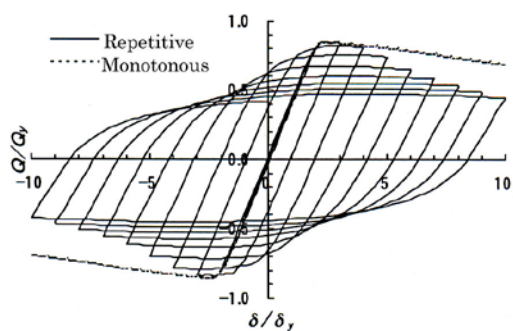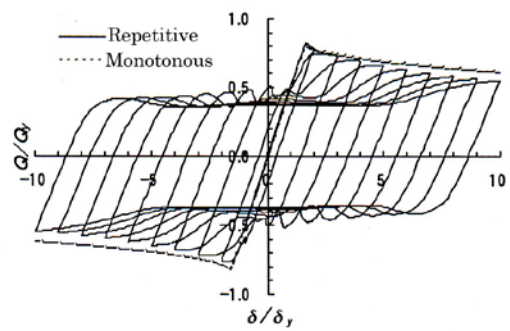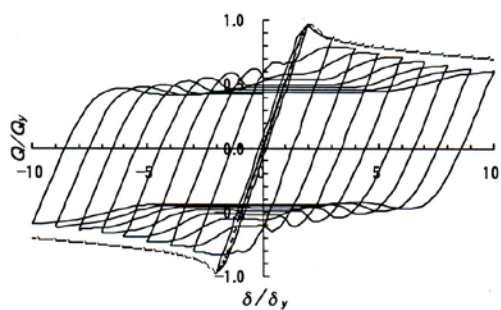
Fig.12 Repetitive loading ($R_f=1.5$)

(a) $R_{\tau w}=1.5$

(b) $R_{\tau w}=1.9$

(c) $R_{\tau w}=2.5$

Fig.13 Repetitive loading ($R_f=2.5$)

The shape of the hysteretic loop is considerably different according to the width-to-thickness ratio of the web plate. That is to say, the strength is decre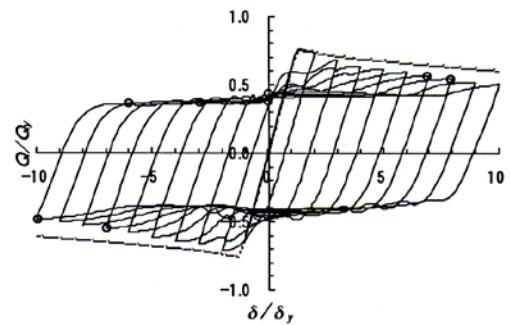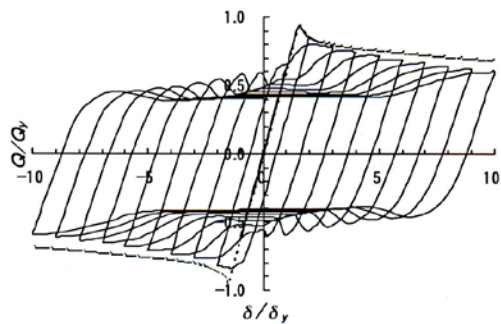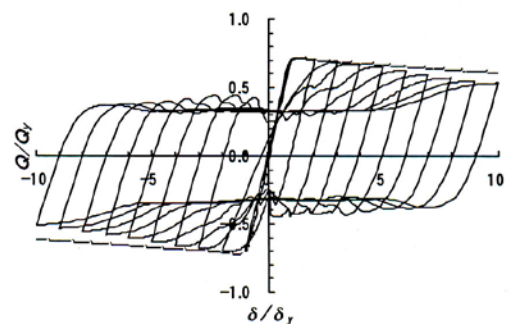asing temporarily and considerably owing to the disappearance of the diagonal tension field, when the sign of the shear force changes. However, the stable loop is obtained according to the recovery of the strength, when the diagonal tension field is formed again. In the steel beam with the large width-to-thickness ratio of the web plate and the low rigidity, this phenomenon remarkably appears.

Considering the characteristic of the above-mentioned hysteretic loop, the idea of the energy dissipation is produced by utilizing the preceding generation of shear buckling in the web plate of the steel beam. As the results, a structural system that guarantees earthquake proofing seems to become possible by not the strength but the deformation.

The deformation on the web plate panels for the every iterative stage of the repetition is shown in Fig.14. Fig.14 is the deformation diagram in the condition of Fig.13 (R_f=2.5 and $R_{\tau w}$=1.9), and each figure is correspondent to the loading stage that ◯ seal in Fig.13 shows. The intensity at the figure shows the magnitude of the out-of-plane deformation. Namely, in the web plate, the deformation to the here side is defined as positive, and it is drawn in the thick color, as this is bigger.

As it is clear from these figures, in the initial loading stage the adjacent panels to the center panel has also been deformed. However, the deformation on the thinner web plate panel at the beam center becomes remarkable with the increase of the repetitive loading, and the difference between the deformations at the adjacent panels gradually increases. The deformation of the center panel becomes more remarkable in the load stage ④. In the load stages ⑤ and ⑦, the

① (δ/δ_y=7. 0, Q/Q_y=0. 59)   ⑤ (δ/δ_y=−10. 0, Q/Q_y=−0. 51)

② (δ/δ_y=−7. 0, Q/Q_y=−0. 58)   ⑥ (δ/δ_y=−6. 0, Q/Q_y=−0. 36)

③ (δ/δ_y=±0, Q/Q_y=0. 32)   ⑦ (δ/δ_y=−3. 0, Q/Q_y=0. 33)

④ (δ/δ_y=8. 0, Q/Q_y=0. 57)   ⑧ (δ/δ_y=±0, Q/Q_y=0. 31)
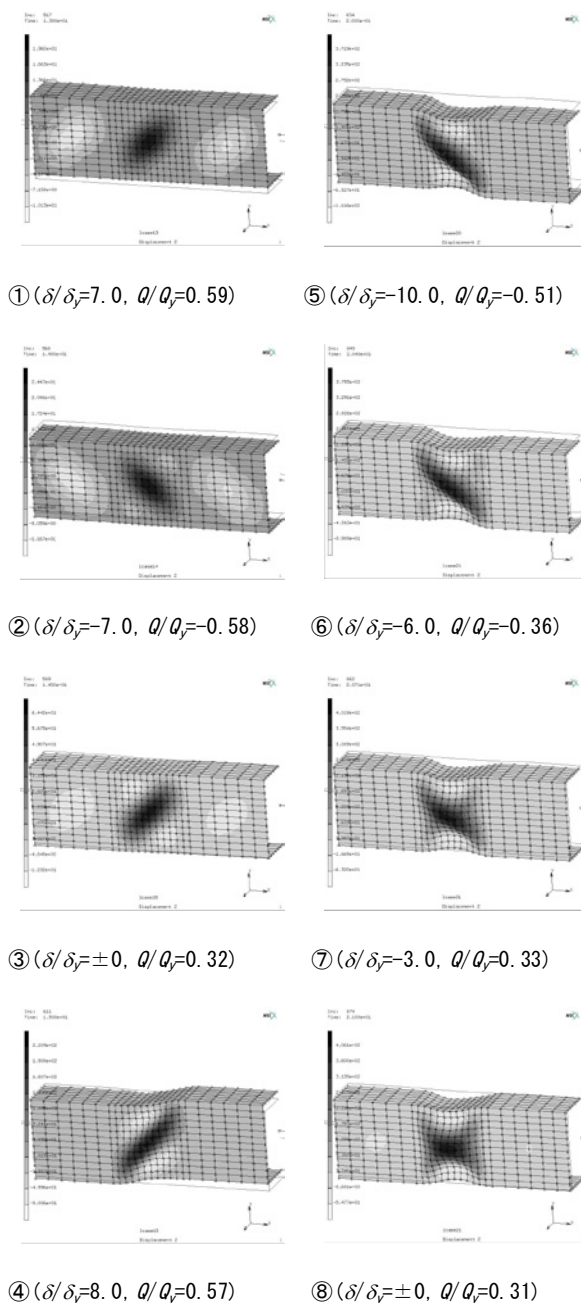
Fig.14 Deformation of web panels

reversal for the direction of the diagonal tension field due to the out-of-plane deformation is generated. In the load stage ⑧, the diagonal tensions occur in the direction of both crossing diagonal lines. Such damage pattern is very much similar to the damage mode on the center web plate at the horizontally layered intermediate beam of two-story portal steel piers in the Great Hanshin-Awaji earthquake as shown in Fig.1. Therefore, it is strongly supposed that the intermediate beam was subjected to the alternatively repetitive shear force examined in this paper.

7.3 Evaluation of earthquake proofing of steel beam

(1) Quantification of dissipation energy

In the hysteretic loop which shows the relationship between the shear force and vertical displacement of the steel beam under alternatively repetitive shear forces, the area of the part surrounded by the loop curve shows the absorbed energy of the steel beam. In other words, it can be also interpreted as the dissipation energy by the deformation of the steel beam. Here, the energy of the steel beam is investigated from the latter viewpoint.

Fig.15 shows the relationship between the dissipation energy of the steel beam and cycle numbers of the load. In this figure, the ordinate shows the accumulated dissipation energy divided by $Q_y \delta_y$. The dissipation energy decreases with the lowering of the cross-sectional rigidity, as it is clear from Fig.15. However, the dissipation energy hardly changes, even if the cross-sectional rigidity is fixedly kept and the width-to-thickness ratio of the web panel of the beam center is increased. Therefore, it is supposed that the evaluation based on the dissipation energy is appropriate. However, as the width-to-thickness ratio of the web plate is larger peculiar snap through buckling in the shear panel and afterwards the increase of the strength remarkably appear.
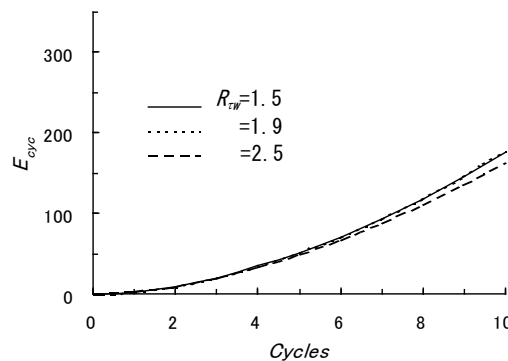
The out-of-plane deformation of the web plate at the beam center becomes remarkable, as the difference between the width-to-thickness ratio of the web panel at
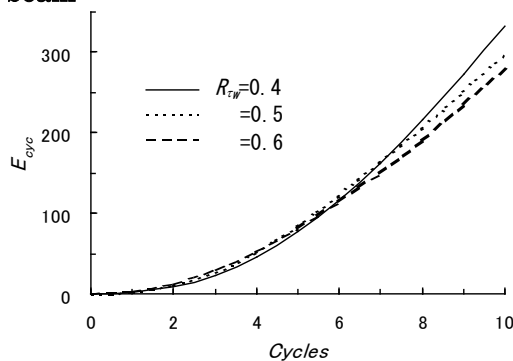
(a) R_f=0.7
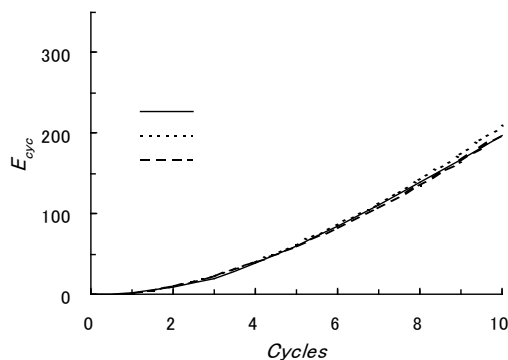
(b) R_f=1.5

(c) R_f=2.5

Fig.15 Accumulated dissipation energy

the beam center and that of the adjacent panel increases. As the width-to-thickness ratio of the web plate at the beam center increases, the smooth energy dissipation by the out-of-plane deformation of the web plate becomes difficult because both ends of this panel at the beam center yields at early stage. Therefore, it is necessary that the difference with the width-to-thickness ratio of the adjacent panel would not remarkably differ without extreme increase of the width-to-thickness ratio so that the energy may smoothly dissipate.

In this study, the energy dissipation on single steel beam was investigated. Therefore, the examination on the effect of the energy dissipation for the whole steel portal pier is needed. It should be examined from the viewpoint of the coupled behavior among the intermediate beam, the corner connection and the column and the deformability evaluation for the whole frame structure.

(2) Deformability evaluation for steel beam by ductility factor

There is a ductility factor in the standard for evaluating the deformability of steel beam. Here, it is assumed that the ductility factor is defined as the ratio between the displacement δ_{95} as the strength of the beam decreases to 95% after the arrival at the maximum load Q_{max} and the yield displacement δ_y. It is shown as following:

$$\mu_u = \frac{\delta_{95}}{\delta_y} \tag{16}$$

In order to consider the effect due to the cyclic loading, δ_{95} was obtained from the envelope curve of the hysteretic loop showing the relationship between the shear force and vertical displacement in the steel beam under the repetitive shear.

The relationship between the width-to-thickness ratio parameter of the web panel at the beam center and ductility factor is shown in Fig.16. In this figure, the following are also shown: Analytical result for the single panel between diaphragms of un-stiffened box section beam by Kasai et al[9] and analytical result for the whole structure of two-story portal steel frame piers by Araki et al[18].

As it is clear from this figure, in the region where $R_{\tau w}$ is smaller than 0.8, the present analysis (● seal) is

Fig.16 Relationship between width-to-thickness ratio parameter and ductility factor

lower a little than the analytical result (△seal) for the single panel by Kasai et al. However, the relation between the width-to-thickness ratio of the web plate and ductility factor shows the almost similar tendency in both solutions. In the region where the width-to-thickness ratio parameter is smaller than 1.0, the ductility factor rapidly decreases with the increase in width-to-thickness ratio of the web plate. In the meantime, the ductility factor becomes almost constant when the width-to-thickness ratio parameter exceeds 1.0. The cross section with the thick plate will be excellent in
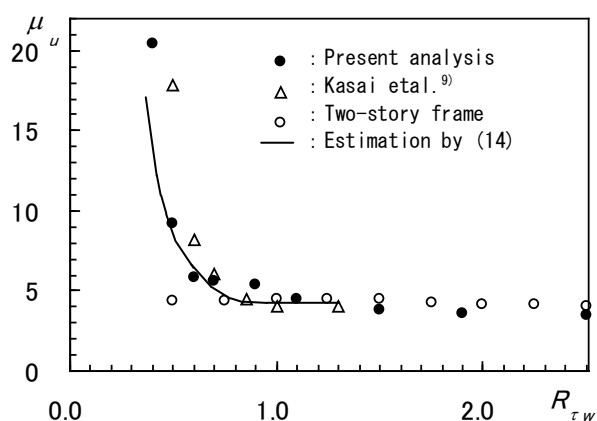
the deformability of the steel beam, as long as the ductility factor is used for evaluation. In the whole analysis on two-story portal steel frame pier, the ductility factor as the width-to-thickness ratio parameter of the center web panel in the intermediate beam variously changes has been obtained as ○ seal in this figure[18]. In this case, the ductility factor is almost constant without being related to the width-to-thickness ratio parameter of the center web panel in the intermediate beam. This fact means the following: Since the strength and deformability of the two-story portal steel frame pier are related to the proportion of the whole frame, the partial correction for the cross section in the intermediate beam does not almost influence on the ductility factor. Namely, it seems to be possible that the center web panel at the intermediate beam has the function for the dissipation of the energy with the development of the deformation without the deterioration of the whole frame.

By analyzing the relationship between the ductility factor and width-to-thickness ratio parameter of the web panel shown in this figure, the limiting value of the deformation corresponding to the lower limit of the ductility factor can be decided. That is to say, the limiting value of the deformation in which the ductility factor becomes constant without relating to $R_{\tau w}$ is about $4 \sim 5 \delta_y$ in the case of monotonous loading and about $3.5 \delta_y$ in the case of repetitive loading. On the other hand, the limiting value of the deformation in the research by Kasai et al.[9] is about 4 times of shear yielding strain γ_y in the case of the repetitive loading. The value obtained in this study is lower than the value obtained by them. This reason seems to be because the considerably thin plate for web plate was used.

By estimating the limiting value of the deformation as $3.5 \delta_y$ in the case of the repetitive loading, the relation between the width-to-thickness ratio parameter of the center web panel in the intermediate beam and the limiting value of the shear displacement will be approximated in the following equation.

$$\frac{\delta_u}{\delta_y} = \frac{0.685}{R_{\tau w}{}^{3.5}} + 3.5 \tag{17}$$

7.4 Discussions
In this chapter, a steel beam that simulated the intermediate beam in the bridge piers of two-story portal steel frame was analyzed. The strength and deformability of this steel beam subjected to the monotonously increasing shear force or alternatively repetitive shear force were clarified by the elasto-plastic finite displacement analysis using the finite element method. The results obtained by the numerical analysis will be summarized as following:
1) As the width-to-thickness ratio of the web plate is larger, the effect of the reversal in the buckling mode that is peculiar in the shear panel under alternatively repetitive shear force remarkably appeared in hysteretic loop between shear force and vertical displacement. The shear strength that remarkably lowered owing to the reversal of the buckling mode rises again by the formation of the new diagonal tension field. Therefore, a stable hysteretic behavior is generally obtained.
2) The energy absorption capacity is better, as the width-to-thickness ratio of the web plate is smaller.

3) If a thin plate is used in the center web panel of the beam, the rigidity of the cross section lowers and the deformation is concentrated in this part. Therefore, the effect of the energy dissipation is obtained. This phenomenon is more remarkable, as the plate thickness of the web plate is less.

4) Because the flange works as an anchor of the diagonal tension field, its plate thickness greatly affects the degradation of the web plate after the maximum load.

5) The prediction expression for the limiting value of the shear displacement was presented.

In this research, when the cross beam established in the steel portal frame pier is subjected to repetitive shear force, the effect of the rigidity of the web panel in the beam center on the shear strength and deformability was examined. That is to say, the energy dissipation effect by the deformation of the web panel was noticed in order to reduce the damage in the earthquake of the bridge pier as much as possible.

Here, the strength and deformability of single steel beam were clarified. The strength and deformability for the steel bridge piers of two-story portal frame type under the repetitive shear force have been investigated for the whole structure[18]. In the future, the results of both researches are developed and the effect of the behavior of the steel beam on the corner connection and the basal part of bridge pier should be examined in detail. In addition, the effect on the steel type of the web plate should be also clarified. In this research, the analysis for the un-stiffened box-beam was carried out. Therefore, the investigation for the stiffened box-beam will be also necessary.

7.5 References

1) Miki, T.: Inelastic earthquake response of steel portal frames with shear collapse in middle of beam, Journal of Structural Engineering, JSCE, Vol.44A, pp.169-178, 1998 (in Japanese).

2) Miki, T. and Yamada, O.: Inelastic earthquake response analysis of steel two-story frames with shear collapse in middle of beam, , Journal of Structural Engineering, JSCE, Vol.45A, pp.227-234, 1999 (in Japanese).

3) Miki, T.: Effect of strain rate on inelastic earthquake response of steel portal frames with shear collapse of beam, Journal of Structural Engineering, JSCE, Vol.47A, pp.771782, 2001 (in Japanese).

4) Morishita, H., Takaku, T., Aoki, T., Fukumoto, Y., Okamoto, T. and Matsui, E.: Experimental study on strength and ductility of a rigid-frame steel pier with intermediate cross beam, Journal of Structural Engineering, JSCE, Vol.46A, pp.831-840, 2000 (in Japanese).

5) Takeda, H., Uchida, Y., Sasaki, D. and Dogaki, M.: Evaluation of Ultimate Strength and Ductility for Plate Girders under Cyclic Shear Loading, Journal of Construction Steel, JSSC, Vol.8, pp.33-40, 2000 (in Japanese).

6) Niinobe, Y.: Study on the post-buckling strength of webplates of plate girders under shear, Proceedings of the Japan Society of Civil Engineers, JSCE, pp.15-30, 1980 (in Japanese).

7) Fukumoto, Y., Uenoya, M., Nakamura, M. and Kobayashi, Y.: Strength and Ductility of plate girder panels under cyclic shear, Journal of Structural Engineering, JSCE,

Vol.46A, pp.143-150, 2000 (in Japanese).

8) Kasai, A., Watanabe, T. Amano, M. and Usami,T.: Strength and ductility evaluation of stiffened steel plates subjected to shear loading, Journal of Structural Engineering, JSCE, Vol.47A, pp.761-770, 2001 (in Japanese).

9) Kasai, A., Watanabe, T., Usami, T. and Chusilp, P.: Strength and ductility of unstiffened box section members subjected to cyclic shear loading, Journal of Structural Mechanics and Earthquake Engineering, JSCE, No.703/ I -59, pp.129-140, 2002 (in Japanese).

10) Specification for Highway Bridges, Japan Road Association, 1990.

11) Scheer, J., Pasternak, H. und Ruga, J.: Kastentraeger mit schlanken Stegen-Verhalten und Braunschweig, Bauingenieur, Vo.69, No.9, S.353-362, 1994.

12) Watanabe, T., Hanbin, GE and Usami, T.: Analytical study on strength and ductility of steel stiffened plates under cyclic loading, Journal of Structural Engineering, JSCE, Vol.45A, pp.185-195, 1999 (in Japanese).

13) Takahashi, Y. and Shinabe, Y.: Experimental Study on Restoring Force Characteristics of Shear Yielding Thin Steel Plate Elements, Journal of Structural and Construction Engineering (Transactions of AIJ), No.494, pp.107-114, 1997(in Japanese).

14) Takahashi, Y. and Tanaka, K.: Development of Hysteretic Damper using Eccentrical Brace System, Journal of Construction Steel, JSSC, Vol.4, pp.39-52, 1997 (in Japanese).

15) Fukumoto, Y. (Edited by): Guidelines for Stability Design of Steel Structures, Subcomittee on Stability Design Committee on Steel Structures, JSCE, 1987.

16) Nakai, H., Kawai, A., Yoshikawa, O., Kitada, T. and Miki, T.: Investigation of actual results for steel frame piers (I), THE BRIDGE AND FOUNDATION ENMGINEERING, Kensetutosho, Vol.16, No.6, pp.35-40, 1982 (in Japanese).

17) Nakai, H., Kawai, A., Yoshikawa, O., Kitada, T. and Miki, T.: Investigation of actual results for steel frame piers (II), THE BRIDGE AND FOUNDATION ENMGINEERING, Kensetutosho, Vol.16, No.7, pp.43-49, 1982 (in Japanese)

18) Araki, T., Takeda, H. and Dogaki, M.: Cyclic Strength and Deformation Capacity for Steel Bridge Piers of Two-Story Portal Frame Type, Journal of Structural Engineering, JSCE, Vol.46A, pp.1455-1465, 2004 (in Japanese).

19) Watanabe, E., Takeda, H. and Kunishi, R.: Inelastic Repetitive Shear and Flexural Buckling of Plate Girders, First International Conference on Structural Stability and Dynamics, pp.183-188, 2000.

Chapter 8

Concluding remarks

The summary on the results obtained in this study and the problems in the future on this study are described in the following.

In Chapter 2, the elastic lateral buckling of plate girders with relatively thin web was investigated as the simultaneous buckling between the flanges and web by means of the theory of orthotropic plate. The numerical computations were carried out by the finite difference method. Loading tests were also carried out for the verification of the theory. The end moment ratios, the flexural and torsional rigidities of the flange and the flexural rigidity of the transverse stiffeners on the critical loads have been clarified. And the mono-symmetric girder was also treated. Furthermore, the method in order to obtain the position of the equivalent uniform moment was presented for the case of the girder panel subjected to unequal end moments. The position of the equivalent uniform moment was expressed as the function of the panel aspect ratio and the end moment ratio. In this study, the deformation of the web plate was considered in the analysis. Such problems are especially important for the girder under construction. Therefore, as future study, initial imperfections and residual stresses must be accurately considered. Furthermore, the overall lateral buckling of the bridge composed of several girders should be also solved with sufficient accuracy.

In Chapter 3, an approximate calculation method to predict the bending strength of multi-stiffened plate girders and the inelastic coupled buckling of the compressive flange and web plate by using the orthotropic plate theory were presented. It was clarified that these estimations were simple and useful method.

The following subject must be settled as a future study. The validity of the reduced coefficients for the rigidities in the inelastic region should be confirmed by means of some way, for example, finite element method.

In Chapter 4, the static load carrying capacity and behavior of girder panels subjected in shear were investigated experimentally and theoretically. The results obtained by the modal analysis, elasto-plastic finite displacement analysis and experimental works were presented for the girder with equal web depth. Furthermore, the results obtained by the modal analyses and tests were given for the girder with linearly varying web depth. As a result, the effect of panel aspect ratio, panel width-to-thickness ratio, flange stiffness and intermediate vertical stiffener rigidity on the ultimate shear strength and the ultimate behavior was clarified. And an

approximate prediction expression on ultimate shear strength for the girder with linearly varying web depth was given.

In the following study, longitudinally stiffened web panel should be researched by the elasto-plastic finite displacement analysis. Then, simple and accurate design methods for such stiffened panel must be developed. Furthermore, the accurate research on the inelastic behavior for tapered panel with varying depth in shear is required analytically. The research on such problem seems to be almost lacking. On the required stiffness of intermediate stiffeners, further examination is necessary.

In Chapter 5, a simple expression to predict the ultimate strength on the trapezoidal panel of plate girders with linearly varying web depth under the combined action of bending and shear was presented. Furthermore, the loading tests were carried out in order to compare the theoretical results. A modal analysis was adopted in the theoretical estimation.

In the following study, an elasto-plastic finite displacement analysis must be tried for general application and the verification on the obtained results is needed.

In Chapter 6, to begin with the ultimate strength and hysteretic behavior of the single girder panel subjected to the repetitive shear force are investigated numerically. Next, the theoretical and experimental studies on the strength and ductility of multi-panel under the repetitive inelastic buckling subjected to shear or the combined shear and bending were examined. The influence of panel aspect ratio, panel width-to-thickness ratio, flange rigidity and the loading pattern on the hysteretic behavior was clarified. As the result, it was proven that the shear panel subjected to cyclic loadings shows the excellent energy dissipation capacity.

In Chapter 7, a steel beam that simulated the intermediate cross beam in the bridge piers of two-story portal steel frame was analyzed. The strength and deformability of this steel beam subjected to the monotonously increasing shear force or alternatively repetitive shear force were clarified by the elasto-plastic finite displacement analysis using the finite element method. Namely, the strength and deformability of single steel beam were investigated in the use of coupled elements. Effect of energy dissipation due to the shear buckling deformation in the relatively thin web plate near the center of the crossbeam was clarified. Namely, the energy dissipation effect by the deformation of the web panel was examined in order to reduce the damage in the earthquake of the bridge pier as much as possible.

In future study, the following examination subjects seem to have been left. To begin with, the behavior in using the low yield ratio steel for the shear panel should be examined in detail. Next, the utilization of the demountable shear panel as a damper

system in steel bridge structures should be investigated. By the use of this realistic damper system, in huge earthquake it is expected that considerably great destruction can be prevented.